Republic of Iraq
Ministry of Higher Education and Scientific Research
University of Babylon
College of Engineering
Civil Engineering Department

Repair of Fire Damage for Normal and High Strength Reinforced Lightweight Concrete T-Beams Using Slurry Infiltrated Fiber Concrete Jackets

A Thesis
Submitted to the College of Engineering / University of Babylon in Partial Fulfillment of the Requirements for the Degree of Master in Engineering / Civil Engineering / Construction Materials

By

Hasanain Sameer Hamdy Hakeem

Supervised by

Prof. Dr.
Mohammed M. Kadhum

Prof. Dr.
Nameer A. Alwash

Ayah from the Holy Quran

سورة البقرة (الآية رقم 255)

Dedication

To the great person

Dad, Mom, My family, Wife and Son …...

……

……

……

……

……

……

……

……

That's for you

Hasanain Sameer Hamdy AL-ameedy

Supervisor Certification

We certify that the preparation of this thesis entitled "**Repair of Fire Damage For Normal and High Strength Reinforced Lightweight Concrete T-Beams Using Slurry Infiltrated Fiber Concrete Jackets**" and submitted by the student "**Hasanain Sameer Hamdy**" was prepared under our supervision at the Department of Civil Engineering / College of Engineering, Babylon University, as a part of the requirements for a Master degree of Science in Civil Engineering (Construction Materials).

Signature:
Name : **Prof. Dr. Mohammed M. Kadhum**
Date : / /

Signature:
Name : **Prof. Dr. Nameer A. Alwash**
Date : / /

We certify that this thesis mentioned above has been completed in Civil Engineering department in the college of Engineering / University of Babylon.

Signature:
Head of Department: Asst. Prof. Dr. Zaid H. Majeed AL-Hasson

Date

Examining Committee Certificate

We certify that we have read this thesis entitled "**Repair of Fire Damage For Normal and High Strength Reinforced Lightweight Concrete T- Beams Using Slurry Infiltrated Fiber Concrete Jackets"** and as an examining cee examined that student **"Hasanain Sameer Hamdy"** in its content and that in our opinion it meets a standard of a thesis for the degree of master in Engineering / Civil engineering / Construction Materials

Signature:
Name:
Prof. Dr. Zainab H. Mahdi
(Chairman)
Date: / /2023

Signature:
Name:
Prof. Dr. Nabeel Hasan Ali Al-Salim
(Member)
Date: / /2023

Signature:
Name:
Assis. Prof. Dr. Ali H. Nahhab
(Member)
Date: / /2023

Signature:
Name:
Prof. Dr. Mohammed M. Kadhum
(Supervisor)
Date: / /2023

Signature:
Name:
Prof. Dr. Nameer A. Alwash
(Supervisor)
Date: / /2023

Approval of Head of Department

Approval of the Dean of Collage

Signature:
Name:
Asst. Prof. Dr. Zaid H. Majeed AL-Hasson
Date: / /2023

Signature:
Name:
Prof. Dr. Laith Ali Abdul- Rahaim
Date: / /2023

Acknowledgements

In the name of ALLAH, the most compassionate, the most merciful. Praise be to ALLAH and pray and peace be on his prophet Mohammed and his relatives' companions and on all those who follow him.

I might want to communicate my genuine appreciation and most profound appreciation to ***Prof. Dr. Mohammed M. Kadhum*** and ***Prof. Dr. Nameer A. Alwash,*** whom I had the magnificent karma and the distinction of being under their watch, for their consistent consolation and significant direction all through this application.

All love and great thanks to ***My Second home "Babylon University"***, especially those people who works in the college of Engineering as well as Civil Engineering Department from Deans, Heads, Lecturers and Staff that I knew during all the study time.

Thanks, are also extended to the staff of the Laboratories at the College of Engineering/University of Babylon for their help in using various devices in the experimental test.

I do not know how can I pass my high respect and thank to my family, especially ***My Dear Father***, ***My Dear Mother, My Brothers and My Lovely wife*** for their care, patience and encouragement throughout the study period, I am really will be in debt to them.

Lastly, special thanks and gratitude are for all people that love subsistence in peace.

Hasanain Sameer Hamdy AL-amiedy

Abstract

An experimental analysis of the behavior of simply supported T-beams is included in the present study. In order to create a stable lightweight concrete, **l**ightweight **e**xpanded **c**lay **a**ggregate (LECA) was employed as a coarse aggregate.

The planned experiments include a series of tests, Fourteen T-beams constructed from lightweight reinforced concrete and subjected to (**S**ymmetric **T**wo-**P**oint **C**oncentrated **L**oads) **STPCL**, where the sample dimensions of T- beam are always the same: (Web 25 X 7.5 cm, Flange 10 X 17.5 cm, and length 150 cm).

The primary factors that were taken into account to find out how fire affects the mechanical characteristics of concrete, burned and unburned samples of **l**ight **w**eight **r**einforced **c**oncrete (LWRC) T-beams manufactured from two different type strength of lightweight concrete; **n**ormal **s**trength **l**ight **w**eight **c**oncrete and **h**igh **s**trength **l**ight **w**eight **c**oncrete (NSLWC and HSLWC).

Burned LWRC T-beams are repaired and strengthened with U-shaped **S**lurry **I**nfiltrated **F**iber **Con**crete (SIFCON) thin jackets, and the effect of several factors on the T-beams such as ductility, stiffness, and energy absorption. The mechanical characteristics of concrete were determined by testing cylindrical and cubical specimens of each mix.

The results showed that by using LECA a lightweight concrete can be achieved with dry density in the range of 1610-1965 Kg/m^3 and compressive strength in the range of 34-67 MPa based on (150*150) mm cube specimens.

The experiments in this study were conducted in three distinct Segments: In the first Segment, investigated characteristic and properties of reference normal and high strength T- beams sample, In the second segment, studying changed in NSLWC and HSLWC T- beams if they were burned according to IS0-834 curves, In the third Segment, studying characteristic of post-

production method for protecting T-beams from further damage caused by fire by applying a layer of SIFCON material. In addition to the control samples, other factors of concrete T-beams and conditions were investigated. These included fire exposure period and SIFCON jacket thickness. The conditions were 15 and 30 min. of fire exposure and 15 and 30 mm of SIFCON jacket thickness.

Several thermocouple sensors were strategically placed inside the T-beam to monitor the temperature distribution across its cross section.

In all, fourteen samples from each of the three Segments (references, fired samples, and repairing by SIFCON) were tested for concrete T-beams. The test specimens were compared using several metrics, including the ultimate load capacity and deflection, ductility index, cracking load, initial stiffness, secant stiffness, and energy absorption.

The results of the experimental tests showed a considerable improvement for the reinforced T-beams compared to samples destroyed by fire, also repair T-beams were restored to perform good or better than unharmed (reference T- beam) variants with the given parameters.

All of the SIFCON-jacketed reinforced T-beams performed well in load tests, as expected. Burning lowered the load bearing capacities of the burned T-beams. NSLWC and HSLWC T-beams experienced a degradation rate of 24.4 and 20.5 %, and 41.5 and 35.6 %, respectively. For 15 and 30 min of fire exposure respectively. The reinforcing T-beams greatly enhanced the carrying capacity, by (159 and 207%) for the NSLWC and (180 and 220%) for the HSLWC for 15 and 30 mm of SIFCON thickness jacket.

Finally, a **f**inite **e**lement **m**ethod (FEM) was built to model and simulate the concrete T-beams that were verified experimentally in the lab, and a simulated theoretical expression was carried out to verify the results.

Numerical validation utilizing by the ABAQUS programmed was used for this purpose, The results shows that the lowest and highest absolute errors

"variation" in **load** bearing capacity determined for the specimens were around 1.97% and 14.28% respectively, for NSLWC and around 0.39% and 9.67% respectively, for HSLWC.

The minimum and highest absolute errors "variation" for the specimen's **deflection** that matched the maximum load were, respectively, 1.59% and 13.43% for NSLWC and 3.93% and 13.89% for HSLWC and an absolute error of 15% or less was considered acceptable.

List of Contents

Ayah from the Holy Quran ..... **I**
Dedication ..... **II**
Supervisor Certification ..... **III**
Examining Committee Certificate ..... **IV**
Acknowledgements ..... **V**
Abstract ..... **VI**
List of Contents ..... **IX**
Abbreviations ..... **XII**
List of Figures ..... **XIV**
List of Plates ..... **XIX**
List of Tables ..... **XX**
Chapter ONE INTRODUCTION **1**
1.1 Introduction 2
1.2 Lightweight Concrete (LWC) 4
1.3 Benefit of Structural Lightweight Concrete 5
1.4 Problems with Lightweight Concrete Structures 5
1.5 Applications and Uses of SLWC 6
1.6 Scope and Objectives of Study 7
1.7 Standard fire curve (ISO 834) 8
1.8 Thesis Outline 10
Chapter Two Literature Review **11**
2.1 Overview 12
2.2 Application of Lightweight Aggregate Concrete in Iraq 14
2.3 Main types of Lightweight Aggregate Concrete 14
2.4 Previous Studies on Mechanical Properties of LWC 18
2.5 Previous Studies on Structural Behavior of LWC 23
2.6 T-Beam Behavior under Fire Exposure 26
2.7 High Range Water Reducing Admixture (HRWRA) 27

2.8 Summary....28
Chapter Three Experimental Work....31
3.1 Introduction....32
3.2 Research Methodology Flowchart....33
3.3 Materials....35
3.4 Mix Design....43
3.5 Trial mixes....45
3.6 Mixing procedure....46
3.7 Preparation, Casting and Curing of Test Specimens....47
3.8 Fresh Concrete Tests....49
3.9 Hardened Concrete test....51
3.10 T-Beam Moulds Description....52
3.11 Fire Test Furnace Description....54
3.12 Preparing the SIFCON Thin Jackets....61
3.13 Repaired Technique of Fired Damaged NSLWC and HSLWC T-beam Specimens....62
3.14 Instruments and Testing Procedure of T-Beam....65
3.15 Testing of Control Samples (Destructive Tests)....69
3.16 Testing Non-Destructive Tests....74
Chapter Four Experimental Results and Discussion....76
4.1 General....77
4.2 Introduction....77
4.3 Mechanical Properties of Concrete....77
4.4 Experimental Results of T-Beam specimens....91
4.5 NSLWC and HSLWC T-Beam Load Carrying Capacity....92
4.6 Load-Deflection of NSLWC T-Beam Specimens....97
4.7 Load-Deflection of HSLWC T-Beam Specimens....99
4.8 The effect of concrete cover....101
4.9 Effect of Fire Exposure on Steel Reinforcement....101
4.10 Effectiveness of SIFCON Jackets....103

4.11 Ductility Index 105
4.12 Flexural toughness “Energy Absorption” 110
4.13 Initial and Secant stiffness 112
4.14 Crack Width 114
4.15 Surface Condition and Fire burning Endurance of T- Beam Specimen 116
Chapter Five Finite Element Modelling and Simulation 120
5.1 General “Overview” 121
5.2 Finite Element Modelling with ABAQUS Program 121
5.3 SEGMENT A: Reference T-Beam Modelling 122
5.4 SEGMENT B: Modelling the Thermal Distribution on Concrete Samples 131
5.5 SEGMENT C: Modelling of Fired Samples Subjected to Mechanical Loading 132
5.6 SEGMENT D: Modelling of The Improvement of Concrete T-Beams Using SIFCON Jacketing 137
5.7 Finite Element Method Result 140
Chapter SIX Conclusions and Recommendation 160
6.1 Conclusions the Results 161
6.2 Recommendations for Future works 163
References 164
Reference 165
Appendices 177
A.1 Appendix 179
A.2 T-beam dimensions: 179
A.3 Min. reinforcement ratio 179
A.4 Flexure calculation 179
A.5 Shear calculation 180
A.6 ABAQUS Appendix 180
الملخص **.....191**

Abbreviations

Symbol	Description
ACI	American Concrete Institute
ASTM	American Society for Testing and Materials
BS	British Standards (BSI: British Standard Institute)
BS EN	British Standard European Norm
C–S–H	Calcium Silicate Hydrate
CDP	Concrete Damage Plasticity
CSC	Concrete Smeared Cracks
FEM	Finite Element Method
FRC	Fiber-Reinforced Concrete
HPFRCC	High-Performance Fiber-Reinforced Cementitious Composite
HRWRA	High Range Water Reducing Admixture
IQs.	Iraqi Standards Specification
ISO	International Organization for Standardization
LECA	Light Expanded Clay Aggregate
LWC	Lightweight Concrete
MOR	Modulus Of Rupture
NWC	Normal-weight Concrete
NSLWC	Normal strength lightweight Concrete
HSLWC	High strength lightweight Concrete
LVDT	Linear Variable Differential Transformer
LWA	Lightweight Aggregate
LWAC	Lightweight Aggregate Concrete
LWRC	Lightweight Reinforce Concrete
ODD	Oven Dry Density
PID	Proportional Integral Derivative
RPC	Reactive Powder Concrete
RILEM	International Union of Laboratories and Experts in Construction Materials, Systems and Structures
SP	Super Plasticizer
STPCL	Symmetric Two Point Concentrated Load
SIFCON	Slurry Infiltrated Fiber Concrete
SCC	Self-Compacting Concrete
SSD	Saturated Surface Dry
SOP	Standard Operating Procedure
USA	The United States of America
UK	The United Kingdom
kN	Kilo-newton

GPa	Giga-pascal
MPa	Mega-pascals
Kg	Kilo-gram
W/C	Water-Cement ratio
W/B	Water-Binder ratio
No.	Number
λ	Reduction Factor
ºC	Centigrade temperature symbol
Ec	Modulus Of Elasticity
f_{cu}	Cube Compressive Strength
f_r	Modulus of Rapture
FRC	Fiber-Reinforced Concrete
f_{sp}	Splitting Tensile Strength
Min.	Minutes
%	Percent
≤	Less than or Equal
≥	Greater than or Equal
=	Equal
≈	Approximately Equal
Ø	Bar Diameter
1st	First
2nd	Second
3rd	Third
4th	Fourth

List of Figures

Figure 1-1: ISO 834 Standard fire curve. ---------- 9
Figure 3-1: Experimental program Flow chart----------34
Figure 3-2: Fine aggregate sieve analysis----------37
Figure 3-3: Percent Materials proportion used in HSLWC mixture----------44
Figure 3-4: Percent Materials proportion used in NSLWC mixture----------44
Figure 3-5: Percent Materials proportion used in SIFCON mixture----------45
Figure 3-6: The longitudinal section of the T-beam with Symmetric two-point concentrated load ----------53
Figure 3-7: The cross section of the T-beam----------53
Figure 3-8 :Details of the furnace and equipment. ----------56
Figure 3-9: Furnace description details ----------57
Figure 3-10: The location of the thermocouples in the cross section----------59
Figure 3-11: Experimental and ISO-834 Standard recommended temperature-time curves for 30 min. ----------61
Figure 3-12: Strengthened section using three-faces SIFCON jacket. ----------62
Figure 3-13: Repair and strengthening technique process of LWC T-beams by using three-faces SIFCON jacket. ----------65
Figure 3-14: Case study of the T-beam specimen identification procedure------66
Figure 3-15: Loading setup and measurements----------67
Figure 3-16: The loading setup of two-point load system ----------68
Figure 4-1: Oven dry density at age 28,56 and 90 days ----------78
Figure 4-2: Development of compressive strength. ----------79
Figure 4-3: Cylinder compressive strength----------80
Figure 4-4: Concrete residual strength at various ages ----------81
Figure 4-5: Ratio compressive strength ----------81
Figure 4-6: Splitting Tensile Strength----------82
Figure 4-7: Calculated and Predicted splitting tensile strength ----------83
Figure 4-8 : Development of Flexural strength. ----------84
Figure 4-9: Predicted and Experimental result cylinder modulus of elasticity for NSLWC and HSLWC sample ----------86
Figure 4-10: % Residual of compressive strength ULTRASONIC ----------87
Figure 4-11: ULTRASONIC T-beam position ----------88
Figure 4-12: Rebound number - compressive strength relation----------91
Figure 4-13: Effect of load carrying capacity of NSLWC T-beams with different SIFCON jacket thickness.----------95
Figure 4-14: Exposure fire duration effect on HSLWC T-beams load carrying capacity with different SIFCON jacket thickness. ----------97
Figure 4-15: Load versus deflection at mid-span of NSLWC T-beam specimen before and after exposure to fire.----------98
Figure 4-16: Load - deflection curve at mid-span of HSLWC T-beam specimen

before and after exposure to fire. ---------- 100
Figure 4-17: Effectiveness of SIFCON jacket on the load carrying capacity of NSLWC T-beams before and after burning ---------- 103
Figure 4-18: Effectiveness of SIFCON jacket on the load carrying capacity of HSLWC T-beams before and after burning ---------- 104
Figure 4-19: Result the value of Δ_y using the load-deflection curve (Azizinamini et al.,1999) ---------- 105
Figure 4-20: Calculating the yield Deflection point on load –deflection curves of NSLWC. ---------- 106
Figure 4-21: Calculating the yield Deflection point on load –deflection curves of HSLWC. ---------- 107
Figure 4-22: Ductility values of NSLWC with different fire exposure time before and after burning ---------- 109
Figure 4-23: Ductility values of HSLWC with different fire exposure time before and after burning ---------- 109
Figure 4-24: Values of energy absorption capacity for NSLWC before and after burning and strengthening ---------- 111
Figure 4-25: Values of energy absorption capacity for HSLWC before and after burning and strengthening ---------- 112
Figure 4-26: Secant and Initial stiffness of NSLWC T-Beam Specimen ------- 113
Figure 4-27: Secant and Initial stiffness of HSLWC T-Beam Specimen ------- 114
Figure 4-28: Relation between applied load and crack width for NSLWC before and after burning ---------- 115
Figure 4-29: Relation between applied load and crack width for HSLWC before and after burning. ---------- 116
Figure 4-30: The relationship between measured temperatures and fire exposure time of NSLWC T-beam. ---------- 117
Figure 4-31: The relationship between measured temperatures and fire exposure time of HSLWC T-beam. ---------- 118
Figure 5-1: Parts geometrical modelling ---------- 123
Figure 5-2: Concrete damage plasticity model: Giovanni Castellazzi,2017 --- 125
Figure 5-3: General types of steel stress strain representation and simplification - 126
Figure 5-4: Section assignment of concrete T-beams and steel bars ---------- 126
Figure 5-5: Stress - Strain relation LWAC at different temp. ---------- 127
Figure 5-6: Compressive inelastic strain defined by ABAQUS ---------- 128
Figure 5-7: Part assembling of the concrete T-beam ---------- 128
Figure 5-8: Element types library in ABAQUS ---------- 131
Figure 5-9: Meshing of the concrete T-beam using structural mesh algorithm techniques ---------- 131
Figure 5-10: Concrete stress – strain behavior under elevated temperatures -- 133
Figure 5-11: Normalized Values of the residual f`c and Ec for concrete subjected to high temperatures (Dabbaghi et al.,2021b) ---------- 134
Figure 5-12: Normalized Value of the concrete strain corresponded to the f`c (Dabbaghi et al.,2021b). ---------- 134

Figure 5-13: Normalized concrete compressive strength at high temperatures (Dabbaghi et al.,2021b) ---------- 135
Figure 5-14: (Lie, 1972) calculated residual Fy and E values for steel bars heated to extreme temperatures. ---------- 136
Figure 5-15: Concrete Poisson's ratio at high temperatures (Bahr et al., 2013). ---------- 136
Figure 5-16: SIFCON jacket layer part along the three faces of the concrete ----- 138
Figure 5-17: Unconfined, uniaxial loading and tensile stress in SIFCON and the resulting stress-strain behavior ---------- 139
Figure 5-18: SIFCON jacket strengthening model meshing ---------- 139
Figure 5-19: N-C-0 Experimental and Finite Element Method Load-Deflection Curve Comparison ---------- 142
Figure 5-20: T-beam N-C-0 deflection and principal stress distribution for concrete and steel reinforcement ---------- 142
Figure 5-21: H-C-0 Experimental and Finite Element Method Load-Deflection Curve Comparison ---------- 143
Figure 5-22: T-beam H-C-0 deflection and principal stress distribution for concrete and steel reinforcement ---------- 143
Figure 5-23: Comparison of FEM & Exp. Temp. distribution of NSLWC for 30 min. fired ---------- 144
Figure 5-24: Comparison of FEM & Exp. Temp. distribution of HSLWC for 30 min. fired ---------- 144
Figure 5-25: N-F15-0 Experimental and Finite Element Method Load-Deflection Curve Comparison ---------- 145
Figure 5-26: T-beam N-F15-0 deflection and principal stress distribution for concrete and steel reinforcement ---------- 145
Figure 5-27: N-F30-0 Experimental and Finite Element Method Load-Deflection Curve Comparison ---------- 146
Figure 5-28: T-beam N-F30-0 deflection and principal stress distribution for concrete and steel reinforcement ---------- 146
Figure 5-29: H-F15-0 Experimental and Finite Element Method Load-Deflection Curve Comparison ---------- 147
Figure 5-30: T-beam H-F15-0 deflection and principal stress distribution for concrete and steel reinforcement ---------- 147
Figure 5-31: H-F30-0 Experimental and Finite Element Method Load-Deflection Curve Comparison ---------- 148
Figure 5-32: T-beam H-F30-0 deflection and principal stress distribution for concrete and steel reinforcement ---------- 148
Figure 5-33: N-F15-S2 Experimental and Finite Element Method Load-Deflection Curve Comparison ---------- 149
Figure 5-34: T-beam N-F15-S2 deflection and principal stress distribution for concrete and steel reinforcement ---------- 149
Figure 5-35: N-F15-S3 Experimental and Finite Element Method Load-Deflection Curve Comparison ---------- 150

Figure 5-36: T-beam N-F15-S3 deflection and principal stress distribution for concrete and steel reinforcement ---------- 150
Figure 5-37: N-F30-S2 Experimental and Finite Element Method Load-Deflection Curve Comparison ---------- 151
Figure 5-38: T-beam N-F30-S2 deflection and principal stress distribution for concrete and steel reinforcement ---------- 151
Figure 5-39: N-F30-S3 Experimental and Finite Element Method Load-Deflection Curve Comparison ---------- 152
Figure 5-40: T-beam N-F30-S3 deflection and principal stress distribution for concrete and steel reinforcement ---------- 152
Figure 5-41: H-F15-S2 Experimental and Finite Element Method Load-Deflection Curve Comparison ---------- 153
Figure 5-42: T-beam H-F15-S2 deflection and principal stress distribution for concrete and steel reinforcement ---------- 153
Figure 5-43: H-F15-S3 Experimental and Finite Element Method Load-Deflection Curve Comparison ---------- 154
Figure 5-44: T-beam H-F15-S3 deflection and principal stress distribution for concrete and steel reinforcement ---------- 154
Figure 5-45: H-F30-S2 Experimental and Finite Element Method Load-Deflection Curve Comparison ---------- 155
Figure 5-46: T-beam H-F30-S2 deflection and principal stress distribution for concrete and steel reinforcement ---------- 155
Figure 5-47: H-F30-S3 Experimental and Finite Element Method Load-Deflection Curve Comparison ---------- 156
Figure 5-48: T-beam H-F30-S3 deflection and principal stress distribution for concrete and steel reinforcement ---------- 156
Figure 5-49: T-beams of NSLWC ultimate load, compared (experimentally and numerically) ---------- 157
Figure 5-50: T-beams of HSLWC ultimate load, compared (experimentally and numerically) ---------- 157
Figure 5-51: Midspan deflection comparison (experimental and numerical) data for NSLWC T-beams ---------- 158
Figure 5-52: Midspan deflection comparison (experimental and numerical) data for HSLWC T-beams ---------- 158
Figure A-1: Principal strain of the T-beam and steel reinforcement, N-C-0 --- 180
Figure A-2: Principal strain for H-C-0 T-beam and steel reinforcement ---------- 181
Figure A-3: Time- temperature distribution of NSLWC for 15 min. fire burning along the T-beam cross section ---------- 181
Figure A-4: Time- temperature distribution of NSLWC for 30 min. fire burning along the T-beam cross section ---------- 182
Figure A-5: Comparison of FEM & Exp. Temp. distribution of NSLWC for 15 min. fired ---------- 182
Figure A-6: Time- temperature distribution of HSLWC for 15 min. fire burning along the T-beam cross section ---------- 183

Figure A-7: Time- temperature distribution of HSLWC for 30 min. fire burning along the T-beam cross section ---------- 183
Figure A-8: Comparison of FEM & Exp. Temp. distribution of HSLWC for 15 min. fired ---------- 184
Figure A-9: Principal strain (concrete and steel) of N-F15-0 ---------- 184
Figure A-10: Principal strain of N-F30-0 ---------- 185
Figure A-11: Principal strain of H-F15-0 ---------- 185
Figure A-12: Principal strain of H-F30-0 ---------- 186
Figure A-13: Principal strain for T-beam N-F15-S2 ---------- 186
Figure A-14: Principal strain for the N-F15-S3 T-beam ---------- 187
Figure A-15: Principal strain for the N-F30-S2 T-beam ---------- 187
Figure A-16: Principal strain for N-F30-S2 T-beam and steel reinforcement ----- 188
Figure A-17: Principal strain for H-F15-S2 T-beam and steel reinforcement ----- 188
Figure A-18: Principal strain for H-F15-S3 T-beam ---------- 189
Figure A-19: Principal strain for the H-F30-S2 (T-beam and SIFCON) and Steel reinforcement ---------- 189
Figure A-20: Principal strain for H-F30-S3 (T-beam and SIFCON) and Steel reinforcement ---------- 190

List of Plates

Plate 1-1: Constructions with lightweight concrete 6
Plate 2-1: Babylonian Buildings, Iraq, Built by Sumerian 12
Plate 2-2: The Great Roman Amphitheatre 12
Plate 2-3: San Francisco Oakland Bay Bridge 13
Plate 2-4: Martyr's Memorial “Al Shaheed Monument” 14
Plate 3-1: LECA raw material 38
Plate 3-2: LECA after dry in air 39
Plate 3-3: Testing machine of steel reinforcement 42
Plate 3-4: Hook-end steel fiber geometry 43
Plate 3-5: Concrete mixer 47
Plate 3-6: LECA saturated surface dry (SSD) condition 47
Plate 3-7: Vibrating rode tool 48
Plate 3-8: Curing of concrete 48
Plate 3-9: Moulds and test specimens used 49
Plate 3-10: Slump test for: - (A) NSLWC, (B) HSLWC 50
Plate 3-11: V-Funnel test apparatus 50
Plate 3-12: Mini V-Funnel used for SIFCON mortar 51
Plate 3-13: Plywood moulds for T-beam 52
Plate 3-14: Furnace used in research with all content 55
Plate 3-15: Furnace floor and wall insulation. 57
Plate 3-16: Type- K thermocouple used. 58
Plate 3-17: Thermocouples Fixing inside LWC T-beam. 60
Plate 3-18: Wooden moulds used for casting SIFCON jacket 63
Plate 3-19: Processes of strengthening T-beam specimen. 64
Plate 3-20: Arrangement of LVDTs and Load Cell within test Device 68
Plate 3-21: A- Crack meter device; B- crack development observation. 69
Plate 3-22: Compressive machine test 70
Plate 3-23: Modulus of elasticity test device 71
Plate 3-24: Splitting tensile strength test of concrete 72
Plate 3-25: Flexural strength test 73
Plate 3-26: Ultrasonic pulse velocity test for cube and T-beam samples. 75
Plate 3-27: Schmidt hammer test for lightweight concrete specimens. 75
Plate 4-1: Splitting crack path 83
Plate 4-2: Ultrasonic test of T-beam sample 88
Plate 4-3: Reference Cracks shape “pattern” of NSLWC T-beams. 94
Plate 4-4: Crack’s pattern of NSLWC T-beams after burning. 94
Plate 4-5: Cracks pattern of HSLWC T-beam before burning 96
Plate 4-6: Cracks pattern of HSLWC T-beams after burning. 96
Plate 4-7: Spalling after burning T-beam 101
Plate 4-8: Hairline cracks after burning 117

List of Tables

Table 1-1:Time-temperature data for the ISO 834 standard fire curve. 9
Table 2-1: Technical description of (MasterGlenium 54) *. 28
Table 3-1: Cement Physical properties 35
Table 3-2: Portland cement chemistry test composition 36
Table 3-3: Fine aggregate sieve analysis 36
Table 3-4: Fine aggregate Chemical and Physical properties 37
Table 3-5: Limits of water using in concrete mixing 37
Table 3-6: Physical and chemical properties of LECA* 39
Table 3-7: Sieve analysis of LECA lightweight aggregate 40
Table 3-8: Technical description of (MasterGlenium 54) *. 41
Table 3-9: Properties of steel reinforcement 42
Table 3-10: Properties of hooked end steel fiber. 43
Table 3-11: Details of LWC mixes (Kg/m3) 44
Table 3-12: SIFCON Materials mix proportion. 45
Table 3-13: Trial mixes proportions 46
Table 3-14: Furnace materials specification 58
Table 3-15: Summary of NSLWC and HSLWC T-beam test specimen 66
Table 4-1: Results of experimental cylinder and cube compressive strength of NSLWC, HSLWC and SIFCON samples 78
Table 4-2: NSLWC and HSLWC burned cube compressive strength 80
Table 4-3: Results of experimental test of cylinder splitting tensile strength of NSLWC, HSLWC LWC and SIFCON samples. 82
Table 4-4: Results of experimental test of prism flexural strength of NSLWC, HSLWC and SIFCON samples. 84
Table 4-5: Results of experimental test of cylinder modulus of elasticity of NSLWC, HSLWC and SIFCON samples 85
Table 4-6: comparison between predicted and experimental result of cylinder modulus of elasticity of NSLWC and HSLWC samples 86
Table 4-7: Results of experimental test for reference and burned cube samples under Ultrasonic Pulse Velocity of NSLWC, and HSLWC 87
Table 4-8: Results of experimental for reference and burned cube samples compressive strength by using “Raouf and Ali” eq. of NSLWC, and HSLWC. 88
Table 4-9: Results of experimental T-beam samples compressive strength by using “Raouf and Ali” eq. of NSLWC, before and after burning 89
Table 4-10: Results of experimental T-beam samples compressive strength by using “Raouf and Ali” eq. of HSLWC, before and after burning 89
Table 4-11: Rebound Number of control and burned NSLWC, and HSLWC. .. 90
Table 4-12: First crack load, ultimate load, and maximum deflection for NSLWC and HSLWC T-beam specimens 92
Table 4-13: Fire exposure effect on the yield stress of steel reinforcement bar 102

Table 4-14: Ductility Index for NSLWC and HSLWC T-beam 108
Table 4-15: Energy absorption capacity of NSLWC and HSLWC lightweight concrete T-beams 111
Table 4-16: Secant and Initial stiffness of NSLWC and HSLWC T-beam 113
Table 4-17: Thermocouples Distribution 119
Table 5-1: Selected CDP material parameter for unfired concrete 124
Table 5-2: Behavior model of elastic perfect plastic for Steel 126
Table 5-3: NSLWC summary results 141
Table 5-4: HSLWC summary results 141

Chapter ONE

INTRODUCTION

1.1Introduction

Reinforced concrete is one of the most essential construction materials on earth,[1]. Reinforced concrete is made out of cement, gravel, sand, water, additive and steel which has been effectively employed in construction.

However, materials have benefits and problems. The high self-weight of reinforced concrete, which ranges from 2200 Kg/m^3 to 2600 Kg/m^3,[2] is one of its problems. Heavy loads, especially on the building foundations, are an inevitable result. Therefore, this problem may be solved by using lightweight concrete, [3].

Concrete is the main user of land resources including water, sand, gravel, and crushed rock as well as admixtures,[4]. By its very nature, construction is not always an ecologically favorable endeavor,[5]. Moreover, that industry has a major effect on the natural world,[6]. Using waste and by-product materials in place of raw materials in the concrete mixture is the greatest option for achieving sustainable development in the concrete industry,[7]. As a result, concrete may be regarded an ecologically benign and sustainable building material for a wide range of applications in the civil and structural engineering industry, contributing to a higher quality of life for all humanity,[8].

The artificial aggregate found in **l**ight**w**eight **a**ggregate **c**oncrete (LWAC) includes expanded clay, slate, shale and blast furnace slag, making it a green building material. Lightweight concrete reduces the building dead weight, which is a major factor. However, it is important to note that a lot of energy is needed to create a lightweight aggregate. The burning of coal and, more recently, combustible liquid waste products, and gas are the source of this energy,[9].

The alternatives lightweight aggregate resources, such as natural lightweight aggregates, that do not require as much energy in their production as artificial lightweight aggregates. Natural lightweight rocks can offer some of these aggregates. In the building business, using waste materials from

manufacturing, in lightweight concretes will be more efficient,[10],[11],.

Several buildings made excellent use of lightweight concrete. Lightweight concrete primary advantage over normal concrete is its ability to reduce building weight, which might result in a 20% reduction in construction costs. For decades, lightweight concrete (LWC) has been a popular building material. Reduced self-weight is the primary motivation for employing LWC in structural applications also dead load reduction is especially crucial in earthquake-prone areas, for high-rise structures and for specialized concrete constructions.[8],[12].

When concrete is subjected to a high temperature during a fire, its qualities such as compressive strength and ductility are drastically reduced. Furthermore, the vapors pressure in the pores causes a large rise in internal tension, resulting in cracks of varied widths and lengths, especially at temperatures above 550 °C. Dehydration of calcium hydroxide occurs at high temperatures, such as 550 °C, and aggregates begin to weaken. The binding components, such as hydrated cement, begin to breakdown at higher temperatures (700 °C or above), causing a drastic reduction in RC's mechanical properties (such as its stiffness and compressive strength). Cracking and the concrete's lay both deteriorate drastically as a result of link loss between the aggregate and the cement paste. Accordingly, the following academics points of view are generally in agreement that the structural components' capacities cannot handle dead and living loads unless they are enhanced, **(Alarcon-Ruiz et al., 2005; Haddad and Shannis, 2004),** [13],[14]**.**

High strength-to-weight ratios, higher toughness, greater durability, and lower costs are just a few of the reasons why composite materials are quickly becoming the standard repair material of choice.

Composites may help structural restoration projects save money on maintenance, increase safety, and prolong the life of the structure.

1.2Lightweight Concrete (LWC)

It’s a form of concrete that has a lower density than normal concrete, which have three approaches for producing lightweight concrete,[15]:

Lightweight concrete that doesn't compromise on the coarse aggregate is known as "no-fines concrete".

Second variety, called "aerated air concrete", which air is trapped in the concrete at a concentration of 30–50 percent.

Third, lightweight aggregate concrete can be made by substituting normal coarse aggregate with lightweight aggregate, either in part or in whole mixture.

Lightweight concrete is also defined by, ACI 318-14,[16] in two categories:

1- Concrete made entirely of only lightweight (fine and coarse) aggregates.
2- In sand-lightweight concrete, the fine lightweight aggregate is replaced entirely by sand, making it a type of structural lightweight concrete have density ranges between 105 and 120 lb./ft^3 (1680 and 1920 Kg/m^3), which is often constructed using a combination of expanded clay, shale, slag, slate, or sintered fly ash and natural sand.

Concrete meeting the requirements of ASTM C567,[17] for equilibrium density, which is employed by ACI 318-19,[18] and including lightweight material, has a density of 1440 to 2160 Kg/m^3.

Lightweight structural concrete is distinguished by its high compressive strength and low density. Structural lightweight concrete meets a variety of criteria for oven-dry densities ≤ 2000 Kg/m^3,[7].

Its defined by ACI 213R-14, [19] as concrete with a cylinder compressive strength of no less than 17 MPa and an equilibrium density in the range of 1120-1920 Kg/m^3 after 28 days, also defined by Norway code, (NS 3473),[20] as a concrete with 1200-2200 Kg/m^3 as an oven dry density and contains lightweight aggregate.

RILEM [21] and European standard (CEN ENV) [22] considered concrete

having an oven-dry density of less than 2000 Kg/m^3 as lightweight concrete.

British code (BS EN, 2004),[23] defines term "structural lightweight concrete" as concrete has a dried density of less than 2200 Kg/m^3.

1.3 Benefit of Structural Lightweight Concrete

It's can be itemized as follows, [24]:

1- By decreasing the composite structure cross-section and the number of required supports, dead load is reduced and longer spans are achievable which lead to reduce the construction cost.

2- Provide superior thermal and acoustic insulation as compared to plain concrete.

3- Because lightweight concrete has a lower heat conductivity than normal concrete, it reduces the amount of damage caused by fires,[25].

4- Sometimes conservation of the natural resources is made by producing structural lightweight concrete from production waste.

1.4 Problems with Lightweight Concrete Structures

It's can be listed below, [26]:

1- Structural lightweight concrete has a lower abrasion resistance than normal weight concrete.

2- The structural lightweight concrete demands more care throughout the mixing process in order to produce the required workability and strength.

3- The structural lightweight concrete requires certain techniques during the pumping operation,[27].

4- The structural lightweight concrete requires special methods when it comes to placement and finishing.

5- Because of the high strength cement paste, structural lightweight concrete has a lesser ductility than normal weight concrete.

1.5Applications and Uses of SLWC

Due to its many benefits, lightweight concrete is rapidly rising in popularity and importance. It finds widespread application in buildings of varying heights, bridges, oil platforms, and precast and prestressed structural sections,[19],[24],[28],[29],[30],[31], as shown in (Plate 1-1):

Heart of America Bridge

Antioch Bridge

William Preston Lane Bridge

Bank of America, 1994

Finished lightweight concrete precast facade

Hibernia offshore Platform

Tunnel built, Norway

Plate 1-1: Constructions with lightweight concrete

1.6 Scope and Objectives of Study

It's can list as:

1- Investigating how heat from a fire affects the mechanical properties of lightweight concrete samples. Some of the properties to evaluate include the modulus of elasticity, flexural strength, and compressive strength.

2- To conduct a comprehensive literature research on the effect of fire flames on the load-carrying capacity of reinforced NSLWC and HSLWC T-beam specimens (Pu) and to evaluate the efficacy of U-shaped SIFCON jackets as external shear strengthening in repairing T-beams.

3- Cracking behavior (crack width, crack length, and position of these cracks), deformation properties, and load versus deflection of LWRC T- beams are investigated as a function of (concrete compressive strength, concrete cover, and fire duration).

4- Investigating how reinforcing and repairing fire-damaged LWRC T- beams with U-shaped SIFCON thin jackets affects their ductility, stiffness, and energy absorption.

5- To By modelling the interface behavior in a finite element programmed package, such as ABAQUS, and the load capacity of NSLWC and HSLWC LWRC T-beams, it is possible to predict the durability and failure modes of LWRC T-beams following exposure to fire.

6- The response and prediction of the behavior of the LWRC repaired with U-shaped SIFCON thin jacket reinforcement is discussed, along with comparisons between experimental and theoretical results.

Light**w**eight **a**ggregate **c**oncrete (LWAC) has significant interest to scientists across the world. However, due to the low volume of LWAC used in construction in Iraq, there is a lack of data on its technical qualities. Therefore, the main causes for structural reinforcement and maintenance are,[32]:

- Restoring lost load carrying capacity due to overloading, earthquake, and other types of degradation caused by aging, such as corrosion, erosion, etc.

- Improving resistance to withstand underestimated loads.
- Increasing load-carrying capacity for higher permissible loads.
- Preventing failure due to inadequate detailing.

Lightweight concretes of varying strengths are needed for urgently needed research on the effects of actual fire flame and rehabilitation utilizing SIFCON jackets. T-beams made of Reinforced Lightweight Concrete (RLWC) are the focus of the current experiment, which will seek to examine the impact of SIFCON jackets as a composite material. The burning and post-burning behavior of RLWC T-beams containing SIFCON will be investigated. Investigating the characteristics of load bearing, stiffness deterioration, ductility, and energy absorption capacity.

1.7 Standard fire curve (ISO 834)

Standard, heating conditions, test steps, and criteria for the measurement of the fire endurance of building construction elements in different categories are specified by International Standard ISO 834. This testing technique allows the fire resistance of construction elements (walls, columns, beams, floors, and roofs) to be determined based on the time length for which the test samples satisfy the specified criteria. According to ISO-834, the following equation applies to the increase in the furnace temperature of the test sample:

$$T = 345*\log_{10}(8*t+1)+T_0 \qquad 1\text{-}1$$

Where:

t = Time (min.)

T = Temp. of furnace at Time (t), by ($^{\circ}$C),

T_o = Initial furnace Temperature, in ($^{\circ}$C).

Values obtained from the above relationship are presented in (Table 1-1). The curve representing this relationship between the time - temperature which is called the standard time-temperature curve as presented in (Figure 1-1).

Table 1-1:Time-temperature data for the ISO 834 standard fire curve.

Time (t) (min.)	Temp. (T) (°C)	Time (t) (min.)	Temp. (T) (°C)	Time (t) (min.)	Temp. (T) (°C)
5	576	45	902	85	997
10	678	50	918	90	1006
15	739	55	932	95	1014
20	781	60	945	100	1022
25	815	65	957	105	1029
30	842	70	968	110	1036
35	865	75	978	115	1043
40	884	80	988	120	1049

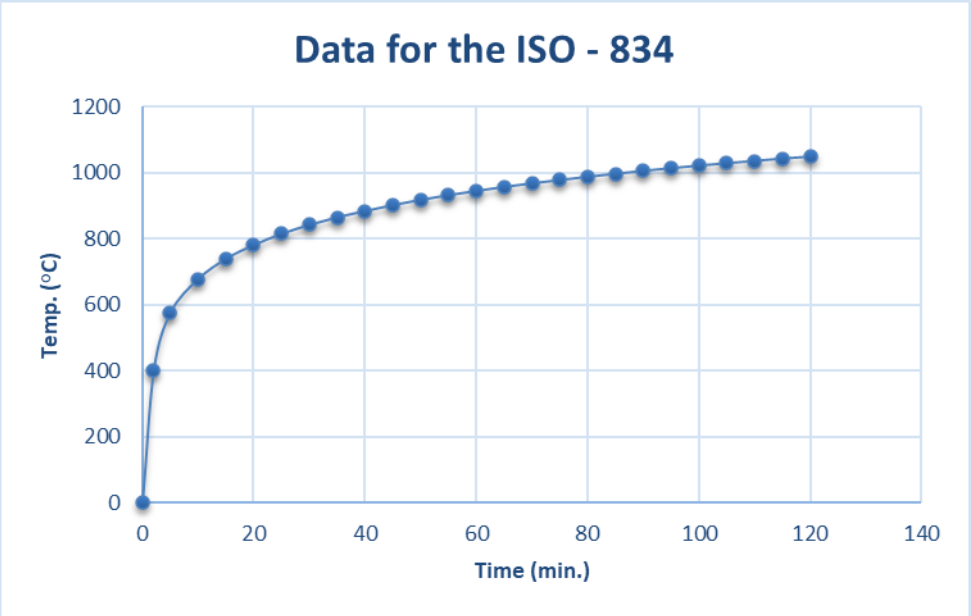

Figure 1-1: ISO 834 Standard fire curve.

The specimen fire resistance represents the time (in min.) of heating until failure occurs, and is defined by one of the following specifications:

• **Load-bearing capacity:** Failure occurs when the test sample collapses in such a manner that it, no longer performs the load-bearing function which is intended.

• **Insulation**: The failure happens in construction elements that separate two building parts (e.g., floors and walls) in three cases. One, the temperature on the unexposed face rises by more than (140°C) over the initial temperature. Two, the maximum temperature rises more than the initial value by over 180°C at any point on the unexposed surface. Three, the unexposed surface

temperature exceeds 220°C.

• **Integrity:** Construction elements like floors and walls collapse occurs when the element shows holes, cracks, or other openings that hot gasses or flames may pass. This can be tested by using standard cotton pads or observation. The element loses its integrity if cotton pads with 100 mm^2 in area of 20 mm thickness are ignited when held at a distance up to 30 mm from any opening on the unexposed side. Similarly, the element loses its integrity when sustained flaming of at least 10-sec duration appears on the unexposed side.

1.8Thesis Outline

This research consists of six chapters, as follows:

First Chapter, introduces structural lightweight concrete, its characteristics, advantages, and disadvantages, and the overall purpose of this work. **Second Chapter**, covers the relevant theoretical and experimental studies. While experimental programmed specifics, including material characteristics, T-beam specimen information, and testing procedures, are reported in **Third Chapter**. The results of the experiments are presented along with some thoughts about them in **Forth Chapter**. In **Fifth Chapter**, the finite element approach of simulation using the ABAQUS programmer is presented and contrasted with experimental results. **Sixth Chapter** presents the results of the current study as well as suggestions for further study.

Chapter Two

Literature Review

2.1Overview

The origins of lightweight concrete may be traced back to ancient times, when the natural lightweight aggregates utilized to make lightweight aggregate concrete where the same elements were employed in ancient architecture, such as scoria, pumice, and other similar materials.

The Sumerians utilized this in Babylonian construction in the third century B.C., as demonstrated in (Plate 2-1), [24].

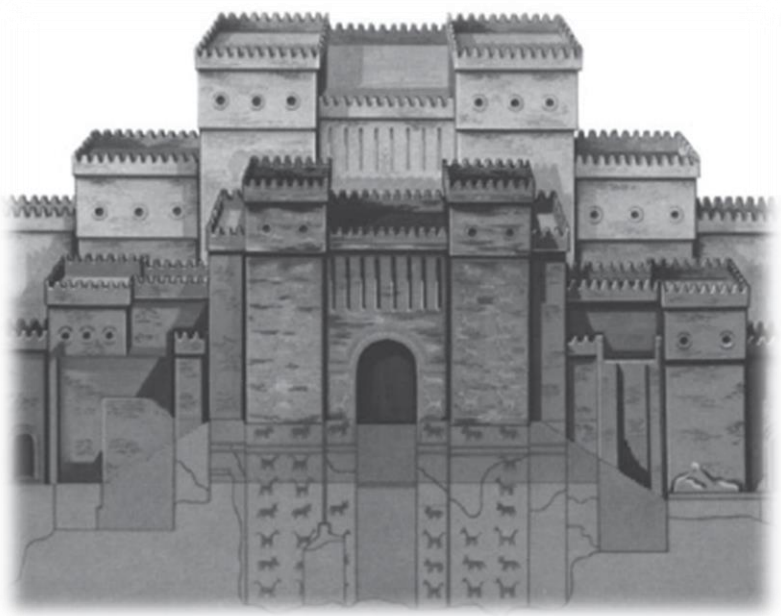

Plate 2-1: Babylonian Buildings, Iraq, Built by Sumerian

Plate 2-2: The Great Roman Amphitheatre

Ferdinand Nebel utilized pumice to make masonry blocks in 1845, and pumice was employed in Iceland's local building industry in 1928,[8]. The top highway of the San Francisco Oakland Bay Bridge was built using lightweight concrete,[24] as demonstrated in (Plate 2-3).

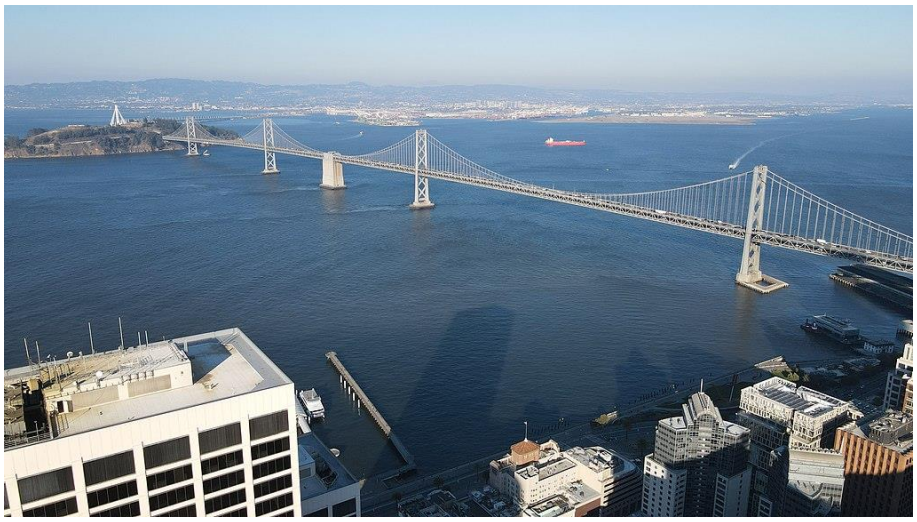

Plate 2-3: San Francisco Oakland Bay Bridge

Large constructions including multistory buildings, such as the Bank of America Corporate Center in Charlotte and the Watergate Apartments in Washington, were constructed with lightweight aggregate concrete in 1950. In addition, highway bridges were built with lightweight aggregate concrete,[33].

The first reinforced lightweight aggregate concrete construction, a three-story building, was constructed in Brantford, near London, in 1958. A pair of bridges in Rotterdam, Holland, were also constructed using structural reinforced lightweight aggregate concrete in 1968, [34].

In 1974, two towers with heights of 122 and 145 meters were built in the United Kingdom utilizing lightweight aggregate concrete with a cubic compressive strength of 30 MPa, In 1975, in Sweden. At 28 days, the lightweight aggregate concrete had a 35 MPa cube compressive strength and a bulk density of 1800 Kg/m^3,[27].

2.2Application of Lightweight Aggregate Concrete in Iraq

In Iraq, structural lightweight aggregate concrete is rarely utilized in structural building, and the lightweight aggregate used is almost always imported.

In Baghdad, expanded clay aggregate was utilized in the building of the Martyr Monument's dome and the flooring of telephone exchanges as presented in (Plate 2-4) ,[8].

Plate 2-4: Martyr's Memorial "Al Shaheed Monument"

Polystyrene aggregate was utilized to make lightweight concrete for the University of Baghdad's penthouse walls in 1980,[35].

In the 1970s, the building research center was particularly interested in producing lightweight aggregates from Iraq central and southern clay deposits,[36].

2.3Main types of Lightweight Aggregate Concrete

The components of LWAC are comparable to those of normal weight concrete, with the exception that (LWA) is used instead of normal weight aggregate.

LWA are required by several international standards, including (**EN 13055,2016, ASTM C330,2006; ASTM C331,2010; ASTM C332,2017**). Long-term weathering-ability (LWA) of structural concrete, masonry concrete, and thermal insulating concrete are all described by ASTM standards. For any

type of lightweight concrete, LWA is mandated by the European standard (**EN 13055,2016**). However, the provided criteria only account for mineral-derived LWA. Instead, then providing a list of LWA by common name, EN 13055 focuses on their histories. Natural LWA is derived from renewable natural resources, whereas artificial LWA is generated from either industrial waste or recycled materials. This specification applies to both man-made and naturally occurring lightweight aggregates. Man-made lightweight aggregates include those made by expanding, pelletizing, or sintering products like blast-furnace slag, clay, diatomite, fly ash, shale, or slate.

2.3.1 Natural Lightweight Aggregate:

They are not readily available in many countries and have varying degrees of quality. For this reason, they are not always employed to create lightweight concrete, it is further classified as:

1- Pumice:

Pumice is the only natural light weight aggregate that sees significant application, and it was employed in Roman buildings. It is extracted from the ground, processed, and put to practical use. It can be made stronger by heating to the point of fusion. Pumice has a bulk density that is anywhere from 600 to 900 Kg/m^3. Density ranges from 700 to 1400 Kg/m^3 for concrete made using high-quality pumice varieties.

It's a rock that formed in volcanoes and may be found all around the globe. Coloration is subtle or nonexistent, and they are a pale shade. They can be utilized as LWA due to their low mass and high strength. Due to gas being released from the molten lava, these rocks are incredibly light. There is a somewhat uniform microstructure of interconnected cells. It contains around 75% silica and is chemically inert.

LWA made of pumice date back to antiquity; they were even utilized in Roman construction. It is mined, processed, and utilized. This concrete has excellent insulating properties, but excessive absorption and shrinkage,[24].

2- Diatomite:

It is hydrated amorphous silica made from the fossilized remains of microscopic aquatic plants. These aquatic plant deposits are typically found well below the surface of the ocean. In later epochs, when the sea floor was reclaimed to form continents, diatomaceous earth was also made accessible on land. Diatomite is a type of sedimentary rock that forms in cold water environments and is only partially cemented. Impure diatomite often weighs more than the average density of pure diatomite, which is around 450 Kg/m^3.

3- Scoria:

This glassy, volcanic rock is full with tiny cavities (called vesicles). In most cases, it has a black hue, and its cells are bigger and more disorganized than usual.

4- Volcanic Cinders:

Loose products of volcanic origin that resemble synthetic cinder.

5- Saw Dust:

In very limited contexts, saw dust has been employed as a lightweight aggregate in flooring and the production of precast pro-ducts. The use of saw dust has been plagued by many challenges. Where it has a very high rate of shrinkage and moisture movement.

6- Rice Husk:

It has been used as light weight aggregate on a very limited scale.

2.3.2 Artificial Lightweight Aggregates:

The artificial aggregates are classified on the basis of raw materials used and the method of manufacture.

i. The aggregates that are created by heating the raw materials are one type of raw material classification, such as expand clay, shale, slate, diatomaceous shale, perlite, obsidian, and vermiculite.

ii. The aggregates results from a unique cooling procedure that enlarges blast furnace slag.

iii. Partially fused particles from coal combustion are called cinder, clinker, or Breeze. Pulverized coal has replaced lump coal in many applications, therefore less of these materials are needed. Dry shrinkage and moisture migration are both significant in cinder aggregates. Too many un-brunt coal particles can cause cinder or clinker to expand or be otherwise unsound. There may be as much as 15–25% of unburned particles in there. Cinder, clinker, and other similar materials produce unsound concrete because the particles expand while wet and compact when dry. Construction blocks, including those used for dividing walls, screeding over flat roofs, and plastering, etc., have all been made from cinder aggregate.

Expanded Clay Aggregate made by the rotary kiln technique is used to create the expanded slate aggregates. After being stored in silos, raw slate is put into preheaters where it is heated gradually before being fed into the rotary kiln's top end, where it gently rotates and descends into the "firing zone" below. The temperature in the firing zone rises to around 2 milligrade (about 1200 ºC). In this area, the slate softens enough to let expanding gases to form clumps of tiny, disconnected cells. These cells are preserved while the expanding slate cools, giving the aggregate its light weight and low absorption. At this stage, the enlarged material, known as clinker, exits the kiln's bottom end and is cooled by a stream of pressurized air.

After being cooled, the clinker is transported to a crushing and screening section for classification. After the ingredients have been mixed together, the moisture content is adjusted to the desired amount. Gradation, moisture, specific gravity, and unit weight tests are subsequently performed on the enlarged slate aggregate. Aggregates are stored when testing is complete.

Variation in aggregate size, and thus bulk density, can lead to segregation in storage. Two methods are used to reduce this: Low-elevation stockpiles with a moisture control system are used to hold coarse aggregates. Storage for fine

aggregates is done in silos with a perimeter port feeding arrangement and a low height, [24].

The multi-separated air gaps within and between the aggregates in LECA may contribute to the material lightness. The density of loose LECA varies from around 250 to about 710 Kg/m^3, mostly as a function of particle size. SiO_2, Al_2O_3, Fe_2O_3, CaO, and a few alkalis like Na_2O and K_2O make up the bulk of LECA's chemical content.

The outstanding adaptability of LECA is evidenced by the wide range of its uses. It has several applications in the building industry, including structural backfill against foundations, lightweight blocks, and concrete and precast,[37].

2.4Previous Studies on Mechanical Properties of LWC

The previous experimental works on lightweight aggregate concrete (LWC) were displayed as follow:

1- Previous studies on the mechanical properties of LWC with natural aggregate.
2- Previous studies on the mechanical properties of LWC with aggregate manufactured from natural materials.
3- Previous studies on the mechanical properties of LWC with aggregate manufactured from industrial by-products.
4- Previous studies on the mechanical properties of LWC with recycled aggregate.

2.4.1 Natural Lightweight Aggregate

In 2006, Mesut,[27] investigated the effect of replacing cement with perlite grain aggregate and perlite powder mix on the mechanical characteristics of lightweight concrete. Natural perlite aggregates with a compressive strength of 20-40 MPa can be utilized to make SLWC, according to the results. Perlite powder can also help to minimize dead weight and enhance the performance of concrete.

In 2012, Saleh,[35] Porcelains lightweight aggregate was investigated as

a coarse aggregate in lightweight concrete. Porcelains lightweight aggregate was used in place of normal weight coarse aggregate in percentage of 0 %, 25 %, 50 %, 75 %, and 100 % by weight. The results showed that adding porcelains to concrete reduces its compressive strength, splitting strength, and density. Porcelain aggregate did, in fact, induce a drop in the dry density of standard weight concrete ranging from 8% to 23%. While standard weight concrete's cylindrical compressive strength was reduced by 53% (to 77.6%).

In 2012, Hachim,[38] investigated the mechanical characteristics of lightweight aggregate concrete when lightweight aggregate (porcelain or Thermo-stone) with a water-cement ratio of 0.32 was used. The results showed that employing porcelain or Thermo-stone as coarse lightweight aggregate may generate structural lightweight aggregate concrete. Porcelain aggregate concrete had a higher compressive strength and air-dry density than thermo-stone aggregate concrete by around 14.8 % and 7.9 %, respectively.

In 2014, Al-Attar,[39] examined high-performance concrete, and the following two methods of internal curing were examined: the first method involved using crushed porcelain to partially replace normal weight coarse aggregate (gravel), whereas the second method involved using crushed porcelain to partially replace normal weight fine aggregate (sand). The coarse material (crushed porcelains) was replaced with two ages: 7.5 % and 15% by volume, while the fine material (crushed porcelains) was replaced with two ages: 5 % and 10% by volume. The results showed that fine porcelain aggregate was more successful as an interior curing medium than coarse porcelain aggregate. Compressive strength increased by 4.4 % to 5% when finely crushed porcelain was partially replaced; splitting tensile strength increased by 5.48% to -6.85%; and flexural strength increased by 11.76 % to 12.74%. When the compressive strength of the material is greater than 28 days, it's be more durable. The use of finely crushed porcelain as a substitute for lightweight aggregate concrete has increased insignificantly.

In 2018, Naser et al.,[40] investigated the characteristics of structural lightweight concrete utilizing three different types of lightweight coarse aggregate (porcelain, pumice, and composite aggregates (75 % clay bricks and 25 % theme stone)). According to the results, the composite aggregate concrete (25 % theme stone and 75 % bricks) had the lowest solidified density (1869 Kg/m^3) and the smallest cylinder compressive strength (25.3 MPa). Pumice aggregate concrete, on the other hand, had the greatest cylinder compressive strength (38.5 MPa) and hardened density (1888 Kg/m^3). Furthermore, the porcelain aggregate concrete had the highest maximum density (1905 Kg/m^3) and the highest cylinder compressive strength (28.5 MPa). Pumice aggregate concrete had a higher modulus of elasticity than porcelain and composition aggregate concrete by around 20.4 % and 22.2 %, respectively. Pumice aggregate concrete also had greater splitting and flexural strengths than porcelain aggregate concrete by approximately 37 % and 37.2 %, respectively, and by approximately 49.5 % and 65.3 % than composition aggregate concrete.

2.4.2 Manufactured aggregate from natural materials

In 1999, Alduaij et al.,[41] used crushed brick lightweight aggregate, expanded clay lightweight aggregate (LECA), and standard weight aggregate to study lightweight concrete in coastal locations, with natural fine aggregate being excluded (no-fines concrete). The results showed that employing LECA with a cube compressive strength of 29 MPa and a dry unit weight of 1520 Kg/m^3 at 28 days, structural lightweight concrete could be produced.

In 2011, Al-Baghdadi,[42] investigated the influence of cement content and crushed clay bricks as a lightweight coarse aggregate on the mechanical characteristics of high-strength lightweight aggregate concrete with cement concentrations ranging from 300 to 600 Kg/m^3. The results showed that crushed clay bricks as a lightweight coarse aggregate can produce high-strength lightweight concrete with cube compressive strengths of 27.2-49.6 MPa, splitting tensile strengths of 3.1-4.0 MPa, oven dry densities of 1900-

1960 Kg/m^3, and flexural tensile strengths of 4.5-7.1 MPa after 28 days.

In 2012, Al-Bayati,[43] investigated lightweight aggregate as a coarse aggregate in lightweight concrete. The results showed that porcelain aggregate with a concrete dry density of 1841 Kg/m^3 and a cylindrical compressive strength of 17.5 MPa may be used to make structural lightweight aggregate concrete.

In 2014, Shafigh et al.,[11] studied the effect of using two waste materials from the palm oil industry as coarse and fine aggregates. The normal weight fine aggregate is replaced with oil palm furnace clinker (OPBC) in volume percentages of 0%, 12.5%, 25%, 37.5%, and 50% in oil palm shell (OPS) lightweight coarse aggregate concrete. The results indicated that it is possible to produce structural lightweight concrete by using oil palm shell as coarse aggregate with 1900 Kg/m^3 oven dry density, 37.8 MPa cube compressive strength, 2.64 MPa splitting tensile strength, and 4.18 MPa flexural strength. The partial replacement of normal fine aggregate with oil palm furnace clinker (12.5%, 25%, 37.5%, and 50%) resulted in a decrease in density of approximately 21.7%, 22.2%, 26.2%, and 27.4%, a decrease in splitting tensile strength of approximately 2.7%, 57%, 8.7%, and 16.7%, and a decrease in flexural strength of approximately 0.7%, 8.1%, 10.8%, and 23%. The compressive strength of OPS concrete containing oil palm furnace clinker fine aggregate up to 25% was approximately equal to the compressive strength of control OPS concrete (without oil palm furnace clinker). It is not advised to use oil palm furnace clinker fine aggregate with a percentage greater than 37.5%.

In 2015, Balasubramanya,[44] made lightweight concrete. Researchers used two types of lightweight aggregates: light expanded clay aggregate (LECA) and scoria aggregate. The proportions of the two types of lightweight aggregate are blended differently. The lightweight aggregate mix completely replaces the normal weight of coarse aggregate. The results showed that using

40% LECA and 60% scoria aggregates instead of normal weight coarse aggregates produced superior results, with a cube compressive strength of 29.9 MPa and a density of 1837 Kg/m^3.

In 2017, Farahani et al,[45] used oil palm shell as a coarse aggregate and cement was substituted with fly ash and rice husk in weight percentages of 35% RHA, 35% FA**.** The results showed that employing oil palm shell as coarse aggregate with an oven dry density of 1840 Kg/m^3 and a cube compressive strength of 40 MPa could be used to make structural lightweight concrete. The use of a 70% RHA-FA mix (35 % RHA plus 35 % FA) reduced the oven-dry density and compressive strength of concrete by 13.6% and 52%, respectively.

In 2018, Zukri, A,[46] investegated that low density aggregate, is a catchall term for a variety of building materials that are less dense than normal aggregates including sand, gravel, and crushed stone. Lightweight aggregates vary greatly in particle form, texture, and characteristics, depending on their origin and mode of manufacturing. Common lightweight materials that have been successfully employed in civil engineering works include lightweight expanded clay aggregate (LECA). The effectiveness of LECA in structural and geotechnical applications has been the subject of several investigations. Dead loads and lateral stresses can be reduced by more than half in installations over structures and those with soft soils, making these materials attractive for use in projects where weight is a concern. The advantages of brick tiles are also shared by LECA, an eco-friendly waste product derived from nature. It was discovered that LECA had a variety of properties while being made from the identical ingredients. The features of LECA demonstrate its potential and appropriateness for substituting natural aggregates in a variety of civil engineering projects.

2.5 Previous Studies on Structural Behavior of LWC

In 2006, Teo et al,[47] investigated the flexural behavior of reinforced concrete beams made from lightweight coarse aggregates made from oil palm shell (OPS) at different reinforcing ratios (0.52 % to 3.90%). The oven dry density for singly reinforced beams was 1965 Kg/m^3, and the cube compressive strength was 26.3 MPa, whereas the oven dry density for double-reinforced beams was 1940 Kg/m^3, and the cube compressive strength was 25.3 MPa. Under two-point symmetrical stress, all beams were simply supported and tested. The results showed that OPS concrete beams had high ductility and a reasonable degree of deflection.

In 2008, Alengaram ,[48] studied the structural behavior of palm kernel shell concrete with a compressive strength of 37 MPa and a density of 1888 Kg/m3 after 28 days. The lightweight coarse aggregate made from palm kernel shells was a waste product from the palm oil industry. Palm kernel shell lightweight concrete had a cement content of 480 Kg/m3, whereas normal weight concrete had a cement content of 320 Kg/m3. All beams were simply supported and loaded symmetrically at two points. The lightweight palm kernel shell concrete beams were more ductile than the normal weight concrete beams, according to the study. Palm-kernel lightweight concrete beams had a moment capacity that was roughly 3% greater than normal weight concrete beams.

In 2013, Altun and Aktas,[49] investigated the impact of steel fiber on the structural behavior of lightweight reinforced concrete beams. In this study, pumice-origin coarse and fine aggregate with 450 Kg/m^3 cement content was used to make concrete with a cylinder compressive strength of 20 MPa and a concrete density of 1532 Kg/m^3. In the lightweight concrete mixes, two different steel fiber proportions (30 and 60 Kg/m^3) were utilized. The beams were evaluated under two intense symmetrical loads, and the results showed that lightweight aggregate-reinforced concrete beams weighed about 42% less

than conventionally reinforced concrete beams. Using 30 and 60 Kg/m^3 steel fiber resulted in a 100 % and 79.2 % increase in mid-span vertical deflection, respectively, and a 51 % and 63.5 % increase in the ultimate load, respectively.

In 2013, Vázquez-Herrero et al,[50] investigated the impact of employing Arleta lightweight coarse aggregate on structural lightweight concrete prestressed girders with a dry density of 1800–2000 Kg/m^3 and a cube compressive strength of 70–75 MPa at 28 days. Two symmetrical loads were used to test the beams. The flexural strengths of lightweight and normal weight concrete beams exceeded the intended flexural strengths, and the ductility of lightweight concrete beams was lower than that of normal weight concrete beams, according to the results. In addition, because of the significant elastic shortening of lightweight concrete, the initial prestressed losses in lightweight concrete beams were larger than those in conventional-weight concrete beams, as predicted. Finally, lightweight concrete was not suggested for use in prestressed concrete bridge girders owing to splitting cracks detected on the lower face of the beams after the prestress was released, resulting in a loss in strand confinement, durability, and bearing capacity.

In 2013, Carmo et al,[51] tested reinforced lightweight aggregate concrete beams for bending strength and ductility. Three different types of lightweight aggregate (LECA) concrete were produced, with densities ranging from 1870 to 1900 Kg/m^3, compressive strengths of 35, 55, and 70 MPa, five different longitudinal reinforcement ratios ranging from 0.55 to 2.96 %, and three different transversal confinement stirrup ratios (0 %, 0.6 %, and 1.68 %). The results showed that as the tensile reinforcement ratio was increased, the deformation capacity of reinforced lightweight aggregate concrete beams dropped for the same concrete strength. while the vertical displacement increased as concrete strength increased, notably in beams with a lower tensile reinforcement ratio. A brittle failure was seen in the middle zone of beams without transverse reinforcing.

In 2016, Abtan and Jaber,[52] used a reactive powder concrete (RPC) (RPC was employed in the compression layer) and lightweight concrete (LWC) to investigate the flexure behavior of hybrid reinforced concrete beams (LWC was used in the tension layer). The following were the most important variables: concrete type (LWC and RPC), RPC layer thickness (HR), and RPC layer thickness (HR) (0 %, 25 % and 50 % of beam height). Porcelain aggregate concrete, polystyrene aggregate concrete, and sawdust aggregate concrete were employed in the study as lightweight aggregate concrete. There was no evidence of slippage between the two concrete layers, according to the results. The ultimate loads of beams increased by 32 % and 105 % for porcelains aggregate concrete, 42 % and 83 % for polystyrene aggregate concrete, and 40 % and 133 % for sawdust aggregate concrete as the RPC layer thickness increased (25 % and 50 % of beam height). While increasing the RPC layer thickness (to 25% and 50% of the beam height), they reduced maximum deflection by about 2% and 5% for porcelain aggregate concrete, 3% and 13% for polystyrene aggregate concrete, and 11% and 17% for sawdust aggregate concrete, respectively. Porcelain aggregate concrete beams had a higher ultimate load than polystyrene aggregate concrete and sawdust aggregate concrete beams for the same RPC thickness.

In2022, Chandramouli, P,[53] attempted to produce lightweight clay aggregate (LECA), lime-free clay is fired in a kiln until the water evaporates, leaving behind angular clay balls with porous structures. Because of its porous nature and increased ability to absorb water, LECA have the same internal curing qualities as any other lightweight aggregate. It’s looked at the performance of LWC beams made with 100% LECA as a replacement for coarse aggregate in both laboratory and real-world settings. The load-deflection, energy-absorbing capacity, and ductility index of the LWC beams were compared to those of the normal concrete beams. The load-carrying capacity of the LWC beam was improved by providing internal mesh

reinforcement with **w**elded **w**ire **m**esh (WWM) in four different configurations: 15 mm square spacing, 10 mm square spacing, 15 mm and 10 mm mesh placed alternately, and 40 mm square spacing. The WWM-reinforced beam was able to bear more weight and withstand more deflection without snapping in half. WWM internal reinforcement was used to strengthen steel rebars, and the material acts as a single unit under load, reducing tension bar stress and maximizing load capacity. When compared to experimental data, the resulting analytical results showed that the model was able to accurately represent how LWC beams behave when equipped with WWM.

2.6T-Beam Behavior under Fire Exposure

It is generally known that concrete's macroscopic and microscopic structures are severely damaged by high temperatures, resulting in enormous mechanical deterioration and potentially adverse impacts at the structural level due to spalling. High temperatures degrade concrete mostly due to damage to the binder or aggregates; their impacts on the mechanical characteristics of the concrete at high temperatures have previously been documented (**Choi et al., 2017**[54]**; Gao et al., 2017**[55]). Volcanic eruptions and cremation are common sources of lightweight particles. This means they are resistant to heat and have a low heat conductivity. Therefore, concrete with such aggregates should have higher mechanical qualities at high temperatures than concrete with normal aggregates (**Sancak et al., 2008**[56]**; Tanyildizi & Coskun, 2008**[57]**; Turkmen & Findik, 2013**[58]**; Yoon et al., 2015**[59])

Direct fire exposure causes a quick rise in reinforcement temperature, which in turn causes a rapid loss of structural member strength (capacity). Spalling of concrete and resulting loss of reinforcing strength greatly impair a structural member ability to withstand fire. Spalling can happen in any concrete, but fire can accelerate spalling in HSC due to its limited permeability and high water-cement ratio.

In2022, Ahmed Youssef,[60] extrapolated the response of lightweight (LECA) high strength concrete beams to extreme fire burning. In the standard recipe, the LECA aggregate served as the coarse component. It was also looked into whether or not there was a post-development procedure involving the jacketing of fire-damaged beams with a coating of SIFCON materials. Beams of concrete were also subjected to testing for a number of conditioning characteristics in addition to the standard samples, including fire exposure time, concrete coverage, and SIFCON layer thickness. All of the materials utilized in this investigation were put through rigorous tests of their chemical and physical characteristics. For each of the three stages (normal or reference, fire damaged samples, and repaired with SIFCON jacket). As a consequence of the study experimental testing, it was shown that the reinforced beams performed noticeably better than the damaged ones. The results also showed that the reinforced beams are, with the exception of the absorption energy, as good as or better than the reference beam.

2.7 High Range Water Reducing Admixture (HRWRA)

Ahigh-performance concrete superplasticizer based on modified poly-carboxylic ether, designed for use in precast and ready-mix concrete applications that demand the greatest durability and performance Master Glenium54 superior cement dispersion is due to its unique carboxylic ether polymer with long lateral chains, which sets it apart from other superplasticizers like sulphurated melamine and naphthalene formaldehyde condensate. The same electrostatic dispersion happens at the start of the mixing process, but the existence of the lateral chains, which are attached to the polymer backbone, creates a steric barrier that stabilizes the cement particles' ability to split and disperse. This technique results in flowable concrete with a lower water requirement and improved early strength. MasterGlenium 54's exceptional dispersion qualities make it an appropriate additive for precast or ready-mix applications requiring low water-cement ratios. This feature enables

the construction of concrete with very high early and final strengths, as well as few voids and hence optimal density. The removal or decrease of steam curing in precast works may be viewed as a cost-effective solution because of the strength development features.

It can be applied and compacted in crowded reinforcement with great workability without segregation or bleeding and with minimal vibration. For a better surface finish, fewer workers are required, MasterGlenium 54 is an able concrete additive that is used during the batching operation.

MasterGlenium 54 is most effective when used after 70 % of water has been added, dry materials should not be treated with MasterGlenium 54. Following the addition of the MasterGlenium 54, thorough mixing is necessary, with at least a mixing period of 60 seconds for forced action mixers. The proportion of 3.7 % is employed in this investigation to create acceptable slurry for SIFCON. (Table 3-8) shows the technical description, [61].

Table 2-1: Technical description of (MasterGlenium 54) *.

Chemical basis	**Aqueous Solution of modified poly-carboxylic ether**
Color	Whitish to straw
Specific gravity	1.07
PH	5-7
Chloride content	None
Toxicity	Danger hazardous material.
Storage	Stored above 5°C in closed containers
Fire	Not fire-propagating

*Manufacturer and Safety data-sheet Properties

2.8 Summary

Factors influencing fire-induced spalling include concrete permeability, fire exposure type, and concrete tensile strength, as the following are some conclusions drawn from prior research on lightweight aggregate concrete and the structural behavior of lightweight and normal weight concrete[62],[63]:

- An RC beam's ultimate load is increased by 2.15 times when an HPFRC jacket 40 mm thick is added to it, compared to an increase of just 1.90 times for a beam that was already damaged. The proposed method is successful in

increasing load bearing capacity in both strengthening and repair situations, as evidenced by experimental and computational results.

- The suggested technique greatly improves the structure at the serviceability limit state, with benefits including reduced mid-span displacement as a result of higher beam stiffness under service load. By preventing the material from cracking, the jacket acts as a form of external pre-stressing.

- It appears that SIFCON (cement-based composite comprising steel fibers) is an effective method for strengthening reinforced concrete beams against shear forces. Beams that were mended with a SIFCON jacket showed an increase in ultimate shear strength from 48% to 60%, and brittle shear failure was completely removed. This might be associated with the energy absorbed during debonding, the stretching of the fibers, or the process that prevents cracks.

- Fresh concrete testing is important for SIFCON mix manufacture. The matrix should be sufficiently liquid and fine to penetrate the network fiber bed. Because of its great fluidity, the SIFCON mix considers **S**elf-**C**ompacting **C**oncrete (SCC) to guarantee full penetration through the optical fiber

Cement slurry is infiltrated into a bed of preplaced fiber to create SIFCON when analyzing a SIFCON specimen, there are four primary factors to think about. Slurry strength, fiber volume, fiber alignment, and fiber type are the factors that must be considered.

A SIFCON specimen's behavior is greatest influenced by fiber orientation and size. Fibers may be positioned parallel or perpendicular to the loading direction. The fiber strength has an impact on the ultimate strength, residual strength, ductility, and energy absorption. Fiber orientation is deeply influenced by fabrication process and craftsmanship (technique) quality, and size factors make in-situ SIFCON qualities difficult to predict

- Due to its self-leveling property, HPFRC can be cast in a thin layer;

normal sand blaster of the beam surface ensures good jacket adhesion without the need for any primer-c curing at ambient temperature and humidity is sufficient to allow the development of the HPFRC's strength characteristics.

Chapter Three

Experimental Work

3.1Introduction

The experimental procedure is discussed by details in this chapter. It describes the research methodology used to achieve the goals of study, as well as the raw material used (cement, sand, steel fiber, mineral and chemical admixtures), mix proportions, preparation, mixing, casting procedures, curing, and testing of (NSLWC and HSLWC) T-beams are also explained.

Application of SIFCON as a means of studying the effect of such a treatment on existing structures. Researchers are looking at the effects of SIFCON jackets on the structural behavior of NSLWC and HSLWC T-beams after being subjected to an actual burning flame. As a result, the goal of this experiment is to investigate the structural behavior of post-fire LWRC T- beams that have been rebuilt and reinforced utilizing U-shaped SIFCON jackets. For the LWRC T-beam specimens, the experimental variables evaluated are: -

1. Grade of concrete (normal and high strength of lightweight concrete).
2. Period of exposure to fire flame [15 and 30 min.].
3. Thickness of SIFCON jacket [15 and 30 mm].

Details of the tests on Lightweight concrete and SIFCON specimens used throughout this study are explained such as: -

1. Tests of fresh SIFCON (mini slump flow and V- funnel test)
2. Compressive strength
3. Modulus of elasticity
4. Load deflection relationship
5. Splitting tensile strength
6. Flexural strength
7. T-beam Specimens Ultimate load capacity

Understanding the attributes and characteristics of the basic materials of concrete, such as SIFCON and lightweight concrete, and crucial (NSLWC and HSLWC). SIFCON is a composite material made up of a variety of materials

such as sand, water, cement, fiber, and admixtures.

Unit weight, specific gravity, gradation, and water content are only some of the properties and features of these materials. LECA aggregates are used in the production of LWAC.

Strict methods in material selection, control, and proportion of the whole component were applied for ensuring accurate results.

All essential experiments were conducted in the Civil Engineering Department laboratories at the University of Babylon, and information on the materials origins, chemical compositions, and physical properties is provided.

3.2 Research Methodology Flowchart

The experimental program of this thesis consists of two stages as presented in (Figure 3-1).

The Raw materials were initially selected, prepared, and evaluated based on their physical and chemical characteristics. In accordance with the overarching plan for structural LWC, many types of LWAC with two distinct concrete compressive strengths have been manufactured.

Lightweight concrete with a desired compressive strength of 30 and 60 MPa is classified as normal and high strength, respectively.

Lightweight concretes with normal and high strengths were made using the produced lightweight aggregate LECA. Guidelines for the correct proportioning of LWAC mixes are few and lack specificity, consequently to achieving the desired strength and workability.

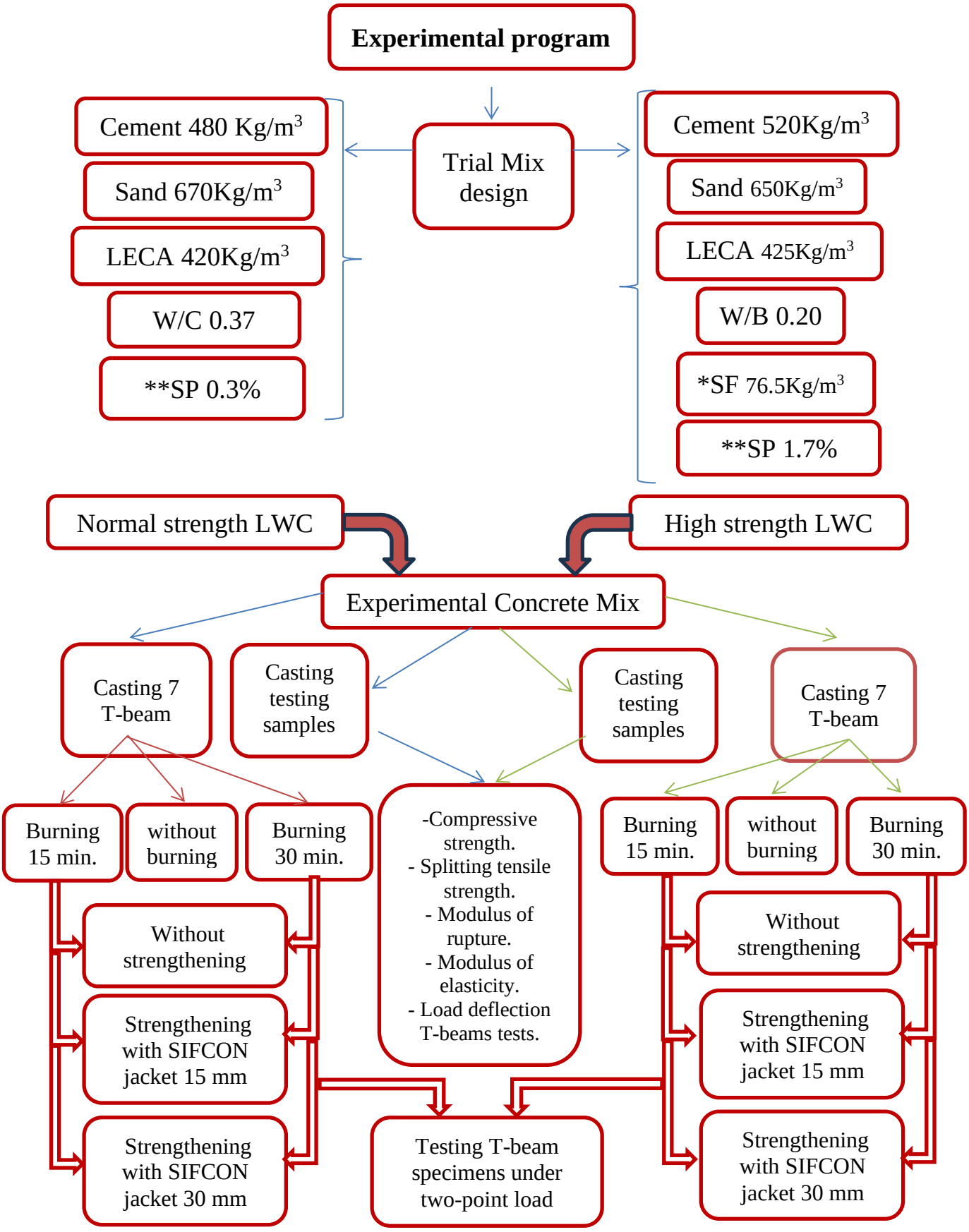

Figure 3-1: Experimental program Flow chart

(Where: *mean silica fume and **mean super plasticizer).

In this research, it was performed the necessary trial mixes for the use of LECA. All required workability was accomplished by adding superplasticizer and mineral admixtures to the mixes.

The next step involves the application of SIFCON to trail mixes in order to establish optimal mix proportions and the most appropriate mineral and chemical additives. Next, the components are mixed using the right mixing procedure and the right mix proportions. Finally, 7 and 28 days of curing time were given to the cast samples and T-beam specimens, respectively.

After achieving the requisite age (28 days), the T-beams specimens and samples are burned for varied duration of fire exposure (15 and 30 min.).

Following the burning process, the third phase involves the repaired and strengthened post-fired T-beams using a U-shaped SIFCON jacket, followed by the preparation and testing of exposed (with and without repairs) and unexposed concrete samples, and finally the testing of the LWC T-beams.

The flowchart in (Figure 3-1) shows the whole experimental inquiry. This chapter merely covers the testing technique; the outcomes of the tests will be detailed in Chapter Four.

3.3 Materials

3.3.1 Cement

In all of the mixes, MASS (MASS Iraq Company) Ordinary Portland cement was employed. The cement is tested to ensure conformity with Iraqi Standard No. 5/2019,[64]. (Table 3-1) and (Table 3-2) show the physical and chemical parameters of the cement that are employed.

Table 3-1: Cement Physical properties

Physical properties		Unit	Result	IQS-5/1984
Initial setting time		Min.	144	≥ 45
Final setting time		hour	3:25	≤ 10
Fineness		m^2/Kg	326	≥ 250
Compressive strength	3days	MPa	25.3	≥ 15
	7days	MPa	32.49	≥ 23

Table 3-2: Portland cement chemistry test composition

Oxide	% By weight	Limits of IQS No.5/1984
SiO_2	20.88	-
CaO	62.41	-
Al_2O_3	4.06	-
Fe_2O_3	5.40	-
Lime **S**aturation **F**actor	0.91	0.66-1.02
MgO	1.60	≤ 5%
SO_3	1.19	≤ 2.5%
Loss on **I**gnition	2.68	≤ 4%
Insoluble **R**esidue	0.56	≤ 1.5
Main component		
C3S	53.57	-
C2S	19.45	-
C3A	1.62	≤ 3.5
C4AF	16.43	-
Al_2O_3 / Fe_2O_3	0.75	-
Free lime (free CaO)	0.84	-

The test results indicates that the used cement conforms to the Iraqi Specification No. 5/1984[65],[66].

3.3.2 Fine Aggregate

As a fine aggregate, AL-Ekhaider quarries natural sand is employed, (Table 3-3), (Table 3-4) and (Figure 3-2) demonstrated the sieve analysis of natural fine aggregate Before usage, the fine aggregate was speared out and let too dry in the open air, also Chemical and Physical properties.

According to the results fine aggregate grading met the standards of Iraqi Specification No. 45/1984,[67], ASTM C29,[68] and ASTM C128,[69].

Table 3-3: Fine aggregate sieve analysis

Sieve Size (mm)	Passing%	IQS 45/1984 Zone (2)
10	100	100
4.75	96	90-100
2.36	78	75-100
1.18	61	55-90
0.60	45	35-55
0.30	20	8-30
0.15	3	0-10

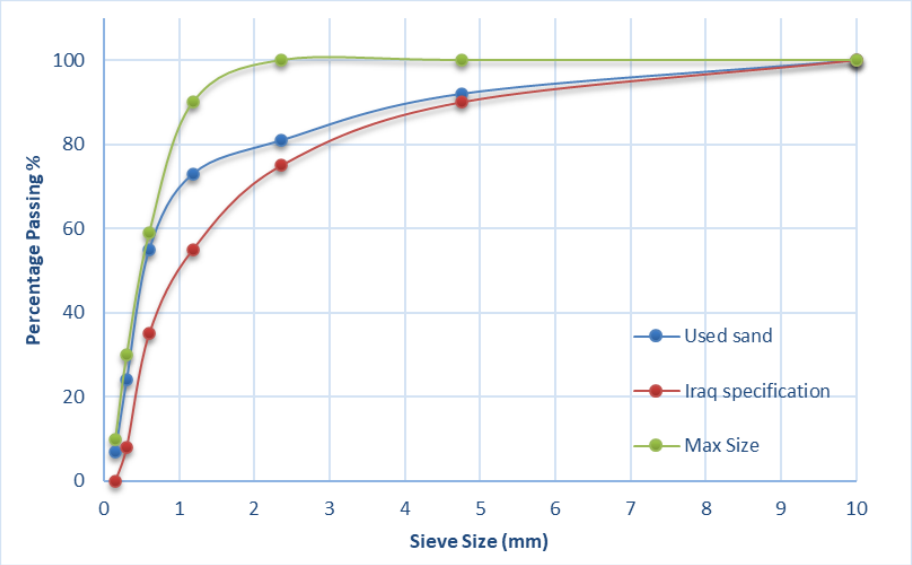

Figure 3-2: Fine aggregate sieve analysis

Table 3-4: Fine aggregate Chemical and Physical properties

Tests	Test results	Specification	Limits of Specification
Relative density (OD)	2.3	ASTM C128	-
Dry loose unit weight (Kg/m^3)	1671.0	ASTM C29	-
Dry rodding unit weight (Kg/m^3)	1822.0	ASTM C29	-
Absorption %	2	ASTM C128	-
Materials finer than75 μm %	4.5	IQS 45/1984	≤5
Fineness modules	2.96	IQS 45/1984	-
SO_3 content%	0.27	IQS 45/1984	≤0.5

3.3.3 Water

Water from the tap was used to make all concrete mixtures and cure all concrete samples, this water was free of salts, turbidity, and organic debris. for mixing, tap water is often regarded as enough. When tested in accordance with IS 3025[70], the (Table 3-5) presented maximum allowable limits of solids in water, Soil water analysis and tests are required to determine the water's physical and chemical properties if IS 456-2000 standards are to be met,[70].

Table 3-5: Limits of water using in concrete mixing

Solids type	Limits
Organic solids	200 mg/l
Inorganic solids	3000 mg/l
Sulphates	400 mg/l
Chlorides	2000 mg/l for concrete not containing embedded steel, and 500 mg/l for reinforced concrete work
Suspended matter	2000 mg/liter

Good-quality mixing water can also be used for the curing process Nevertheless:

1. Water for curing must not leave behind any undesirable stains or unattractive deposits on the surface.
2. It is forbidden to combine or cure substances with wastewater.
3. Testing the water must be done prior to the start of the work.

3.3.4 Lightweight Coarse Aggregate

The 0.475-1 cm uniformly sized LECA that was supplied from the Islamic Republic of Iran was used. It's made from porous ceramic materials that have uniformly small closed-cell pores, as well as firmly sintered and durable exterior surfaces, a considerable increase in particle volume results from swelling during the production of LECA from clay mineral raw materials, as shown in (Plate 3-1) after being burned in rotary kilns at temperatures between 1100 and 1200 °C, Sieve analysis of LECA must be meet with Limits of ASTM C330-17a, 2017,[71] as list in (Table 3-7), where (Table 3-6) shown LECA physical and chemical properties which tests were conducted from factory.

Plate 3-1: LECA raw material

Because of its high-water absorption capability, LECA is soaked in water for at least 48 hours, as indicated in (Plate 3-2), to prevent it from absorbing

water during mixing, the LECA was next distributed in laboratory air until the surface dried, resulting in a **s**aturated **s**urface **d**ry (SSD) state in the aggregate, as recommended by ACI 211.2-98[72].

Plate 3-2: LECA after dry in air

Table 3-6: Physical and chemical properties of LECA*

Physical Properties	
Properties	**Test Results**
Specific Gravity	1.2
Absorption	12%
Bulk density Kg/m^3	700
Chemical Properties	
Chemical Composition	**%Age by Weight%**
CaO	3.78
SiO_2	61.58
Al_2O_3	16.99
Fe_2O_3	7.62
MgO	2.56
SO_3	0.19
TiO_2	0.80
MnO_2	O.10
Na_2O	1.03
K_2O	2.34
Loss on Ignition (L.O.I.)	0.2

*Chemical tests were conducted from factory.

Table 3-7: Sieve analysis of LECA lightweight aggregate

Sieve Size (mm)	Cumulative Passing %	Limits of ASTM C330-17a, 2017
12.5	100	100
10	100	80-100
8	79	-
6	46	-
4.75	5	5-40
2.36	2	0-20
1.18	0	0-10

3.3.5 Micro Silica Fume (SF)

The by-product of the manufacture of elemental silicon or alloys in electric arc furnaces is silica fume (SF), which is an extremely fine non-crystalline silica. The amorphous silicon dioxide in the silica fume, which condenses from the gases leaving the furnaces, is made up of extremely tiny spherical particles with a diameter of 0.1 to 0.2 mm. Silica fume is formerly assumed to be apart cement alternative (react with calcium hydroxide produced Jel), but it is now most widely employed in the production of high-performance concrete, which benefits from the inclusion of silica fume. Silica fume has been utilized in this function to manufacture concrete with an increased compressive strength and very long durability.

Silica fume used in this research; which is commercially known as (MasterRoc®MS 610 OR BASF silica fume) from chemical company (Master Builders Solutions), and it was utilized in this investigation as a partial replacement (15%) by weight of cement. Silica fume improves the micro structure of the cement paste and makes it of more resistance to any type of external influence and have TECHNICAL DATA; (Form Powder, Color Grey, Density 0.55 - 0.7 Kg/L, Chloride content <0.1%)[73].

3.3.6 High Range Water Reducing Admixture (HRWRA)

This technique results in flowable concrete with a lower water requirement and improved early strength, this feature enables the construction of concrete with very high early and final strengths, as well as few voids and

hence optimal density, MasterGlenium 54 is most effective when used after 70% of water has been added, dry materials should not be treated with MasterGlenium 54. Following the addition of the MasterGlenium 54, thorough mixing is necessary, with at least a mixing period of 60 seconds for forced action mixers. The proportion of 3.7 % is employed in this investigation to create acceptable slurry for SIFCON.

(Table 3-8) shows the technical description (**MasterGlenium 54**)[61].

Table 3-8: Technical description of (MasterGlenium 54) *.

Chemical basis	**Aqueous Solution of modified poly-carboxylic ether**
Color	Whitish to straw
Specific gravity	1.07
PH	5-7
Chloride content	None
Toxicity	Danger hazardous material.
Storage	Stored above 5°C in closed containers
Fire	Not fire-propagating

*Manufacturer and Safety data-sheet Properties

3.3.7 Reinforcement Steel-bar

In research, deformed steel bars with nominal diameters of 12mm, 8mm, and 6mm are employed for tensile reinforcement, upper reinforcement, and shear reinforcement, respectively.

Laboratory of the Mechanical Engineering Department, University of Babylon, has implemented steel bar reinforcement tests utilizing a computerized testing equipment, as illustrated in (Plate 3-3).

The tested specimens were conformed with ASTM A615M,[74]. And according to ASTM A370,[75] the steel reinforcing rods are 12 mm in diameter and meet all of the grade 60 steel's technical requirements. The steel reinforcement, with nominal 8 and 6 mm, met all of the grade 40 steel technical requirements. The results from the tests conducted on steel reinforcement are compiled in (Table 3-9).

Plate 3-3: Testing machine of steel reinforcement

Table 3-9: Properties of steel reinforcement

Property	Results				Tensile requirement ASTM- 615 Minimum	
	Ø 12	**Ø 10**	**Ø 8**	**Ø 6**	**Grade 40**	**Grade 60**
Nominal diameter (mm)	12	10	8	6	-	-
Actual diameter (mm)	11.75	9.83	7.85	5.96	-	-
Actual Weight (Kg/m)	0.858	0.608	0.368	0.213	-	-
Yield strength, fy (MPa)	576	510	507	533	≥280	≥420
Ultimate strength fu (MPa)	710	631	540	583	≥500	≥620
Elongation %	17	-	-	-	≥12%	≥9%

3.3.8 Steel Fibers

Previous research has revealed that bundles of bonded fibers are not recommended use in SIFCON, where it is preferable to permeate the fiber bed without blocking or honeycombing. As a result, bonded fibers have to be fell apart and separated before being placed in the moulds, (**Gilani, 2007**)[76].

Type of steel fiber employed in this study was hooked end with a length of 30 mm and a diameter of 0.5 mm.

(Plate 3-4) shows the hooked end steel fiber that was employed in this study. According to the manufacturer, (Table 3-10) shows the technical parameters of the hooked end.

Table 3-10: Properties of hooked end steel fiber.

Property	Results of hooked end steel fiber
Description	Deformed shape hooked end
Appearance	Bright and clean wire
Length (l), mm	30
Diameter (d), mm	0.5
Aspect ratio(l/d)	60
Density (Kg/m^3)	7800
Tensile strength (MPa)	1100
Description	Of shape hooked ends
Appearance	Bright and clean wire

*Manufacturer Properties.

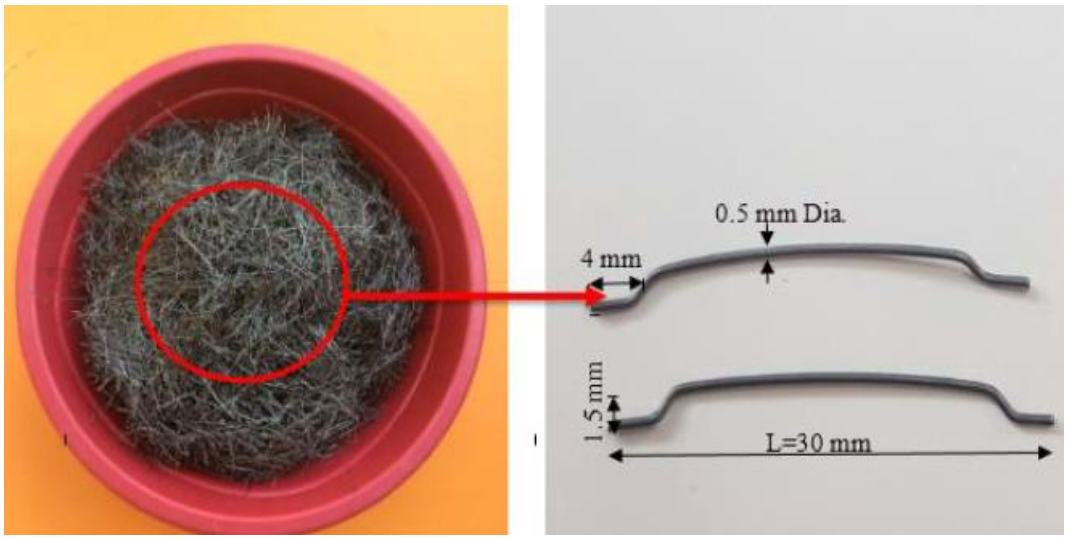

Plate 3-4: Hook-end steel fiber geometry

3.4 Mix Design

3.4.1 Lightweight concrete Mix Design

To construct concrete mixes that meet the standards for density and compressive strength of normal and high strength concrete, ACI Committee 211.2-98,[72] and ACI 211.4R-08,[77] are utilized as a reference.

In this study, two classes of LWC mixes (NSLWC and HSLWC) are created for comparative purposes. The concrete mix design goal is to achieve a slump of 65 mm and 75 mm also a 28-day cube compressive strength of 30 MPa for NSLWC and 60 MPa for HSLWC, respectively.

To attain the requisite strength, a variety of trial mixes are tested; the mix specifics for normal and high strength lightweight aggregate concrete are shown in (Table 3-11) which displays the mixture ratio, compressive strength, fresh density, and slump, while (Figure 3-3) and (Figure 3-4) shown the fraction of LWC mix elements as a percent by weight.

Table 3-11: Details of LWC mixes (Kg/m3)

Grade of LWC	Cement Kg/m^3	Sand Kg/m^3	LECA Kg/m^3	Silica Fume Kg/m^3	Water Kg/m^3	SP by wt. of cm (%)	W/Cm	Slump mm	Fresh Density Kg/m^3	28-day Compressive Strength *f*cu MPa
NSLWC	480	670.6	420	0	153	0.15	0.32	65	1810	39.38
HSLWC	520	650	425	76.5	117.3	0.15	0.20	75	1965	62.5

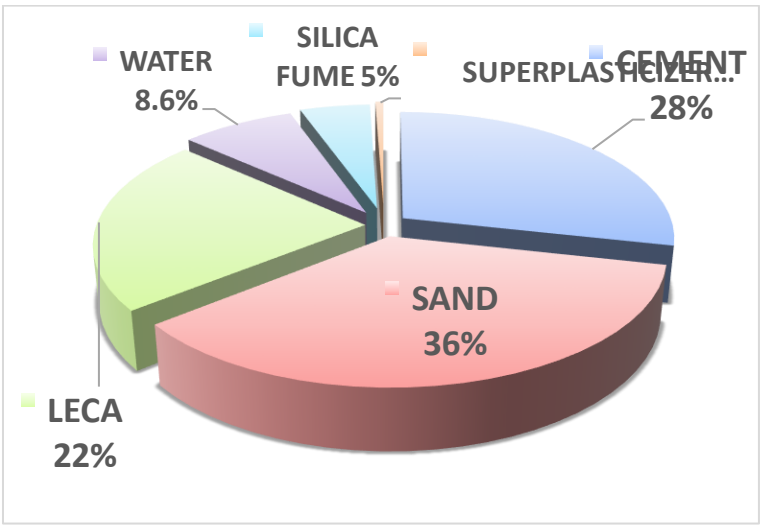

Figure 3-3: Percent Materials proportion used in HSLWC mixture

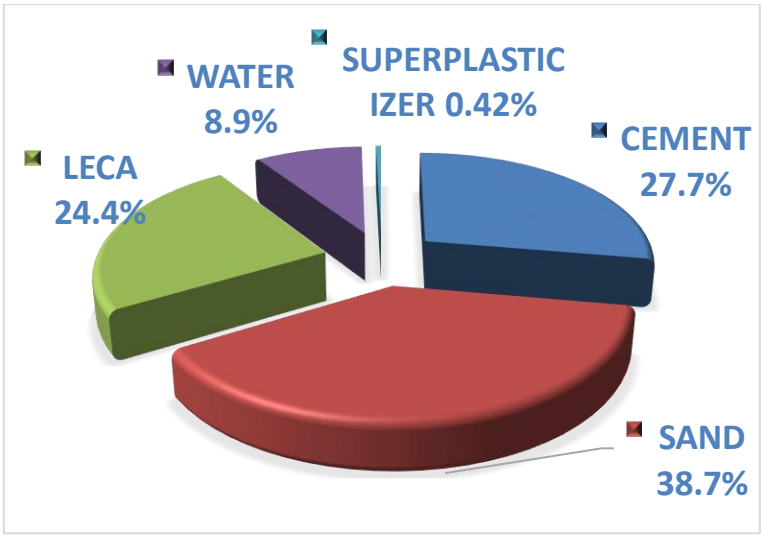

Figure 3-4: Percent Materials proportion used in NSLWC mixture

3.4.2 Mix Design of SIFCON

Many trail slurry combinations are tested in order to discover the one that has the best qualities in the fresh condition in terms of fluidity, viscosity, and filling ability without bleeding, segregation, or pore pockets in the fiber network, which may reduce the mechanical properties of SIFCON dramatically.

The kind of SIFCON used in this study is (hooked end steel fiber SIFCON), which is made using mortar and hooked end steel fiber with a volume friction of 6%. And (Table 3-12) and (Figure 3-5) show the weight proportions of the optimal mixtures employed in this investigation.

Table 3-12: SIFCON Materials mix proportion.

Mix Proportions					
Cement Kg/m^3	**Sand Kg/m^3**	**Silica Fume Kg/m^3 10% rep.**	**Hooked end Steel Fiber Kg/m^3**	**W/Cm**	**Super Plasticizer by wt. of Cementous (%)**
872.4	969	96.9	468	0.33	3.7

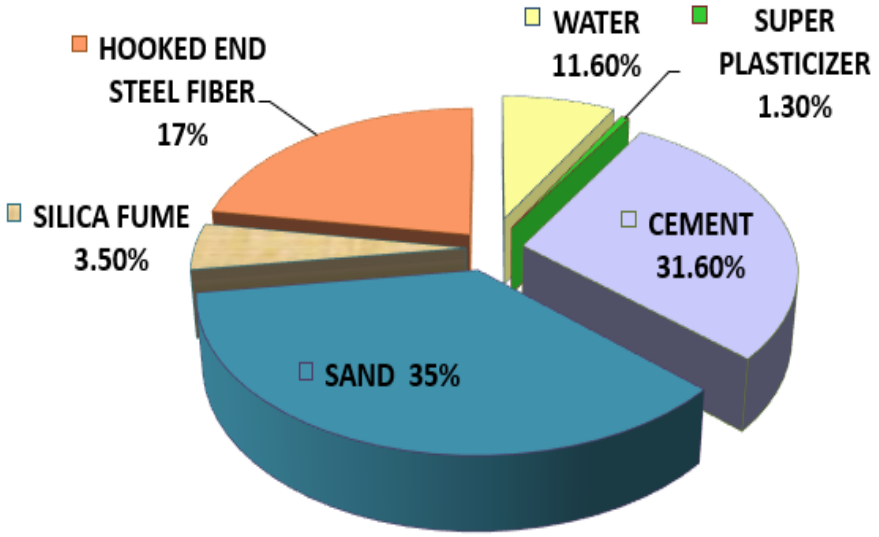

Figure 3-5: Percent Materials proportion used in SIFCON mixture

3.5 Trial mixes

The different experimental mixing material in the study are presented in (Table 3-13):

Table 3-13: Trial mixes proportions

Mix	N1	N2 Selected	N3	H	H1 Selected	S1	S2 Selected
Cement Kg/m^3	480	480	480	540	510	900	872.4
Fine aggregate (sand) Kg/m^3	670	670	670	680	650	890	969
Coarse aggregate (LECA) Kg/m^3	420	420	420	425	425	---	---
W/C %	31.8	34.3	40	26	29	450	468
Superplasticizer %	1.5	1.47	3	1.7	5.1	3.7	3.7
Slump, mm	400	650	1100	1100	750		
Cube Compressive strength, MPa	36	39.38	41.15	47.1	62.5	95	117.6
Oven dry density, Kg/m^3	2100	1797	1810		1975	---	2141

N: Normal light-weight concrete, H: High strength light-weight concrete,
S: SIFCON (Slurry Infiltrated Fiber Concrete)

3.6Mixing procedure

As stated in (Plate 3-5), mixing is done using a 0.31 m^3 rotary mixer. Before putting the components, the internal surface of the pan was cleaned and wetting. ASTM C192/C192M-05,[78] is used to combine the components, the LECA aggregate is mixed with some mixing water and chemical additives in the mixer.

Before adding the chemical additive to the mixer, it is best to combine it with some mixing water. The fine aggregate is added to the mixer with some mixing water after a few seconds of mixing.

Finally, in the mixer, the cement and the remaining mixing water are added. After all of the concrete components have been added, the mixture mixed for another five min., then allowed to rest for three min. before being mixed for two min.

Plate 3-5: Concrete mixer

Lightweight aggregates should be soaked in water at least for 48 hours to avoid absorption of concrete mixing water by the lightweight particles. The aggregate particles are exposed to air for 2 hours to reach the **S**aturated **S**urface **D**ry (SSD)[79], as indicated by ACI 211.2-04,[72] As shown in (Plate 3-6).

Plate 3-6: LECA saturated surface dry (SSD) condition

3.7 Preparation, Casting and Curing of Test Specimens

To prevent adhesion with concrete after hardening, the inside surfaces of cubes, cylinders, and the built moulds of T-beam specimen are thoroughly cleaned and lubricated. Cube and cylinder specimens are cast in steel moulds. Fresh concrete was put into moulds, three equal layers for cubic and cylinder

moulds, with 36 strokes for each layer, after the concrete had been mixed by a rotary mixer [78],[80].

The T-beams are cast in two layers,[81] directly “to ensure there is no segregation or honey-combing”, each layer is compressed using a vibrating rode as indicated in the (Plate 3-7). Within 15 seconds, each layer vibration is confined to the elimination of entrapped air, and the concrete surface got reasonably smooth and glazed,[78]. With a steel trowel, the top layer was smoothed and leveled with the top of the mould after it has been placed casted. Specimens are soaked in tap water then dry about 24 hours before being tested, which T-beam covered by canvas then plastic layers as indicated in (Plate 3-8).

Plate 3-7: Vibrating rode tool

Plate 3-8: Curing of concrete

The moulds and test specimens' material used in this research as indicated in (Plate 3-9) are:

1. T-beam moulds (80×250) mm for flange and (100×170) mm for web where the length 1500 mm to determine the flexural strength of concrete.
2. Cubic moulds (150×150×150) mm to determine the compressive strength of concrete.
3. Cylindrical moulds (150×300) and (100×200) mm to determine the splitting tensile strength of concrete, oven dry density, water absorption and the static modulus of elasticity.
4. Prism moulds (100*100*400) mm.

Plate 3-9: Moulds and test specimens used

3.8 Fresh Concrete Tests

3.8.1 Slump test

Slump test was used to determine the workability of all concrete mixtures immediately after mixing, as stated in ASTM C143– 12,[82] as shown in the (Plate 3-10). For comparison purposes, the superplasticizer content was changed with the type of Concrete to achieve a constant workability for NSLWC and HSLWC respectively.

Plate 3-10: Slump test for: - (A) NSLWC, (B) HSLWC

3.8.2 Slump test SIFCON slurry

V-Funnel flow time is a good indicator of the slurry's viscosity. The calculated time value is proportional to the slurry flow rate and not its viscosity. The V-funnel test indicates that the slurries with the longest flow rate times have a high viscosity. (Plate 3-11) show the testing equipment, which consists of a V-Funnel, bucket, scoop, trowel, and stopwatch. Ten liters of mortar are enough for the experiment.

Plate 3-11: V-Funnel test apparatus

The V-funnel is set up on solid ground. Then, while the trap door is open for water to drain, it was moistened the inner parts of the funnel and the bottom gate. After that, it was lowered the bucket into the opening and shut the trap door. Without compacting the mixture, the device is filled to capacity, and the trowel struck mortar at the same height as the funnel rim. Within ten seconds of being filled, the trap gate is unlocked, and releasing the mortar. Stopwatches are started and flow times are recorded as soon as the gate to the trap is opened. This shot is taken when sunlight is shining down on the funnel. SIFCON mortars should have a flow time of 7-11 seconds (**EFNARC, 2005**)[83].

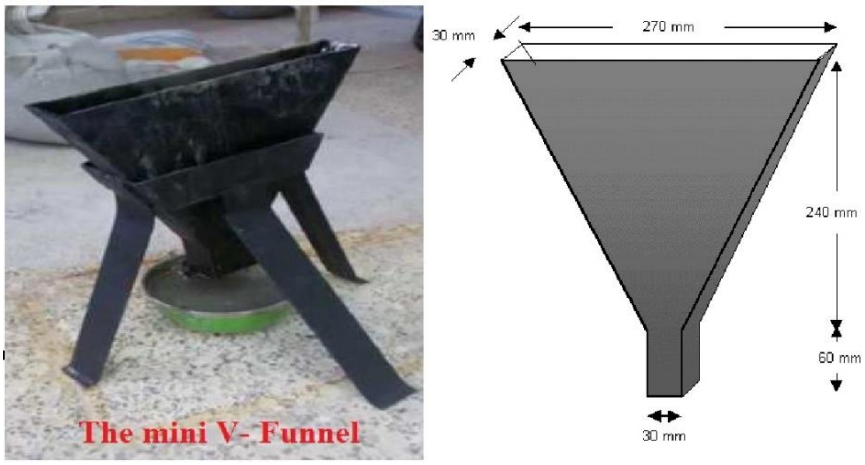

Plate 3-12: Mini V-Funnel used for SIFCON mortar

3.9 Hardened Concrete test

3.9.1 Oven Dry Density

This test is conducted according to ASTM C567,[17] on 100×200 mm cylinders. The test is conducted at 28, 56 and 90 days, where three specimens are tested at each age. oven-dry density is determined from Eq. below:

$$O_m(Density, \frac{Kg}{m^3}) = \left[\frac{(D*997)}{(F-G)}\right]/V \qquad 3\text{-}1$$

Where: O_m = measured oven-dry density, Kg/m^3

D = mass of oven-dry cylinder, Kg.

F = mass of the saturated surface-dry cylinder, Kg.

G = apparent mass of suspended-immersed cylinder, Kg

V =volume of concrete cylinder, m^3.

3.9.2 Water Absorption

The test is carried out according to ASTM C642,[84] on cylindrical specimens with a diameter of 100 and length 200 mm. The increased amount in weight due to immersion is computed for each specimen and given as a percentage of the dry weight of the specimen. At the age of 28, the test is done. Three specimens on average were chosen. ASTM C642 is used to determine the absorption from Eq. below:

$$\text{Absorption after immersion, } \% = [(B - A)/A] \times 100 \quad \textbf{3-2}$$

Where:

A = mass of oven-dried sample in air, g

B = mass of surface-dry sample in air after immersion, g

3.10 T-Beam Moulds Description

3.10.1 Moulds Preparation

The T-beam is casted in plywood moulds to achieve clear dimensions fair face as shown in (Plate 3-13).

Plate 3-13: Plywood moulds for T-beam

3.10.2 Details of Reinforced Concrete T-Beam Models

The experimental program consisted of testing fourteen reinforced lightweight concrete T-beams and tested under **s**ymmetric **t**wo-**p**oint **c**oncentrated **l**oad (STPCL) as shown in (Figure 3-6), cross-section of T-beam

and reinforced details are illustrated in (Figure 3-7), with a 10 mm bottom and side coverings, all beams are the same size. The length of the reinforcing bars is determined. Following the oiling of the T-beam sample moulds, reinforcing bars carefully placed within the moulds, for all T-beams, the distribution of tensile and shear reinforcement is constant.

The T-beam specimens are simply supported and the ends of all T-beams extended 100 mm beyond the support's centerlines to prevent slipping (crushing) failure and any local failure. Therefore, the effective T-beam span was 1300 mm.

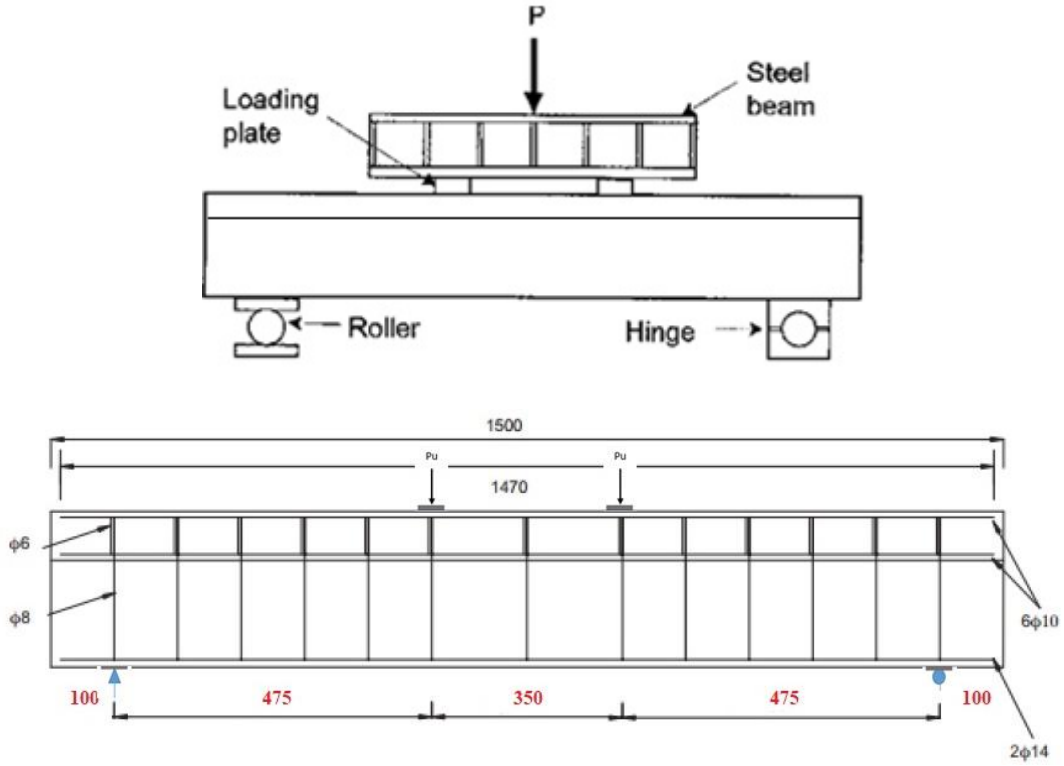

Figure 3-6: The longitudinal section of the T-beam with Symmetric two-point concentrated load

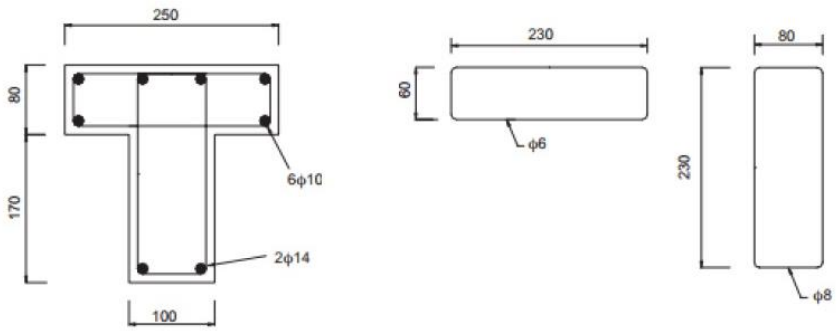

Figure 3-7: The Cross Section of the T-beam

3.11 Fire Test Furnace Description

The components of the fire test furnace include a burner combustion chamber or furnace with a gas evacuation system, a steel frame with a hydraulic linear actuator, and loads applied to the elements, see (Plate 3-14).

It was made to adhere to a time-temperature curve that was defined in fire standards ISO-834 by used **P**roportional-**I**ntegral-**D**erivative (**PID**) to maintain temperature the furnace.

The European Directives on Safety Compatibility criteria are met, which regulates the structural test procedure under fire circumstances.

Burner adjustment and the refractory qualities of all industrial furnace components are important features of the design and operation of this equipment. The burners control the flame to regulate the furnace's internal temperature. The bottom and side walls of this furnace are represented to twenty-four burners that evenly heat the room. Refractory materials help keep heat within the furnace by preventing heat loss and ensuring that the standard temperature-time curve is followed. Finally, a gas evacuation system is used in the standard fire test to collect heat flux and gases.

To manage pressure and temperature in real-time and adhere to standard time-temperature curves, a PID controller is incorporated. In order to guarantee that the furnace runs in the event of a fire, PID controllers feature an emergency power down mechanism. To reduce current risks, the system's control is essential.

Thermocouples are positioned close to the specimen and within the furnace to measure temperature. Three main components of furnace designs are the fuel, the burners, and the refractory lining. The purpose and fuel type of different furnace designs may be found [**Juan Enrique Martinez, 2020**],[85]. The primary function of the fire flame kiln is to increase the temperatures of LWC T-beam modeling to the desired levels and maintain those temperatures for the necessary amounts of time. the following equipment

is used to regulate the burning process:

1. Brick furnace.
2. Network methane burners.
3. Thermocouple.
4. Electrical gas regulator control.
5. Digital gage.
6. Electrical grid.
7. Methane gas bottle.
8. Oxygen gas bottle.
9. Gas connections and pipelines.
10. Furnace steel cover.
11. Ignition tool.
12. Air injection motor

The details of the furnace and equipment are shown in (Figure 3-8),[60]**.**

Plate 3-14: Furnace used in research with all content

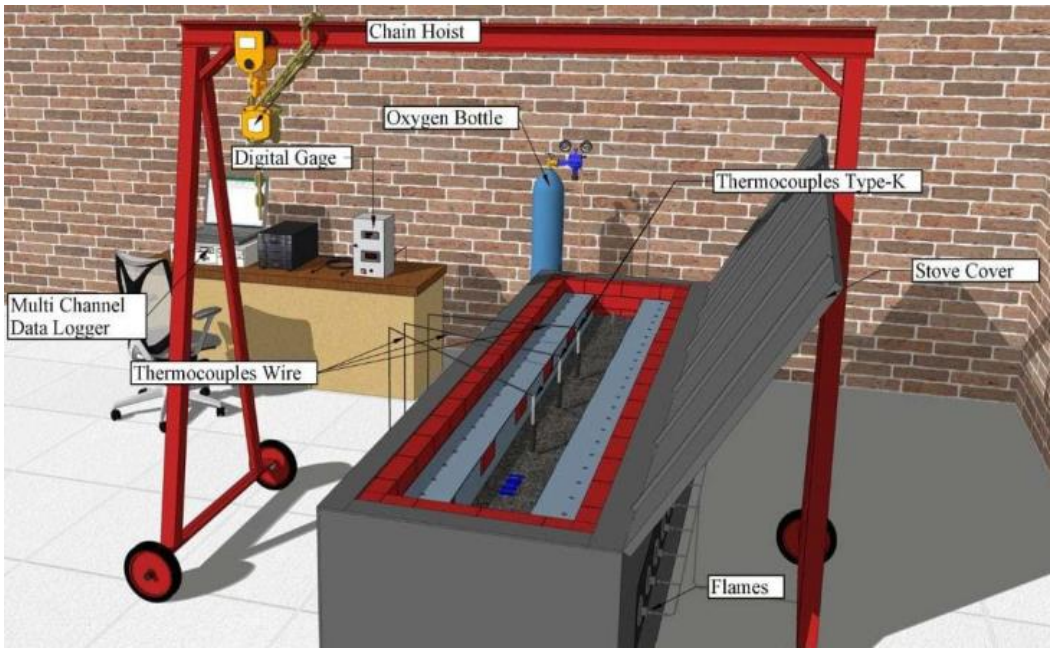

Figure 3-8 :Details of the furnace and equipment.

3.11.1 Brick Furnace: Dimensions and Description

This furnace is meant to simulate the temperature and heat transfer that a structural part might experience in a real fire. The furnace has an inside length of 2200 mm, width of 450 mm, and height of 650 mm. (Plate 3-15) and (Figure 3-9) depicts the three layers of refractory materials that make up the insulation of a furnace floor and walls. In this way, the furnace is properly insulated and maintained at a constant temperature.

Constant heat is maintained by an insulator plate 8 mm thick covering the top of the furnace, and the walls are a uniform 136 mm thick, because they are made of thermal bricks and mortar with small hole openings that are connected to an iron pipe from an air motor. There are a total of twenty-four burners in the system, spread across three lines (one at the base, one on each side). Two valves regulate the flow of gas from bottles of oxygen and methane to the burners, and the entire system controlled by an electrical regulator. Two networks are set up to imitate the heating state of a real fire by burning three situations. The fire-flame bars are designed to mimic (similar) the heating environment of an actual fire, as presented in (Figure 3-9) and specification materials in (Table 3-14).

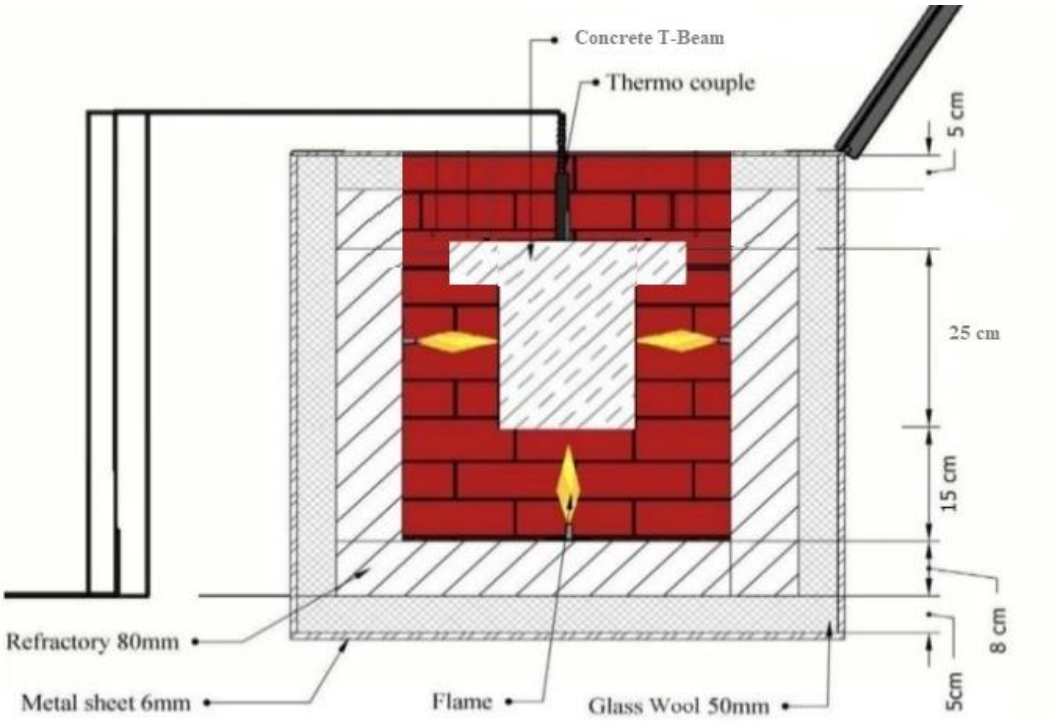

Figure 3-9: Furnace description details

Plate 3-15: Furnace floor and wall insulation.

Table 3-14: Furnace materials specification

Layers (mm)	Thickness (mm)	Density (Kg/m^3)	Thermal conductivity (W/m K)
Steel plate	6	7800	54.37
Ceramic fiber blanket	50	128	0.324
Dense refractory bricks	80	2600	2.398

3.11.2 Thermocouple

A thermometer consists of a metal tube with two wire legs made of different metals (thermocouple's "cover"). Welding is used to link the wires together at their terminals. The temperature is detected. When the temperature of the junction changes, the voltage produced their changes with it. An insulated wire is normally used to transmit readings from a thermometer to other thermocouple-capable device (a digital gauge is used in this experiment) during the burning process. Thermocouple parts information is provided in the (Plate 3-16).

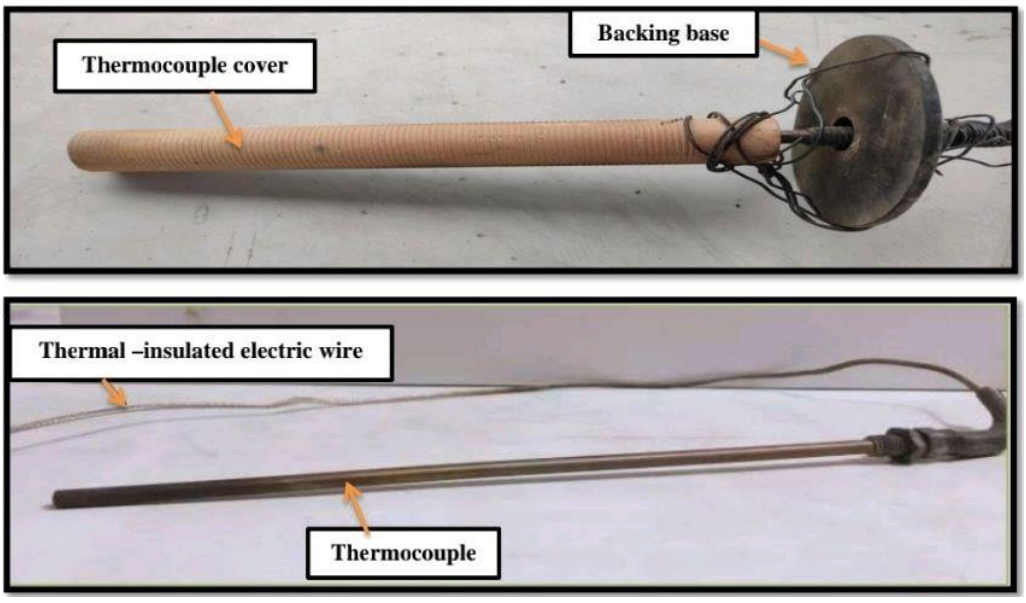

Plate 3-16: Type- K thermocouple used.

The test T-beams are outfitted with a number of different instruments, such as thermocouples, and data transducers. At each of the three intersections, 0.91 mm thick Type-K chrome-lalumel thermocouples are set up (mid-span, quarter-depth and reinforcement).

The fourth is installed in each T-beam to monitor the ambient burning

temperature, which is used to calculate the temperature of fire flame subjected to the lightweight concrete. Figure 3-10) displays the cross section, locations and numbers of thermocouples.

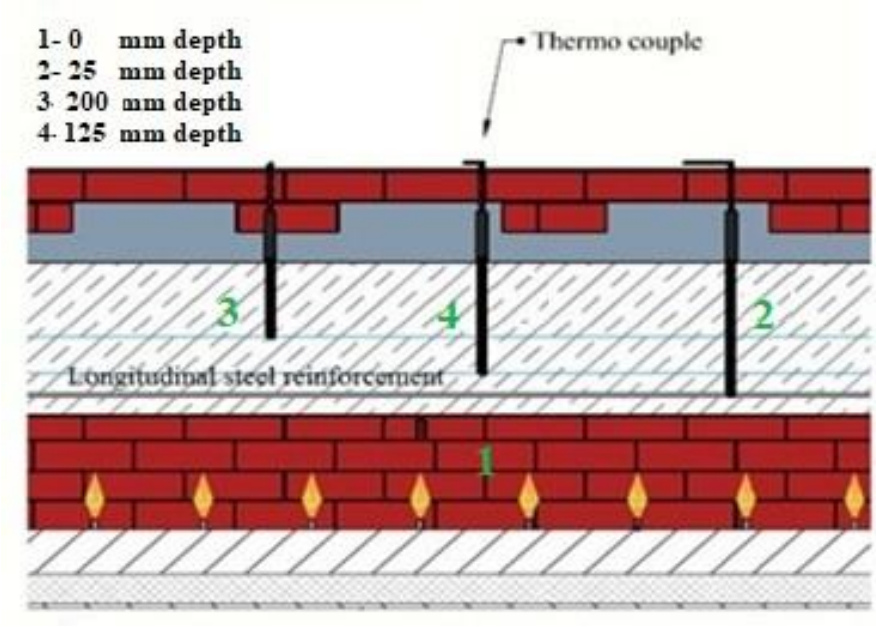

Figure 3-10: The location of the thermocouples in the cross section

3.11.3 Burning Procedure of the Specimens

The burning process is carried out once curing completes. The specimens are fired to the desired temperature in a brick furnace using direct fire flame from a network of Oxy-methane burners. The steps taken to accomplish the burning are as follows:

1. The furnace is outfitted with all the necessary connections, and then the lightweight concrete samples and beam specimens are carefully hoisted inside using a chain hoist.
2. The LWC specimens are placed towards the Oxy- methane burners and are spaced uniformly apart from the burners in both rows.
3. The gas valve is turned on, the burners are lit, and the temperature is gradually raised in accordance with the standard curve of ISO-834 which presented in chapter one (page 8).
4. (Figure 3-9) and Figure 3-10) shows that only the bottom and the two sides of the specimens T-beams section are exposed to fire, while the top

surface of the T-beam has to remain under adiabatic conditions during the whole process when a concrete slab is placed on top of the beam, as is typically the case in real life.

5. The networks of oxygen-methane burners are designed to combust samples of low-temperature cobalt chromium. All methane burners, at the bottom of the furnace and on each side, are positioned directly under and alongside the T-beam specimen, with a space of 15 cm between the T-beam's exposed surface and the burner nozzles.
6. Once the desired study time fire exposed is reached, two digital thermometers, one placed in the flame contact region and the other at the face of the specimen, continuously monitored the temperature to ensure it does not deviate from the set point. The placement of the thermocouples within LWC T-beam is shown in (Plate 3-17).

Plate 3-17: Thermocouples Fixing inside LWC T-beam.

7. Following 15 and 30 min. of fire exposure, the gas is turned off and the reinforced lightweight concrete samples are allowed to cool. Writing down the specimen starting and finishing weights.

3.11.4 Fire Loading

The testing period and fire line history are crucial factors in high-temperature studies. Brick furnaces carried loads of fuel (gas) to get them the right temperature for burning. The T-beam samples are put in a furnace to

required time study.

The greatest temperature that may be reached within the furnace is 1200 °C. The furnace's temperature was set to mimic (similar) the ISO-834 fire burning curve increased, as shown in (Figure 3-11). The fire loading lasted for 15 or 30 min. in all study cases.

The specimen is monitored every one min. for any significant changes, such as spalling-induced fire also fire flame shape where air injection motor used to exhaust the CO_2 gases produced from burning operation. When the fire loading test is finished and each T-beam is cooled to ambient air temperature (about 25-30 °C), final careful notes are taken on the cracking and spalling.

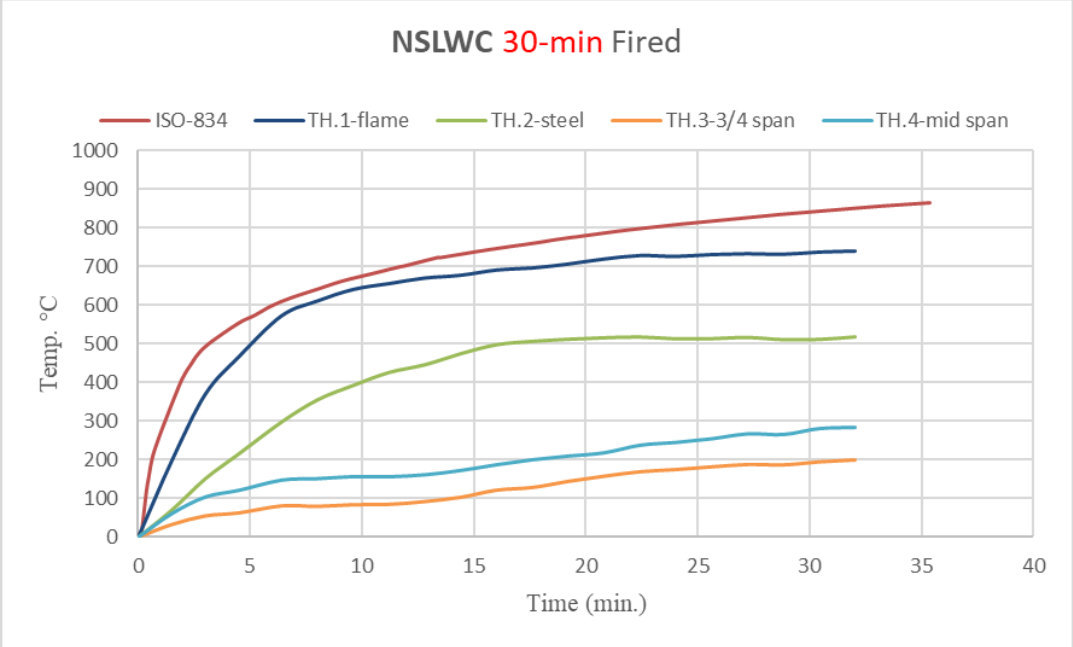

Figure 3-11: Experimental and ISO-834 Standard recommended temperature-time curves for 30 min.

Around 300 mm of flame, the thermostat methane gas is also control by hand. Three sides T-beam, including the bottom, are directly hit by flames.

3.12 Preparing the SIFCON Thin Jackets

It is determined in this research that randomly infiltrating discrete fibers with a cement-based slurry would be the most effective method for producing the SIFCON thin jacket (15- and 30-mm thickness) 6% (by volume) of hooked fibers have an aspect ratio (Lf/Df) of 60 was adequate to completely fill the

mould, therefore it was used in the experiment. The mechanical behavior of the matrix and SIFCON are discussed, as well as the ratio of materials used.

The slurry mixture was designed to have optimal compressive strength and workability.

3.13 Repaired Technique of Fired Damaged NSLWC and HSLWC T-beam Specimens

Applied to test specimens are T-beams that have destroyed in a fire and subsequently strengthened using a SIFCON thin jacket.

There is no need to repair concrete surface before practical three-faces SIFCON jacket on the specimens that are exposed to shorter fire periods and suffered less serious damage (U-shaped jackets), A customized wooden mould was used to create the jacket.

Moulds made of wood with a cross section identical to the T-beam samples. Several layers of fibers are used to fill the moulds to the desired volume proportion. The slurry mixture is infused into each successive layer.

The infiltration process is carefully monitored to check for leaks and ensure that fibers are evenly dispersed. As well as the joints between the wooden components are sealed using a specialized rubber strip, As indicated in (Figure 3-12).

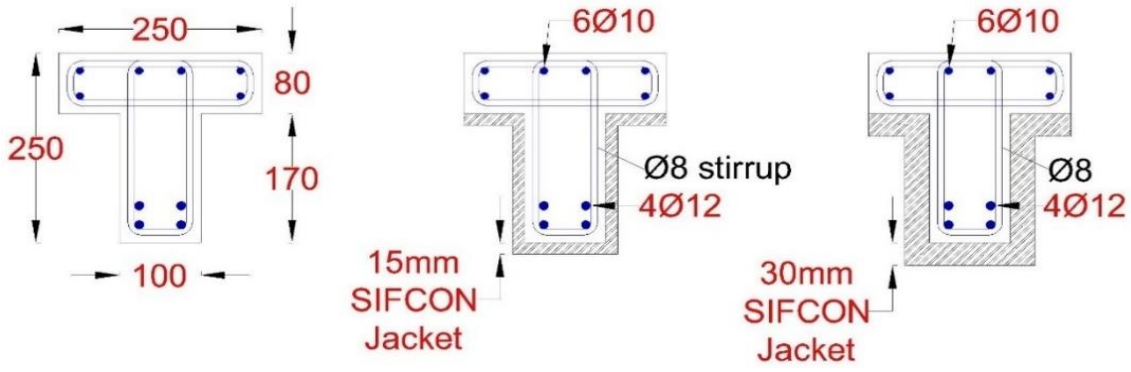

Figure 3-12: Strengthened section using three-faces SIFCON jacket.

Casting the three-sided SIFCON jacket required larger-than-usual moulds prepared, as seen in (Plate 3-18). Cover jackets of 15- and 30-mm thickness could be cast in these moulds and adhesives could be applied from below and

on both sides (U-shaped jackets), Cracked and destroyed T-beams caused by the fire, SIFCON was used to replace the broken piece (spalling parts).

Plate 3-18: Wooden moulds used for casting SIFCON jacket

The T-beams strengthening process used SIFCON thin jacket as indicated in the (Plate 3-19) and (Figure 3-13) [60].

Then, the fibers are laid down in a series of layers, with the slurry added after each layer so that it may thoroughly permeate the fibers and fill any gaps.

During the casting of SIFCON thin jacket, the multi-layer approach for inserting fiber in the slurry was used, which was found to be more effective and simpler in practice than the single layer technique, especially when dealing with a high steel fiber content.

This process was done as many times as necessary to ensure that the desired quantity of fibers would completely fill the mould.

Plate 3-19: Processes of strengthening T-beam specimen.

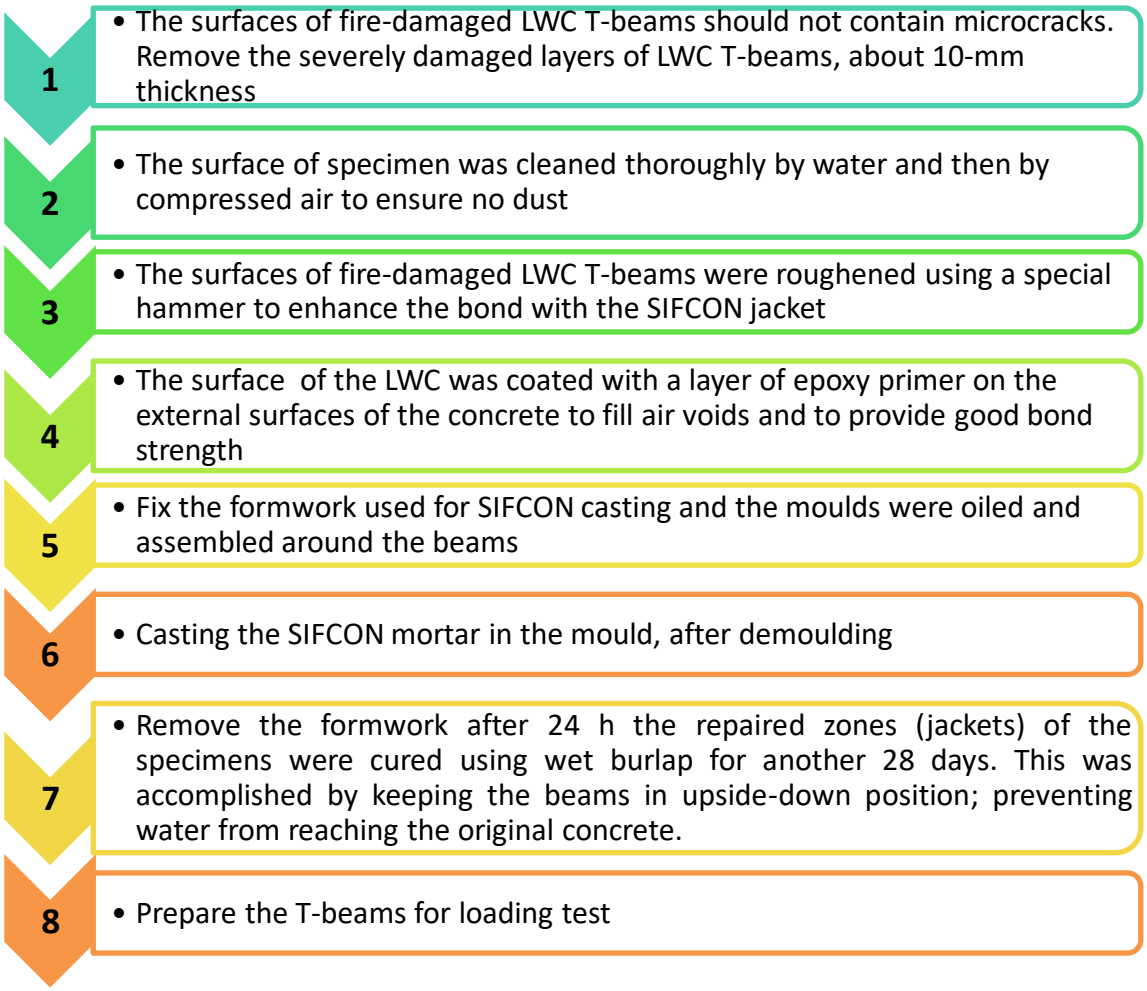

Figure 3-13: Repair and strengthening technique process of LWC T-beams by using three-faces SIFCON jacket.

3.14 Instruments and Testing Procedure of T-Beam

3.14.1Description of the Tested Lightweight T-Beam

The complete experimental program involves fourteen both of normal and high strength reinforced lightweight concrete T-beam specimens, that are cast in the lab, burned and repaired then testing under two-point load stress, as indicated in (Figure 3-14). Twelve T-beams are subjected to fire flame and compared to two reference T-beam specimens that are not (used as reference).

The data for LWC T-beam samples are shown in (Table 3-15), All of the T-beams are produced at the same time, which kept the exposure conditions consistent. After lubricating the moulds of T-beam specimens, reinforcing bars are kept securely fastened to ensure 10 mm covers in place within these moulds for casting of LWC T-beam specimens, as illustrated in (Plate 3-9).

Table 3-15: Summary of NSLWC and HSLWC T-beam test specimen

Grade of concrete beam	SIFCON jacket thickness (mm)	T-Beam's designation	Fire duration (Min)
NS LWC T-Beams	None	N-C0	0
		N-F15	15
		N-F30	30
	15	N-F15-S2	15
		N-F30-S2	30
	30	N-F15-S3	15
		N-F30-S3	30
HS LWC T-Beams	None	H-C0	0
		H-F15	15
		H-F30	30
	15	H-F15-S2	15
		H-F30-S2	30
	30	H-F15-S3	15
		H-F30-S3	30

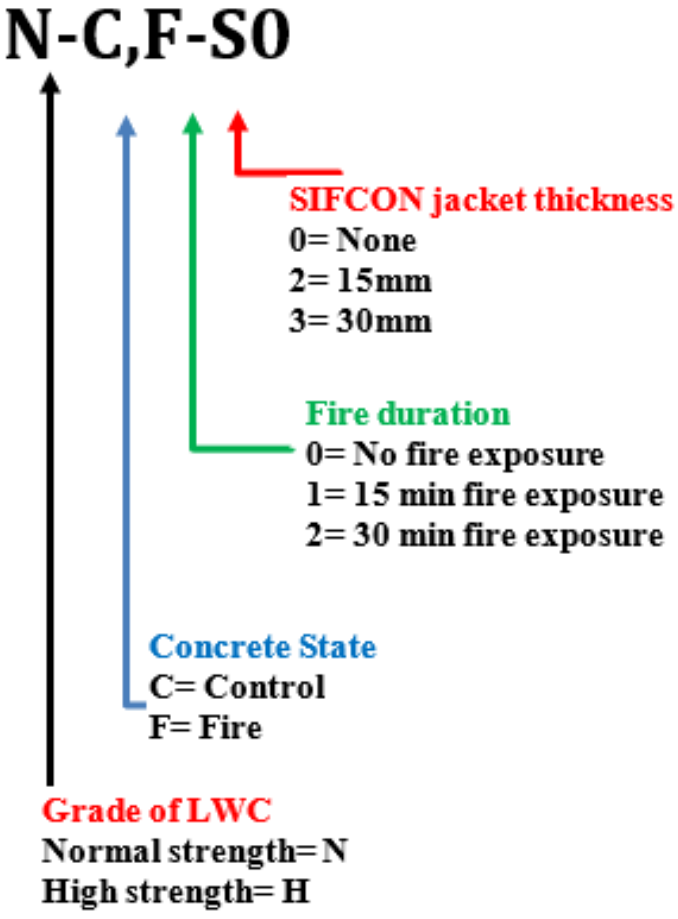

Figure 3-14: Case study of the T-beam specimen identification procedure

3.14.2 Condition and Procedure of Test Reinforced T-Beams

The T-beams' flexural performance is tested using a two-point loading methodology, which is believed to produce a zone of pure bending throughout the T-beam whole span, resulting in uniform load application and moment failure. The distance between each T-beam end supports is 1.3 meters, as shown in (Figure 3-15). The tested LWC T-beam is divided into three sections and subjected to a simulated load that is applied and distributed using a steel T-beam at two places, they put 350 mm between the two load points, the 20 mm thick hardened steel plates used to construct the special supports are able to withstand the imposed stress without deforming, and without interruption.

At age of 28 days All T-beams are subjected to two-point loads at constant rate of 0.02 mm/s using stroke-controlled electro hydraulic testing equipment with a capacity of 2500 kN. Each T-beam is stressed up to the point of failure then being discarded. Acquired and stored data collection system are the measurements shown in (Figure 3-16). The primary features of the structural behavior of the specimens at each loading level are identified during testing, midspan and point loading deflection are measured with these LVDTs by connecting them to a computerize data gathering (collecting) system, as illustrated in (Plate 3-20).

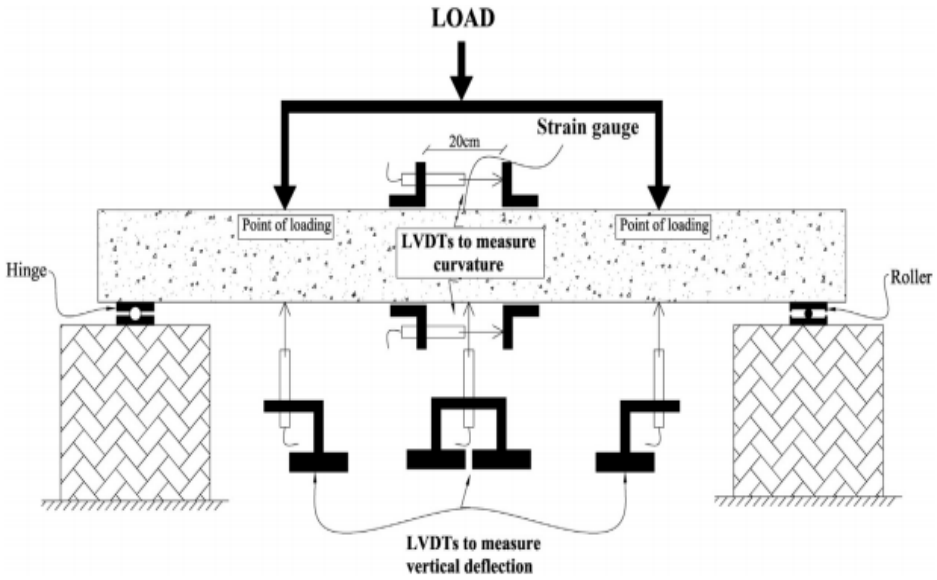

Figure 3-15: Loading setup and measurements

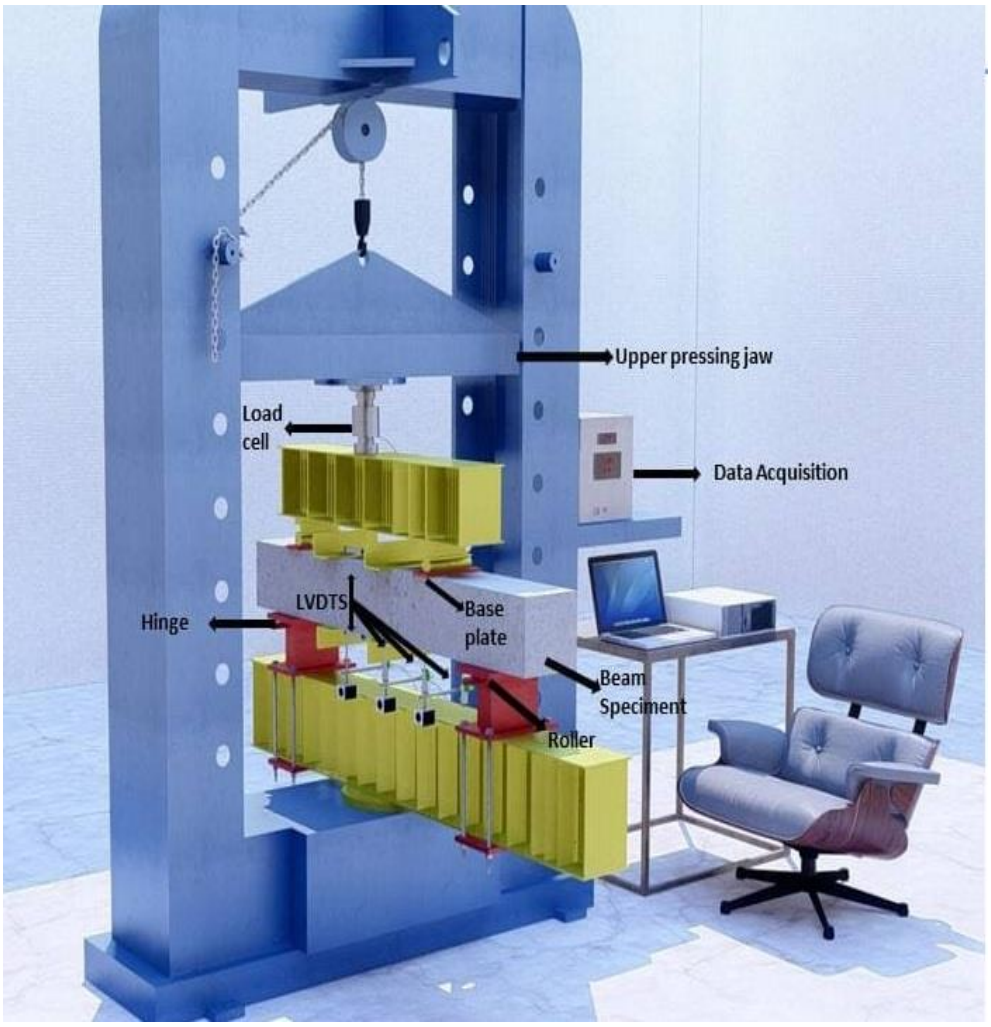

Figure 3-16: The loading setup of two-point load system

Plate 3-20: Arrangement of LVDTs and Load Cell within test Device

The experiment is carried out in the engineering lab at University of Babylon. The crack meter is used to detect the initial crack and track its progression. T-Beam specimens crack patterns documented, and the load values for each as shown in (Plate 3-21) have been recorded in order to assess the failure mode. Also, visual inspections are reported the various failure modes.

Plate 3-21: A- Crack meter device; B- crack development observation.

3.15 Testing of Control Samples (Destructive Tests)

Following the selection of the SIFCON mixes, cubes, cylinders, and prisms are cast for testing at ages of 7 and 28 days at room temperature and after exposing to a fire flame with the same procedures and conditions of burning T-beam specimens, while SIFON is tested only at room temperature. All of the following are tested: splitting tensile strength (*f*sp), cube compressive strength (*f*cu), elastic modulus (Ec), and modulus of rapture (*f*r).

The Civil Department's Building Materials Laboratory at Babylon University College of Engineering served as the site for all the tests.

3.15.1 Compressive Strength

This test is conducted on 100 mm and 150 mm cube according to B.S. 1881: part 116:1989[80] and 100×200 mm cylinder according to ASTM C 39/C 39M – 18[86] by using a digital compression testing machine of 2000 kN

capacity as shown in (Plate 3-22) The test was conducted at ages 7 and 28 days, and three specimens are tested at each age.

Plate 3-22: Compressive machine test

3.15.2 Static Modulus of Elasticity

The elastic modulus was obtained by using the uniaxial compression tests, the ACI 318-14,[16] formula is used to find the elastic modulus of concrete.

$$E_c = W_c^{1.5} * 0.043 * (f_c')^{1/2} \qquad \textbf{3-3}$$

Where:

Ec = Modulus of elasticity, MPa

Wc = Equilibrium density of lightweight concrete (1440 - 2560 Kg/m^3)

f `c = Cylinder compressive strength, MPa

At laboratory by using (100*200 mm) cylindrical specimens, the static modulus of elasticity of concrete is determined according to (ASTM C469, 2014)[87].

The top surface of the cylinder was properly polished and smoothed using an electric grinding machine. The specimens are put through their paces in a

hydraulic machine with a capacity of (2000 kN). For the elastic module test, 40 percent of the concrete sample ultimate compressive strength is delivered to the concrete cylinders, as indicated in (Plate 3-23), For each grade of (NSLWC and HSLWC).

The following equation is used to calculate the static modulus of elasticity:

$$\mathbf{Es} = (\boldsymbol{S_2} - \boldsymbol{S_1})/(\mathbf{e_2} - \mathbf{0.0005}) \qquad \textbf{3-4}$$

Where:

Es: static modulus of elasticity, (GPa).

S_2: stress corresponding to 40% of ultimate load, (MPa).

S_1: stress corresponding to a longitudinal strain (0.00005), (MPa).

e_2: longitudinal strain produced by stress S_2.

Plate 3-23: Modulus of elasticity test device

3.15.3 Splitting Tensile Strength

This test is performed according to ASTM C496-11 [88], which 100×200 mm cylindrical concrete specimens are used. The specimens are tested with a machine capacity of 2000 kN at rate loading (0.3 MPa/sec) as shown in (Plate 3-24). This test is conducted at ages of 28 and 56 days. For splitting tensile strength test of lightweight aggregate concrete, at least eight cylindrical specimens are required at each age for each grade of LWC (NSLWC and HSLWC) and three cubes for SIFCON,[71].

The experimental splitting tensile strength of cylinders is calculated by using the ASTM C496-11 [88] equation:

$$f_{sp}=2P/\pi\, d\, L \qquad 3\text{-}5$$

Where:

f_{sp} = Splitting tensile strength, (MPa)

P =Maximum applied load, (N).

d = Diameter of the specimen, (mm).

L= length of the specimen, (mm)

Plate 3-24: Splitting tensile strength test of concrete

The ACI 318-14,[16] provide an equation to predict splitting tensile strength of concrete based on concrete compression strength.

$$f_{sp} = \lambda * 0.56 * f'^{1/2}_{c} \qquad 3\text{-}6$$

Where:

λ = A reduction factor (λ = 1 for normal weight concrete,

λ = 0.85 for sand LWC, and λ = 0.75 for all lightweight concrete)

f_{sp}= Splitting tensile strength, MPa.

f'_c = Cylinder compressive strength, MPa.

3.15.4 Modulus of Rapture (Flexural Strength)

Concrete prisms of 100x100x400 mm are used to evaluate the modulus of rupture (MOR) in line with ASTM C78/2002,[89].

Similar to how T-beam specimens are cast and cured, prisms are as well. Each figure was the average of three prisms for each age (7, 28, and 56) days.

A hydraulic machine controls digital with a 150 kN capacity was used for third-point loading (MOR) tests, as shown in (Plate 3-25).

Plate 3-25: Flexural strength test

The ultimate modulus of rupture (*f*r) for all lightweight concrete was calculated using the following equation:

$$fr = 0.46\sqrt{f`c} \qquad \textbf{3-7}$$

Where within the middle third of the span, following equation is used to determine the MOR:

$$fr = 2Pa/bh^2 \qquad \textbf{3-8}$$

Where:

fr: Modulus of rupture, (MPa). P: Failure load, (N).

l: distance between the supports, (mm). b: Prism's width, (mm).

h: Depth of prisms, (mm). **a**: average distance between line of fracture and the nearest support measured on the tension surface of the beam (mm).

3.16 Testing Non-Destructive Tests

The compressive strength of the beams is determined using nondestructive testing in order to assess the impact of fire on the lightweight concrete. The ultrasonic pulse velocity test; however, the results are inconclusive, owing to random cracks that formed during the fire. In order to estimate concrete compressive strength, the Schmidt hammer is utilized, an average of 10 readings.

3.16.1 Ultrasonic Pulse Velocity Test (U.P.V)

Direct transmission is used to determine the transit durations of ultrasonic pulses. This test is done in accordance with the following guidelines: (ASTM C597,[90]). Before and after the controlled lightweight concrete examples are burned, the velocity of ultrasonic pulses passed through them is measured. (Plate 3-26) shows the portable ultrasonic concrete tester PUNDIT 54 K-Hz that is utilized for this purpose.

Prior to testing, the PUNDIT is calibrated to ensure that transit time readings are accurate. Calibration using the reference bar is used to accomplish this, to function as a compliance and prevent dissipation of transmitted energy, a tiny coating of grease is placed to the surface of the tested locations. The length of the pulse transit route is precisely measured, and the time it took to travel is recorded to the order of 0.1 μsec. The test is carried out at the concrete laboratory at College of Engineering University of Babylon.

Raouf and Ali (1983)[91] developed Equation from 650 tests results collected from the previous studies, the developed equation is given as :

$$C = A * e^{\wedge B * D} \quad \textbf{3-9}$$

Where:

C = concrete compressive strength in N/mm^2 (MPa)

D = direct Ultrasonic velocity (Km/s).

A = 2.016 and B = 0.61

Plate 3-26: Ultrasonic pulse velocity test for cube and T-beam samples.

3.16.2 Rebound Hammer Test

LWC specimens surface hardness is estimated using a Schmidt hammer, with the rebound number recorded as a proxy for the LWC's strength and void content. For each LWC sample, the rebound number is measured at eight different locations across the specimens' faces. As a result, the average rebound number for each LWC specimen region (exposed to realties fire flame) are determined. In this study, a Schmidt hammer of the MC kind is employed (Plate 3-27). Specifications from (BS-1881:part 202 ,1986)[92] dictate the testing procedure must be followed.

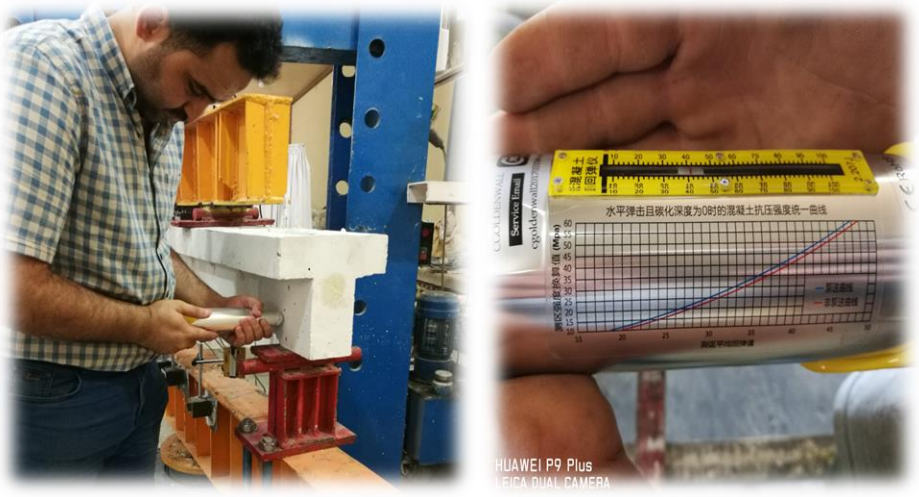

Plate 3-27: Schmidt hammer test for lightweight concrete specimens.

Chapter Four

Experimental Results and Discussion

4.1 General

The experimental results of this research study outlined in Chapter 3 are presented in this chapter, together with the discussion of the results.

The mechanical properties of concrete, such as its compressive strength, oven-dry density, splitting tensile strength, water absorption, and predicted modulus of elasticity, are first analyzed and discussed, based on data from tests conducted on both normal and high strength lightweight aggregate concrete.

4.2 Introduction

The primary purpose of this study is to investigate experimentally the structural behavior of light-weight concrete T-beams outed to fire flame and strengthened with SIFCON U-shape jackets. The bottom and both lateral sides of the T-beams are covered with various parameters, including compressive strength of the concrete (normal and high), exposure duration, and thickness of the reinforcing jacket. The experiment objective is to examine the flexure behavior and failure process of simply supported T-beams that are received external SIFCON jacket reinforcement.

The research technique is focused on analyzing and contrasting the behaviors, mode of failure, and resistance to apply two-point loads of T-beams damaged and repaired with SIFCON jacket, then comparing the outcomes of the experimental test with those of the simulation program (ABAQUS) to ensure that the behavior in both is consistent.

4.3 Mechanical Properties of Concrete

The properties of materials, effect of fire damage, repairing by SIFCON jacket and behavior of T-beam section “research study” on the mechanical properties of NSLWC and HSLWC are discussed here.

4.3.1 Oven Dry Density

As presented in (Figure 4-1), concrete produced from LECA aggregate, conformed to the ACI 213R -14,[19] requirements, and oven dry density are

conformed to the requirements of (CEN ENV 1992-1-4),[22] "unified European standard" and "RILEM",[21] which caps density at 2000 Kg/m^3.

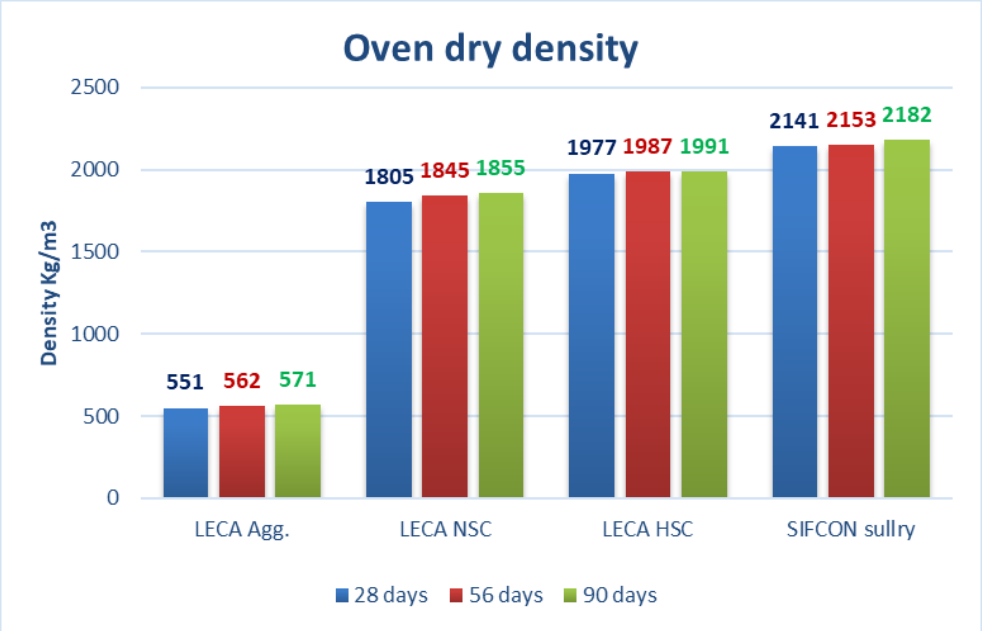

Figure 4-1: Oven dry density at age 28,56 and 90 days

4.3.2 Compressive Strength

The test used to determine the capacity strength of the concrete which categorized according to its compressive strength. (Table 4-1) displays the SIFCON compressive strength as well as that of normal and high strength lightweight concrete. The outcome represents the average value of six cubes.

Table 4-1: Results of experimental cylinder and cube compressive strength of NSLWC, HSLWC and SIFCON samples

Symbol	Age	Compressive strength *f* cy (MPa)	Compressive strength *f* cu (MPa)	% *f*cu development with respect to 90 days age
NSLWC	7	17.81	21.36	59.25
NSLWC	28	26.87	32.22	89.38
NSLWC	56	28.02	33.6	93.2
NSLWC	90	30.07	36.05	100
HSLWC	7	44.29	50.79	71.13
HSLWC	28	56.95	65.31	91.47
HSLWC	56	60.05	68.87	96.46
HSLWC	90	62.26	71.4	100
SIFCON	7	82.71	93.56	72.62
SIFCON	28	101.18	114.46	88.85
SIFCON	56	111.18	125.77	97.62
SIFCON	90	113.89	128.83	100

(Figure 4-2) shows development concrete compressive strength over time. Regarding the strength after 28 days, both the HSLWC and NSLWC have the same level of growth, which is about 70%. A strength growth of nearly 87% was seen in the SIFCON combination. At 90 days, the NSLWC combination had the strongest strength development, which is about 119%, followed by the SIFCON mixture, which has the second-strongest growth 114%, while the HSLWC has the weakest development 104%.

SIFCON, on the other hand, improvements strength quickly during the initial stages of development (In 7 days, at 25 °C, the material has attained about 80% of its compressive strength, and in 28 days, it has reached about 91% of its compressive strength), considering that the resistance at the age of 90 days represents the semi-final outcome of the concrete element. When compared to HSLWC and NSLWC, the strength gains are 66 and 69.7% of compressive strength at 7 days of age and 96 and 87.5% of compressive strength at 28 days of age, respectively.

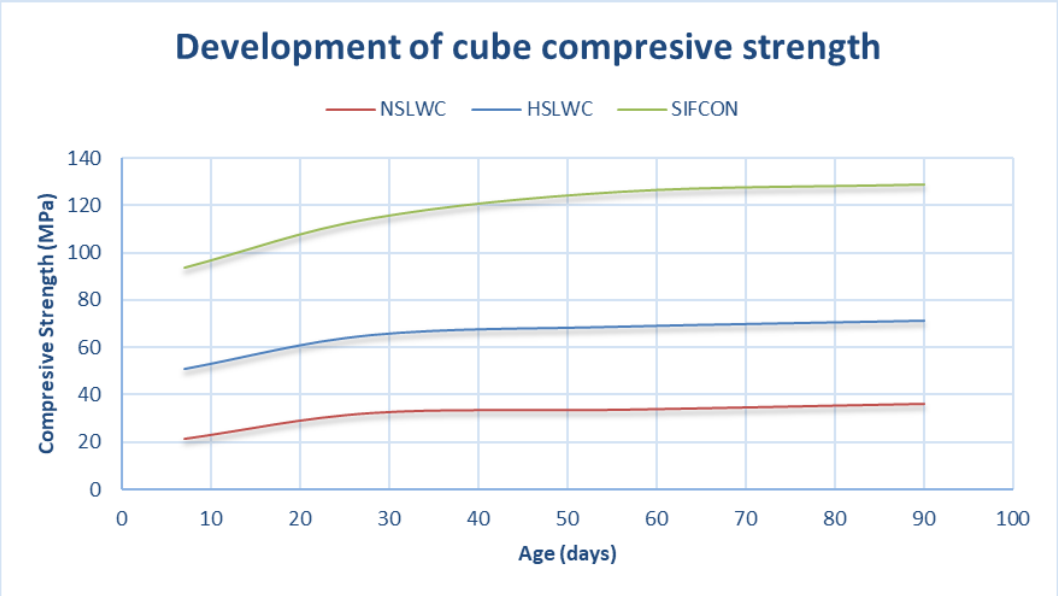

Figure 4-2: Development of compressive strength.

(Table 4-2) shows development concrete compressive strength over time for cubical burned sample up to 600 °C, due to crashing and spalling for both NSLWC and HSLWC.

Table 4-2: NSLWC and HSLWC burned cube compressive strength

Symbol	Age (days)	Compressive strength f_{cu} (MPa)		% Residual of compressive strength
		At 25°C	At 600°C	
NSLWC	7	21.36	12.78	59.83
NSLWC	28	32.22	20.48	63.56
NSLWC	56	33.6	23.91	71.16
NSLWC	90	36.05	26.1	72.4
HSLWC	7	50.79	24.69	48.61
HSLWC	28	65.31	36.65	56.12
HSLWC	56	68.87	41.15	59.75
HSLWC	90	71.4	43.17	60.46

Compressive strengths of cylinders (*f* 'c) and cubes (*f*cu) are displayed for both normal and high strength LWAC as in (Figure 4-2), and (Figure 4-3) respectively.

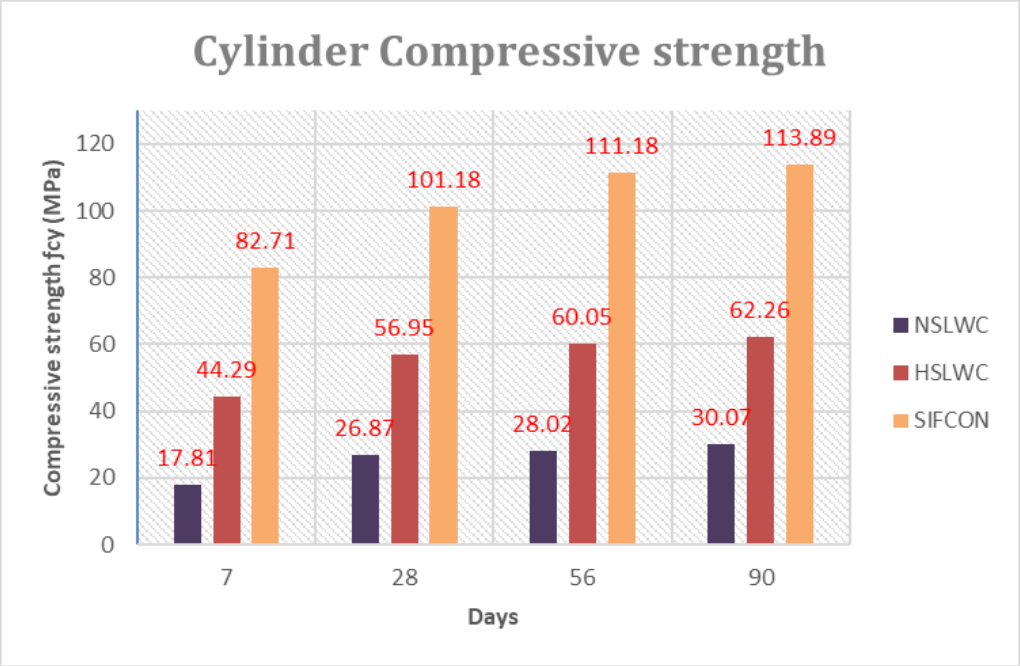

Figure 4-3: Cylinder compressive strength

The residual strength calculated from eq (4-1) of concrete cube specimens for NSLWC and HSLWC mixtures is shown in (Figure 4-4). Comparing the NSLWC combination to the HSLWC mixture as a whole, the NSLWC mixture has maintained higher residual strength. Between 7% and 10% less residual strength is found between these combinations at different ages.

$$\%\ Residual\ of\ compressive\ strength = \frac{fcu\ (T = 600°C)}{fcu\ (T = 25°C)}\ X\ 100 \quad \textbf{(4-1)}$$

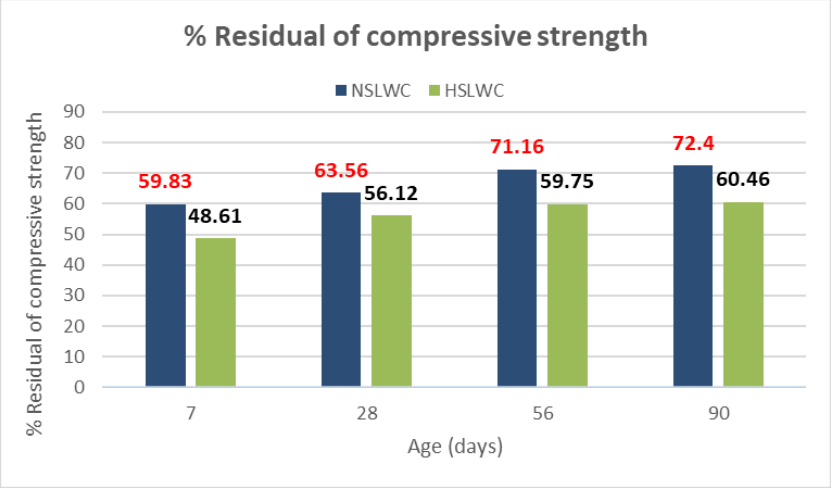

Figure 4-4: Concrete residual strength at various ages

Results showed that after 28 days, NSLWC cube compressive strength is approximately 42.8% lower than HSLWC. This is because, in comparison to HSLWC, the limited cement causes a weaker contraction (transition zone).

Compressive strength ratio of cubes and cylinders (*f* `c, *f*cu) at 28 days are shown in (Figure 4-5) for typical lightweight concrete samples.

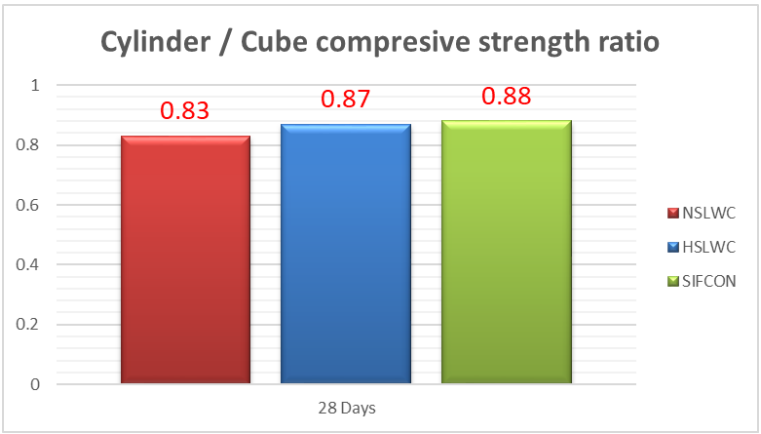

Figure 4-5: Ratio compressive strength

4.3.3 Splitting Tensile Strength

According to (ASTM C330,2017)[71], structural LWAC requires a minimum splitting tensile strength of 2.0 MPa over a period of 28 days, results displays that both the NSLWC and HSLWC mixtures is significantly higher than the minimum criterion as shown in (Table 4-3), and often increases with

age. Splitting tensile strength is significantly lower than its compressive strength because the crack propagates fast under tensile pressure. Matrix hydration progresses as its internal microstructure is completed, increasing the strength given to the composite material over time.

Table 4-3: Results of experimental test of cylinder splitting tensile strength of NSLWC, HSLWC LWC and SIFCON samples.

Symbol	Age (days)	Splitting tensile strength *f sp* (MPa)
NSLWC	28	3.81
NSLWC	56	4.17
HSLWC	28	4.8
HSLWC	56	5.64
SIFCON	28	14.17
SIFCON	56	18.5

The splitting tensile strength results for NSLWC, HSLWC and SIFCON were tabulated in (Table 4-3) and graphed in (Figure 4-6).

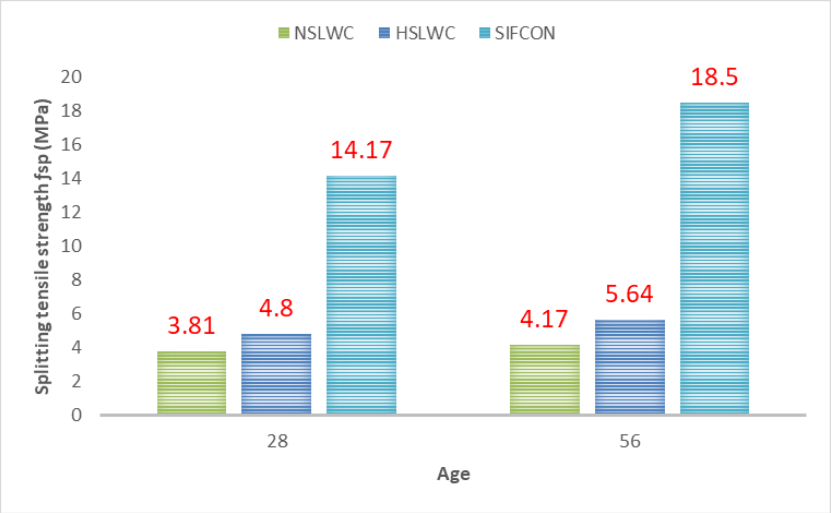

Figure 4-6: Splitting Tensile Strength

Results showed that, SIFCON splitting tensile strength greater than NSLWC and HSLWC by about 73.11% and 66.13% at 28 days as well as about 77.46% and 69.51% at 56 days respectively. This is due to the high density and steel fiber of SIFCON, also, development of SIFCON splitting tensile strength is in excess of NSLWC and HSLWC as presented in (Figure 4-6), Compared to NSLWC and HSLWC, SIFCON's hydration procedure is clearly better there, because the water absorption of Cement (high quantity) more than that

of HSLWC and NSLWC. The tests showed that crack path line through NSLWC and HSLWC, are closely similar but different about SIFCON due to steel fiber in the mixture as shown in (Plate 4-1)

Plate 4-1: Splitting crack path

In general, the average experimental results value exceeded the value indicated by ACI 318-2014,[16] equation where (reduction factor) λ=0.75 as shown in (Figure 4-7).

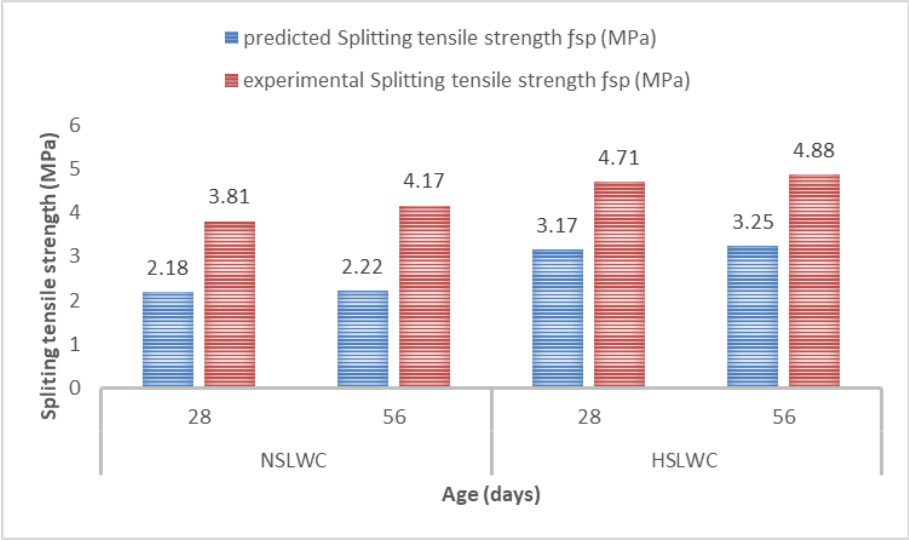

Figure 4-7: Calculated and Predicted splitting tensile strength

4.3.4 Flexural Strength (Modulus of Rupture)

For both LWAC and SIFCON, the flexural strength f_r test was conducted using (100x100x400) mm prism specimens, with each prism being tested as simply supported and subjected to two-point loading using the same method.

(Table 4-4) shows that the flexural strength values are similar for both LWC mixes, with little improvement for the high strength, but that SIFCON is far superior in acquiring the strength at all ages, with a value of more than 4.5 times that of HSLWC and more than 7.3 times that of NSLWC at 28 days of age. Furthermore, as shown in (Figure 4-8), the flexural strength development of HSLWC is anywhere from 33 % to 62 % higher than that of NSLWC. On the other hand, SIFCON demonstrates substantially more rapid strength growth, with its strength in 7 days age exceeding the highest strength reached in the ultimate age of 90 days for both LWC mixes by 2.76 and 3.98 times, for NSLWC and HSLWC, respectively.

Table 4-4: Results of experimental test of prism flexural strength of NSLWC, HSLWC and SIFCON samples.

Symbol	Age (days)	Flexural strength f_r (MPa)
NSLWC	7	3.64
NSLWC	28	4.08
NSLWC	56	4.81
NSLWC	90	5.22
HSLWC	7	4.91
HSLWC	28	6.67
HSLWC	56	7.28
HSLWC	90	7.62
SIFCON	7	20.9
SIFCON	28	30.1
SIFCON	56	34.66
SIFCON	90	42.31

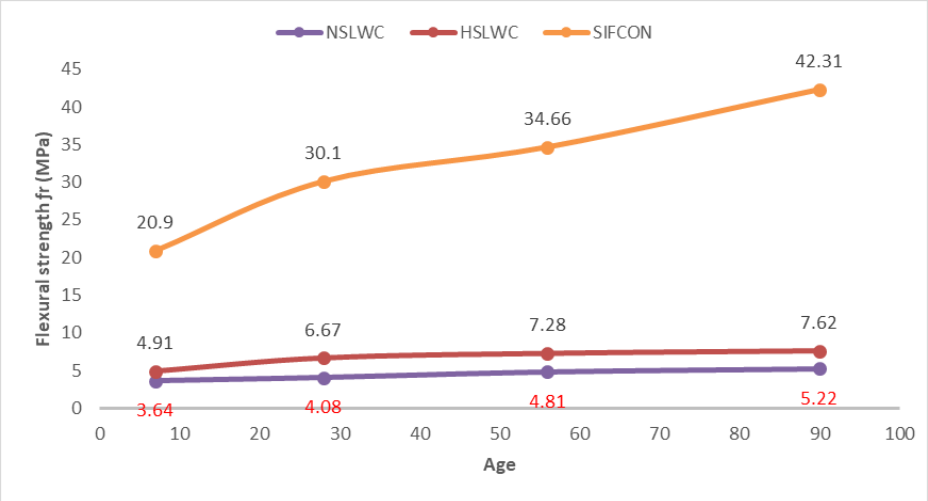

Figure 4-8 : Development of Flexural strength.

4.3.5 Static Modulus of Elasticity

A material stiffness may be quantified by calculating its modulus of elasticity. The modular ratio *n* is used in the design of flexure-prone sections of members, and it is heavily influenced by the modulus of elasticity, which is an essential component in estimating the deformation of members. The modulus of elasticity is used to determine the amount of reinforcement needed, estimate stress from measured strain, and determine the size of reinforced and unreinforced structural parts. Therefore, the modulus of elasticity of concrete is a crucial metric that indicates concrete elasticity.

One of the most essential characteristics of any solid, is its static modulus of elasticity (Ec), which is an indicator of its stiffness. The concrete modulus of elasticity is greatly influenced by the constituent materials and their relative proportions. Because the stress-strain curve steepens with increasing strain, the modulus of elasticity should increase with increasing compressive strength (**Ramezanianpour et al., 2009**),[93].

The results as presented in (Table 4-5) show the modulus of elasticity of both normal and high strength lightweight concrete samples.

Table 4-5: Results of experimental test of cylinder modulus of elasticity of NSLWC, HSLWC and SIFCON samples

Symbol	Age (days)	Modulus of Elasticity Ec (GPa)
NSLWC	28	19.8
NSLWC	56	22.01
HSLWC	28	33.85
HSLWC	56	34.1
SIFCON	28	56.29
SIFCON	56	62.6

The modulus of elasticity for NSLWC at 28 days is 19.8 GPa, while that for HSLWC is 33.85 GPa. The mechanical characteristics of LWC are quite sensitive to changes in the coarse aggregate used (which makes up around 40%-45% of the total volume of the concrete),[60].

(Figure 4-9) displays the expected static modulus of elasticity for NSLWC

and HSLWC concrete as calculated by ACI 318-14,[16], and compared with the experimental result presented in (Table 4-6).

Table 4-6: comparison between predicted and experimental result of cylinder modulus of elasticity of NSLWC and HSLWC samples

Symbol	Age (days)	Predicted	Experimental
		Modulus of Elasticity Ec p (GPa)	**Modulus of Elasticity Ec (GPa)**
NSLWC	28	17.74	19.8
	56	19.06	22.01
HSLWC	28	29.02	33.85
	56	30.7	34.1

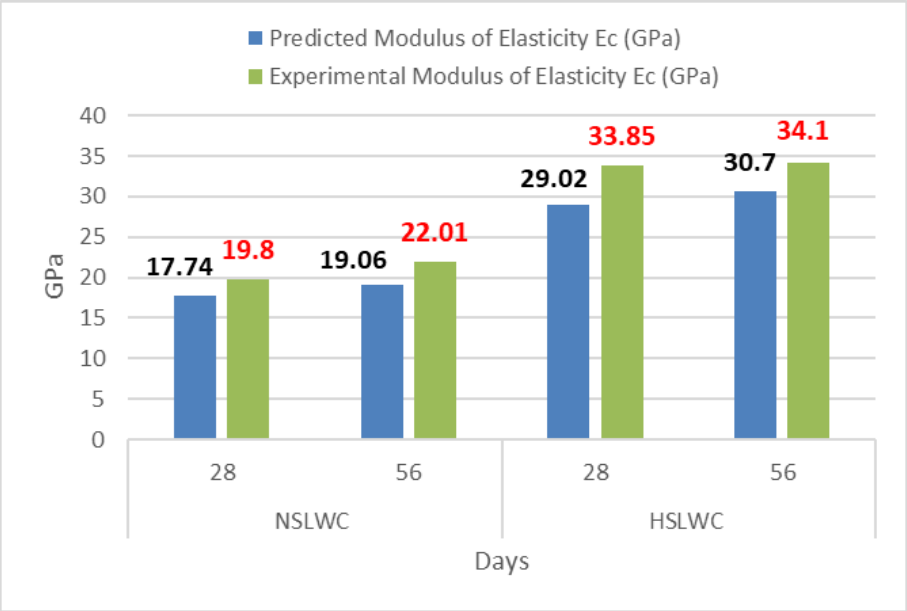

Figure 4-9: Predicted and Experimental result cylinder modulus of elasticity for NSLWC and HSLWC sample

Compressive strength and mixture density are found to be the primary reasons why NSLWC's estimated modulus of elasticity is lower than those of HSLWC and SIFCON.

4.3.6 Ultrasonic Pulse Velocity (U.P.V)

In this investigation, each sample is evaluated wave being transmitted directly. (Table 4-7) displays the results of the experiments, which reveal that after burning, the pulse velocity dropped for all samples, with reduction rates ranging from (28%-37%) for HSLWC to (24%-30%) for NSLWC.

Table 4-7: Results of experimental test for reference and burned cube samples under Ultrasonic Pulse Velocity of NSLWC, and HSLWC

Mix. type	Age (Day)	(U.P.V) (m/sec)		% Residual of (U.P.V)
		At 25°C	At 600°C	
NSLWC	7	3838	2636	68.68
NSLWC	28	4380	3115	71.12
NSLWC	56	4531	3321	73.3
NSLWC	90	4642	3487	75.12
HSLWC	7	5227	2610	49.93
HSLWC	28	5566	3312	59.5
HSLWC	56	5678	3607	63.53
HSLWC	90	5795	3834	66.16

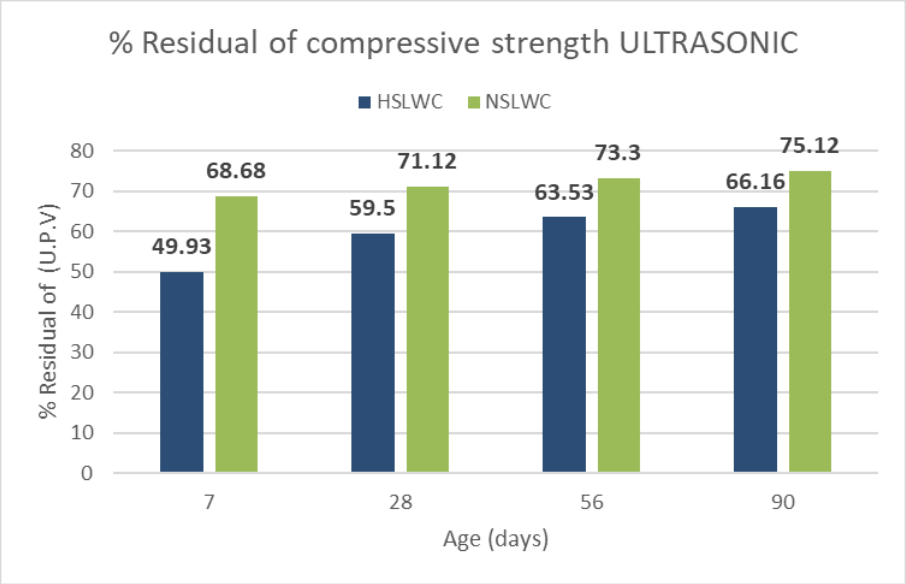

Figure 4-10: % Residual of compressive strength ULTRASONIC

Due to its high absorption rate, LECA contains more water than other forms of aggregate, at higher temperatures the evaporation of this water generates air gaps through which the pulse wave travels at a slower velocity after being exposed to fire. There is an increase in the amount of microcracks and holes, and the chemical components deteriorate as well. The sound wave interaction with air caused a certain amount of energy to be reflected back into space, as predicted by the wave propagation characteristics. A portion of the wave rose vertically, while the remainder twisted around the buildings and continued to grow. The direct method ultrasonic point position T-beam is presented in (Figure 4-11) and (Plate 4-2).

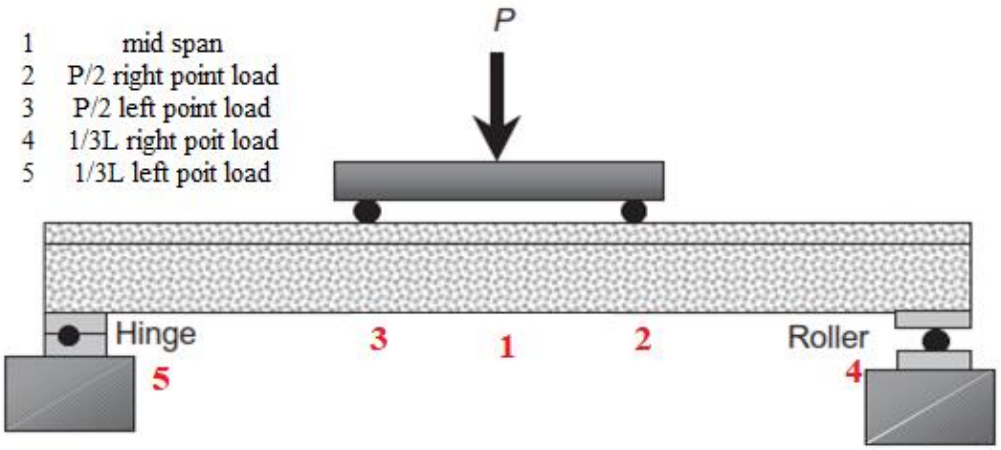

Figure 4-11: ULTRASONIC T-beam position

Raouf and Ali (1983), [91] results presented in (Table 4-8) display the samples compressive strength calculated.

Table 4-8: Results of experimental for reference and burned cube samples compressive strength by using "Raouf and Ali" eq. of NSLWC, and HSLWC

		At 25°C	At 600°C
Mix. type	Age (Day)	RAOUF Eq. (MPa) C=A*e^(B*D)	
NSLWC	7	20.95	10.07
NSLWC	28	29.16	13.48
NSLWC	56	31.98	15.29
NSLWC	90	34.22	16.91
HSLWC	7	48.89	9.91
HSLWC	28	60.12	15.2
HSLWC	56	64.37	18.2
HSLWC	90	69.14	20.9

While for NSLWC T-beams as presented in (Table 4-9).

Plate 4-2: Ultrasonic test of T-beam sample

Table 4-9: Results of experimental T-beam samples compressive strength by using "Raouf and Ali" eq. of NSLWC, before and after burning

N-C-0 direct	Time (Micro second)	Velocity V = l/t (m/s)	Compressive strength (MPa)
1-1	21.05	4751	36.57
2-2	21.2	4717	35.82
3-3	21.3	4695	35.34
4-4	21.4	4673	34.87
5-5	21.1	4739	36.3
		Average	**35.78**
N-F15-0			
1-1	23.2	4310	27.94
2-2	25.6	3906	21.84
3-3	23.8	4202	26.16
4-4	21.9	4566	32.67
5-5	22.5	4444	30.32
		Average	**27.79**
N-F30-0			
1-1	22.7	4405	29.61
2-2	25.8	3876	21.44
3-3	23.4	4274	27.34
4-4	24.2	4132	25.07
5-5	24.6	4065	24.07
		Average	**25.51**

Also, for HSLWC T-beam results are presented in (Table 4-10) which refer to the high temperature that causes large damage

Table 4-10: Results of experimental T-beam samples compressive strength by using "Raouf and Ali" eq. of HSLWC, before and after burning

H-C-0 direct	time (micro second)	Velocity V = l/t (m/s)	Compressive strength (MPa)
1-1	19.86	5035	43.49
2-2	16.76	5967	76.78
3-3	16.86	5931	75.12
4-4	16.96	5896	73.53
5-5	16.66	6002	78.44
		Average	**69.47**
H-F15-0			
1-1	18.92	5285	50.65
2-2	21.33	4688	35.19
3-3	19.52	5123	45.89
4-4	17.63	5672	64.14
5-5	18.22	5488	57.33
		Average	**50.64**

H-F30-0			
1-1	18.9	5291	50.84
2-2	22.15	4515	31.67
3-3	19.53	5120	45.8
4-4	20.32	4921	40.57
5-5	20.73	4824	38.24
		Average	**41.42**

For all SIFCON T-beam, it is difficult to calculate compressive strength by Ultrasonic due to high density of steel fiber uses in repairing jacket which give errors value.

4.3.7 Rebound number result

The Schmidt rebound hammer is still the surface hardness testing device of the most widespread use for concrete. Rebound hammer can be used very easily and the measure of hardness (i.e., the rebound index) can be read directly on the display of the testing device. According to **(Malhotra and Carino,2003)**,[94] the accuracy of assessing the strength of specimens cast, maintained in cure, and tested in labs to compression using correctly calibrated hammers is between 15% and 20%. However, the accuracy of the hammer's estimation of the compressive strength of the concrete structure is 25%.

The results shown in (Table 4-11) that rebound number values reduction clearly when concrete exposed to fire, is (45 and 33%) for high and normal strength lightweight concrete respectively where calculated according to Relation as presented in (Figure 4-12) between compressive strength and rebound number for concrete cylinders made with different aggregates,[3].

Table 4-11: Rebound Number of control and burned NSLWC, and HSLWC.

Symbol T-beam	**Age days**	**Average Rebound No.**	**Compressive strength f_{cu} (MPa)**	**Quality of concrete**
N-C-0	56	33	37.13	Good layer
N-F15		28	31.49	Fair
N-F30		20	22.48	destroyed layer
H-C-0	56	51	57.33	Very good hard layer
H-F15		36	40.5	Good layer
H-F30		30	33.76	Fair

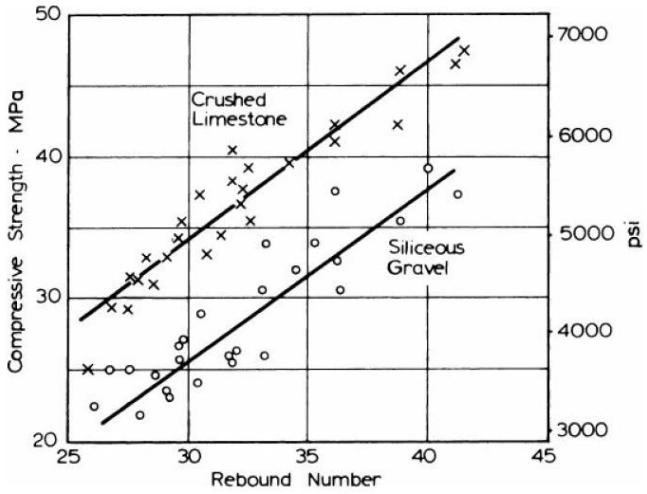

Figure 4-12: Rebound number - compressive strength relation

4.4 Experimental Results of T-Beam specimens

Fourteen T-beam specimens are tested, split evenly between two groups: those constructed from a NSLWC mixture and those constructed from a HSLWC mixture.

Four distinct subgroups may be extracted from each of these larger groups:

First, T-beams that are not subjected to fire and aren't repaired with SIFCON which used as a **control** in the study.

Second, T-beams that are burned for 15 and 30 min. we're not repaired.

Third, T-beams that had been exposed to fire repaired with a 15-mm SIFCON jacket.

Fourth, T-beams that are fire-exposed repaired by a 30-mm SIFCON jacket.

initial crack load, ultimate load, modes of failure, load-deflection behavior, and longitudinal strain distribution of each tested T-beam are all documented.

To accomplish this, a flexural loading mechanism with two points is used. T-beam deflection is measured at the specimen midspan and under the two-point loading position with three LVDT instruments at each loading step.

Gradual increase in load pressure is used by automatic hydraulic pressure to accelerate the breakdown of sample study.

The primary objective is to reduce the deterioration and spalling effects of the main sample lightweight concrete T-beam exposed to a burning flame by using SIFCON jackets as exterior reinforcements to strengthen the repaired T-beams.

The results of the T-beam testing, including the first cracking load, ultimate load, and residual ultimate load, are shown in (Table 4-12):

Table 4-12: First crack load, ultimate load, and maximum deflection for NSLWC and HSLWC T-beam specimens

Grade	T-Beams designation	First crack load kN	Ultimate load kN	Percentage residual ultimate load %
NSLWC	**N-C-0**	**64**	**243.5**	**100**
	N-F15	45	232.12	95.3
	N-F30	40	206.68	84.9
	N-F15-S2	80	265.17	108.9
	N-F30-S2	84	280.19	115.1
	N-F15-S3	88	301.23	123.7
	N-F30-S3	94	330.9	135.9
HSLWC	**H-C-0**	**75**	**270**	**100**
	H-F15	49	247.9	91.8
	H-F30	45	233.8	86.6
	H-F15-S2	98	303.5	112.4
	H-F30-S2	91	325.9	120.7
	H-F15-S3	95	254.7	94.3
	H-F30-S3	118	259.3	96

4.5NSLWC and HSLWC T-Beam Load Carrying Capacity

When testing T-beams, the load-carrying capacity represents the maximum allowable load before the machine reading drops and rapid deformation of the T-beam occurs, indicating failure. Investigating and summarizing the pre- and post-fire features of NSLWC and HSLWC T-beams is necessary for studying the influence of fire exposure on the load-carrying ability of T-beam specimens as follows:

4.5.1 Behavior of NSLWC T-Beams Before and After Burning (Group One)

In this research, the behavior of **NSLWC T-beam** specimens is studied by looking at a number of crucial indicators closely linked to their load-bearing capability. The first sign is a distinctive pattern of cracks that appears when the crack grows in tandem with the external strain, small flexural cracks of limited magnitude developed initially in the pure bending area, reference T-beam, and fire-damaged specimens that have not been repaired (near mid span).

The stress-cracking pattern seen in both the original and damaged samples is identical. When the stress is raised, cracks appeared in both the reference and damaged specimens, and the cracks in the damaged specimen grew larger. When comparing the cracking loads, it was found that the reference has a value of (64) kN and the damaged specimens is (45 and 40) kN, the initial crack started at the mid-span area. It is possible that steel reinforcement effects contributed to the heat-damaged specimens by reducing cracking load. Cracks started showing up within the shear span areas in response to the increased stress because the residual tensions of steel after cooling burnt specimens are significantly higher than those of unburnt LWC. Cracks normally start vertically began migrating in oblique directions due to the presence of shear forces, causing cracks in the shear span to bend towards the loading point and produce diagonal cracks. Within a short amount of time, the developed diagonal crack has spread virtually the whole length of the T- beam. Stress redistribution leads the development of secondary cracks, some of which developed in the T-beam's lowest 100 mm, as shown in (Plate 4-3). When the concrete in the compression zone cracked, the T-beam would withstand a greater weight for a shorter period of time. When the steel in support T-beams gave way, cracks propagated in the compression area toward the loading sites, shattering the concrete just below the load centers. Flexural with yielding of stirrups is the mode of failure for the control T-beams.

Plate 4-3: Reference Cracks shape "pattern" of NSLWC T-beams.

Fired-damaged T-beams, on the other hand, reveal a quick shear failure, most likely due to the losing in shear strength of concrete caused by heating, as in (Plate 4-4). After burning the angle of diagonal cracks inclination is slightly larger, also the extension is little shorter and almost similar on both sides, while hinge side seems longer before burning. The secondary cracks form more after burning and appear so close to each other.

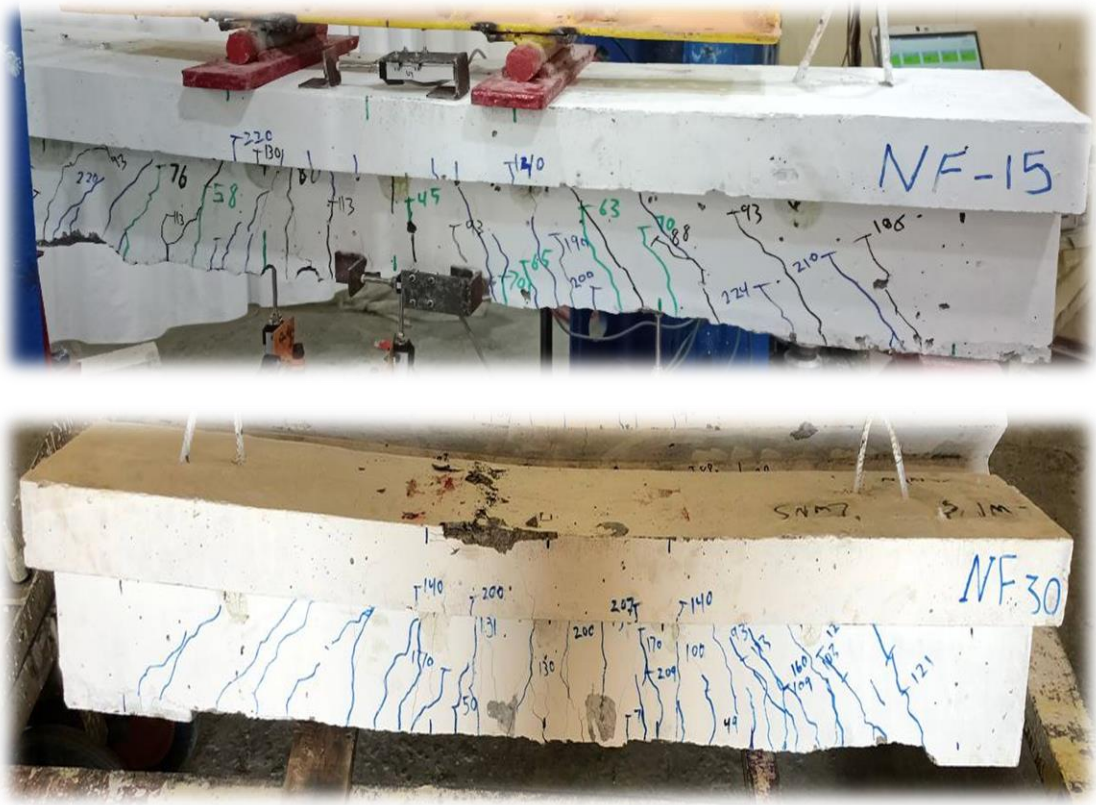

Plate 4-4: Crack's pattern of NSLWC T-beams after burning.

The structural behavior of the T-beam specimen can be studied in relation to the load carrying capacity with different SIFCON jacket thicknesses. There is increase in bending capacity, in thickness of the jacket increases (section

depth) and the ultimate load specimen, which means a good repair to the burned-damaged concrete as presented in (Figure 4-13).

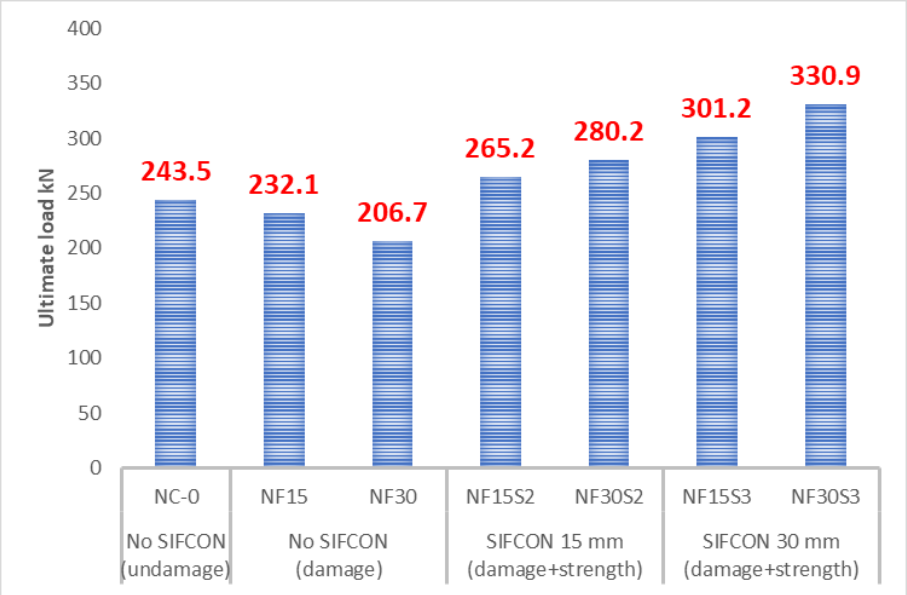

Figure 4-13: Effect of load carrying capacity of NSLWC T-beams with different SIFCON jacket thickness.

4.5.2 Behavior of HSLWC T-Beams Before and After Burning (Group Two)

The behavior of **HSLWC T-beams** is approximately similar to that in **NSLWC**, as in (Plate 4-5) when a crack forms to the left of the load's application in the bending zone, and then further cracks form to the left of the initial cracks in a vertical direction; finally, diagonal cracks form and propagate between the support and applied load locations. (Plate 4-6) evidence that burning increases the inclination angle of diagonal cracks, shortens cracks' extensions, and reduces cracks' numbers.

Prior to the formation of the diagonal cracks, several small cracks appear in the shear zone and at less rate in bending zone as well. **HSLWC** behaves with a much higher sensitivity than **NSLWC** to burning, where after (650°C) of burning, spalling is noticed to be occurred.

The vapor in the **HSLWC** particles found it difficult to exit through the surface, resulting in concrete spalling.

Rapid spalling of the concrete's surface increases the rate of heat

transmission to the T-beam core and reinforcement by exposing them to direct flame.

Plate 4-5: Cracks pattern of HSLWC T-beam before burning

Plate 4-6: Cracks pattern of HSLWC T-beams after burning.

After burning, the results showed a great convergence of the load capacity, which can be attributed to the influence of the steel reinforcement by a slight amount that allowed to reduce difference that is caused by increasing effective depth, what reinforces this hypothesis is that the difference in resistance has decreased from about 8% after burning for 15 min. to about 1.4% after burning for 30 min. The effect of the concrete cover as a protection factor for the rebar, and thus its effect is greater, which changes the amount of its sustainability to the resistance loads.

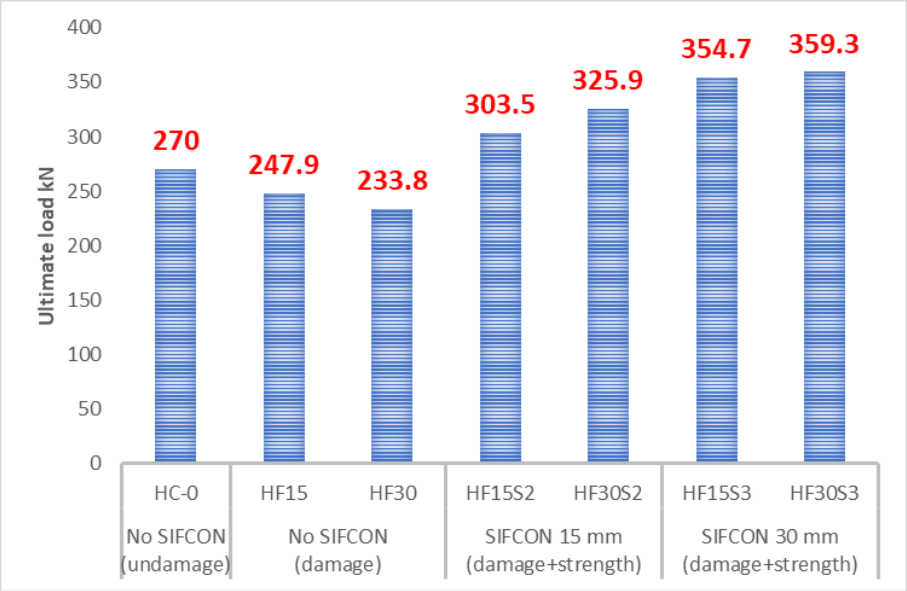

Figure 4-14: Exposure fire duration effect on HSLWC T-beams load carrying capacity with different SIFCON jacket thickness.

4.6 Load-Deflection of NSLWC T-Beam Specimens

All of the curves exhibited elastic behavior before to cracks and inelastic behavior after cracking. The ultimate load-carrying capability of NSLWC LWC T-beams subjected to 30min. is drastically reduced, as shown by the test results. The NSLWC T-beams decayed at a rate of (22,3%).

There is a clear decrease in the load Deflection behavior after burning as shown in (Table 4-12) and (Figure 4-15) for 15 min. and 30 min. compared to the control specimen. While NF15 shows a linear behavior up until the failure load and very little hardening, NF30 shows more ductility but was about on par with NF15 in terms of load capacity. Additionally, in contrast to the NF30, the NF15 is effective at maintaining maximum load for a significant distance.

Increased load capacity, increased stiffness, nearly linear behavior till failure load, decreased ductility, and reduced absorption energies are seen in the fire damaged specimens strengthened with 15 and 30 mm after 15 min. of fire exposure, as compared to un strengthened specimens.

Compared to NF15S2, NF15S3 is demonstrated greater load capacity. Strengthening with a 30 mm SIFCON jacket resulted in increasing stiffness, load capacity, and ductility for specimens exposed to fire for 30 min. (NF30S2

and NF30S3).

In addition, the behavior is nearly linear up until the failure load, after which it failed suddenly without being able to maintain the peak load for a sufficiently large Deflection.

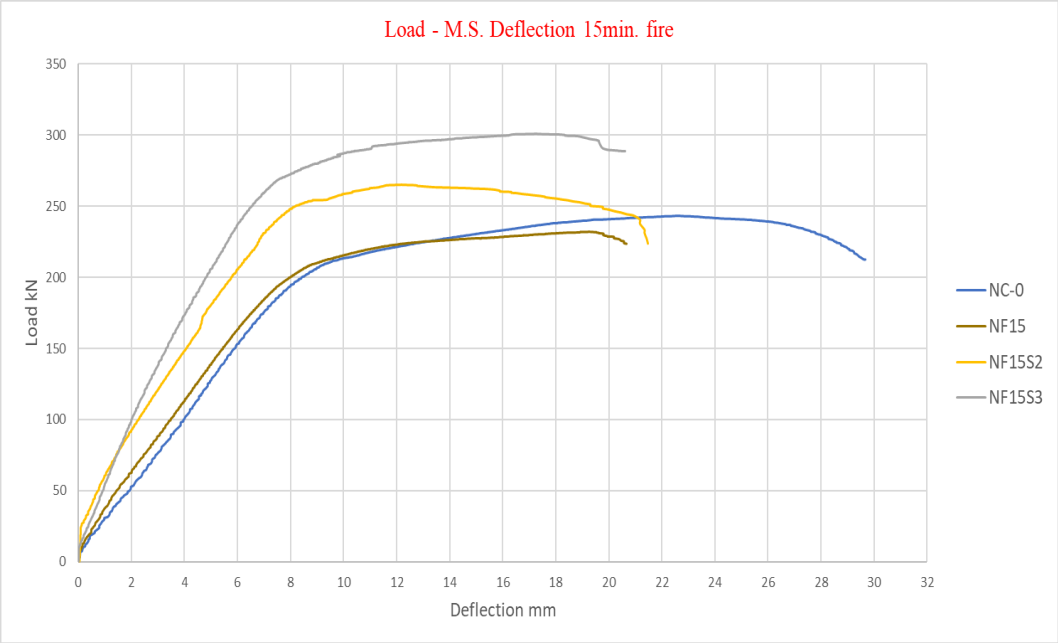

A

B

Figure 4-15: Load versus deflection at mid-span of NSLWC T-beam specimen before and after exposure to fire.

4.7 Load-Deflection of HSLWC T-Beam Specimens

When applied to a high-strength lightweight reinforced T-beam, a SIFCON jacket raise the ultimate load capacity by 22.4% and 43% for 15 min. also by about 39.4% and 53.7% for 30 min., respectively, after fire damage. These results show that technique is effective in increasing bearing capacity during strengthening.

The load Deflection curves of undamaged, burning for 15 min. and 30 min. cause a damage, where SIFCON strengthen of damaged HSLWC T- beams is shown in (Figure 4-16). All of the examples shown in the aforementioned diagram have a concrete covering of 10 mm. After strengthening with a 15mm and 30mm SIFCON jacket, there is no yield loading is seen until attaining failure loading, the linear behavior of reinforced specimens with a SIFCON jacket until the peak load might be seen as a drawback. When compared to the exposed specimens, the reinforced ones showed sharper behavior in the deteriorated region of the curves, which indicates that the specimens failed to endure the maximum load for tolerable limit (ductility issue). Note that, in contrast to the exposed samples, the strengthened ones showed no signs of yielding under stress. Moreover, the maximum load capacity of strengthened T-beams is represented by a smaller mid-span Deflection.

A 30-minute fire exposure drastically weakens LWC T-beams, **HSLWC** T-beams decayed at a rate of 40.3% and 37.4%, respectively. After 15 and 30 min. of burning, the load Deflection behavior exhibited a clear decline in comparison to the reference specimen HC0. Over all, HF30 has demonstrated more ductility. Also, unlike the HF30, the HF15 is able to effectively maintain maximum load for a significant distance.

Increased load capacity, increased stiffness, nearly linear behavior till failure load, decreased ductility, and reduced absorption energies are seen in fire exposed specimens strengthened with 15 and 30 mm after 15 min. of fire

exposure, as compared to un strengthened specimens. Compared to HF15S2, HF15S3 has demonstrated greater load capacity.

A

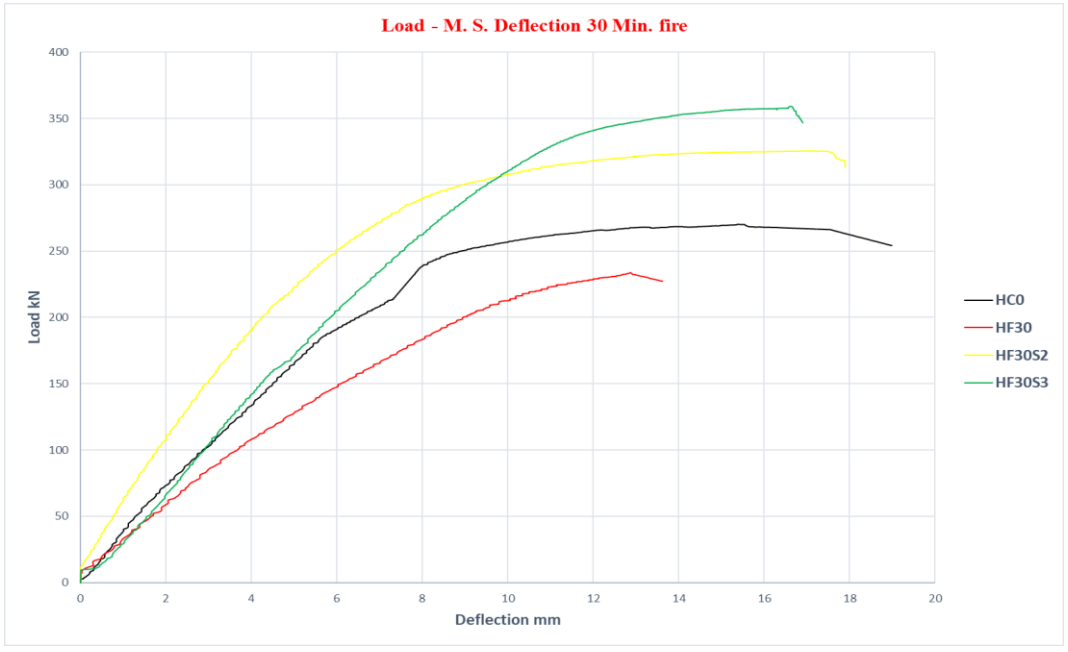

B

Figure 4-16: Load - deflection curve at mid-span of HSLWC T-beam specimen before and after exposure to fire.

For specimens subjected to fire for 30 min., strengthening with a 15 and 30 mm SIFCON jacket enhances stiffness and load capacity for samples (H-F30-S2 and H-F30-S3). Behavior is virtually linear up to the failure load, but then it suddenly fails without being able to hold the peak load for a long enough

time. When failure occurs especially in the elastic zone samples exhibit linear behavior and steep slope.

4.8 The effect of concrete cover

It can be shown, that the concrete T-beam cover has larger amount of loses after burring, due to limitation cover and internal vapor pressure based on the test results of huge spalling, its needs to increase for future research.

Plate 4-7: Spalling after burning T-beam

Increased cover thickness can delay corrosion caused by carbonation and chloride by lengthening the time it takes for those elements to enter concrete reinforcement. Provide thermal insulation, which protects the reinforcement bars from fire, and embedding reinforcement bars deeply enough, so that they remain stationary under strain. Also, to prevent exposure of reinforcement to harsh external conditions and the ensuing rusting and degradation of the cross-sectional area in the structural elements, sufficient concrete cover must be supplied in the reinforced concrete constructions.

4.9 Effect of Fire Exposure on Steel Reinforcement

Steel reinforcing bars are not likely to be significantly impacted by high temperatures if they are provided the minimal amount of protection mandated by building codes. However, structural instability and damage are possible

outcomes of deformation brought on by thermal expansion and the loss of connection between concrete and steel. Many people think that steel reinforcing bars need to be shielded from temperatures over 250°C to 300°C because low-carbon steels exhibit blue brittleness between (200 and 300°C) (**Ünlüolu et al., 2007**),[95]. To examine what happens to steel reinforcing bars when they are exposed to fire, we split them into three groups of 12mm in diameter: 1st group and 2nd group samples of steel reinforcement is implanted into HSLWC and NSLWC T-beam specimens, where 3rd samples are exposed directly to fire flame without concrete cover for two times (15 and 30) min. After three sets of samples are burnt at 700°C as a mean temperature, attained by the ISO-834 chart to which T-beams are subjected to fire, the bar reinforcement steel is recovered from the concrete and done the test of yield stress. Results from yield stress tests on reinforcing bars before and after exposure to 700°C were compared to the control sample as in (Table 4-13).

Table 4-13: Fire exposure effect on the yield stress of steel reinforcement bar

Group No.		**Temperature (°C)**	**Fire exposure (min)**	**Yield Stress f_y (MPa)**	**Reduction Ratio %**
Control	Non exposed	25	-----	**420**	---
Group One	NSLWC	700	15	404.8	3.62
	HSLWC			392.7	6.5
Group Two	NSLWC	700	30	403	4.05
	HSLWC			388	7.62
Group Three	Unprotected	700	15	386.3	8.02
	Unprotected		30	300.2	28.52

As showing in (Table 4-13), the yield stress is reduced by 3.62 and 6.5% for NSLWC and HSLWC, respectively, when exposed to fire for longer than 15 min. for T-beams. The reductions for NSLWC and HSLWC for 30-minute-burning T-beams are 4.05% and 7.52%, respectively. Objects that are put in direct contact with the flames have an 8.02% and 28.5% decreased with fire burning times of 15 and 30 min., respectively. The yield stress reduction for NSLWC is found to be 3.2% and 3.3% lower than for HSLWC T-beams, suggesting that NSLWC provides greater protection for reinforcing bars than

HSLWC under the same fire exposure conditions. Lightweight concrete is suited for use in high-temperature applications due to its low heat conductivity up to 400 °C and very modest rise to over 700 °C while it's not comfortable over that.

4.10 Effectiveness of SIFCON Jackets

Using **SIFCON** to repaired T-beams increases shear strength in four distinct ways. **First**, they lend strength to the longitudinal bars and stirrups by giving them something to rest against applied force. **Second**, the fibers critical function in bridging and transporting tension strains across both sides of a diagonal crack to restrain its spread. **Third**, they enhance T-beam ultimate strength and performance under service loads by delaying the onset of initial flexural and shear cracking in reinforced concrete T-beams. **Finally**, flexural failure is employed instead of shear failure where caracks failure at mid span. Research is conducted on the performance of T- beams subjected to a two-point loading system using SIFCON as an external jacket along the bottom and both sides of the T-beam. The criteria such as strength, stiffness, ductility, and energy absorption were checked. (Figure 4-17) and (Figure 4-18) display test results that demonstrate how employing a **SIFCON** jacket improved the ultimate load bearing capability of T-beam specimens.

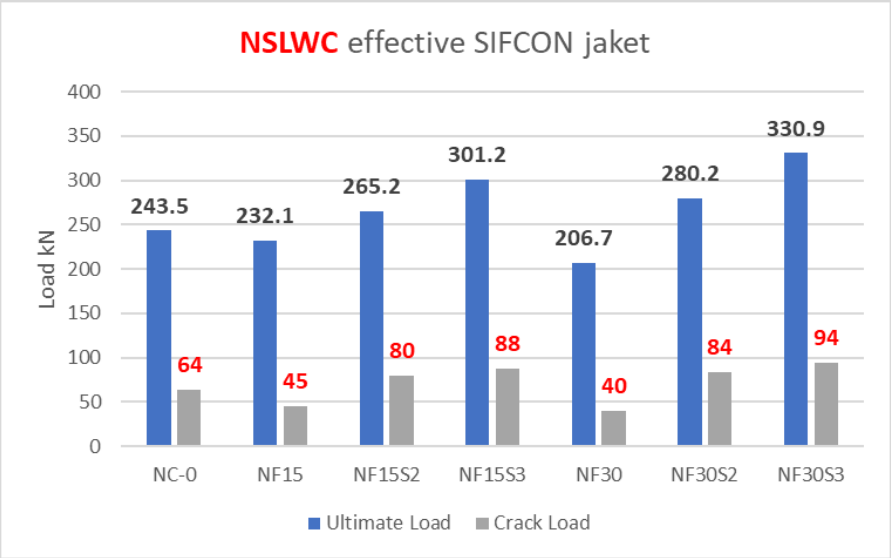

Figure 4-17: Effectiveness of SIFCON jacket on the load carrying capacity of NSLWC T-beams before and after burning

Two axes can be used to discuss the efficacy of the SIFCON jacket in developing the models load carrying capacity. **The first** is the general effect of the reinforcement, where it is found that the use of the SIFCON jacket significantly increases the models load carrying capacity, by 159%-207% for normal strength concrete and 180%-220% for high strength concrete. **The second** impact is that of increasing the thickness of the SIFCON jacket, which is shown to clearly increase the load carrying capacity of the models across all investigated situations by improvement rates of 109%–135% for **NSLWC** and 112.4%–133% for **HSLWC**.

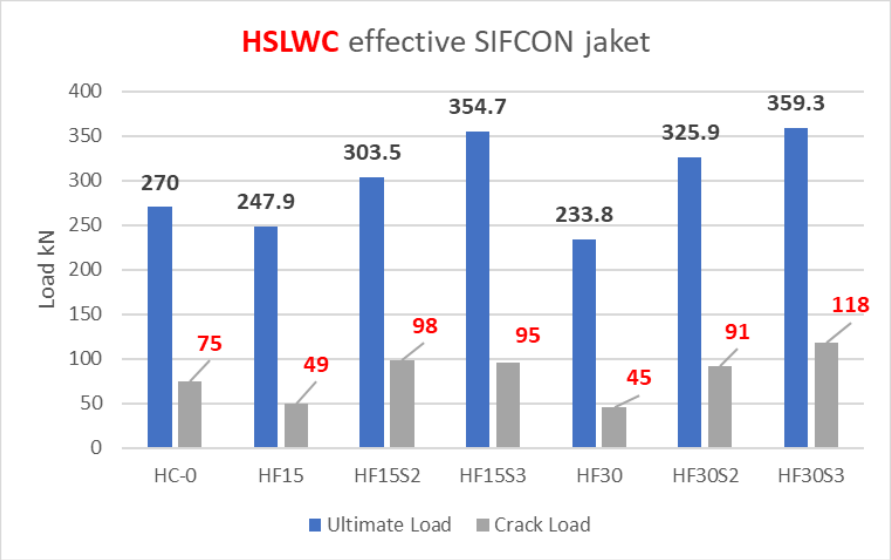

Figure 4-18: Effectiveness of SIFCON jacket on the load carrying capacity of HSLWC T-beams before and after burning

T-beam integrity is maintained all across the post-cracking Segment s of behavior due to the effectiveness of steel fibers in preventing the propagation and restricting the growth of flexure and diagonal cracks inside the T-beam when they cross them. Thus, the T-beam could be able to withstand greater loads and deflections before giving way. Repairing a lightweight broken concrete T-beam with **SIFCON** saves money and time compared to more traditional alternatives, and the results show that it can attain a compressive strength of 93.56 MPa in 7 days. In other words, compared to the time required for repairs using traditional concrete methods, the T-beam is returned to service in a much shorter amount of time.

4.11 Ductility Index

The ability of a material or member to sustain deformation beyond the elastic limit while maintaining a decent load carrying capacity until total failure is defined as ductility. In this way, ductility reflects the total area ratio under the load-deflection curve to a portion area extended up to the service loads.

Ductility may be computed using the formula:

$$\mu = \frac{\Delta u}{\Delta y} \qquad \textbf{4-2}$$

Where μ = Ductility Index.

Δ_u = represents the maximal deformation at failure.

Δ_y = deformation as a result of material yielding.

Δ_y = founded from the load- deflection curves through the intersection point of the curve tangent lines,

where Δ_y represents the deflection opposite this point, (**Azizinamini et al.,1999**)[60] , as shown in (Figure 4-19), (Figure 4-20) and (Figure 4-21).

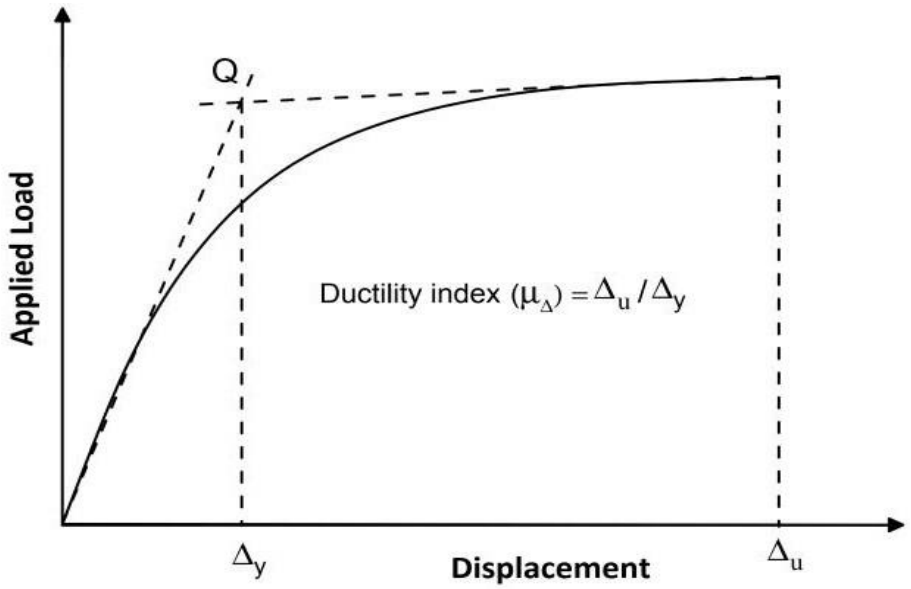

Figure 4-19: Result the value of Δ_y using the load-deflection curve (Azizinamini et al.,1999)

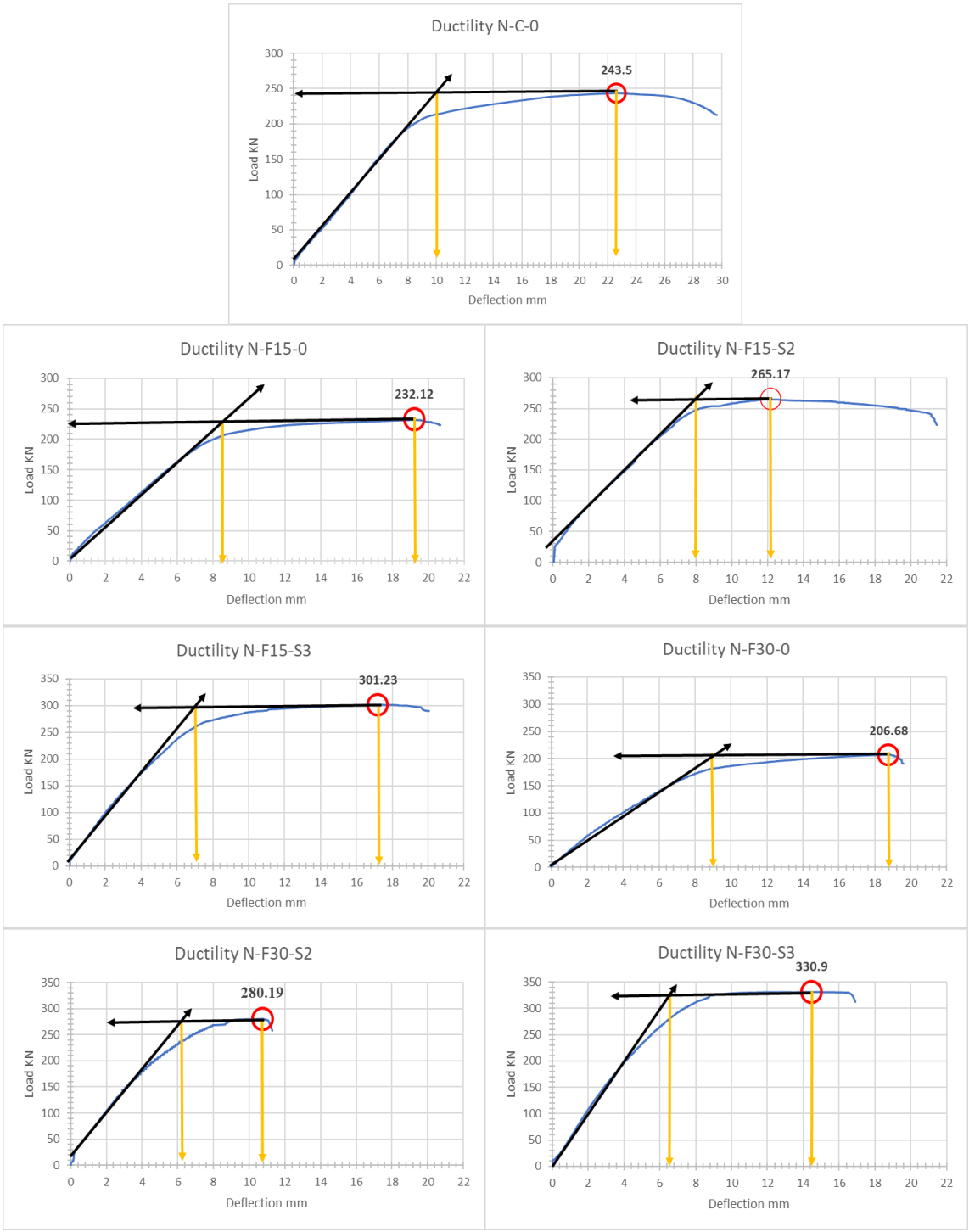

Figure 4-20: Calculating the yield Deflection point on load –deflection curves of NSLWC.

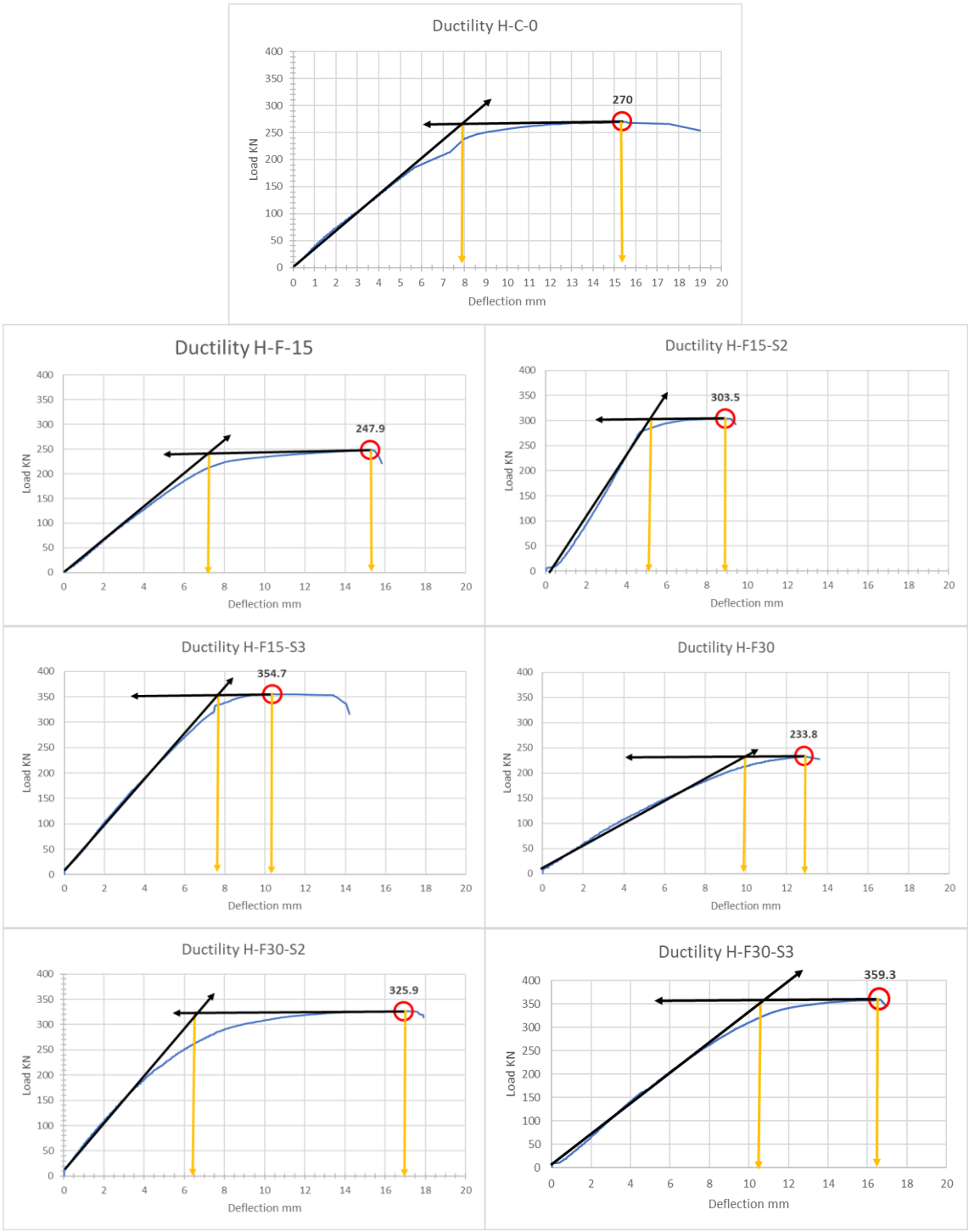

Figure 4-21: Calculating the yield Deflection point on load –deflection curves of HSLWC.

Table 4-14: Ductility Index for NSLWC and HSLWC T-beam

Sym.	Yield Deflection Δy mm	Ultimate Deflection Δu mm	$\mu = \frac{\Delta u}{\Delta y}$
N-C-0	10.25	22.65	**2.21**
N-F15	8.75	19.15	2.19
N-F15-S2	8.03	12.21	1.52
N-F15-S3	7.16	17.25	2.41
N-F30	9.16	18.75	2.05
N-F30-S2	6.44	10.82	1.68
N-F30-S3	6.6	14.45	2.19
H-C-0	7.85	15.45	**1.97**
H-F15	7.25	15.28	2.11
H-F15-S2	5.11	8.93	1.75
H-F15-S3	7.63	10.4	1.36
H-F30	9.91	12.86	1.3
H-F30-S2	7.15	16.88	2.36
H-F30-S3	10.51	16.66	1.59

Form (Table 4-14) ductility index ranged from 1.30 to 2.36 for the T-beam samples that were examined both before and after exposing them to fire.

For NSLWC, the testing results show that fire damage for 15 min. has slightly affected, where the strengthening damaged T-beam resulted decreases by 30.6%. While the ductility index is improved by 1% for T-beam with 15mm and 30mm SIFCON jacket respectively when compared with the fire unstrengthen members N-F15 while for 30 min. burning T-beam decreased by 18% while improved by 6.8% when compared with fire unstrengthen N-F30.

On the other hand, the ductility index is decreased by 31.22% and enhanced by about 9.05% when compared with un-strengthened undamaged (reference) T-beam with 15 and 30 mm SIFCON jacket cover respectively, as can be seen in (Figure 4-20) and (Figure 4-22).

A high ductility index is indicative of a structural member ability to resist large deformations without failure. After 15 min. of fire exposure, the ductility index for NSLWC T-beams declined by 0.09%, while the ductility index for T-beams exposed for 30 min. decreases by 7.23% comparing to reference. Due to the fact, that the ductility index is calculated based only on the displacement

of the T-beams, NSLWC T-beams show a more gradual and linear load-displacement response after being exposed to fire, this decrease in ductility can be due to deterioration of both concrete and steel mechanical properties.

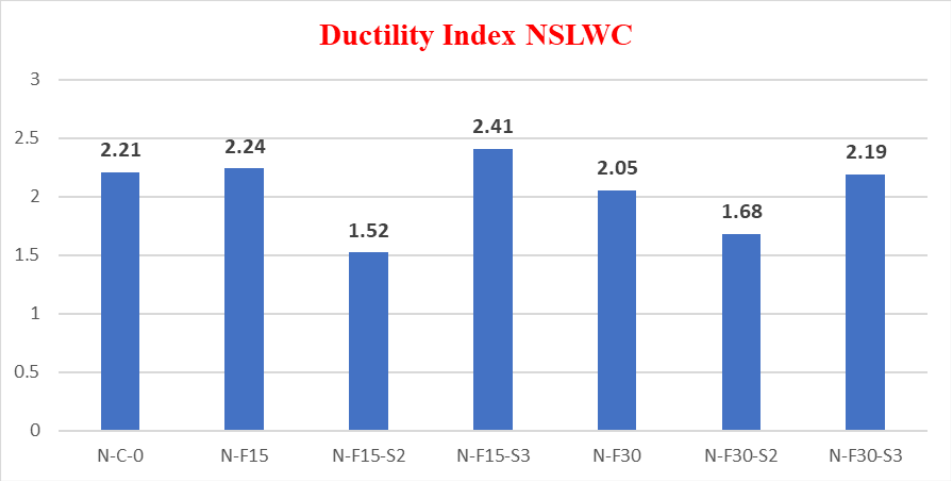

Figure 4-22: Ductility values of NSLWC with different fire exposure time before and after burning

The results of HSLWC comparing to control T-beam show that the ductility index has a slight increase T-beams exposed to (15min.) showing ductility index of (7.10 %) and a decrease (34%) after exposed to (30 min.) as showed in (Figure 4-21) and (Figure 4-23).

In comparing with unstrengthen damage HSLWC T-beam for 15 min. ductility index decrease by 17% and 35.5% while for 30 min. burning ductility increased by 81.5% and 22.3% for 15 and 30 mm SIFCON jacket respectively.

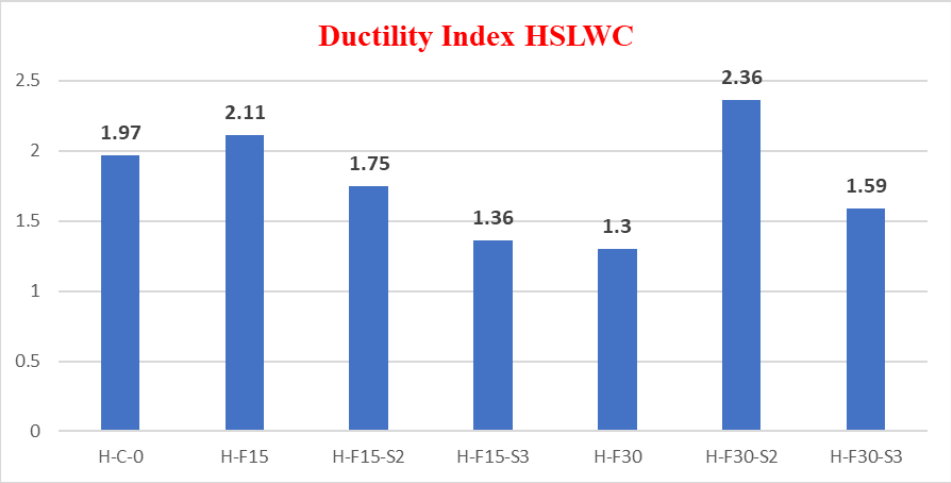

Figure 4-23: Ductility values of HSLWC with different fire exposure time before and after burning

Furthermore, when temperature increases, the bonding strength between reinforcing bars and concrete decreases, indicating that reinforcing bars are unable to acquire adequate strength.

4.12 Flexural toughness "Energy Absorption"

The area under a load-deflection curve is a measure of flexural toughness, which is amount of energy needed to deflect beam by a certain amount, [96].

The area bounded by the load-deflection curve up to the point when the maximum load is attained represents the energy absorption capacity of the concrete T-beam, and hence the maximum load that the beam can support before showing significant deformation.

Energy absorption capacity calculated from an estimate of the area enclosed by the load-displacement curve for each T-beam, has been proposed as a more relevant metric for gauging ductility in light of the decrease in load carrying capacity for these T-beams after fire exposure.

The energy-absorbing capacity is the best measure of a concrete structure ability to endure the effects of natural disasters like earthquakes, as well as man-made ones like fires and terrorist bombings.

(Table 4-15) displays the result from testing the NSLWC and HSLWC T- beams for their ability to absorb energy both before and after exposed to fire, where NSLWC has better energy absorption capacity than HSLWC.

NSLWC T-beams have a residual energy absorption capability of 72.4% of the reference T-beam at a burning temperature, (Figure 4-24) displays the range of residual energy absorption capability after SIFCON jacket, which is between 64% and 70% of the reference T-beam.

(Figure 4-25) shows that after being burned for 30 min. the HSLWC T- beam suffered substantial damage, with a residual energy absorption capability of just 45 %. This figure rises to between 126.2% and 111.1 % after being reinforced with a SIFCON jacket for 15 and 30 mm respectively.

Table 4-15: Energy absorption capacity of NSLWC and HSLWC lightweight concrete T-beams

Concrete grade	Sym.	flexural toughness (kN.mm)
NSLWC	N-C-0	**4179.1**
	N-F15	3429
	N-F15-S2	2258.1
	N-F15-S3	4057.1 *
	N-F30	2898.1
	N-F30-S2	2088.6
	N-F30-S3	3582.3
HSLWC	H-C-0	**2974**
	H-F15	2725.8
	H-F15-S2	1835.5
	H-F15-S3	2348.1
	H-F30	1872.7
	H-F30-S2	4236.6
	H-F30-S3	3952.8

* Refer to the beast T-beam sample that's repaired.

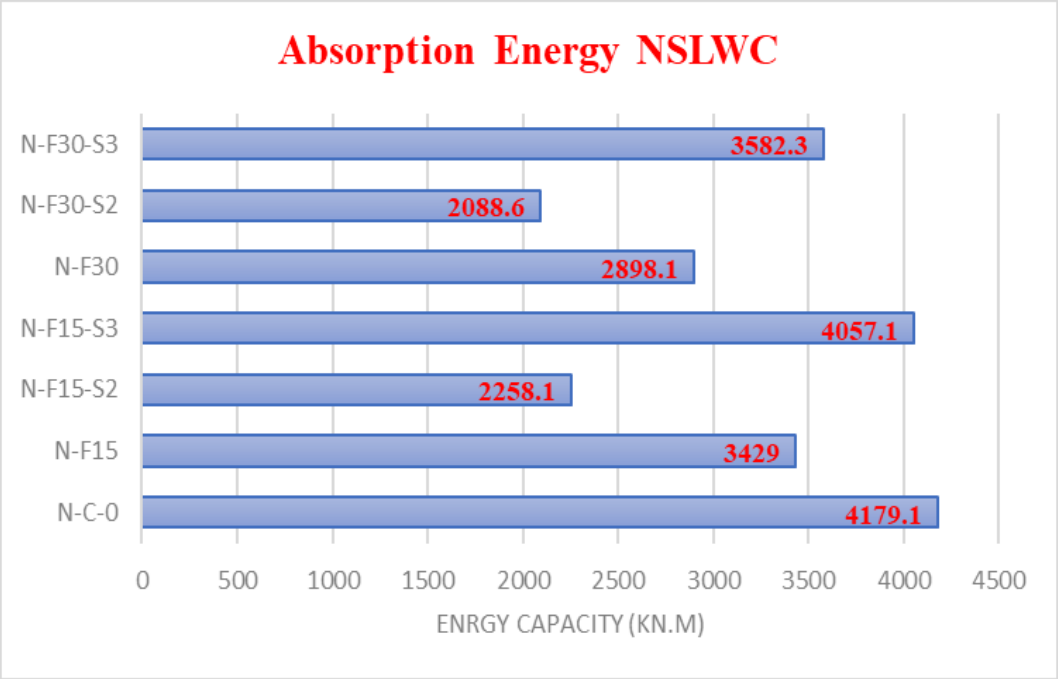

Figure 4-24: Values of energy absorption capacity for NSLWC before and after burning and strengthening

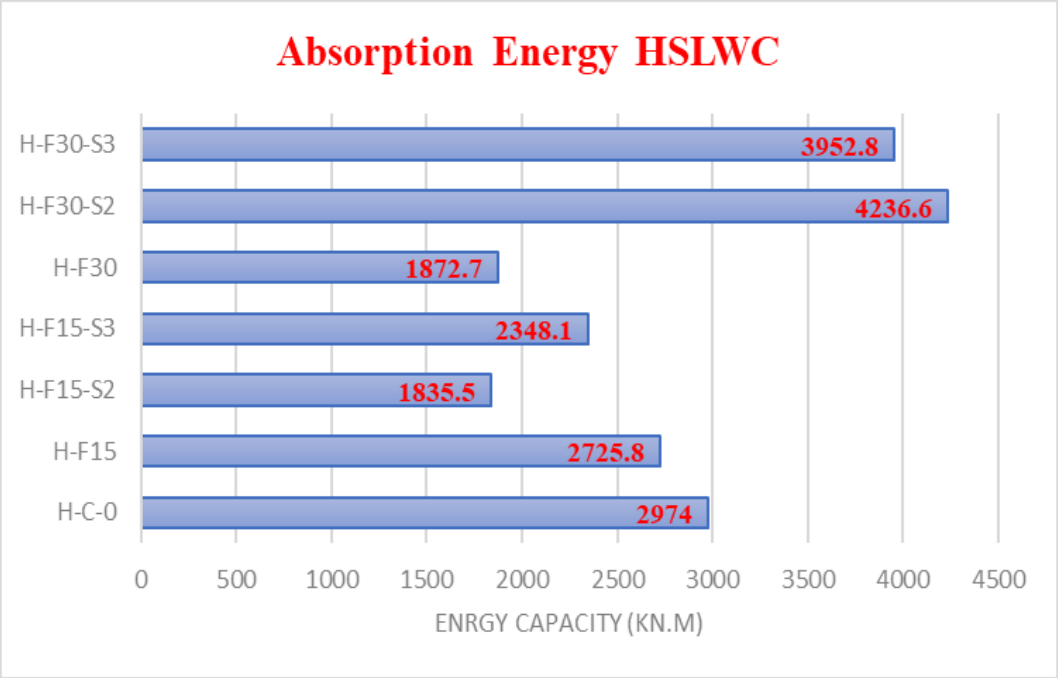

Figure 4-25: Values of energy absorption capacity for HSLWC before and after burning and strengthening

4.13 Initial and Secant stiffness

A beam stiffness is measured in terms of the force required to generate a single unit of beam deflection.

There is a significant increase in secant and decrease initial stiffness after burning at varying exposure times, and this is followed by a decrease in load bearing capacity when the fire burning temperature was increased. At room temperature HSLWC T-beams have a secant stiffness of 100% but after 30 min. of burning at 650°C, it has reduced to around 73%. Nevertheless, after being burned for 30 min. at 650°C, the secant rigidity of NSLWC beams fell from 100% at ambient temperature to roughly 72%. SIFCON jacket repairs result in a greater stiffness value for the 30mm jacketed specimens than the 15mm covered ones (HSLWC and NSLWC). As can be seen in (Table 4-16), the repaired specimens also have an increased rigidity compared to the control specimens, and the damaged specimens exhibited the greatest initial and secant stiffness, as well as the maximum load bearing capacity compared to the (damaged and undamaged) specimens.

Table 4-16: Secant and Initial stiffness of NSLWC and HSLWC T-beam

Sym.	Secant Stiffness				Initial Stiffness			
	Pu	Δu	Ks kN/mm	Residual Ks %	Pu	Δy	Kin kN/mm	Residual Kin%
N-C-0	**243.5**	22.65	**10.75**	----	**243.5**	10.25	**23.76**	----
N-F15	232.1	19.15	12.12	112.74	232.1	8.55	27.15	114.27
N-F15-S2	265.2	12.21	21.72	202.05	265.2	8.03	33.02	138.97
N-F15-S3	301.2	17.25	17.46	162.42	301.2	7.16	42.07	177.06
N-F30	206.7	18.75	11.02	102.51	206.7	9.16	22.56	94.95
N-F30-S2	280.2	10.82	25.9	240.93	280.2	6.44	43.51	183.12
N-F30-S3	330.9	14.45	22.9	213.02	330.9	6.6	50.14	211.03
H-C-0	**270**	15.45	**17.48**	----	**270**	7.85	**34.39**	----
H-F15	247.9	15.28	16.22	92.79	247.9	7.25	34.19	99.42
H-F15-S2	303.5	8.93	33.99	194.45	303.5	5.11	59.39	172.7
H-F15-S3	354.7	10.4	34.11	195.14	354.7	7.63	46.49	135.18
H-F30	233.8	12.86	18.18	104	233.8	9.91	23.59	68.6
H-F30-S2	325.9	16.88	19.31	110.47	325.9	7.15	45.58	132.54
H-F30-S3	359.3	16.66	21.57	123.4	359.3	10.51	34.19	99.42

(Figure 4-26) and (Figure 4-27) depict the stiffness of NSLWC and HSLWC T-beam specimens, respectively, discussed in ductility, the reduction in load carrying capacity of the T-beam specimens after exposure to fire resulted from the deterioration of concrete and steel reinforcement in both chemical and mechanical properties. This in turn leads to a reduction in the difference between yielding point and failure point values and a deterioration in the capacity of specimen to absorb applied loads with less deformation.

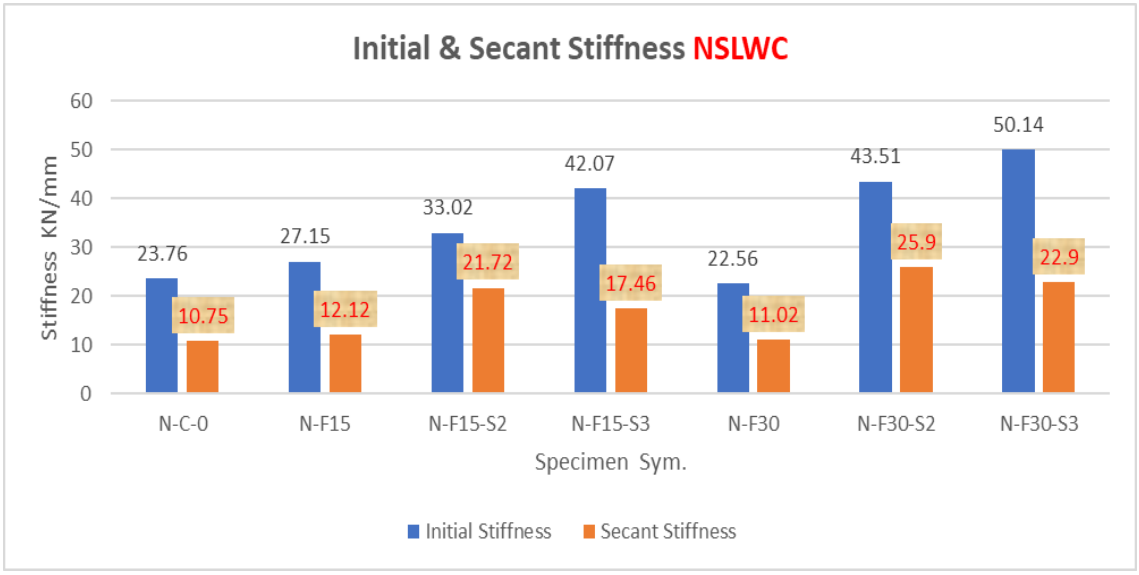

Figure 4-26: Secant and Initial stiffness of NSLWC T-Beam Specimen

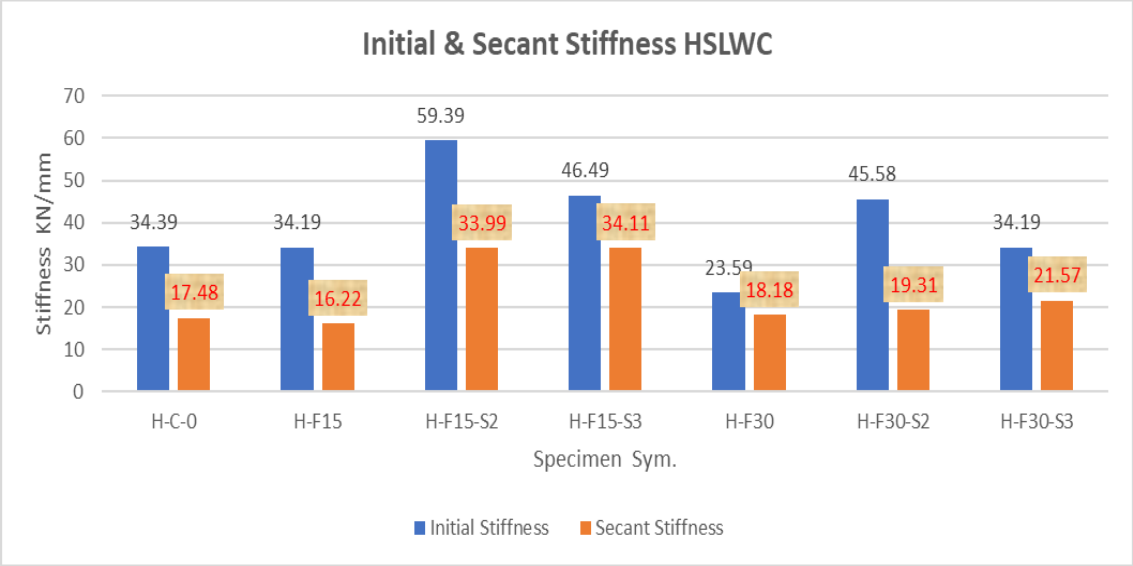

Figure 4-27: Secant and Initial stiffness of HSLWC T-Beam Specimen

4.14 Crack Width

Numerous researches have recently concentrated on the unpredictable nature of crack initiation and propagation in reinforced concrete structures since it can significantly affect structural stability and strength. With a width of less than 0.5 mm, cracks frequently start off as too small, elongated openings that are invisible to the naked eye. Despite the fact crack width restrictions are imposed by design standards and are based on empirical equations, cyclic/seismic stresses frequently lead to ambiguity in crack width propagation. The service life of a structure can be decreased by the entry of moisture, mist, saltwater, and chemical vapors into structural members. This can hasten the corrosion of steel reinforcement. The crack width starts and spread in reinforced concrete members could be calculated using classical theories by assuming the distribution of bond stress while a member is subjected to tension with constant bending moment.

Base and Murray developed the finite difference approach to calculate the crack response of concrete structures using numerical analysis on restrained elements. **Gilbert** created a series of formulas from computing the stresses in concrete and steel components, the quantity of cracks, and the average crack width, also applied fundamental equilibrium and compatibility principles,[60].

Since the steel reinforcement remained constant throughout all tested specimens in this study, the impact of the other element was investigated. Two factors, such as the steel stress and the burning fire duration, may primarily affect the crack width. Although concrete cover limitation is frequently ranked as the second most crucial factor affecting crack width.

As presented in (Figure 4-28),and (Figure 4-29), It's observed that the crack width in both types of concrete (NSLWC and HSLWC) obviously rise after burning for the same degree of applied load, and dramatically decreased after strengthening, which was attributable to the impact of SIFCON jacket in reducing the crack width. **SIFCON** is the best material for enhancing strength because of its low cost, ease of fabrication, and compatibility with both specialist and regular construction machinery.

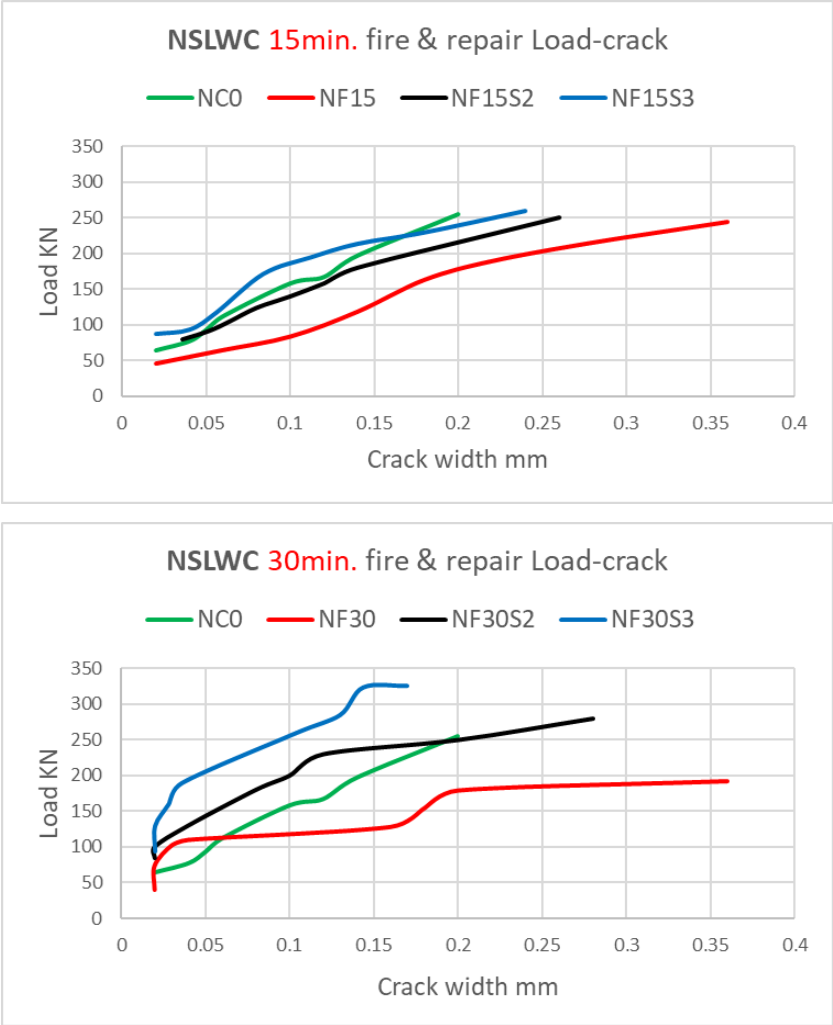

Figure 4-28: Relation between applied load and crack width for NSLWC before and after burning

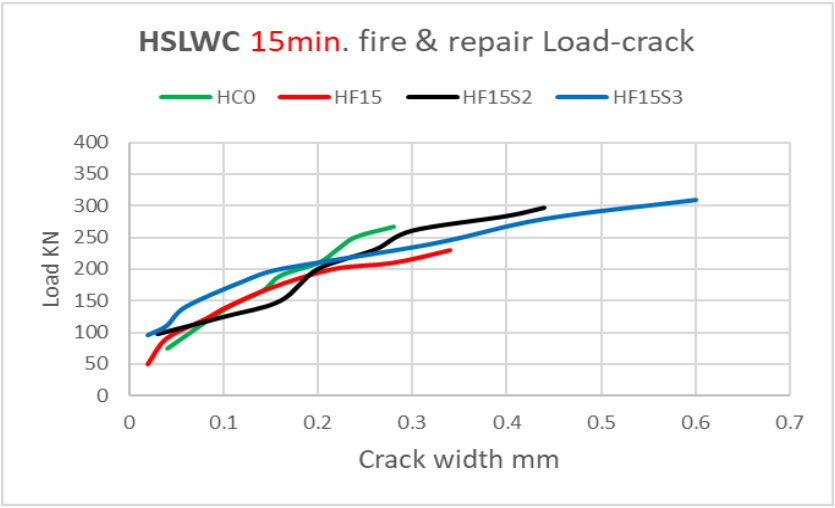

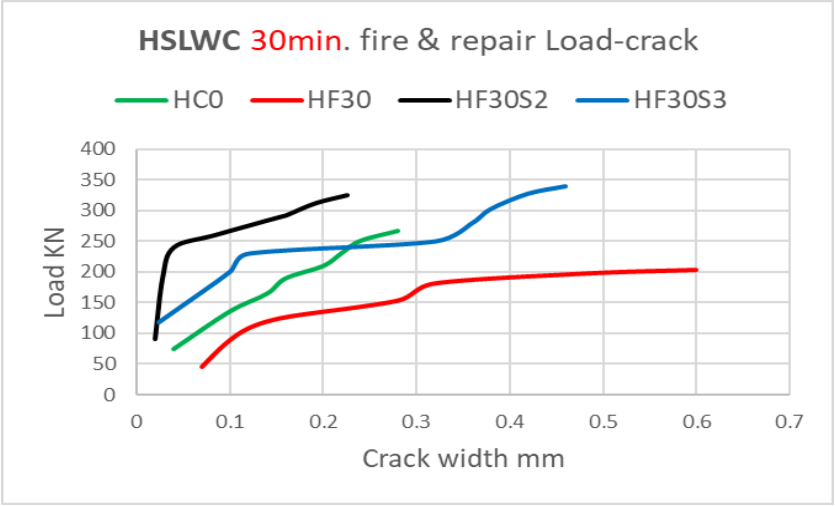

Figure 4-29: Relation between applied load and crack width for HSLWC before and after burning.

4.15 Surface Condition and Fire burning Endurance of T- Beam Specimen

(Plate 4-8) shows that after a period of time when temperatures exceed 600°C for 30 min, random severe hairline cracks of widths 0.03-0.6 mm appeared on concrete surfaces.

The major and transversal reinforcing points of the concrete surface are in close proximity to the areas where the cracking is most severe. The expansion of the concrete mix element might have caused (a) significant tensile strains in the concrete, particularly at the reinforcing contact, and (b) the cement binder and aggregate behave differently to the high temperatures, resulting in the cracks.

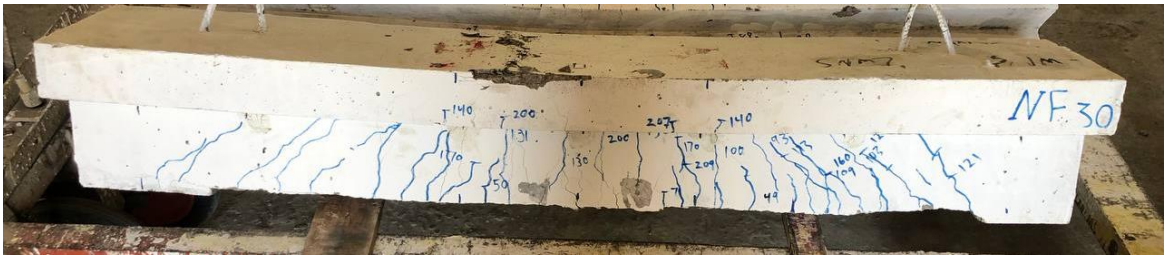

Plate 4-8: Hairline cracks after burning

Furthermore, the T-beam corner spalled concrete to a maximum depth of roughly 15 mm without exposing any steel. The T-beam was checked for curvature, but there none is found. The graph shows how T-beam temperature changes as a function of fire exposure time for NSLWC and HSLWC samples as presented in (Figure 4-30) and (Figure 4-31) respectively.

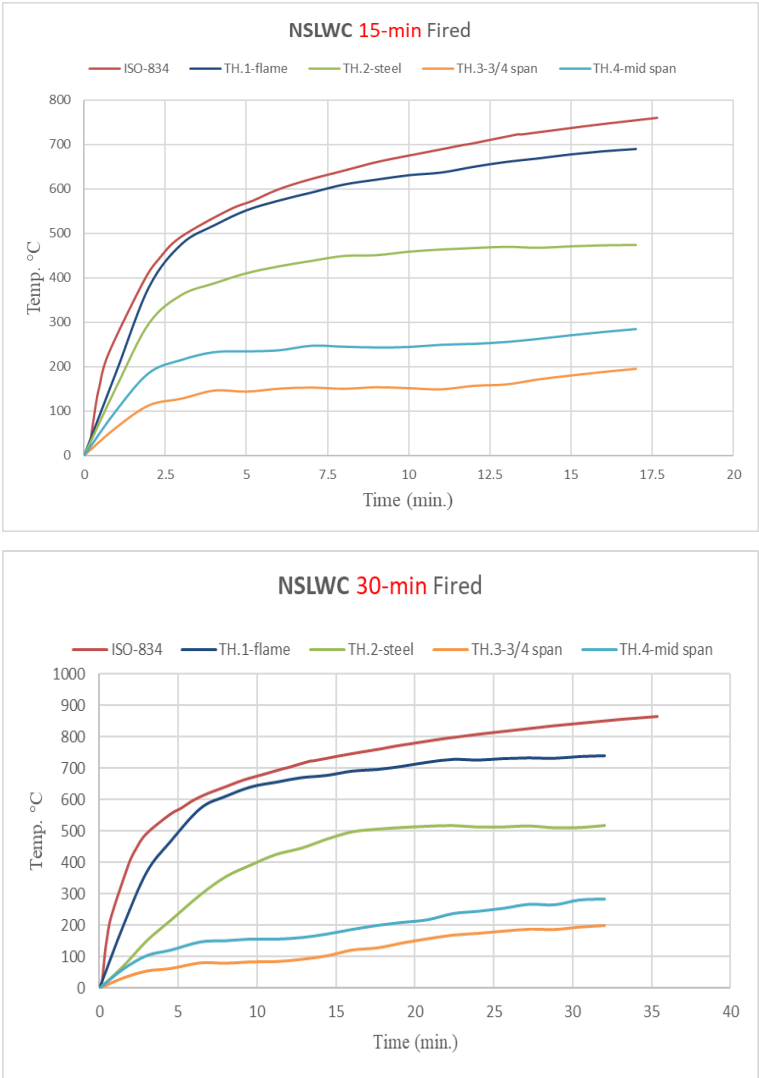

Figure 4-30: The relationship between measured temperatures and fire exposure time of NSLWC T-beam.

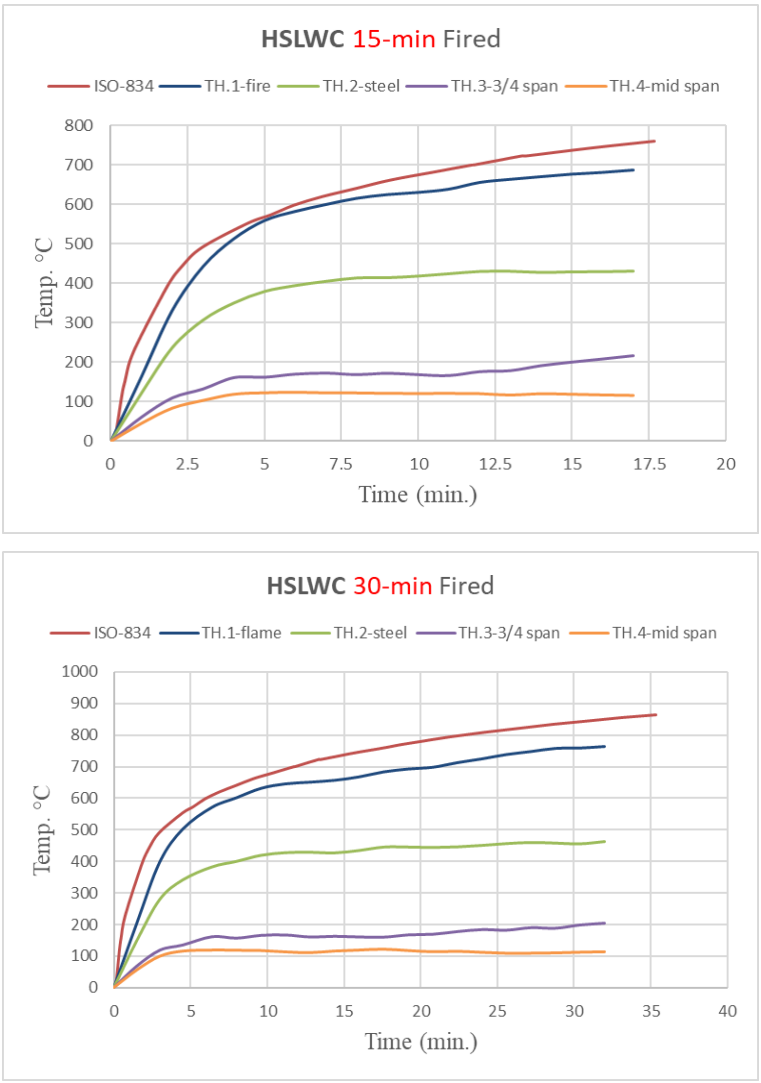

Figure 4-31: The relationship between measured temperatures and fire exposure time of HSLWC T-beam.

(Table 4-17) shows the location and identification of the thermocouples type K which is used in the study, with a deviation of 7% from the ISO-834 burning curve until the specified times are reached, this study successfully replicated the ISO-834 heating curve in the furnace. NSLWC and HSLWC T- beam covers have been shown to suffer damage and severe spalling as temperatures have risen. The concrete near the bottom of the T-beam is subjected to the greatest temperatures, therefore its compressive strength is predicted to decrease more than it does in the deeper sections of the specimen.

The restricted thermal conduction properties of concrete means that the temperature measured at TH.1 at the bottom of the T-beam is significantly higher than that at TH.4 at a distance of 125 mm. The temperatures at TH.3

and TH.4 at the intermediate depth of the T- beam were maintained at roughly 200 °C due to the evaporation pressure of water in the concrete and the consequent loss of heat. Temperatures decreased from the bottom to the top of the T-beam, indicating a distinct gradient. The concrete's strength around TH.3 and TH.4 decreased slightly compared to normal temperature concrete, but the peak temperatures of TH.1 and TH.2, which were higher than TH.3. As a quick summary, the concrete surface temperature reached over 600 °C while the temperature rapidly declined as it moved further inside the structure. Core concrete temperature ranged from around 200 to 240 °C. This mean that the outside layer of concrete was severely compromised and had to be removed before the usable inner concrete could be used. Compressive strength of NSLWC concrete is little impacted by temperatures up to 450 °C. It is common for NSLWC to be porous, allowing water vapor to readily disperse pore pressure. In contrast, the use of several binders in HSLWC produces a denser microstructure with less calcium hydroxide, leading to improve compressive strength at room temperature.

Table 4-17: Thermocouples Distribution

Sym. Thermocouple	Type	Space from exposed surface (mm)	Highest recorded temperature °C at time T-beam Fired			
			NSLWC 15min	NSLWC 30min	HSLWC 15min	HSLWC 30min
TH.1	K	0	690	739.7	686.7	763.8
TH.2	K	25	474.2	518.3	430.9	463.2
TH.3	K	200	194.5	198.9	217.5	205.7
TH.4	K	125	283.7	282.7	114.9	115.8

In contrast, the compact microstructure is highly impermeable and detrimental at high temperatures because it prevents moisture from escaping leading to pore pressure build-up and the rapid development of micro cracks in HSLWC, which leads to a faster deterioration of strength and occurrence of spalling and damage T- beam. Porous LWAC helped to soak up pressure and mitigate the rapid weakness that occurs when exposed to high temperatures.

Chapter Five

Finite Element Modelling and Simulation

5.1 General "Overview"

The development of numerical solver software has been made possible by recent developments in computing technology and its wide acceptance. ABAQUS, created by the SIMULIA corporation, is one of the most important software suites of late. With the help of the finite element method, (ABAQUS ver.2021) can perform numerical simulations of a wide range of applications. This program is enhanced with a materials library that includes concrete, earth, metal, and a variety of failure modes concepts that account for how materials react to a variety of loads (mechanical, thermal, coupled, etc.).

Most academics recommend this kind of program for use in modeling and simulation because of the solid foundations upon which it rests, making it a flexible platform. This chapter provide an overview of the established **S**tandard **O**perating **P**rocedure (SOP) for modeling and simulating laboratory-tested concrete T-beams. By compare the finite element modeling results to the experimental data, pointing out key disparities and discussing their consequences. There are some materials that must be employed in accordance with previous research or guidelines due to their unfortunate lack of complete curve characteristics or under higher temperature.

5.2 Finite Element Modelling with ABAQUS Program

The modelling and simulation processes for samples must be described in detail and discussed. Three segments make up the technique in general:

Segment A: Modelling and simulating the reference samples (a T-beam that has not been fired and has not undergone any "enhancements").

Segment B: Modelling and simulating high-temperature burned concrete T-beam samples without SIFCON jacket augmentation.

Segment C: Simulating and modelling the burned concrete T-beam repaired by SIFCON jacketing.

In general, the following steps should be taken while using ABAQUS to replicate any process or behavior of concrete elements:

Parts Modelling: This is the **First** phase in the simulation of a part.

Second, the qualities of the concrete and steel that are previously utilized and identified.

Third, collect and assemble all simulation-related components.

The **fourth** step is to specify the kind of analysis to be performed, how long the simulation will take, and how the solver should be set up.

Fifthly, constraints and interactions, which defined the characteristics of the interface kind and character of the interacting surfaces.

Sixth, samples must be loaded and given boundary conditions in order to determine the kind of loading (mechanical, thermal, electrical, etc.).

Seventh, a predefined parameter is employed to specify the assembly initial condition with regards to stress, temperature distribution, etc.

Eighth: carrying out and initiating the simulation process.

5.3SEGMENT A: Reference T-Beam Modelling

5.3.1 Geometric Modelling

Flexible modeling provided by ABAQUS environment, accepting files exported from other applications (like AutoCAD) that employ mutually compatible but otherwise distinct file extensions. It has always been the norm in geometrical modeling to produce each piece separately, whether it be a 3D model, a 2D model, or a 1D model. To add extra complexity, the simulation status decides which parts are malleable and which are rigid. The four essential components required for geometric modeling are a concrete T-beam, steel reinforcement, loading and supporting plates, and a steel fiber concrete jacket.

Every step of production needs to be duplicated in three dimensions, Both the concrete T-beam and the jacket are subjected to the extraction method, and then determined an appropriate extraction length for each component, which involves essentially drawing the T-beam “cross section” or the jacket area in the X-Y plane. Most often, this method is used for 3D components that have a flat, longitudinal profile. Ties and other steel reinforcement are represented

using a 1D wire approach to portray flat, flattened surfaces instead of 3D structures. For simplicity and to reduce the time needed to complete the analysis, the most well-known procedure for steel bar modelling in concrete elements is to model them as a wire element. However, while realistic simulation approach necessitates exact modelling to the actual programmed, which consisted various adjustments have been proposed by previously writers. In fact, there are scenarios in which it is necessary to represent steel bars as 3D objects, such as in the case of the steel concrete interaction is an issue to discuss. (Figure 5-1) illustrates the adopted procedure for geometrical modeling of various parts.

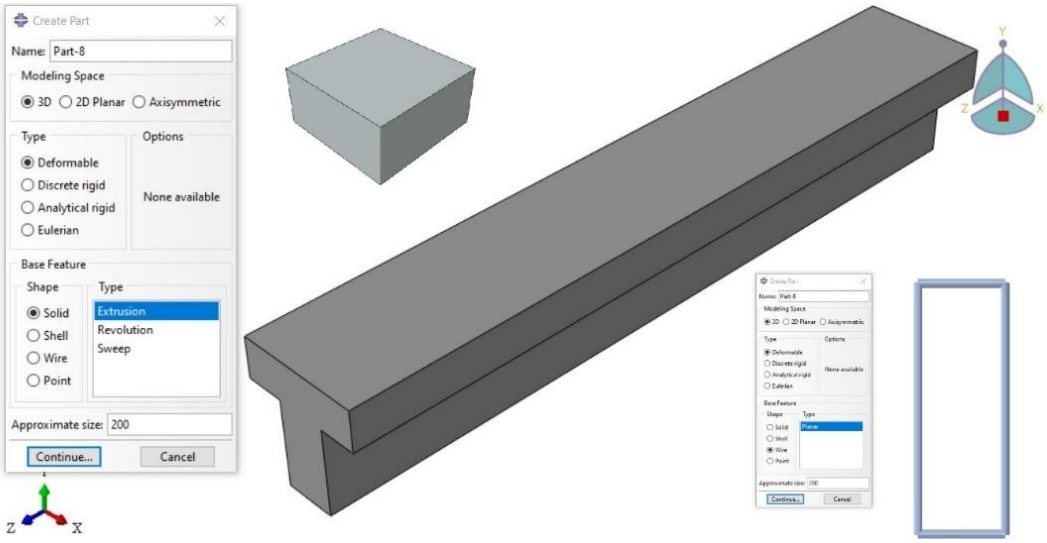

Figure 5-1: Parts geometrical modelling

5.3.2 Material model and assign section

ABAQUS provides a number of material properties, each of which depicts the material behavior in a particular simulation setup. In addition, numerous theories of material failure, applicable to metals, soils, concrete, and so on, are provided. When modeling concrete, it is common practice to divide the process into two distinct Segments, the elastic and plastic Segments are the names given to these states. It is common practice to characterize the elastic Segment of isotropic resources materials through means of the modulus of elasticity and Poisson's ratio.

Two distinct patterns are in effects here:

The **C**oncrete **D**amaged **P**lasticity (CDP) and **C**oncrete **S**meared **C**racks (CSC) models are two ways to describe the plastic Segment of concrete.

A- ABAQUS Parameter Model of Concrete Damaged Plasticity

Five fundamental criteria are required to establish the CDP model: dilation angle, surface plasticity flow number, eccentricity, the ratio of biaxial compressive strength to uniaxial compressive strength, and viscosity. Inelastic stress versus cracking strain and inelastic compressive strength versus plastic strain, both superimposed on the cracking strength, (Figure 5-2) illustrates that extra inputs are required for both the compressive and tensile behaviors, mono-axial inelastic curves,[97] respectively. A breakdown of the CDP failure surface properties is shown in (Table 5-1).

Table 5-1: Selected CDP material parameter for unfired concrete

Parameter	Value	Descriptions
Dilation angle	36	the proportion of the volume change to shear strain for reinforced concrete (30-40)
Ecc	0.1	the flow potential eccentricity, the default value 0.1
$*f\,b_0/f\,c_0$	1.16	the ration between biaxial compressive strength to initial uniaxial strength, its ranged between 1.10 to 1.16
Kc	0.677	the ratio of the second stress invariant on the tensile meridian
Viscosity Parameter	0.01	required when a convergence problem is caused by softening behavior
E		Modula's of elasticity "varied value depends on f`c"
v	0.18	Poisson's ratio = Transverse (Lateral) Strain /Axial (Longitudinal) Strain

* ABAQUS recommended manual

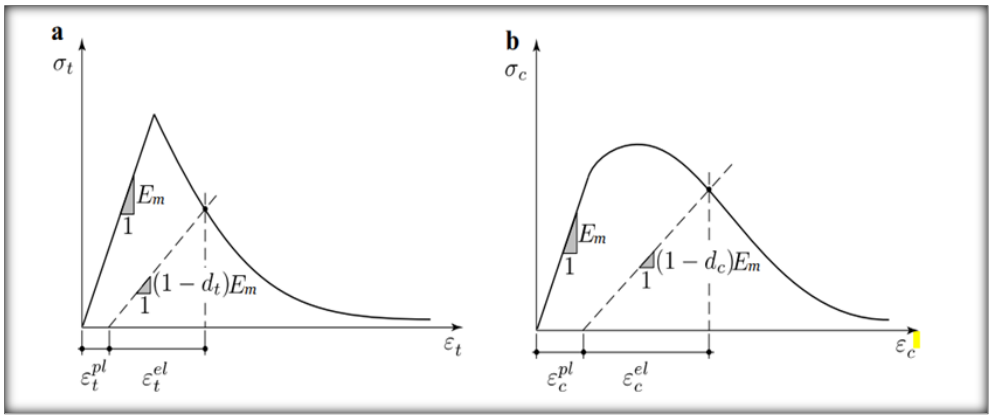

Figure 5-2: Concrete damage plasticity model: Giovanni Castellazzi,2017

Both the compressive and tensile stress-strain curves for unconfined materials at room temperature are required for inclusion in the CDP model (20 °C). These curves may be divided into two parts: an **elastic zone** with a low modulus of elasticity and a high Poisson's ratio, and **plastic region** with a low modulus of elasticity and a high critical dislocation pair (CDP). In concrete, the plastic Segment describes both the tensile and compressive characteristics.

B- Defining Steel Material Behavior

There are four main stress-strain models used to characterize steel's behavior: the engineering stress-strain, the true or logarithmic stress-strain relation, the elastic perfect plastic behavior, and the bi-linear elasto-plastic with hardening. Reinforcing steel bars (rebars) have an elastic ideal, the study has developed a flexible attitude and style of behavior. The yielding point, which is equivalent to zero plastic strain, must be included in the definition of the elastic and plastic model if such behavior is to be taken into consideration. In contrast, the plastic Segment requires at least two places, the yield point and the rapture point, in order to achieve linear hardening. More than just two instances of plasticity are needed to characterize the remaining stated relations. For this research, used the elastic perfect plastic behavior is used instead of the plastic Segment data that is currently unavailable as presented in (Table 5-2).

Table 5-2: Behavior model of elastic perfect plastic for Steel

Parameter	Selected value
Type Model	Theoretical stress-strain behavior
Poisson's Ratio	0.3
E, MPa	Modula's of elasticity = 200000 at (ambient temperature)
Fy, Yielding stress	Depending on the bar's temperature and kind.

Where the general stress-strain behavior is illtreated in (Figure 5-3), [98]

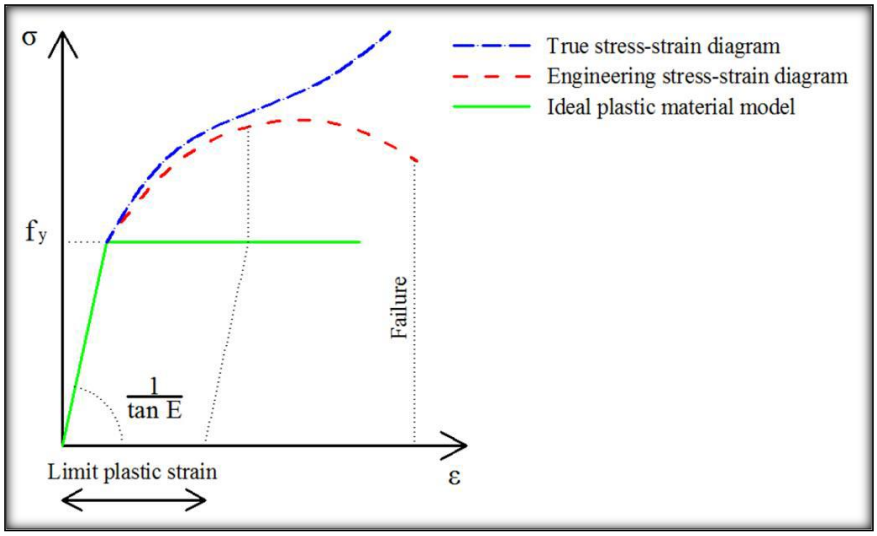

Figure 5-3: General types of steel stress strain representation and simplification

By default, ABAQUS necessitates defining a section for each material shown in (Figure 5-4). Concrete T-beam sections, for example, should be described as homogenous solids; similarly, the terms "T-beam section" and "truss section" can be used to define steel reinforcing sections.

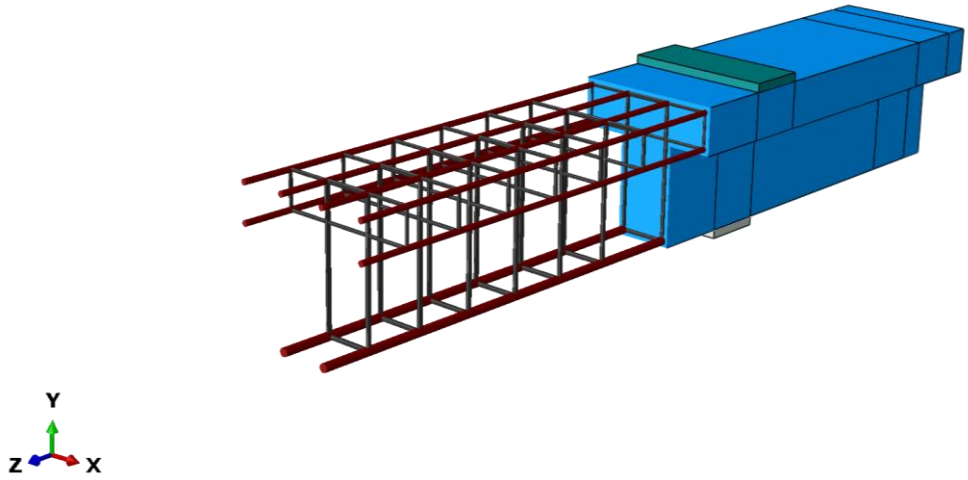

Figure 5-4: Section assignment of concrete T-beams and steel bars

5.3.3 Materials Characteristics and Response Modelling

Different types of concrete mixes (NSLWC and HSLWC) have their stress-strain behavior at ambient and higher "elevated" temperature predicted. But these statistical models are constructed with various aspects like aggregate type, additive type, water-cement ratio, etc.

When LWAC is heated to 250, 500, and 750°C, the compressive strength decreases by 7%, 28%, and 70%, respectively. However, the absorbed water content of LECA needs to escape as vapor during heating, but the rate at which compressive strength decreases is lower in LWAC for a number of reasons described, including free-water evaporation and thermal stress-induced fractures. Crack coalescence at the paste-aggregate interface is responsible for releasing the excess steam pressure generated in the LWAC matrix over 250°C. In this way, the porous network within LECA allowed for a quicker release of internal pressure before damage could accumulate, reducing the severity of the impact. Therefore, additional surface fractures and abrupt spalling accompanied the failure mechanism of the LWAC specimens,[99].

Temperature variations in the compressive stress-strain relation are depicted in (Figure 5-5).

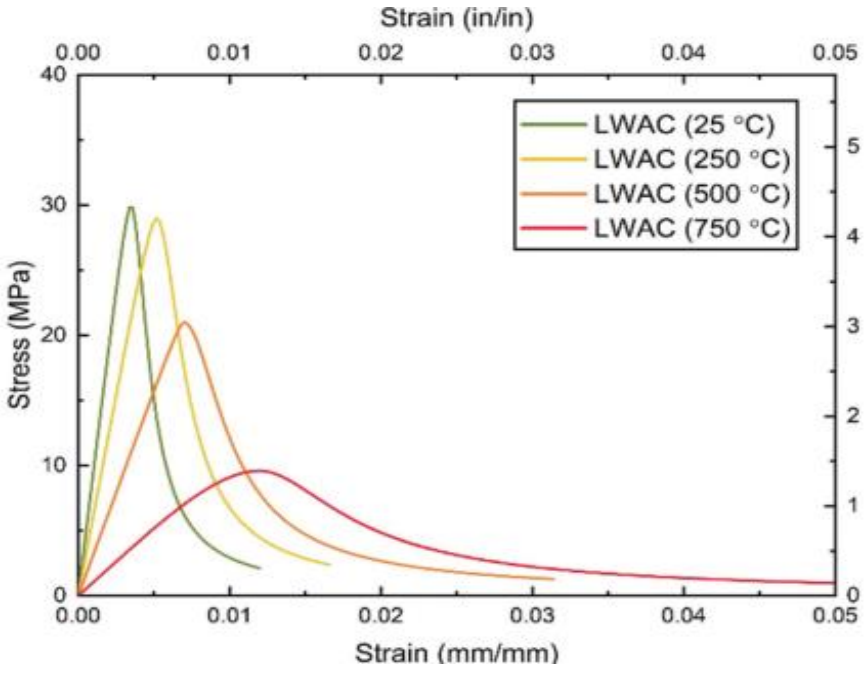

Figure 5-5: Stress - Strain relation LWAC at different temp.

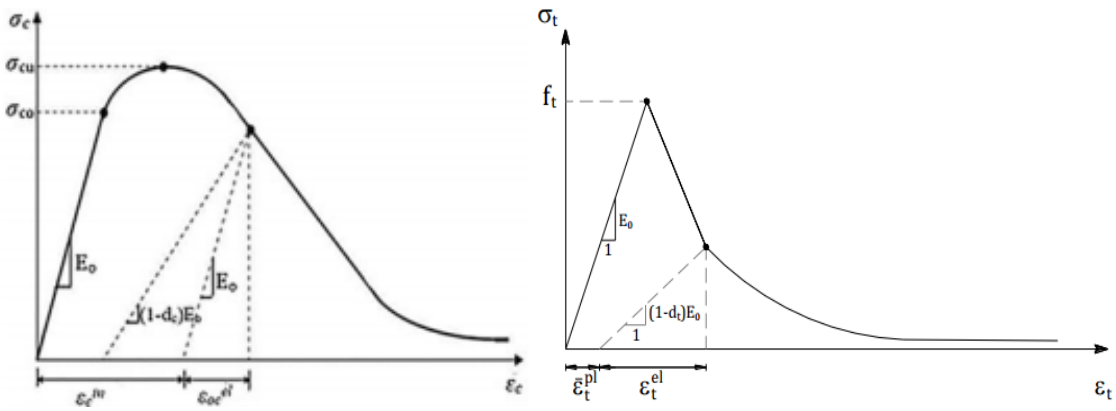

Figure 5-6: Compressive inelastic strain defined by ABAQUS

ABAQUS/CAE User's Guide,[100] defined Compressive inelastic strain as presented in (Figure 5-6).

The current study results are consistent with the projected statistical model for normal and high strength concrete with lightweight clay aggregate.

5.3.4 Assembling Parts

Gathering the manufactured components into the simulation setting is what the assembly module is for. (Figure 5-7) shows how the long steel bars for the top and bottom layers and the stirrups are placed and replicated after the concrete T-beam has been set in place.

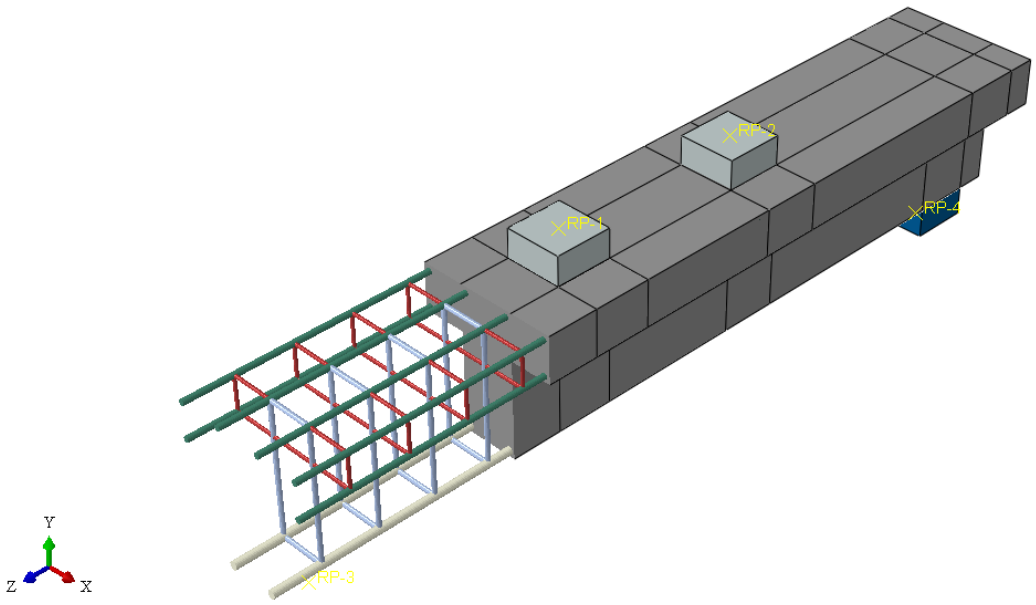

Figure 5-7: Part assembling of the concrete T-beam

5.3.5 Analysis Procedure

ABAQUS offers a number of distinct “steps” of analysis, to accommodate a wide range of engineering problems. Most engineering uses are suited to the static stage when the loading frequency is less than one-third of the structure's inherent frequency or when the kinetic energy is less than five percent of the internal energy. Over that threshold, researchers must turn to quasi-static analysis. This kind of study is inadequate for capturing the impact of loading at a higher frequency. Applications including collision, crashes, earthquakes, and so on are all possible with the dynamic method. Additionally, heat transfer analysis process and coupled thermal-displacement analysis are available in the ABAQUS library to accurately represent the combined influence of mechanical and thermal loads on the structure. In this research, the non-fire-exposed concrete T-beam problems have been solved using the static analysis method. While the heat transfer analysis method is utilized to probe the thermal distribution on the T-beam cross section.

Other concrete T-beams those are tested after exposing to fire and those improved with SIFCON jacketing, are analyzed with the static analysis step.

5.3.6 Constrains and Interactions

ABAQUS working environment includes certain helpful tools, including constraints and interactions. The embedded region constrain is frequently used and recognized as a powerful constraint type in structural research. To prove that the embedded portions of steel reinforcement are fully interacted with the concrete T-beam, these kinds of constrains can be used (the host element). That is to say, even under extreme tension, the lengthy rebars and stirrups must not move. Rigid body constraints are the second most common form of useful constraints. The loading and supporting plates are of this kind because they are in deformable and hence the stress state, strain, or displacement is irrelevant to the simulation. A fixed point of reference must be coupled with the target body in order to apply the rigid body constrain operation.

The connection between the concrete T-beams loads and supporting plates is simulated with the help of the mechanical interaction feature. In general, the simulation process will not function properly if the surfaces that are interacted physically are not specified. In this analysis, normal and tangential features of the commonly used surface-to-surface contact are utilized.

The normal (hard contact) full bond meaning the first surface cannot penetrate the second one. The friction between the concrete T-beam and the steel plates is modeled by assigning the tangential behavior with a penalty or friction coefficient of 0.4, as recommended for the static. The steel plate, being the stiffer component, is chosen as the master surface type, while concrete T-beam is assigned the role of slave surface.

5.3.7 Meshing Properties

The meshing approach is a way for breaking down the simulated objects into smaller pieces utilizing a variety of geometrical forms and subdivision algorithms.

After the manufactured components have called elements. ABAQUS 's library has many distinct sorts of elements, as seen in (Figure 5-8).

Parts in three dimensions (plates, a concrete T-beam, and an SIFCON jacket), are all modeled using the continuum solid element (C3D8R), While steel bars are reinforced with a one-dimensional element family (truss).

To create the mesh distribution, a structural mesh algorithmic approach is applied, element sizes in concrete are 20mm x 20mm x 20mm (8 nodes), steel reinforcements of the same length are also employed.

The concrete T-beam's produced mesh is shown in (Figure 5-9).

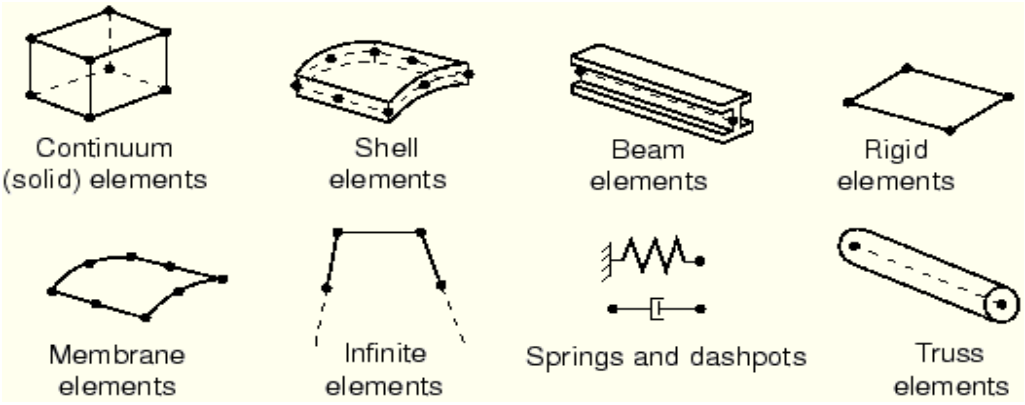

Figure 5-8: Element types library in ABAQUS

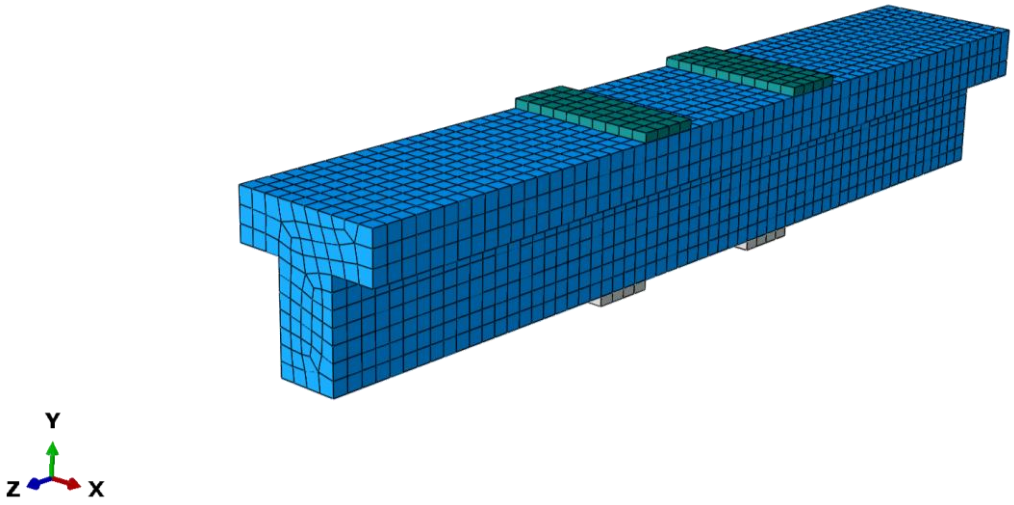

Figure 5-9: Meshing of the T-beam using structural mesh algorithm techniques

5.4 SEGMENT B: Modelling the Thermal Distribution on Concrete Samples

5.4.1 Geometrical Modelling and Assembling

Same techniques and dimensions used in Segment A, are used here this stage.

5.4.2 Material Properties

Concrete strength declines in the same manner as other materials do when subject to high temperatures, such as in a fire. Therefore, it is vital to characterize the thermal characteristics of such concrete type since they are required as input data ABAQUS for heat transfer analysis, in addition to the chemical bonding and expansion of cement mortar components. Concrete thermal qualities, including its thermal connectedness, density, and specific heat, must often be defined. LECA cement, in general, heat is transferred by

one of three mechanisms: conduction, convection, or radiation. Whenever there is a direct contact between two or more bodies, heat is transferred between them. However, convection describes the surface file condition used to represent the medium effect on the model. A material "emissivity" refers to its ability to emit heat into its surroundings.

5.4.3 Type of Analysis (Step)

Thermal analysis procedure has been utilized in this Segment to simulate heat distribution on the fired T-beam.

5.4.4 Constrains, Interactions Properties, and Predefined Field

The heat transmission from the concrete beam interior to the ambient air is modelled by assigning a surface film condition option to the beam sides and bottom edges. One research started with the washbasin prepared to 20 °C to simulate the initial environment. The heat amplitude of TH.1 is mapped to reflect the rise in ambient temperature that occurs as a result of the firing.

The surface film state of concrete is used to illustrate how the model interacts with its surroundings, whereas conductivity represents the transfer of heat from one substance (such as steel or concrete) to another.

The Fib modal,[101] code suggests a surface film condition value of 25 for surfaces that have been exposed to fire, whereas for unfired surfaces is 9.

The full model given a reference point with a temperature of 20 °C.

5.4.5 Meshing Techniques and Type Element Solver Library

In this stage, no mechanical stress has been applied; instead, a temperature boundary is being applied to the base and sides with an amplitude of TH.1 derived from the experiments.

5.5SEGMENT C: Modelling of Fired Samples Subjected to Mechanical Loading

5.5.1 Part Modelling and Assembling

Same techniques and dimensions used in Segment A, are used here this stage.

5.5.2 Materials' Characterization

(Figure 5-10) displays the stress-strain response of postfire concrete exposed to uniaxial unconfined compressive stress loading at a range of temperatures.

When concrete is heated to very high temperatures, it loses a lot of its characteristics, not just its compressive strength, but also its strain at maximum stress and secant modulus of elasticity. At higher temperatures, the material's brittleness decreases and it becomes more ductile; also, the deterioration Segment of its behavior gets more pronounced.

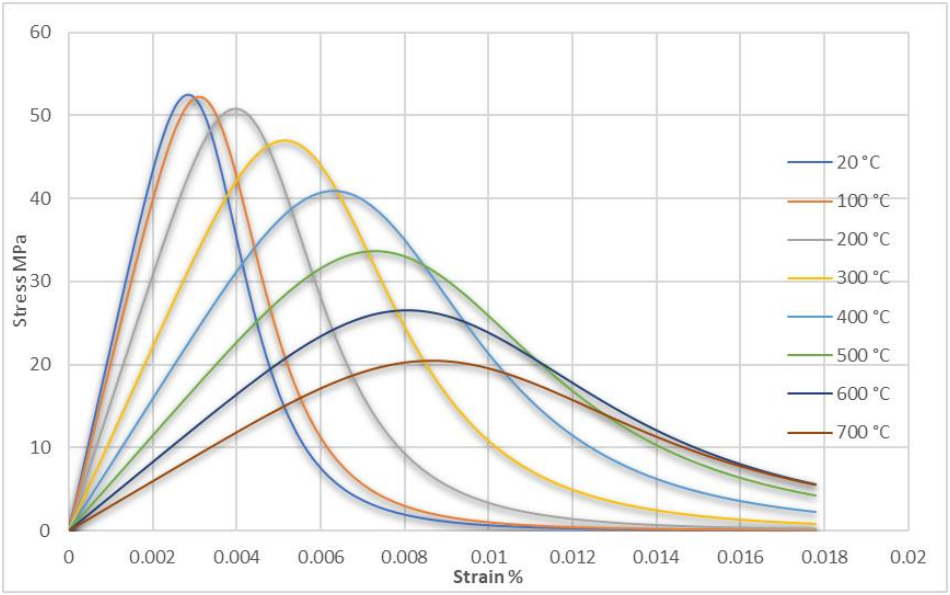

Figure 5-10: Concrete stress – strain behavior under elevated temperatures

Accordingly, (Figure 5-11) displays the normalized residual compressive strength and elastic modulus of lightweight concrete. The offered figure makes it evident that, at temperatures below 150 °C, both f `c and Ec values decrease slightly.

Further, at 300 °C, 10% of the concrete compressive strength and 28% of its elastic modulus values are lost, with the residual values for f `c and Ec reaching 22% and 54% at 650 °C.

In contrast, peak stress normalized strains in concrete are shown in (Figure 5-12), until 150 °C, strain increases at a relatively slow 10%; however, once

over this point, the strain increases at an exponential pace, first to 81% at 300 °C and then to around 181% at 600 °C.

It is worth mentioning that (**Dabbaghi et al.,2021b),**[102] has covered in his research, concrete behavior till temperature 750 °C. Where, at such point, the residual *f* `c and Ec values are approximately 12.8% and 34%, respectively. while to strain corresponding to the peak stress is increased about three times the value at ambient temperatures.

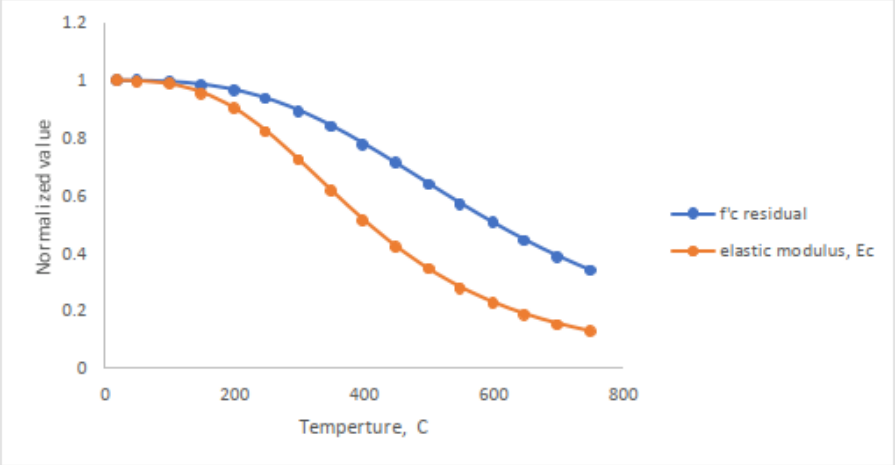

Figure 5-11: Normalized Values of the residual *f* `c and Ec for concrete subjected to high temperatures (Dabbaghi et al.,2021b)

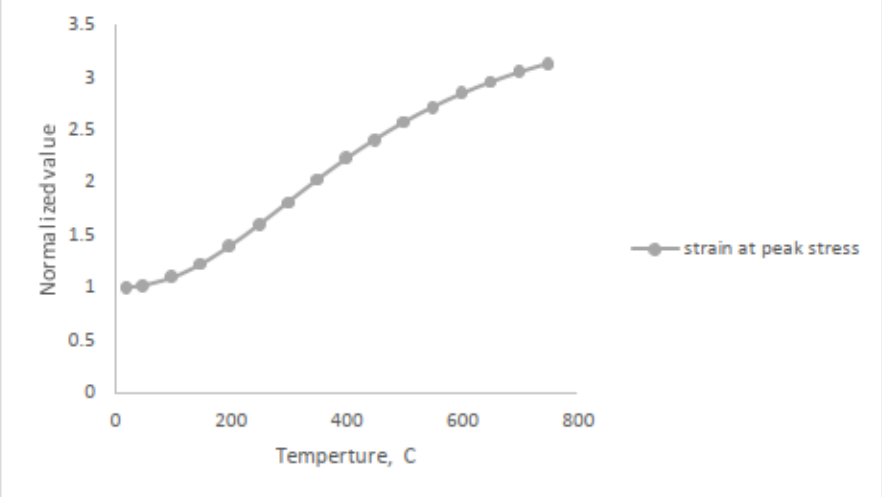

Figure 5-12: Normalized Value of the concrete strain corresponded to the *f* `c (Dabbaghi et al.,2021b).

The performance of concrete suffers as a whole when subjected to prolonged heating and exposing. Compressive strength loss in concrete due to heat has been documented by several studies. At high temperatures, the

residual compressive strength of concrete is shown in (Figure 5-13). It is clear from the preceding diagram that most studies of concrete residual strength are conducted with only small changes in experimental conditions up until a temperature of 300 °C. When this threshold is exceeded, a wide range of residual strength variations (between 43% and 70%) in the concrete are discovered. In addition, studies are similar up to 600 °C (**Dabbaghi et al.,2021b**),[103].

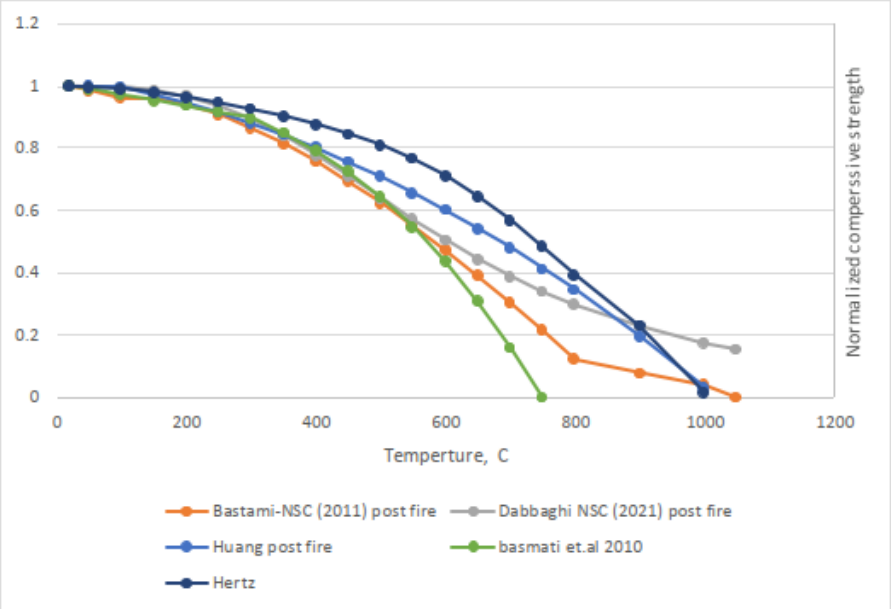

Figure 5-13: Normalized concrete compressive strength at high temperatures (Dabbaghi et al.,2021b)

5.5.2.1. Steel Reinforcement Behavior at Ambient and Elevated Temperatures

Using numerical validation of the experiments, we may infer that the steel reinforcement temperature is around 394 °C in the most extreme instance. Several studies and guidelines have found that heating steel to 400 °C does not noticeably lower the yield stress point. As compared to the elastic modulus, which does not undergo any change even at these temperatures.

Following the explanation provided in (Figure 5-14), These researchers followed **Lie's,**[104] recommendation and used the residual elastic and yield strength of steel bar reinforcement. As shown, at 300 °C, a steel bar's residual normalized yield strength is around 76% and its initial elastic modulus is

around 91%, but at 600 °C, these values drop to around 33% and 72%, respectively. The rate of weakening is greater than that of the elastic modulus, which has been measured. Steel reinforcement, when heated to temperatures close to 500 °C, loses roughly 19% of its elastic modulus and nearly 50% of its yield strength.

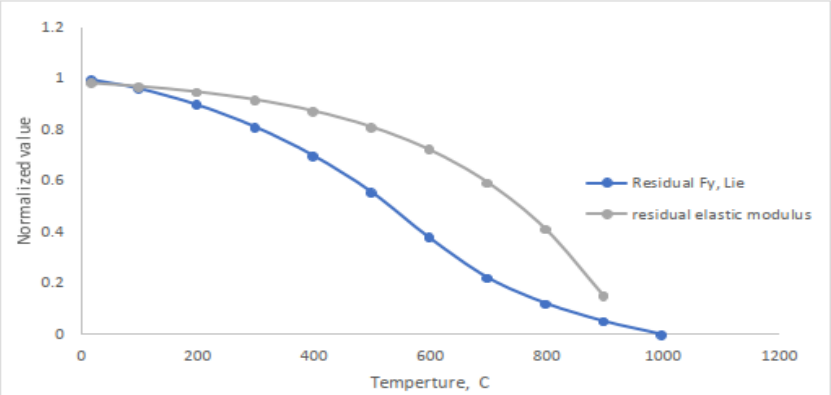

Figure 5-14: (Lie, 1972) calculated residual Fy and E values for steel bars heated to extreme temperatures.

5.5.2.2. Concrete Poisson's Ratio at Elevated Temperatures

It's found in many literatures that the Poisson ratio value of concrete specimens is significantly reduced after being subjected to high temperatures. Experiments on the effects of high temperatures on the behavior of concrete were conducted. It can be observed in (Figure 5-15) and the suggestion of a statistical model that the ratio of Poisson's decreases with increasing temperature (**Bahr et al., 2013**),[105].

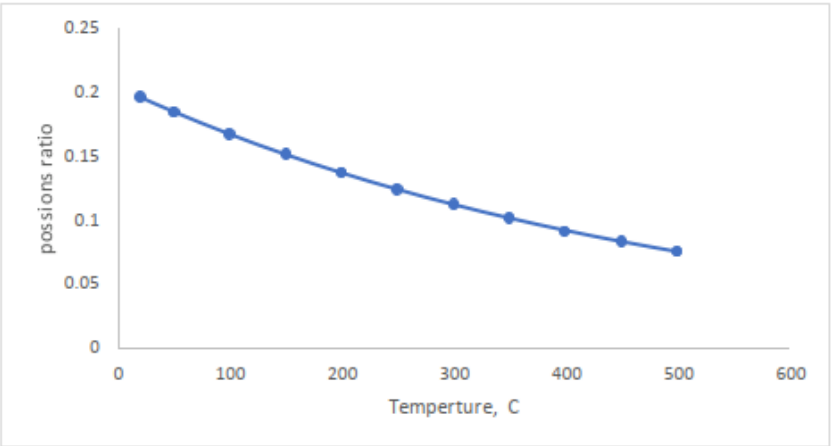

Figure 5-15: Concrete Poisson's ratio at high temperatures (Bahr et al., 2013).

5.5.3 Type of Analysis

This simulation Segment involved modeling the combined impact of thermal and mechanical loads by transient coupled temperature-displacement analysis. In this context, it's important to note that the maximum safe temperature per the increment was established at 20°C to prevent uncontrollable temperature swings and rifts in the simulation. Analysis was used to simulate the coupled effect of thermal and mechanical loading. It is worth mentioning that, the maximum allowable temperature per increment was set to 700°C, to avoid excessive change and disseverance issues during performing the simulation.

5.5.4 Meshing Techniques and Element Type

At this Segment of the modeling process, all aspects of the model including element form and meshing distribution algorithm were carried over from Segment A with the exception of the element type (solver). Element types of **C3D8R** and **T3D2T** were used for concrete and steel reinforcement, respectively, to solve and account for both mechanical and thermal loads.

5.5.5 Predefined Fields

This model makes advantage of a preset option to incorporate the impact of fire on a concrete T-beam. Setting the fired samples' initial temperature distribution using the initial state option. This makes it easier to redistribute the strength qualities of concrete in a way that's in line with the profile's temperature. Researches recollect the firing model output results files (ODB) received in Segment B in preparation for Segment D.

5.6 SEGMENT D: Modelling of The Improvement of Concrete T-Beams Using SIFCON Jacketing

5.6.1 Geometrical Modelling and Assembling

For geometric modeling, the T-beam and steel reinforcement were both measured in the same units as everything else save the jacketing. Concrete T-beams of the same length were modeled in three dimensions using an

extraction technique see (Figure 5-16). It is also important to note that the lengths of the supporting and loading plates were extended to accommodate the wider dimensions of the new concrete T-beam.

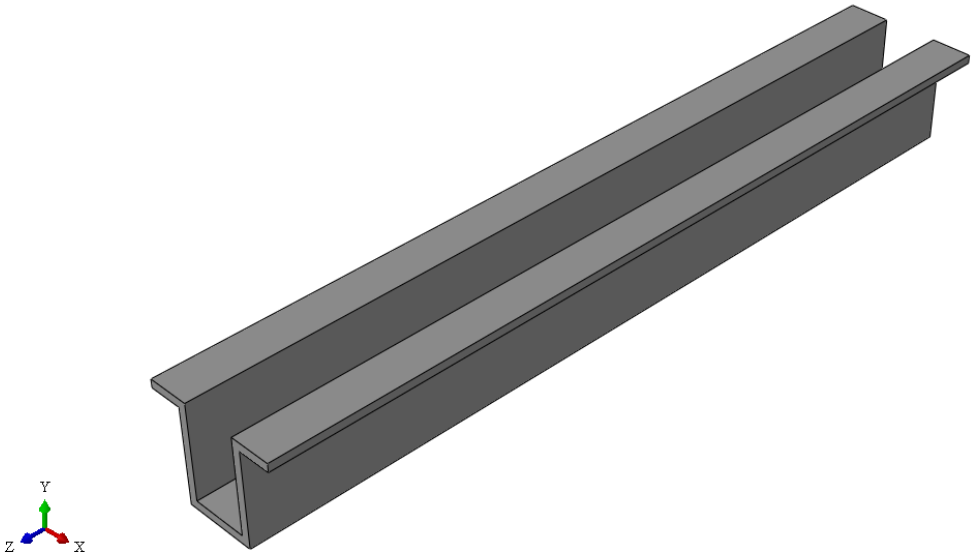

Figure 5-16: SIFCON jacket layer part along the three faces of the concrete

5.6.2 Stress Strain Relations of SIFCON Material

In particular, the addition of tiny steel fibers to the mix causes high strength concrete to behave differently from normal concrete. Under monolithic, uniaxial compressive and tensile stress, the stress strain behavior of a SIFCON combination is depicted as in (Figure 5-17),[60]. The high ductility and stronger ability to resist loading provided by the abundant steel fiber causes the strain at the point of maximum stress to approach (0.02).

ABAQUS stress strain data was refined, and its elastic Segment was isolated. A previously utilized model in concrete characterization (concrete damaged plasticity) was applied for the plastic Segment behavior, giving rise to a definition of the elastic modulus as an elastic isotropic model. The 3D jacket was then given the material property. All the other components, such as the concrete T-beam and the streel reinforcement, were set in place as described in Segment C.

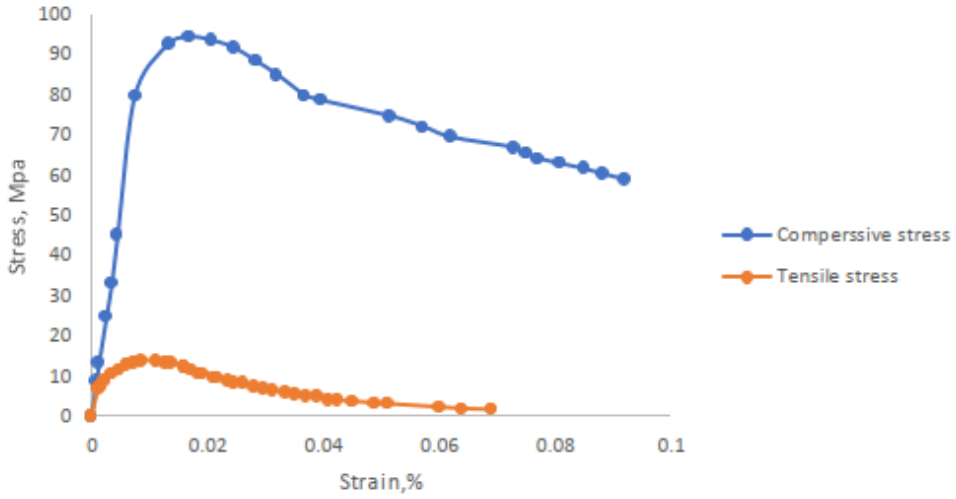

Figure 5-17: Unconfined, uniaxial loading and tensile stress in SIFCON and the resulting stress-strain behavior

5.6.3 Meshing

For the improved models, this step employs the same meshing methods, element shapes, sizes, and types as Modeling Segment C. the size of the part in the direction opposite to the jacket thickness.

As shown in (Figure 5-18), in order to provide more precision in the final product, the dimensions of the allocated elements were set at 4 mm in this direction.

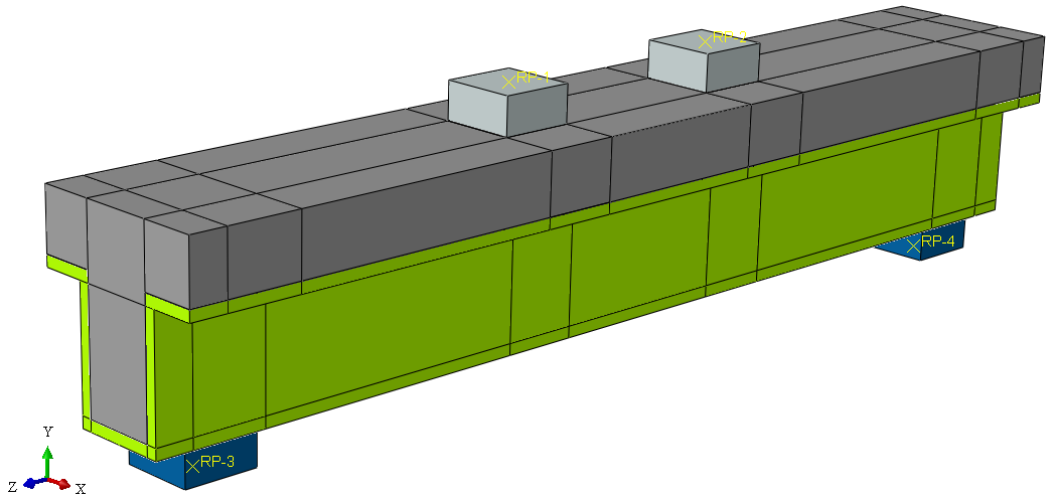

Figure 5-18: SIFCON jacket strengthening model meshing

5.7Finite Element Method Result

In this chapter, looked at how finite element modeling with ABAQUS software may be used to simulate experimental work by studying the behavior of different types of specimens under varying situations.

Validation Results of NSLWC and HSLWC at Ambient Temperatures (segment A) and Validation of distribution Temperature - Time Along T-beam and Simulation Outcomes at damage burning stage (segment B), compared with experimental data before and after fire, as well as before and after the enhancement “repairing” with the SIFCON jacketing process.

According to the curve behavior of numerical and experimental results for “ultimate load-midspan deflection”, it shows that they are similar in (N-C-O, H-C-0, N-F15-0, N-F30-0 and lastly H-F30-0 “which shown failure in elastic area”) T-beam samples, as presented in (Figure 5-19), (Figure 5-21), (Figure 5-25), (Figure 5-27), and (Figure 5-31).

Validation of time – temperature distribution along T-beam cross section for both NSLWC and HSLWC gave the result of heat transfer were remarkably similar to those obtain from experimental work as shown in (Figure 5-23) for NSLWC and (Figure 5-24) for HSLWC respectively.

Then in segment C (validation for the post fire treated NSLWC and HSLWC T-beam with repairing by SIFCON jacket) which show match load - deflection curved up to (7, 6.7, 10.4, 8.5, and 9.4) mm for (N-F15-S2, N-F15-S3, N-F30-S2, N-F30-S3, and H-F15-S3) respectively. While lastly H-F30-S3 shows that there is a gap in the curve line path. However, it shown matches up to 10.2 mm deflation, while in H-F15-0 there is a noticeable variation between experimental and numerical behavior in curve “small variation” as well as a huge noticeable variation between experimental and F.M.E curve in H-F15-S2 starts as a slide and contract at 148 kN, another different behavior is shown with H-F30-S2 which indicates matches curves only in elastic area up to 4 mm deflection distance.

These results are shown in (Figure 5-33), (Figure 5-35), (Figure 5-37), (Figure 5-39), (Figure 5-41), (Figure 5-43), (Figure 5-45), and (Figure 5-47) respectively.

The absolute error "variation" between the experimental and numerical results was calculated Concisely summarizing in (Table 5-3), and (Table 5-4).

Table 5-3: NSLWC summary results

Specimen Identification	Ultimate Load (kN) EXP.	Ultimate Load (kN) FEA	Max Deflection at Mid-span (mm), EXP.	Max Deflection at Mid-span (mm), FEA	Difference in load, %	Difference in deflection, %
N-C-0	243.5	255.08	22.64	22.28	4.75	-1.59
N-F15-0	232.1	243.57	19.25	21.6	4.93	12.21
N-F15-S2	265.2	292.83	12.19	12.85	10.43	5.41
N-F15-S3	301.2	344.24	17.21	18.18	14.28	5.64
N-F30-0	206.7	201.82	18.76	21.28	-2.35	13.43
N-F30-S2	280.2	285.72	10.76	11.31	1.97	5.11
N-F30-S3	330.9	372.96	14.48	15.56	12.71	7.46

Table 5-4: HSLWC summary results

Specimen Identification	Ultimate Load (kN) EXP.	Ultimate Load (kN) FEA	Max Deflection at Mid-span (mm), EXP.	Max Deflection at Mid-span (mm), FEA	Difference in load, %	Difference in deflection, %
H-C-0	270	276.34	15.37	16.54	2.35	7.61
H-F15-0	247.9	248.86	15.27	15.87	0.39	3.93
H-F15-S2	303.5	309.43	8.93	9.7	1.95	8.62
H-F15-S3	354.7	381.75	10.37	11.81	7.63	13.89
H-F30-0	233.8	229.81	12.86	14.42	-1.71	12.13
H-F30-S2	325.9	294.4	16.93	18.1	-9.67	6.91
H-F30-S3	359.3	364.87	16.62	17.81	1.55	7.16

The tables shows that the lowest and highest absolute errors "variation" in **load** bearing capacity determined for the specimens were around 1.97% and 14.28% respectively, for NSLWC and around 0.39% and 9.67% respectively, for HSLWC.

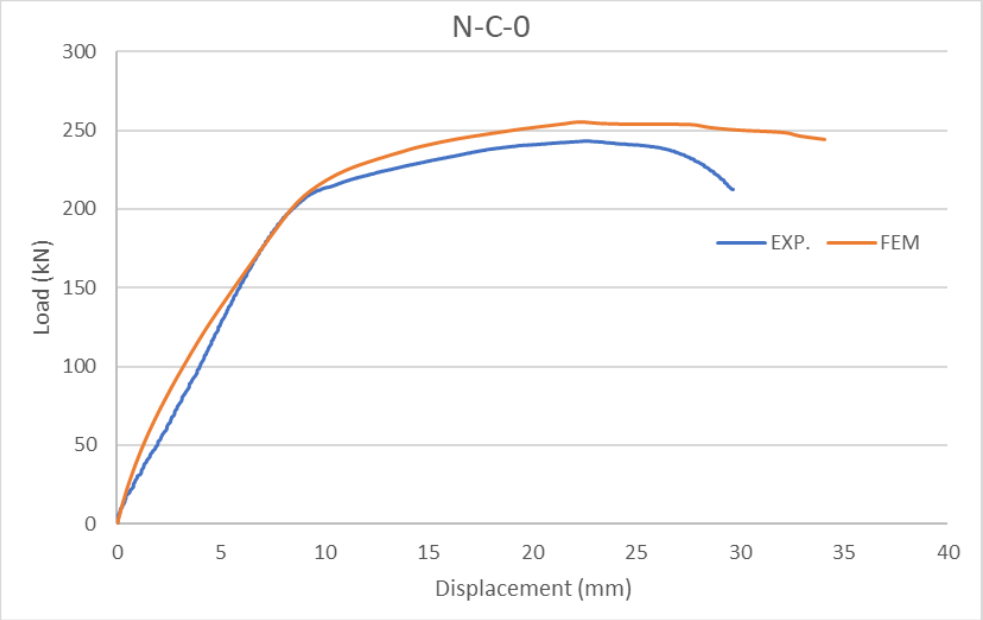

Figure 5-19: N-C-0 Experimental and Finite Element Method Load-Deflection Curve Comparison

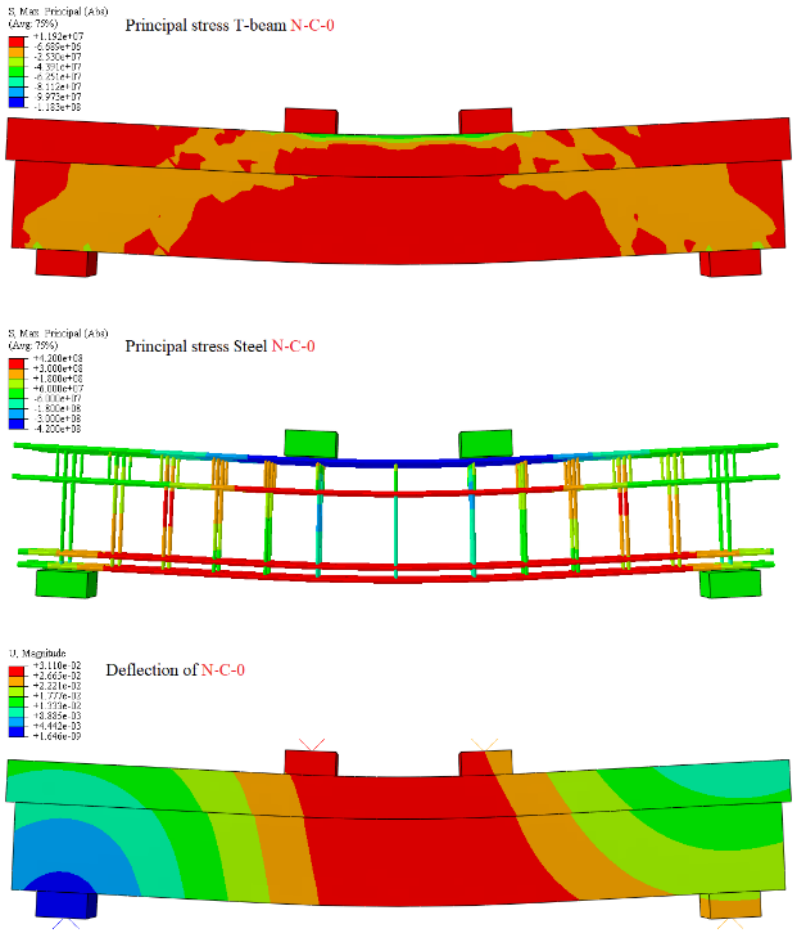

Figure 5-20: T-beam N-C-0 deflection and principal stress distribution for concrete and steel reinforcement

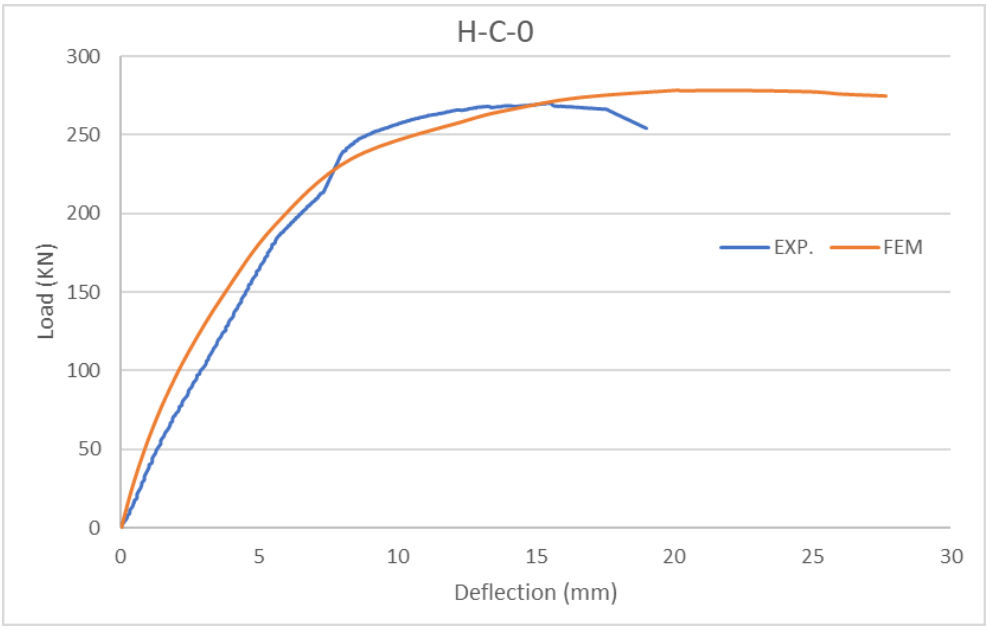

Figure 5-21: H-C-0 Experimental and Finite Element Method Load-Deflection Curve Comparison

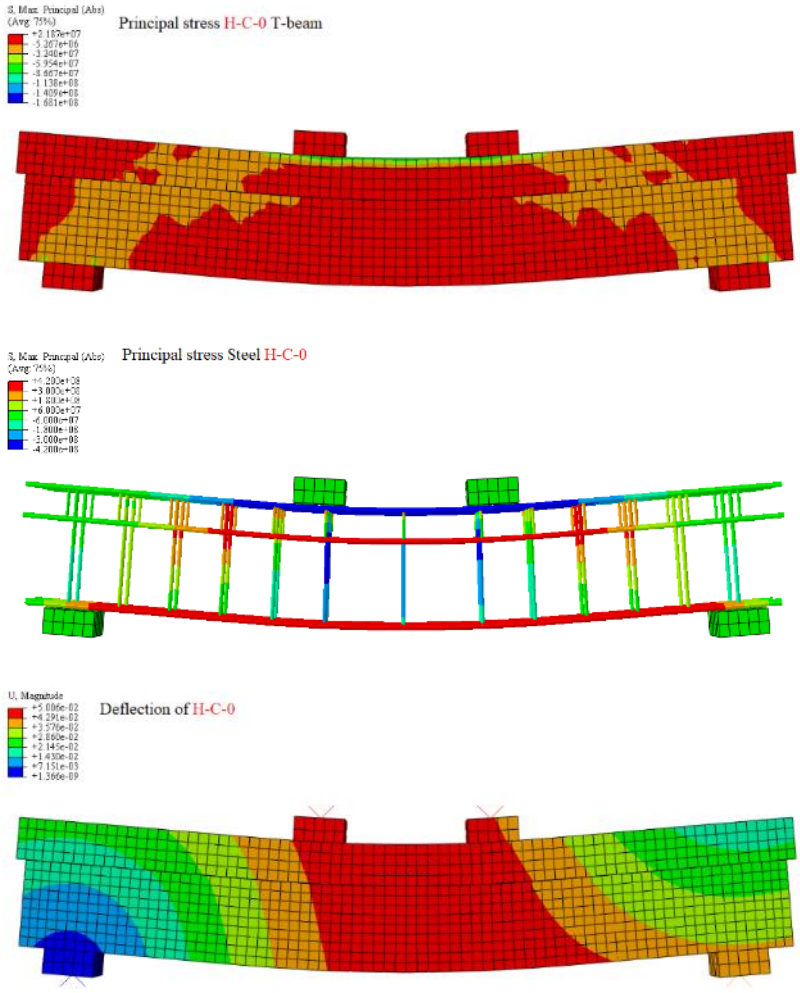

Figure 5-22: T-beam H-C-0 deflection and principal stress distribution for concrete and steel reinforcement

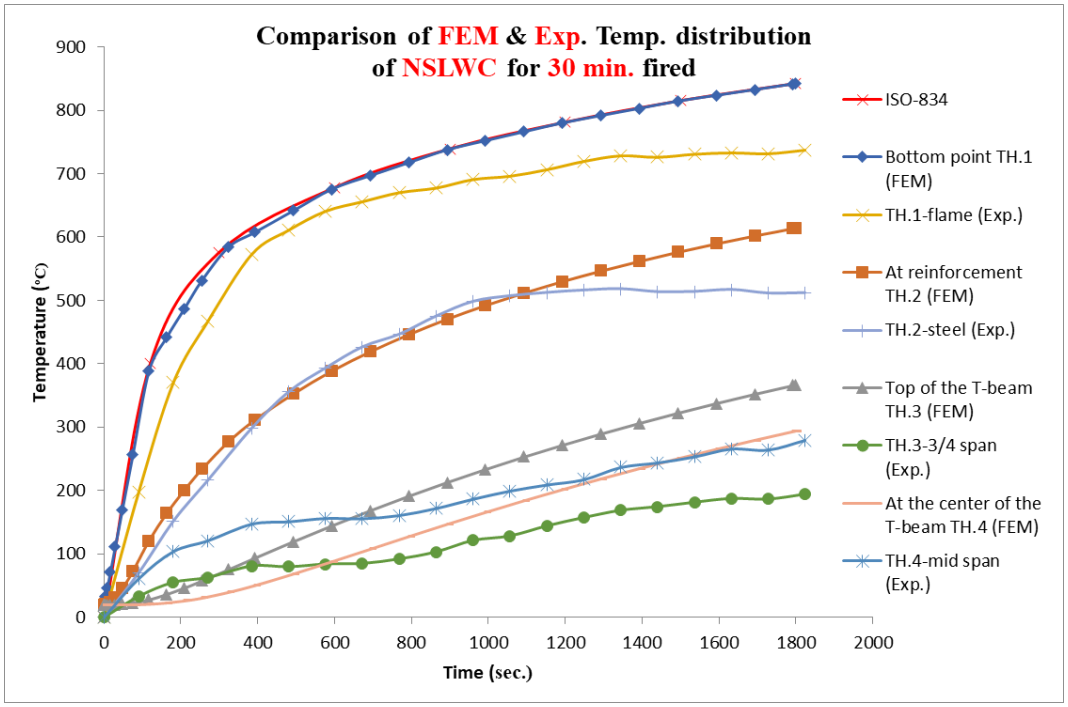

Figure 5-23: Comparison of FEM & Exp. Temp. distribution of NSLWC for 30 min. fired

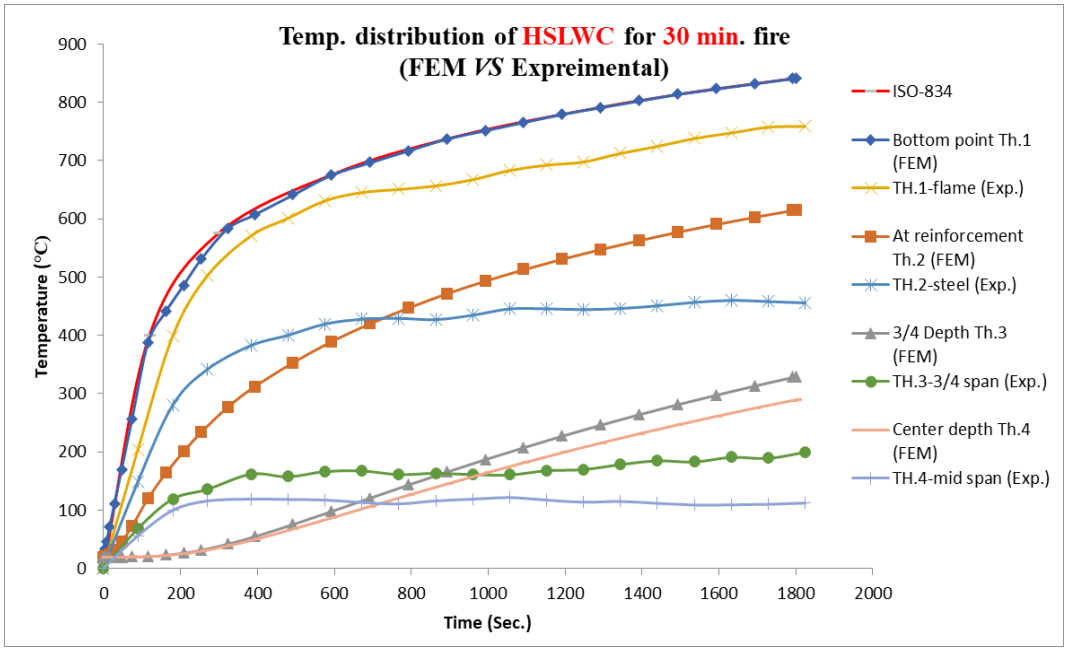

Figure 5-24: Comparison of FEM & Exp. Temp. distribution of HSLWC for 30 min. fired

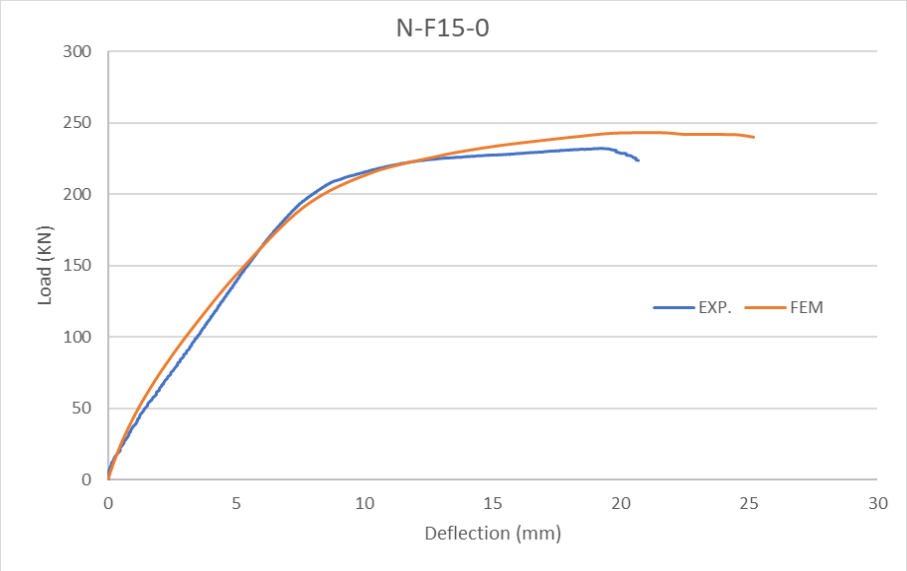

Figure 5-25: N-F15-0 Experimental and Finite Element Method Load-Deflection Curve Comparison

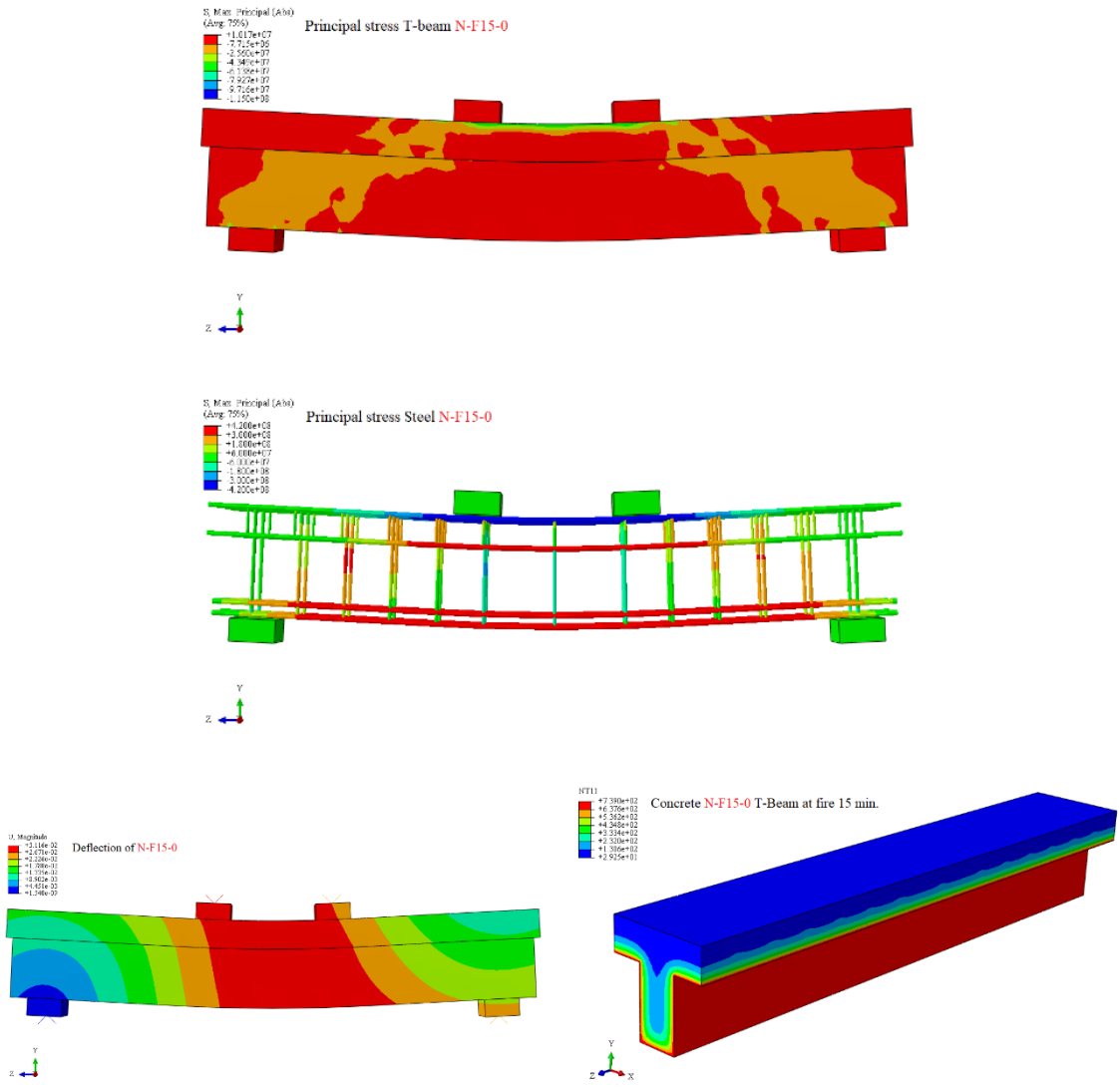

Figure 5-26: T-beam N-F15-0 deflection and principal stress distribution for concrete and steel reinforcement

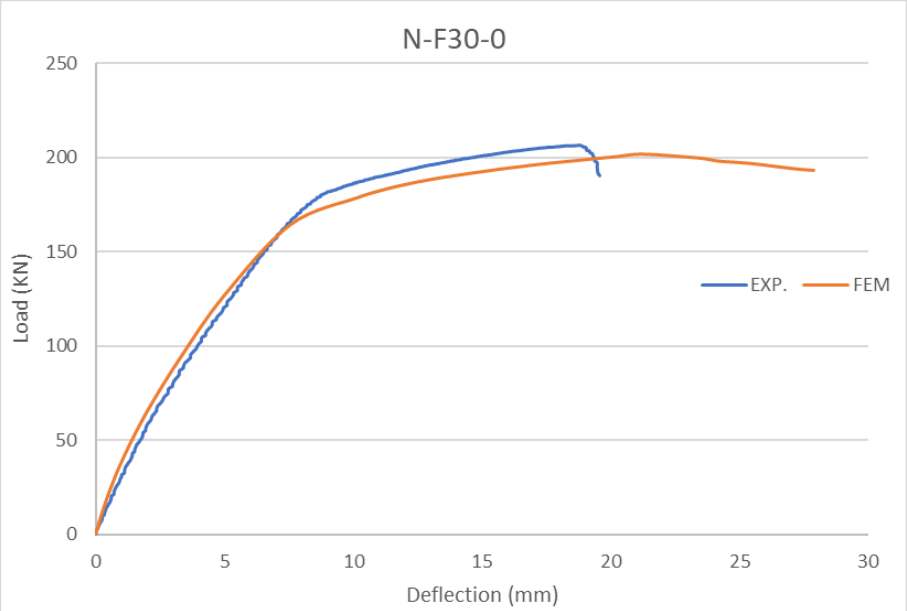

Figure 5-27: N-F30-0 Experimental and Finite Element Method Load-Deflection Curve Comparison

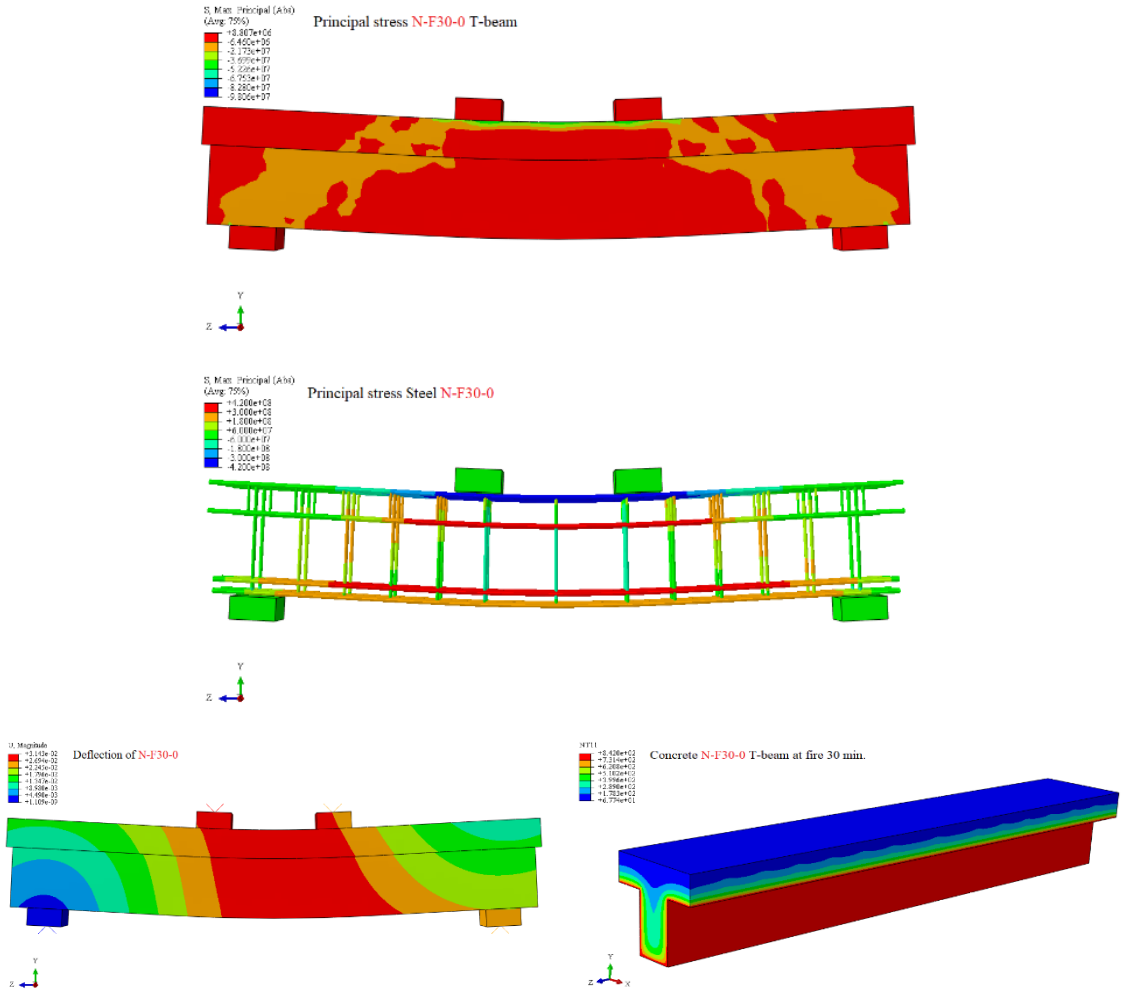

Figure 5-28: T-beam N-F30-0 deflection and principal stress distribution for concrete and steel reinforcement

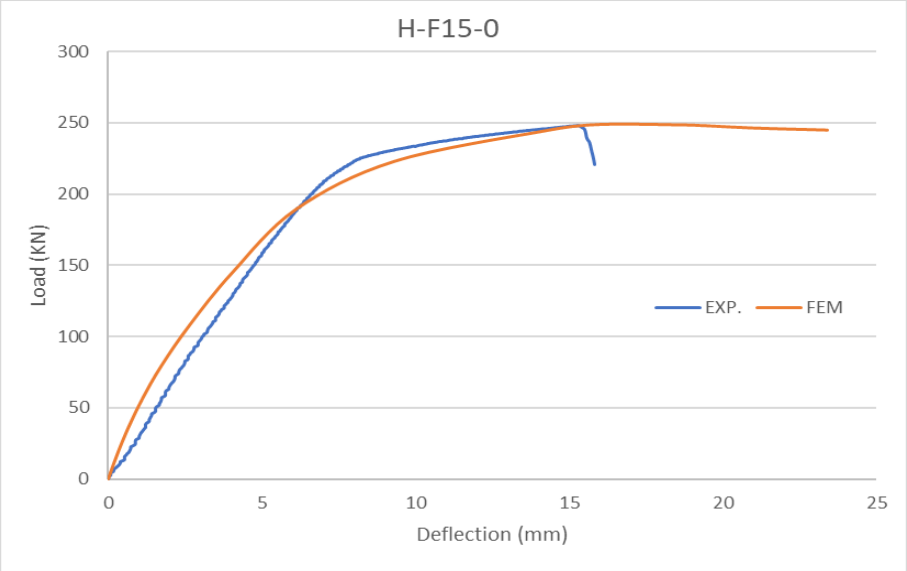

Figure 5-29: H-F15-0 Experimental and Finite Element Method Load-Deflection Curve Comparison

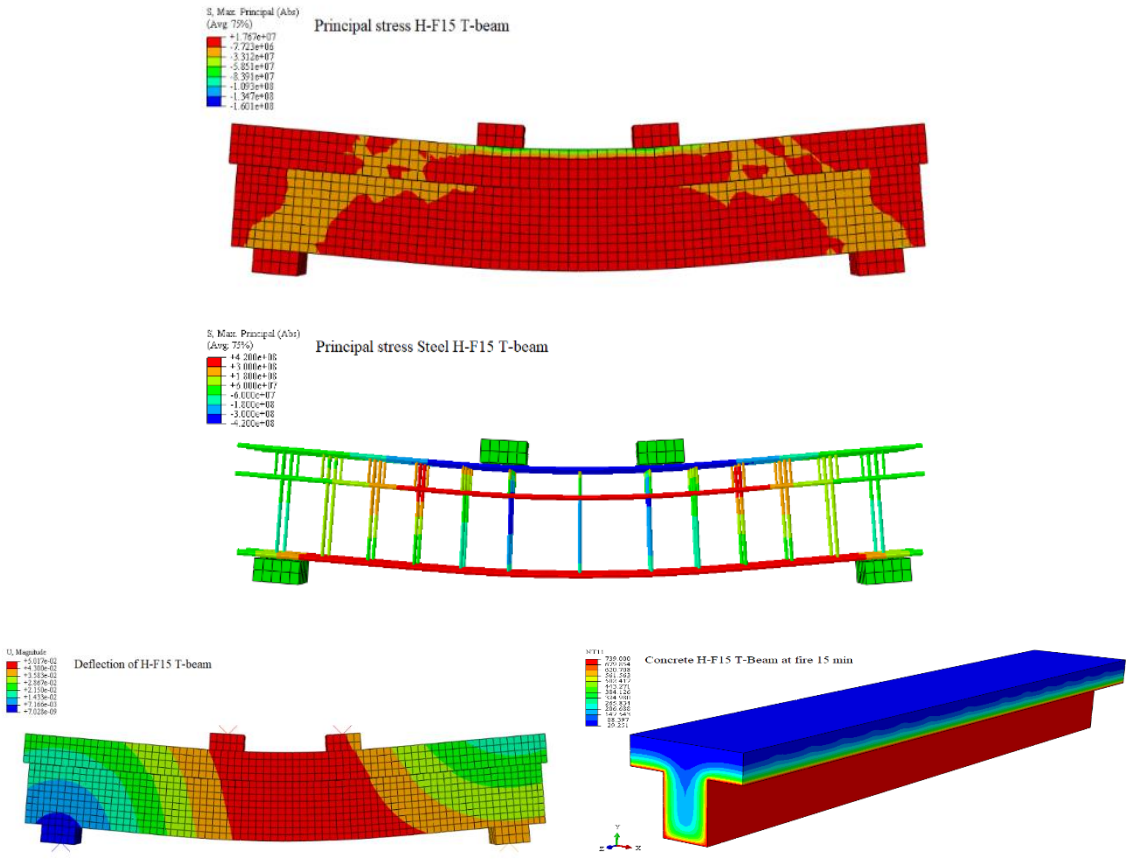

Figure 5-30: T-beam H-F15-0 deflection and principal stress distribution for concrete and steel reinforcement

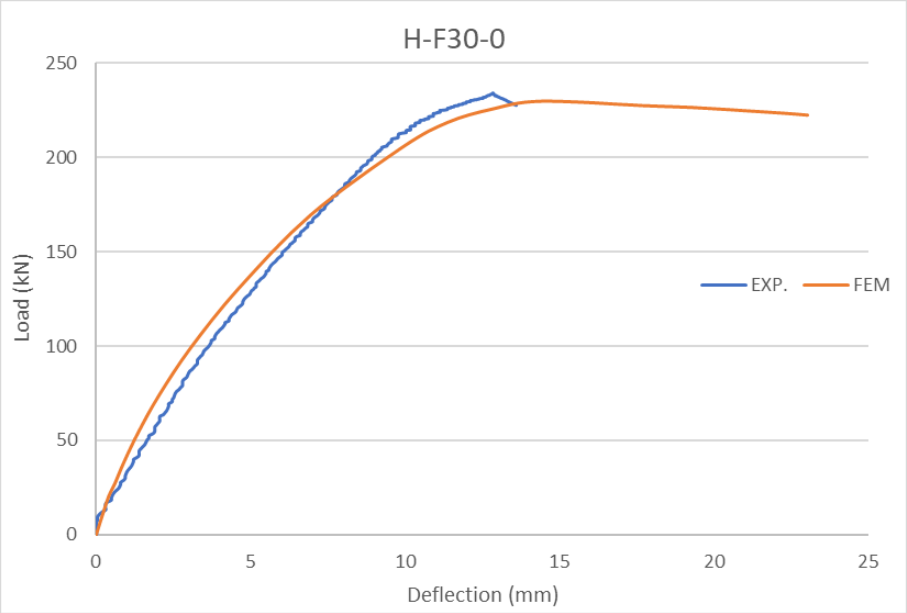

Figure 5-31: H-F30-0 Experimental and Finite Element Method Load-Deflection Curve Comparison

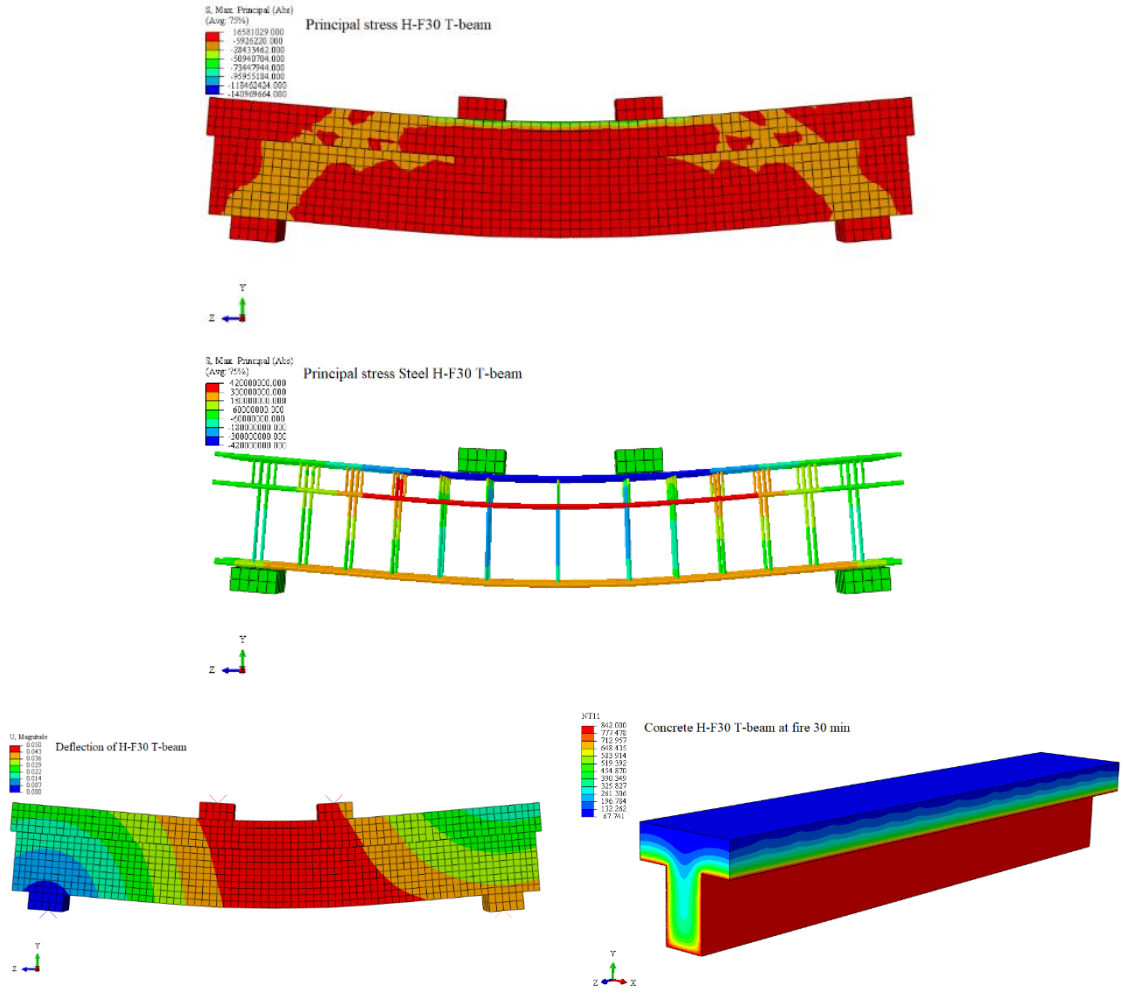

Figure 5-32: T-beam H-F30-0 deflection and principal stress distribution for concrete and steel reinforcement

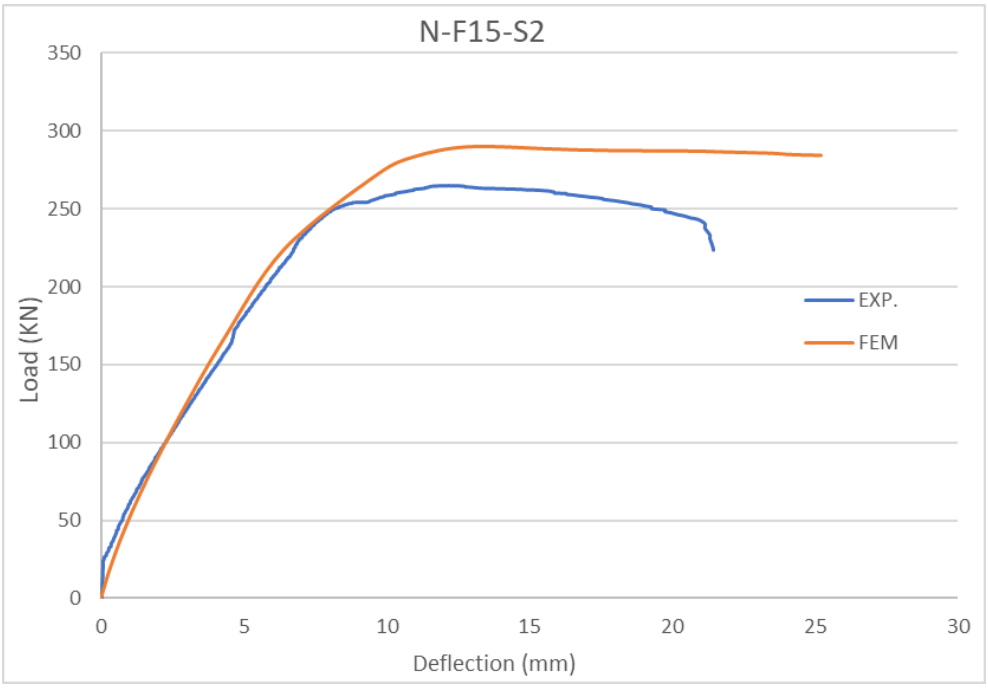

Figure 5-33: N-F15-S2 Experimental and Finite Element Method Load-Deflection Curve Comparison

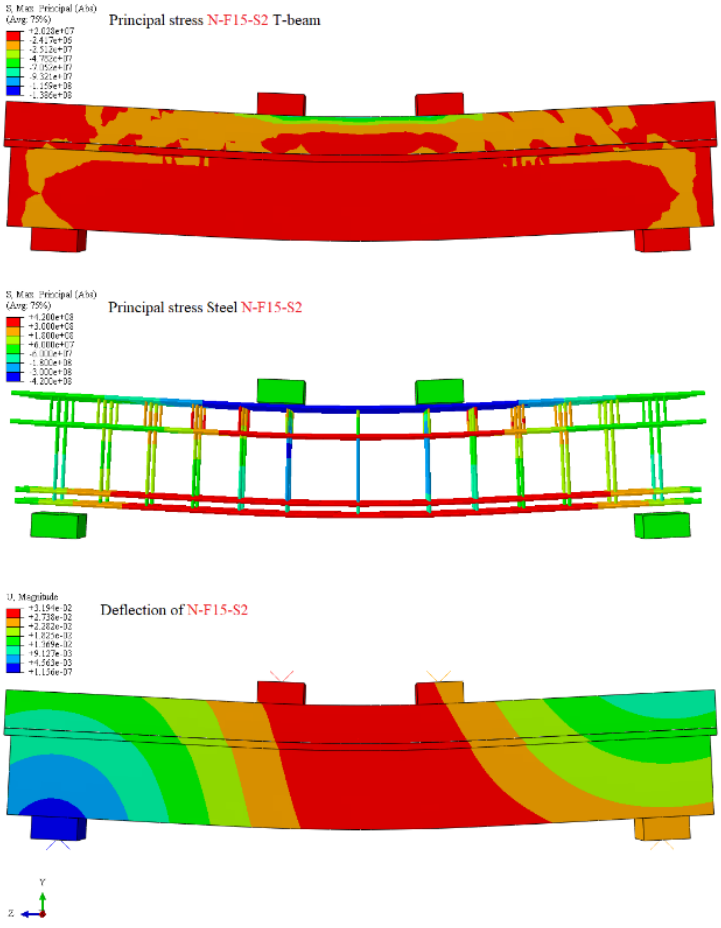

Figure 5-34: T-beam N-F15-S2 deflection and principal stress distribution for concrete and steel reinforcement

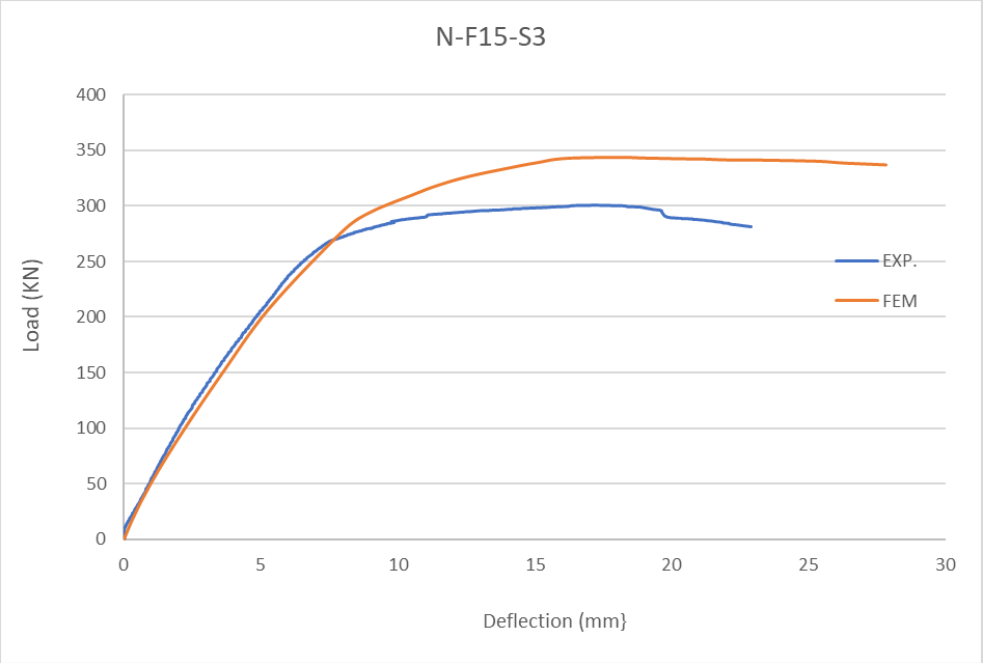

Figure 5-35: N-F15-S3 Experimental and Finite Element Method Load-Deflection Curve Comparison

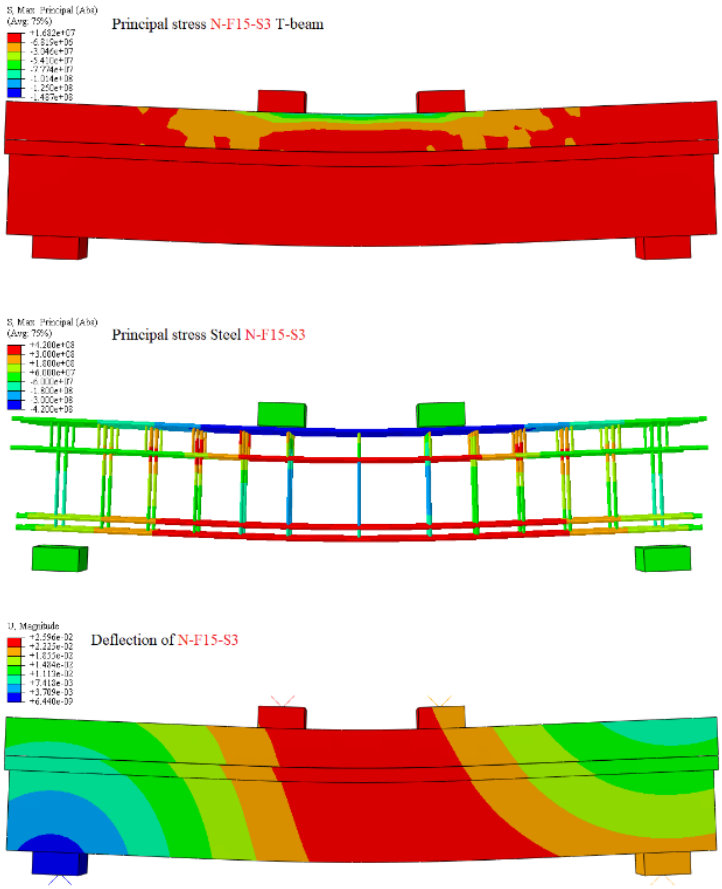

Figure 5-36: T-beam N-F15-S3 deflection and principal stress distribution for concrete and steel reinforcement

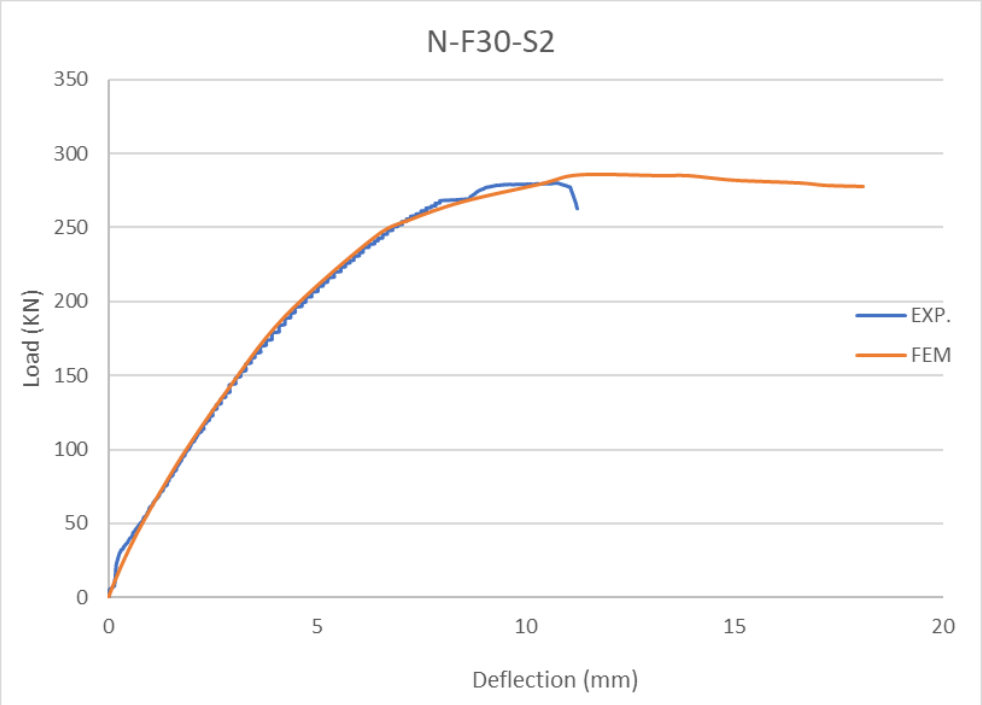

Figure 5-37: N-F30-S2 Experimental and Finite Element Method Load-Deflection Curve Comparison

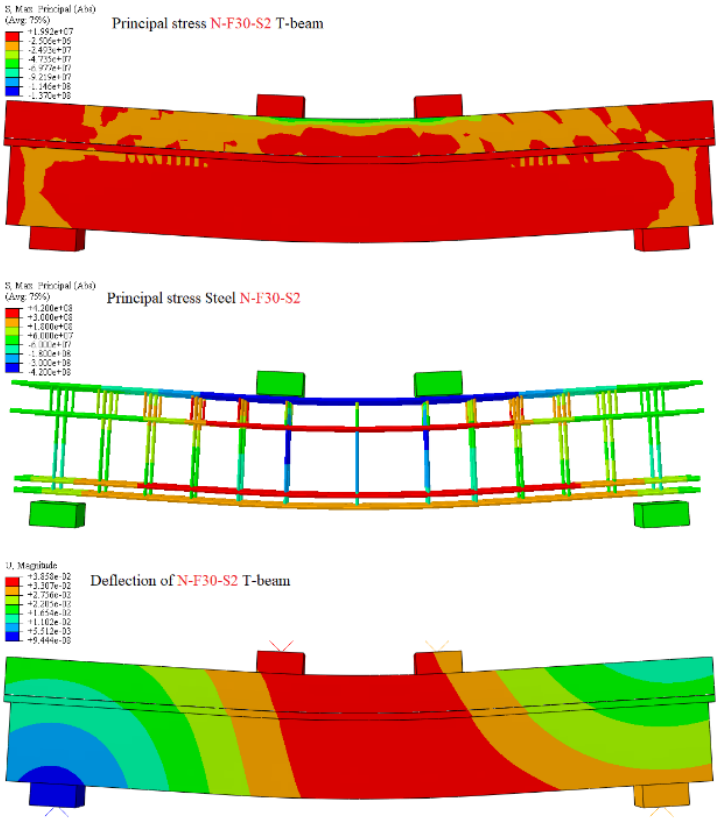

Figure 5-38: T-beam N-F30-S2 deflection and principal stress distribution for concrete and steel reinforcement

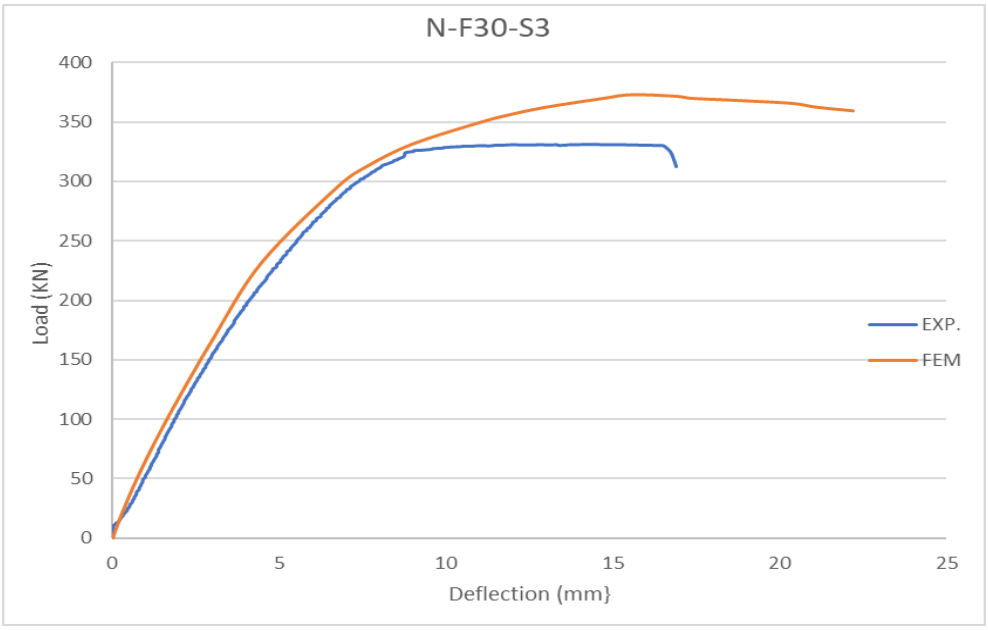

Figure 5-39: N-F30-S3 Experimental and Finite Element Method Load-Deflection Curve Comparison

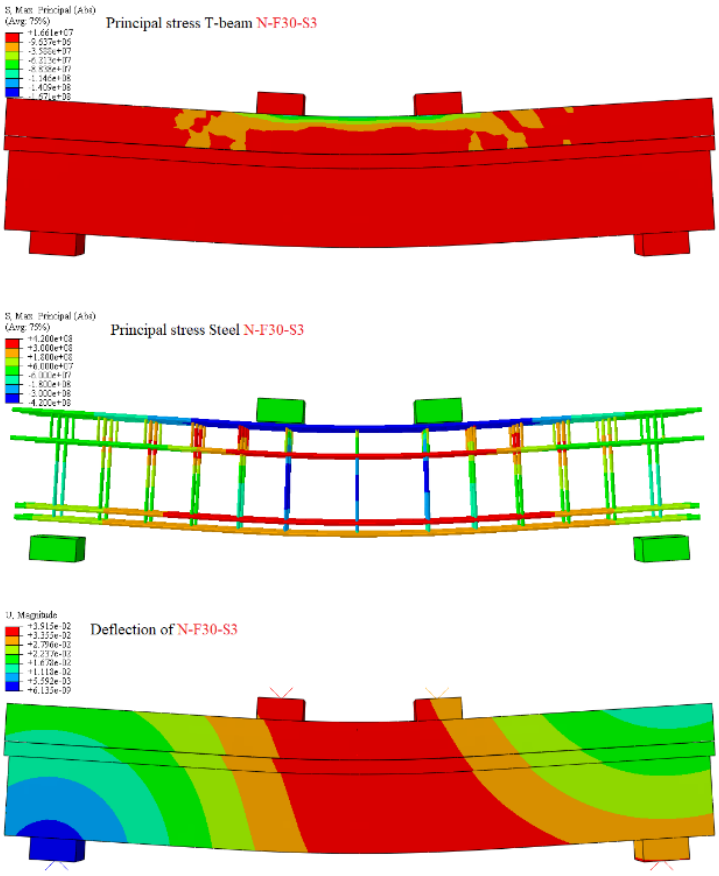

Figure 5-40: T-beam N-F30-S3 deflection and principal stress distribution for concrete and steel reinforcement

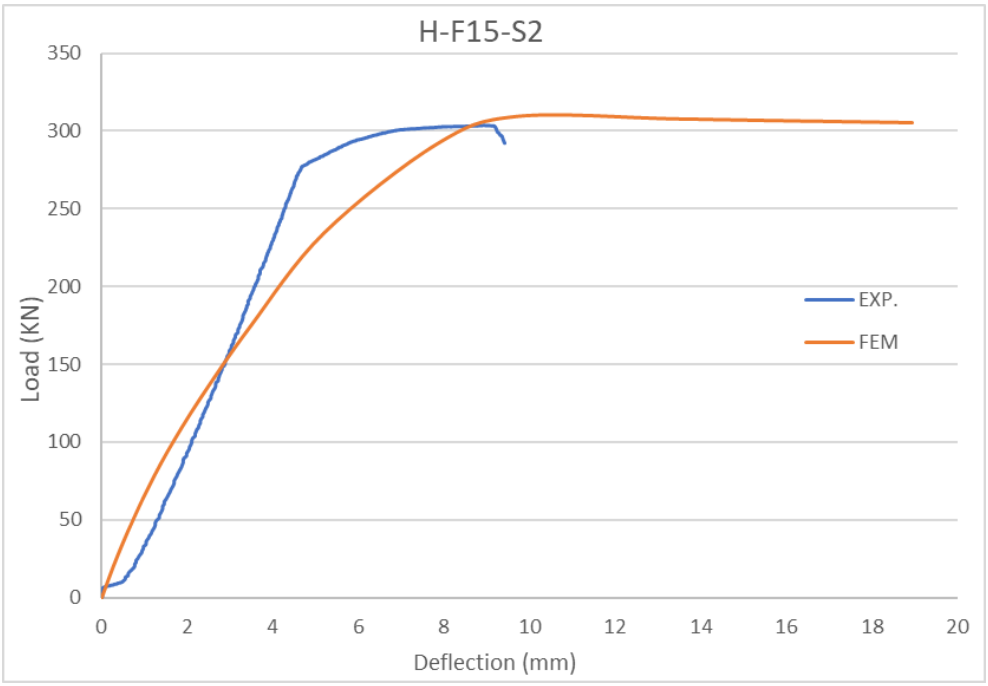

Figure 5-41: H-F15-S2 Experimental and Finite Element Method Load-Deflection Curve Comparison

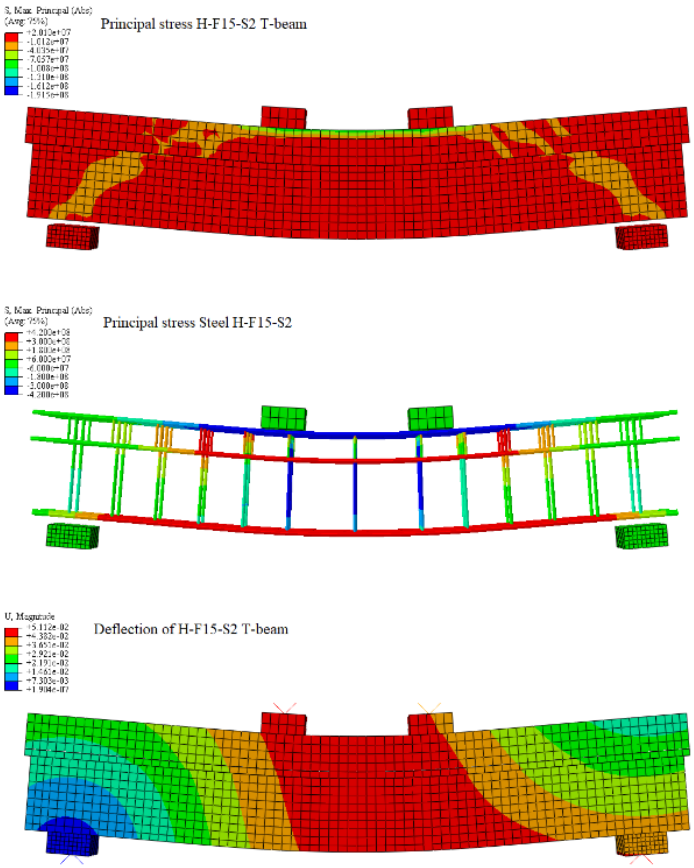

Figure 5-42: T-beam H-F15-S2 deflection and principal stress distribution for concrete and steel reinforcement

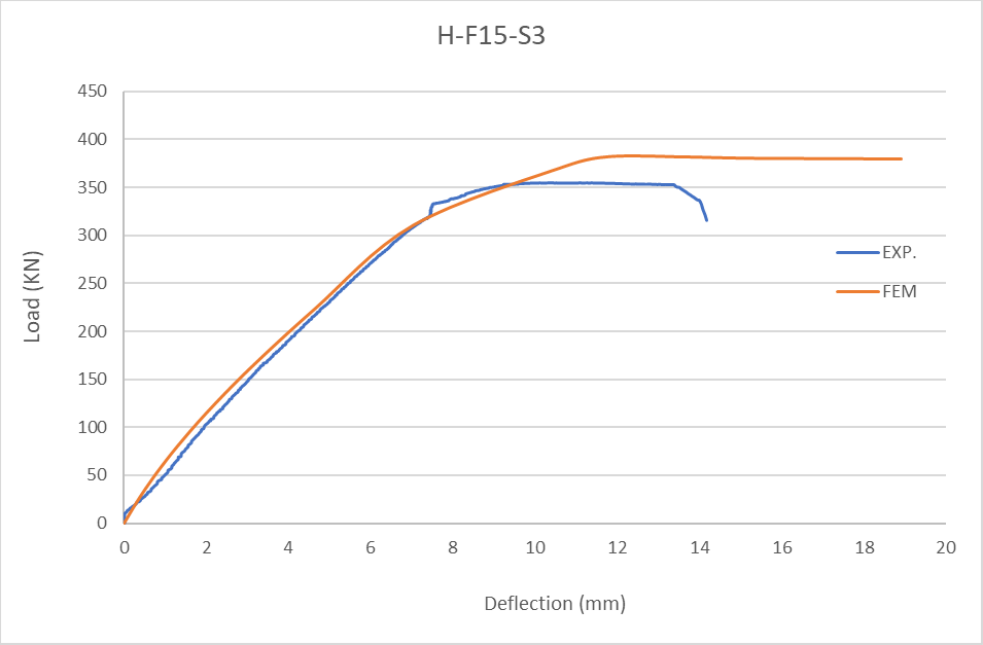

Figure 5-43: H-F15-S3 Experimental and Finite Element Method Load-Deflection Curve Comparison

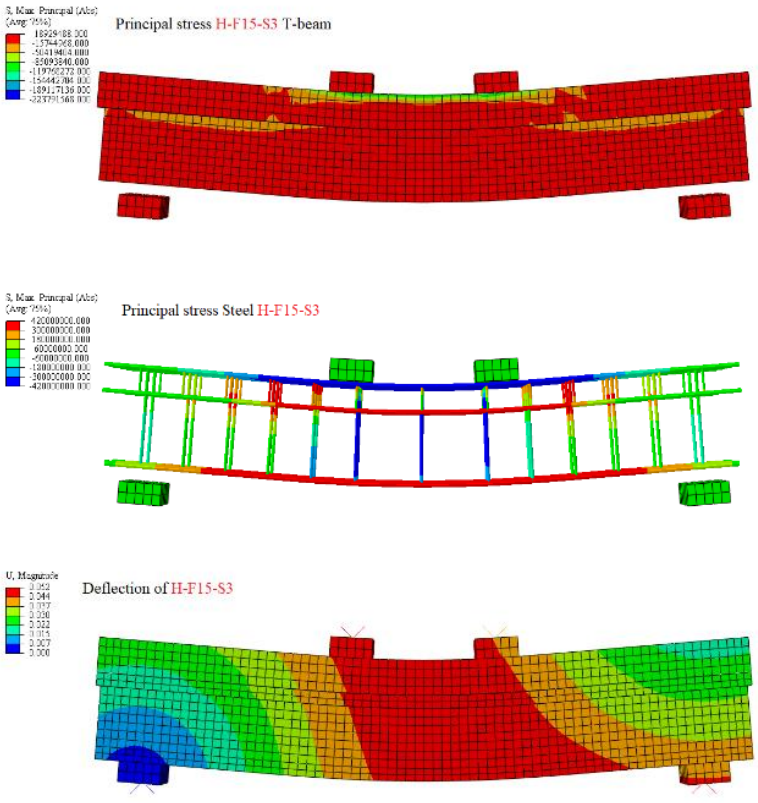

Figure 5-44: T-beam H-F15-S3 deflection and principal stress distribution for concrete and steel reinforcement

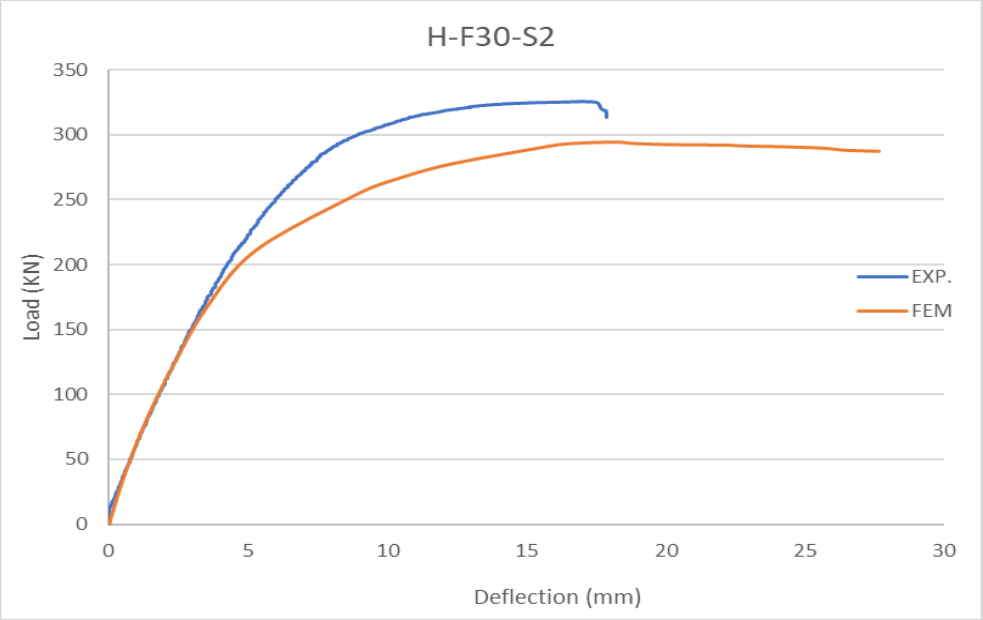

Figure 5-45: H-F30-S2 Experimental and Finite Element Method Load-Deflection Curve Comparison

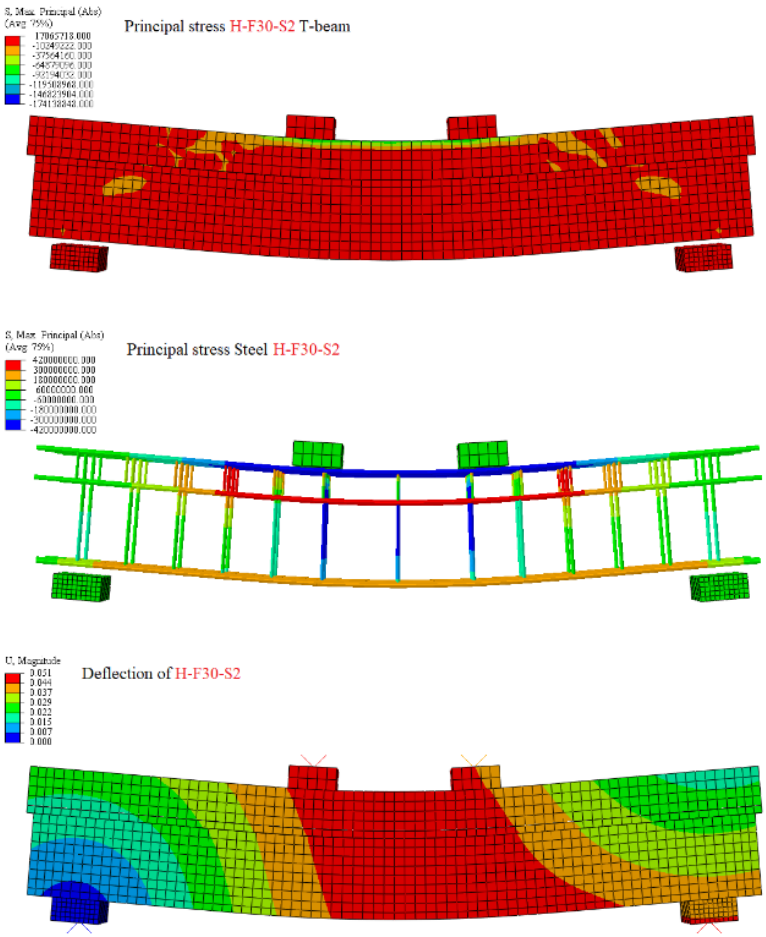

Figure 5-46: T-beam H-F30-S2 deflection and principal stress distribution for concrete and steel reinforcement

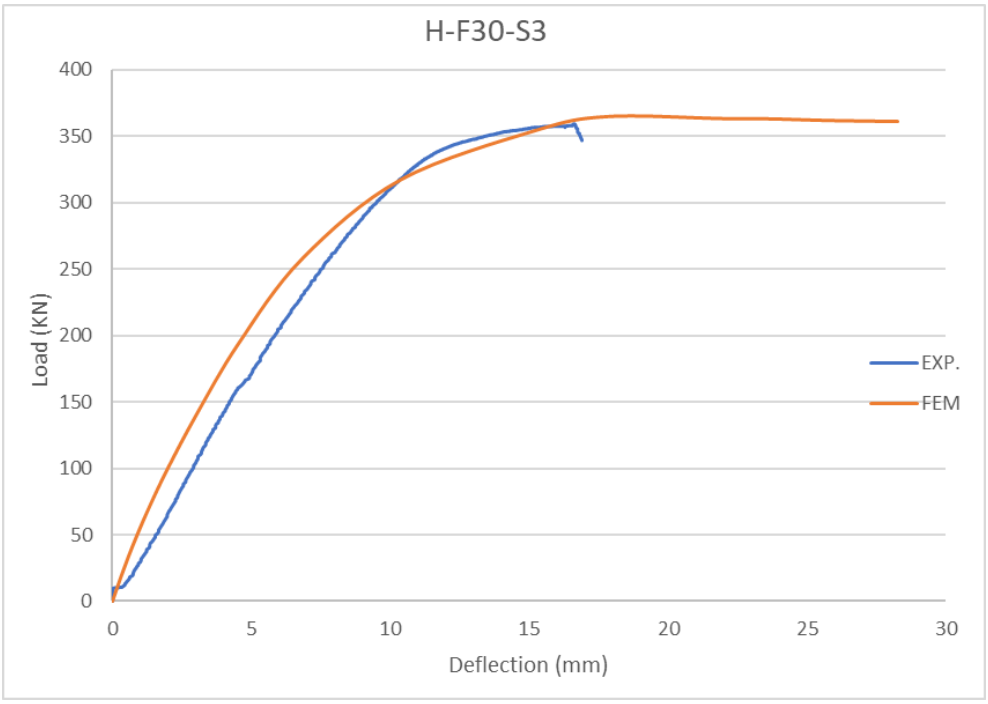

Figure 5-47: H-F30-S3 Experimental and Finite Element Method Load-Deflection Curve Comparison

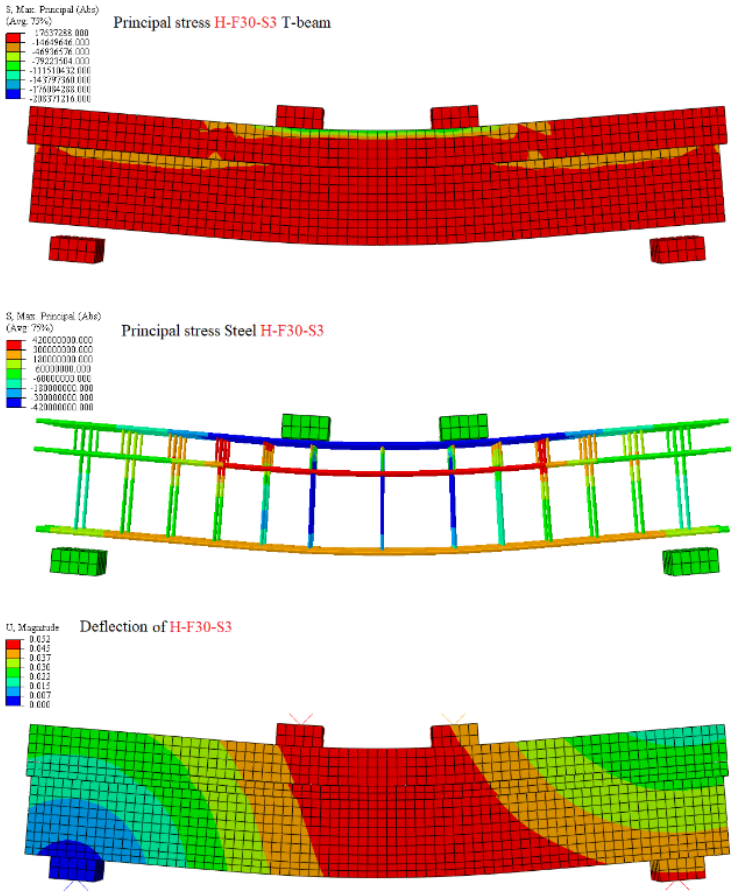

Figure 5-48: T-beam H-F30-S3 deflection and principal stress distribution for concrete and steel reinforcement

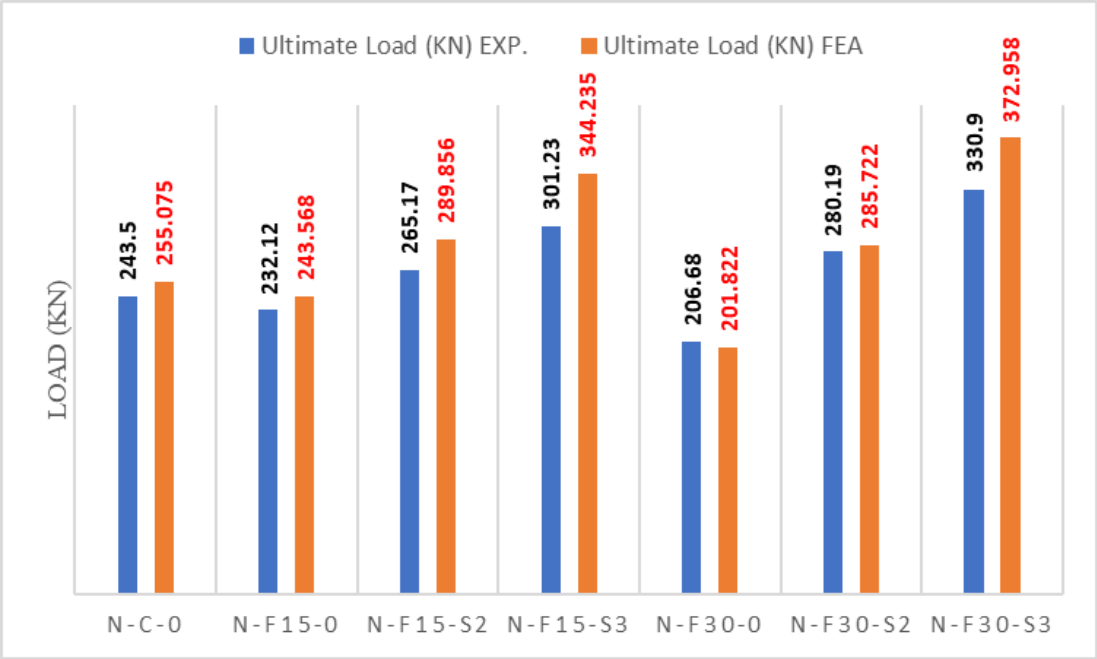

Figure 5-49: T-beams of NSLWC ultimate load, compared (experimentally and numerically)

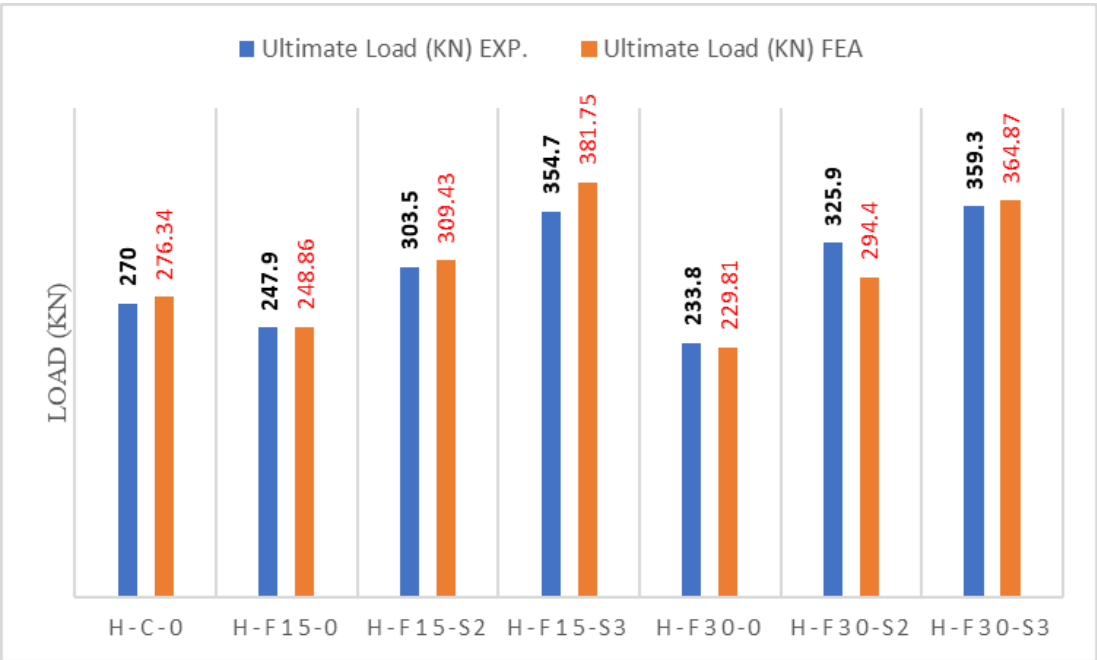

Figure 5-50: T-beams of HSLWC ultimate load, compared (experimentally and numerically)

The minimum and highest absolute errors "variation" for the specimen's **deflection** that matched the maximum load were, respectively, 1.59% and 13.43% for NSLWC and 3.93% and 13.89% for HSLWC.

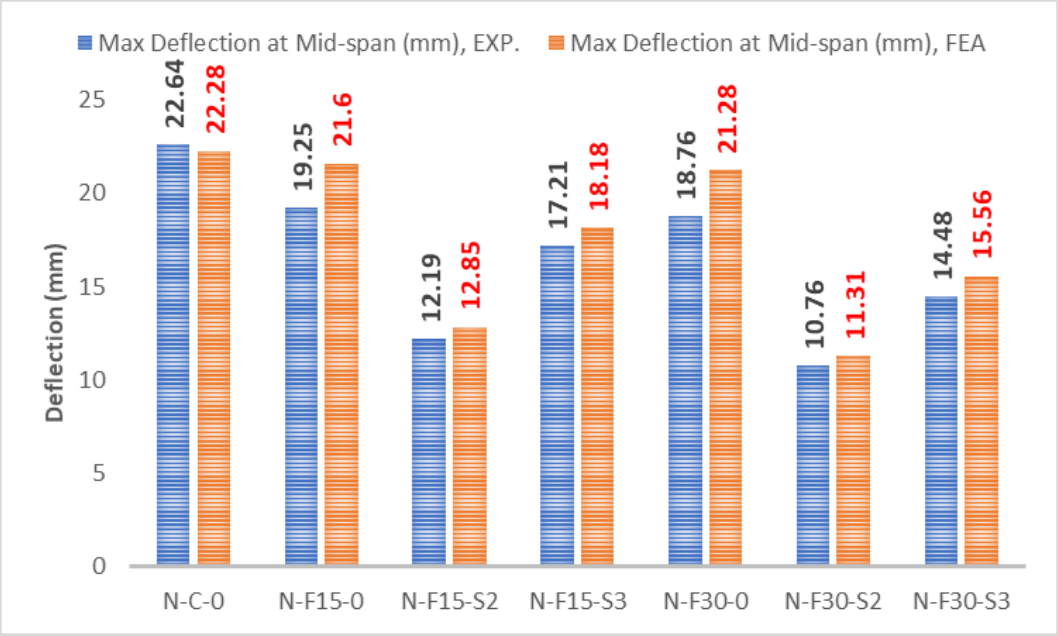

Figure 5-51: Midspan deflection comparison (experimental and numerical) data for NSLWC T-beams

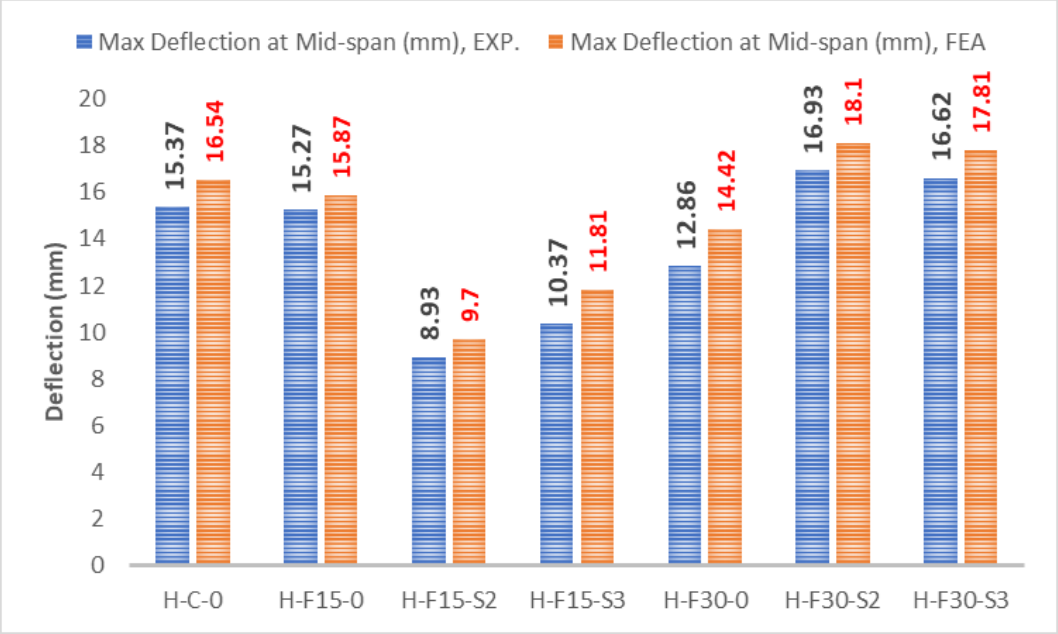

Figure 5-52: Midspan deflection comparison (experimental and numerical) data for HSLWC T-beams

Contour maps which include (T-beam deflection and principal stress distribution for concrete and steel reinforcement) for research study specimen (N-C-0, H-C-0, N-F15-0, N-F30-0, H-F15-0, H-F30-0, N-F15-S2, N-F15-S3, N-F30-S2, N-F30-S3, H-F15-S2, H-F15-S3, H-F30-S2, and H-F30-S3) respectively, are shown in (Figure 5-20), (Figure 5-22), (Figure 5-26), (Figure 5-28), (Figure 5-30), (Figure 5-32), (Figure 5-34), (Figure 5-36), (Figure 5-38),

(Figure 5-40), (Figure 5-42), (Figure 5-44), (Figure 5-46), and (Figure 5-48) respectively, while (Principal strain for T-beam and steel reinforcement) is illustrated in Appendix as shown in (Figure A-1), (Figure A-2), (Figure A-9), (Figure A-10), (Figure A-11), (Figure A-12), (Figure A-13), (Figure A-14), (Figure A-15), (Figure A-16), (Figure A-17), (Figure A-18), (Figure A-19), and (Figure A-20) respectively.

In the light of this and given that the projected errors were fewer than 15%,it can be concluded that, in comparison to other researchers' investigations, the simulation procedure was successful and accurate,[60]. There appears to be a good agreement between the experimental data and the model predictions. As a result, the created model may be conveniently used to the parametric examination of the contested T-beam analysis.

Chapter SIX

Conclusions and Recommendation

6.1 Conclusions the Results

6.1.1 Material Properties Conclusions

The following conclusions were concluded based on the overall results of the experimental work:

1- Structural lightweight concrete made using LECA aggregate satisfies the criteria of the standards codes of ACI 213R-14 and having an average oven dry density of 1977 Kg/m^3 and an average cylinder compressive strength of 31.5 MPa.

2- Expanded clay as a lightweight aggregate has been tested for its physical qualities using the standards set out by ASTM C 330.The results of the laboratory testing indicate that it is effective and can be utilized to make lightweight concrete.

3- When comparing the density of lightweight aggregate concrete to the formulas of ACI318, 2014, it is important to take into account the developed equations between mechanical properties.

4- After using ABAQUS for finite element modelling to determine the absolute deviation between experimental and numerical data, we find that the simulation procedure was successful within an error of 15%.

5- High accuracy in the modelling method was confirmed by numerical validation using the ABAQUS programmed of experimental data on load bearing capability of the reference T-beam, fire damage, repairing damaged T-beam and detailed temperature distribution.

6.1.2 T-beam Actions Conclusions

Based on the overall results obtained from the experimental work, the following conclusions can be drawn:

1- A flexural failure was seen for all T-beams, which was expected.

2- About a 33.87% temperature difference was observed between the midpoint and the periphery of the T-beam cross section. Although there was a temperature disparity of 74.24% between the spots on the steel

bars and the concrete center.

3- The concrete T-beams with a 30-minute firing time had a lower cracking load (service loading) compared to the reference T-beam by 54%-67%. However, when fire-damaged T-beams were strengthened with a SIFCON jacket layer, the result was an improvement that was superior to the reference T-beam by a factor of 2.98-3.27 for a jacket thickness of 15 mm and by a factor of 2.96-5.73 for a jacket thickness of 30 mm.
4- For T-beams HSLWC, the 30 min. fire damaged T-beams showed a significant drop in load capacity of roughly 34.1%, in comparison to the undamaged T-beam.
5- The experimental results demonstrated that, 30 min. fire damage has a major impact on the ductility. In contrast to the un-strengthened (damage) T-beam, strengthening T-beam increased its ductility index by roughly 9.9% and 21.5% for T-beams repairing with 15 mm and 30 mm SIFCON jacket, respectively.
6- Damaged T-beams absorbed about 54% less energy than their undamaged counterparts after 30 min. in the fire, and damaged T-beams reinforced with 15 mm and 30 mm SFICON absorbed about 38% more energy than their undamaged counterparts.
7- The experiments revealed that firing samples for 30 min. reduced the initial stiffness values by around 26%. The rigidity of the reinforced members is expected to be between 3 and 3.5 times that of the damaged members before reinforcement, and 2.25 times that of the undamaged (reference T-beam)

6.2 Recommendations for Future works

The following are some ideas that might be taken into account as future research:

1- Using lightweight aggregate in place of all or some of the natural fine sand in the production of structural lightweight concrete.
2- Using the plastic waste material as coarse aggregate in mater expected to be subjected to fire due to properties of melting and fill crack at high temperature.
3- Examine how high-performance lightweight aggregate concrete behaves structurally.
4- Look at the performance of lightweight aggregate concrete that has been strengthened with carbon fiber reinforced polymer (CFRP) bars.
5- Consider the structural behavior of a T-beam cast from continuous lightweight aggregate concrete.
6- Look at the structural performance of a prestressed T-beam made of lightweight aggregate concrete.
7- Shear failure in structural lightweight aggregate concrete T-beams is a topic that should be looked into.
8- Determine how the addition of steel fibers to RLAC T-beams impacts their performance in terms of shear strength.
9- Examine the response of both a normal weight and a lightweight aggregate concrete T-beam under a dynamic load.
10- Spalling can be prevented or at least mitigated by including polypropylene fiber into the concrete mix, which expands to fill cracks due to its melting properties under fire.
11- Use Scoria lightweight aggregate instead of LECA.

References

Reference

[1] A. H. Nilson, D. Darwin, and C. W. Dolan, *Design Concrete Sructures*. 2016.

[2] S. abdulameer Badar, L. S. Rasheed, and S. A. Salih, "The Structural Characteristics of Lightweight Aggregate Concrete Beams," *J. Univ. Babylon Eng. Sci.*, vol. 27, no. 2, pp. 64–73, 2019, doi: 10.29196/jubes.v27i2.2293.

[3] A. M. Neville, *Properties of concrete*. 2021. doi: 10.4324/9780203967874-11.

[4] H. Mefteh, O. Kebaïli, H. Oucief, L. Berredjem, and N. Arabi, "Influence of moisture conditioning of recycled aggregates on the properties of fresh and hardened concrete," *J. Clean. Prod.*, vol. 54, no. September, pp. 282–288, 2013, doi: 10.1016/j.jclepro.2013.05.009.

[5] V. W. Y. Tam, "Comparing the implementation of concrete recycling in the Australian and Japanese construction industries," *J. Clean. Prod.*, vol. 17, no. 7, pp. 688–702, 2009, doi: 10.1016/j.jclepro.2008.11.015.

[6] F. Pelisser, A. Barcelos, D. Santos, M. Peterson, and A. M. Bernardin, "Lightweight concrete production with low Portland cement consumption," *J. Clean. Prod.*, vol. 23, no. 1, pp. 68–74, 2012, doi: 10.1016/j.jclepro.2011.10.010.

[7] A. D. Kumar, P. Poluraju, and H. Kasagani, "EXPERIMENTAL INVESTIGATION ON MECHANICAL PROPERTIES OF LIGHTWEIGHT AGGREGATE CONCRETE," *Civ. Environ. Eng.*, vol. 18, no. 2, p. 12, 2022, doi: 10.2478/cee-2022-0061.

[8] S. Abdul, A. Bader, S. A. A. Bader, L. S. Rasheed, and S. A. Salih, "Structural Sustainability of Lightweight Concrete girder," University of Kerbala, 2015.

[9] T. Bremner and P. Eng, "Environmental aspects of concrete: problems and solutions," in *Proceedings of the First all Russian Conference on Concrete*

and Reinforced Concrete, Editors: NIIZhB, Moscow, 2001, no. September 2001, pp. 232–246. [Online]. Available: http://unb.ca/civil/materials/materialsgrp/eac.pdf

[10] Z. Jamellodin, L. P. Sim, H. C. Qing, S. H. Adnan, N. Salleh, and N. A. A. Hamid, "Strength Performance of Oil Palm Shell Lightweight Aggregate Concrete," *IOP Conf. Ser. Mater. Sci. Eng.*, vol. 1144, no. 1, p. 012042, 2021, doi: 10.1088/1757-899x/1144/1/012042.

[11] P. Shafigha, H. Bin Mahmuda, M. Z. Bin Jumaata, R. Ahmmad, and S. Bahria, "Structural lightweight aggregate concrete using two types of waste from the palm oil industry as aggregate," *J. Clean. Prod.*, 2014, doi: 10.1016/j.jclepro.2014.05.051.

[12] N. A. A. Alwash, G. M. Habeeb, and F. H. N. Al-Mamoori, "FLEXURAL BEHAVIOR OF LIGHT WEIGHT CONCRETE SLAB PANELS REINFORCED WITH CFRP BARS," *Al-Qadisiyah J. Eng. Sci.*, vol. 10, no. 4, p. 16, 2017, doi: 10.30772/qjes.v10i4.482.

[13] L. Alarcon-Ruiz, G. Platret, E. Massieu, and A. Ehrlacher, "The use of thermal analysis in assessing the effect of temperature on a cement paste," *Cem. Concr. Res.*, vol. 35, no. 3, pp. 609–613, 2005, doi: 10.1016/j.cemconres.2004.06.015.

[14] R. H. Haddad and L. G. Shannis, "Post-fire behavior of bond between high strength pozzolanic concrete and reinforcing steel," *Constr. Build. Mater.*, vol. 18, no. 6, pp. 425–435, 2004, doi: 10.1016/j.conbuildmat.2004.03.006.

[15] J. Newman and Ban Seng Choo, *Advanced Concrete Technology*. Butterworth-Heinemann An imprint of Elsevier Linacre House, Jordan Hill, Oxford OX2 8DP 200 Wheeler Road, Burlington MA 01803, 2003.

[16] ACI Committee 318, *Building Code Requirements for Structural Concrete (ACI 318-14)*, vol. 11. American Concrete Institute 38800 Country Club Drive Farmington Hills, MI 48331, 2014. [Online]. Available:

www.concrete.org

[17] ASTM C 567, “Standard Test Method for Determining Density of Structural Lightweight Concrete 1,” *ASTM Int.*, vol. i, pp. 22–24, 2010, doi: 10.1520/C0567.

[18] ACI-318, *AMERICAN CONCRETE INSTITUTE. ACI 318-19: Building code requirements for structural concrete*. 2019.

[19] ACI 213, *Guide for structural lighweight concrete*. American Concrete Institute 38800 Country Club Drive Farmington Hills, MI 48331, 2014. [Online]. Available: www.concrete.org

[20] Norwegian Standard, “Design of Concrete Structure". Norwegian Standard NS3473.E.” standards Norway, p. 136, 2004.

[21] RILEM, “RILEM Lightweight Concrete Committee Terminology and Definitions,” *Mater. Struct.*, vol. 3, no. 13, p. 10, 1970, [Online]. Available: https://www.rilem.net/publication/119?id_papier=4755

[22] D. ENV, “Part 1.4 General rules — Lightweight aggregate concrete with closed structure,” *Design of Structural Elements*. pp. 334–394, 1996.

[23] CEN, “UK National Annex to Eurocode 2: Design of concrete structures; Part 1-2: Structural fire design,” 2004.

[24] S. Chandra and L. Berntsson, *LIGHTWEIGHT AGGREGATE CONCRETE*. Chalmers University of Technology Göteborg, Sweden: WILLIAM ANDREW PUBLISHING, 2002. [Online]. Available: www.williamandrew.com

[25] I. Asadi, P. Shafigh, Z. F. Bin Abu Hassan, and N. B. Mahyuddin, “Thermal conductivity of concrete – A review,” *J. Build. Eng.*, vol. 20, pp. 81–93, 2018, doi: 10.1016/j.jobe.2018.07.002.

[26] Hjh Kamsiah Mohd.Ismail, M. S. Fathi, and N. bte Manaf, “STUDY OF LIGHTWEIGHT CONCRETE BEHAVIOUR,” *PENGARUH Pengguna. PASTA LABU KUNING (Cucurbita Moschata) UNTUK SUBSTITUSI TEPUNG TERIGU DENGAN PENAMBAHAN TEPUNG ANGKAK*

DALAM PEMBUATAN MIE KERING, vol. 15, no. 1, pp. 165–175, 2016, [Online]. Available: https://core.ac.uk/download/pdf/196255896.pdf

[27] P. B. Castro and SÉBASTIEN CARON, "STRUCTURAL LIGHTWEIGHT CONCRETE WITH NATURAL PERLITE AGGREGATE AND PERLITE POWDER," 2006.

[28] H. K. M. Ismail, M. S. Fathi, and N. bte Manaf, "STUDY OF LIGHTWEIGHT CONCRETE BEHAVIOUR," *CORE – Aggregating world's open access Res. Pap.*, vol. 71908, no. 2, pp. 35–43, [Online]. Available: https://core.ac.uk/display/11780783?utm_source=pdf&utm_medium=banner&utm_campaign=pdf-decoration-v1

[29] T. Y. Lo and H. Z. Cui, "Properties of Green Lightweight Aggregate Concrete," *Int. Work. Sustain. Dev. Concr. Technol.*, vol. 81, no. January 2004, pp. 113–8, 2002.

[30] J. W. C. Iii *et al.*, *State of the Art Report on Full-Depth Precast Concrete Bridge Deck Panels*. Precast/Prestressed Concrete Institute, 2011.

[31] P. R. Bergstresser, "Building bridges," *J. Invest. Dermatol.*, vol. 132, no. 5, pp. 1309–1310, 2012, doi: 10.1038/jid.2012.70.

[32] R. Z. Al-Rousan and M. J. Shannag, "Shear Repairing and Strengthening of Reinforced Concrete Beams Using SIFCON," *Structures*, vol. 14, no. 2017, pp. 389–399, Jun. 2018, doi: 10.1016/j.istruc.2018.05.001.

[33] S. Mindess, J. F. Young, and D. Darwin, "Concrete_2nd edition." Prentice Hall; 0002- edition (January 1, 2002), p. 657, 2002.

[34] JOHN L.CLARKE, *Structural lightweight aggregate concrete*, vol. 33, no. 10. Blackie Academic & Professional, an imprint of Chapman & Hall, Wester Cleddens Road, Bishopbriggs, Glasgow G64 2NZ Chapman, 1999.

[35] H. M. Saleh, "Using of Porcelinite as Coarse Aggregate in Concrete," *Tikrit J. Eng. Sci.*, vol. 19, no. 3, pp. 33–40, 2012, doi: 10.25130/tjes.19.3.04.

[36] E. A. Almajeed and S. K. Turki, “Synthesis of Expanded Clay Aggregate Pellets by Using Local Raw Materials,” *J. Univ. Babylon Eng. Sci.*, vol. 26, no. 4, pp. 345–353, 2018, doi: 10.29196/jub.v26i4.812.

[37] A. M. Rashad, “Lightweight expanded clay aggregate as a building material – An overview,” *Constr. Build. Mater.*, vol. 170, pp. 757–775, 2018, doi: 10.1016/j.conbuildmat.2018.03.009.

[38] Q. J. H. Assist and N. M. Fawzi, “The Effect of Different Types of Aggregate and Additives on the Properties of Self-Compacting Lightweight Concrete,” *J. Eng.*, vol. 18, no. 8, p. 14, 2012.

[39] T. S. Al-Attar, A. M. Abdullatif, and A. J. Al-Saad, “Effect of Internal Curing on StrengthDevelopment of High Performance Concrete by Using Crushed Lightweight Porcelinite,” *Eng. Technol. J.*, vol. 32, no. 11, pp. 2803–2814, 2014, doi: 10.30684/etj.32.11A.16.

[40] F. H. N. Al-Mamoori, M. H. N. Al-Mamoori, and Wissam Nadir Najim, “Production of Structural Light-Weight Aggregate Concrete Using Different Types of Iraqi Local Crushed Materials as Coarse Aggregate,” *J. Univ. Babylon*, vol. 26, no. 1, pp. 362–375, 2018.

[41] J. Alduaij, K. Alshaleh, M. Naseer Haque, and K. Ellaithy, “Lightweight concrete in hot coastal areas,” *Cem. Concr. Compos.*, vol. 21, no. 5–6, pp. 453–458, 1999, doi: 10.1016/S0958-9465(99)00035-9.

[42] H. M. Al-baghdadi, “Using Local Materials Wastes For Development Of High Strength Lightweight Concrete,” *J. Babylon Univ. Appl. Sci.*, vol. 19, no. 1, pp. 226–239, 2011.

[43] A. albayati, nabeel, “BEHAVIOR OF PORCELANITE REINFORCED CONCRETE DEEP BEAMS,” 2012.

[44] N. Balasubramanya, “Experimental investigation on development of light weight BY BLENDING WITH LECA AND CINDER,” VISVESVARAYA TECHNOLOGICAL UNIVERSITY, 2015.

[45] J. N. Farahani, P. Shafigh, and H. Bin Mahmud, “Production of A Green

Lightweight Aggregate Concrete by Incorporating High Volume Locally Available Waste Materials," in *Procedia Engineering*, 2017, vol. 184, pp. 778–783. doi: 10.1016/j.proeng.2017.04.158.

[46] A. Zukri, R. Nazir, K. N. M. Said, and H. Moayedi, "Physical and mechanical properties of lightweight expanded clay aggregate (LECA)," *MATEC Web Conf.*, vol. 250, 2018, doi: 10.1051/matecconf/201825001016.

[47] D. C. L. Teo, M. A. Mannan, and J. V. Kurian, "Flexural behaviour of reinforced lightweight concrete beams made with oil palm shell (OPS)," *J. Adv. Concr. Technol.*, vol. 4, no. 3, pp. 459–468, 2006, doi: 10.3151/jact.4.459.

[48] U. J. Alengaram, M. Z. Jumaat, and H. Mahmud, "Ductility behaviour of reinforced palm kernel shell concrete beams," *Eur. J. Sci. Res.*, vol. 23, no. 3, pp. 406–420, 2008.

[49] F. Altun and B. Aktaş, "Investigation of reinforced concrete beams behavior of steel fiber added lightweight concrete," *Constr. Build. Mater.*, vol. 38, pp. 575–581, 2013, doi: 10.1016/j.conbuildmat.2012.09.022.

[50] C. Vázquez-Herrero, I. Martínez-Lage, H. Vázquez-Vázquez, and F. Martínez-Abella, "Comparative study of the flexural behavior of lightweight and normal weight prestressed concrete beams," *Eng. Struct.*, vol. 56, pp. 1868–1879, 2013, doi: 10.1016/j.engstruct.2013.08.008.

[51] R. N. F. Carmo, H. Costa, T. Simões, C. Lourenço, and D. Andrade, "Influence of both concrete strength and transverse confinement on bending behavior of reinforced LWAC beams," *Eng. Struct.*, vol. 48, no. March 2020, pp. 329–341, 2013, doi: 10.1016/j.engstruct.2012.09.030.

[52] T. jaber G. abtan, "Behavior of Hybrid Reinforced Concrete Beams Combining Reactive Powder Concrete and Varying Ytpes of Lightweight Concrete," *J. Eng. Sustain. Dev.*, vol. 20, no. 2, pp. 204–223, 2016.

[53] P. Chandramouli, D. Muthukrishnan, V. Sridhar, V. Sathish Kumar, G.

Murali, and N. I. Vatin, “Flexural Behaviour of Lightweight Reinforced Concrete Beams Internally Reinforced with Welded Wire Mesh,” *Buildings*, vol. 12, no. 9, 2022, doi: 10.3390/buildings12091374.

[54] S.-K. Kim and J.-H. Choi, “Compressive and Tensile Strength Properties of Slurry Infiltrated Fiber Concrete,” *Journal of the Korea Concrete Institute*, vol. 18, no. 5. pp. 703–708, 2006. doi: 10.4334/jkci.2006.18.5.703.

[55] W. Y. Gao, J. G. Teng, and J. G. Dai, “Fire resistance of RC beams under design fire exposure,” *Mag. Concr. Res.*, vol. 69, no. 8, pp. 402–423, 2017, doi: 10.1680/jmacr.15.00329.

[56] E. Sancak, Y. Dursun Sari, and O. Simsek, “Effects of elevated temperature on compressive strength and weight loss of the light-weight concrete with silica fume and superplasticizer,” *Cem. Concr. Compos.*, vol. 30, no. 8, pp. 715–721, 2008, doi: 10.1016/j.cemconcomp.2008.01.004.

[57] H. Tanyildizi and A. Coskun, “Performance of lightweight concrete with silica fume after high temperature,” *Constr. Build. Mater.*, vol. 22, no. 10, pp. 2124–2129, 2008, doi: 10.1016/j.conbuildmat.2007.07.017.

[58] İ. Türkmen and S. B. Fındık, “Several properties ofmineral admixtured lightweight mortars at elevated temperatures,” *Wiley Intersci.*, no. August 2008, p. 13, 2010, doi: 10.1002/fam.

[59] M. Yoon, G. Kim, G. C. Choe, Y. Lee, and T. Lee, “Effect of coarse aggregate type and loading level on the high temperature properties of concrete,” *Constr. Build. Mater.*, vol. 78, pp. 26–33, 2015, doi: 10.1016/j.conbuildmat.2014.12.096.

[60] Ahmed Habeeb Abdulhussein Youssef, “Shear Repairing and Strengthening of Fire Damaged Normal and High Strength Reinforced Lightweight Concrete Beams Using Slurry Infiltrated Fibre Concrete,” University of Babylon /College of Engineering, 2022.

[61] “MasterGlenium 54 Submittal.pdf.”

[62] V. K. R. Kodur and L. Phan, “Critical factors governing the fire performance of high strength concrete systems,” *Fire Saf. J.*, vol. 42, no. 6–7, pp. 482–488, 2007, doi: 10.1016/j.firesaf.2006.10.006.

[63] M. B. Dwaikat and V. K. R. Kodur, “Hydrothermal model for predicting fire-induced spalling in concrete structural systems,” *Fire Saf. J.*, vol. 44, no. 3, pp. 425–434, 2009, doi: 10.1016/j.firesaf.2008.09.001.

[64] المركز الوطني للمختبرات الانشائية, “_كراس_مواصفات_المواد_والاعمال_الانشائية.pdf.” 2019.

[65] ا. ا. ل. و. النوعية, “المواصفة القياسية العراقية رقم 5 السمنت البورتلاندي.” p. 11, 1984.

[66] Iraqi Directory of Building Materials, “Iraqi Directory of Building Materials.” 2017.

[67] I. S. ‘‘Portland cement. . B.-I. I. C. No and O. for S. and Q. C. (1984), “وزارة التخطيط جمهورية العراق Republic of Iraq Ministry of Planning المواصفات الفنية اعمال البناء-1-المجلد Technical Specifications for Civil Work.”

[68] A. C29/C29M, “Astm-C29/C29M,” *ASTM International: West Conshohocken, PA, USA*. p. 5, 2016.

[69] ASTM C128, “Standard Test Method for Density, Relative Density (Specific Gravity), and Absorption of Coarse Aggregate,” *Annu. B. ASTM Stand.*, pp. 1–5, 2004.

[70] BIS:456, *Plain and Reinforced Concrete - Code Of Practice*, no. July. 2000.

[71] ASTM C330, “Standard Specification for Lightweight Aggregates for Structural Concrete,” *ASTM Int.*, vol. 552, no. 18, p. 4, 2017, doi: 10.1520/C0330.

[72] A. C. 211, “ACI Standard: Standard practice for selecting proportions for structural lightweight concrete,” *Am. Concr. Institute, ACI Spec. Publ.*, vol. 4, no. 2, p. 20, 1982, doi: 10.1016/0262-5075(82)90019-7.

[73] “basf-masterroc-ms-610-tds.pdf.”

[74] ASTM A 615, “Standard Specification for Deformed and Plain Billet-Steel

Carbon Steel Bars for," *Astm a615*, pp. 1–8, 2015, doi: 10.1520/A0615.

[75] ASTM, "A370: Standard Test Methods and Definitions for Mechanical Testing of Steel Products," *ASTM Int.*, pp. 1–50, 2019, doi: 10.1520/A0370-19E01.2.

[76] Z. M. Khalifah and M. M. Rasheed, "Effect of Strengthenig Beam Sides on," *ISSN 0974-5823 Int. J. Mech. Eng.*, vol. 7, no. March, p. 12, 2022.

[77] ACI. 211.4R-08, "Guide for Selecting Proportions for High-Strength Concrete Using Portland Cement and Other Cementitious Materials," *ACI Comm. 211*, 2008.

[78] ASTM C192, "Standard Practice for Making and Curing Concrete Test Specimens in the Laboratory," *Am. Soc. Test. Mater.*, vol. 04, pp. 1–8, 2016.

[79] M. Kharun *et al.*, "Heat treatment of basalt fiber reinforced expanded clay concrete with increased strength for cast-in-situ construction," *Fibers*, vol. 8, no. 11, pp. 1–16, 2020, doi: 10.3390/fib8110067.

[80] B. S. I. Standards, "Testing concrete — compressive strength of concrete cubes," *Br. Stand. Inst.*, no. 1, pp. 1–10, 1983.

[81] M. Alhassan, R. Al-Rousan, and A. Ababneh, "Flexural behavior of lightweight concrete beams encompassing various dosages of macro synthetic fibers and steel ratios," *Case Stud. Constr. Mater.*, vol. 7, no. November, pp. 280–293, 2017, doi: 10.1016/j.cscm.2017.09.004.

[82] ASTM C143/C143M, "Standard Test Method for Slump of Hydraulic-Cement Concrete," *Astm C143*, no. 1, pp. 1–4, 2015, doi: 10.1520/C0143.

[83] EPG, "ERMCO The European Guidelines for Self-Compacting Concrete," *Eur. Guidel. Self Compact. Concr.*, no. May, 2005.

[84] ASTMC642-06, "Astm C 642," *Standar Test Method Density, Absorption, Voids Hardened Concr.*, pp. 11–13, 2008.

[85] J. J. del Coz-Díaz, J. E. Martínez-Martínez, M. Alonso-Martínez, and F. P. Álvarez Rabanal, "Comparative study of LightWeight and Normal

Concrete composite slabs behaviour under fire conditions," *Eng. Struct.*, vol. 207, no. January, p. 110196, 2020, doi: 10.1016/j.engstruct.2020.110196.

[86] S. T. M. for C. S. of C. ASTM C39 / C39M-18 and C. Specimens., "Astm 39," pp. 1–8, 2019, doi: 10.1520/C0039.

[87] ASTM C469-02, "Standard Test Method for Static Modulus of Elasticity and Poisson's Ratio of Concrete in Compression," *ASTM Stand. B.*, vol. 04, pp. 1–5, 2002, [Online]. Available: http://portales.puj.edu.co/wjfajardo/mecanica de solidos/laboratorios/astm/C469.pdf

[88] ASTM C496, "Standard Test Method for Splitting Tensile Strength of Cylindrical Concrete Specimens," *Annu. B. ASTM Stand.*, vol. i, pp. 545-545–3, 2020, doi: 10.1520/C0496.

[89] ASTM, "ASTMC 78: Standard Test Method for Flexural Strength of Concrete (Using Simple Beam with Third-Point Loading)ASTM International. USA," *Annu. B. ASTM Standars*, vol. 04.02, pp. 1–3, 2002.

[90] ASTM C 597-02, "Pulse Velocity Through Concrete," *United States Am. Soc. Test. Mater.*, vol. 04, no. 02, pp. 3–6, 2016, doi: 10.1520/C0597-16.2.

[91] H. Shakir Al-Aasm, "Empirical Formula for Assessment Concrete Compressive Strength by Using Ultrasonic Pulse Velocity," *Int. J. Eng. Technol.*, vol. 7, no. 4.20, p. 113, 2018, doi: 10.14419/ijet.v7i4.20.25860.

[92] B. Standard, *BS 1881-202: 1986 : Recommendations for surface hardness testing by rebound hammer*. BRITISH STANDARD, 1997.

[93] A. A. Ramezanianpour, E. Ghiasvand, I. Nickseresht, M. Mahdikhani, and F. Moodi, "Influence of various amounts of limestone powder on performance of Portland limestone cement concretes," *Cem. Concr. Compos.*, vol. 31, no. 10, pp. 715–720, 2009, doi: 10.1016/j.cemconcomp.2009.08.003.

[94] V. M. MALHOTRA and N. J. CARINO, *Handbook on Nondestructive*

Testing of Concrete, Second Edition. 2004. doi: 10.1201/9781420040050.ch16.

[95] E. Ünlüoğlu, I. B. Topçu, and B. Yalaman, "Concrete cover effect on reinforced concrete bars exposed to high temperatures," *Constr. Build. Mater.*, vol. 21, no. 6, pp. 1155–1160, 2007, doi: 10.1016/j.conbuildmat.2006.11.019.

[96] Y. Wang, H. Jin, C. Demartino, W. Chen, and Y. Yu, "Mechanical properties of SFRC: Database construction and model prediction," *Case Stud. Constr. Mater.*, vol. 17, p. e01484, Dec. 2022, doi: 10.1016/J.CSCM.2022.E01484.

[97] G. Castellazzi, A. M. D'Altri, S. de Miranda, A. Chiozzi, and A. Tralli, "Numerical insights on the seismic behavior of a nonisolated historical masonry tower," *Bull. Earthq. Eng.*, vol. 16, no. 2, pp. 933–961, 2018, doi: 10.1007/s10518-017-0231-6.

[98] www.ideastatica.com, "IDEA StatiCa Connection," *IDEA Statica Connect. - Theor. Backgr.*, no. November, p. 360, 2017, [Online]. Available: www.ideastatica.com

[99] F. Dabbaghi, A. Tanhadoust, M. L. Nehdi, M. Dehestani, H. Yousefpour, and T. Thai, "High-Temperature Behavior of Lightweight-Aggregate Reinforced Concrete Beams," *ACI Mater. J.*, vol. 119, no. 5, pp. 199–212, 2022, doi: 10.14359/51736093.

[100] Simulia, *ABAQUS/CAE User's Guide*. 2014. [Online]. Available: www.3ds.com/simulia

[101] J. Brier and lia dwi jayanti, *fib model code for concrete structures 2010*, vol. 21, no. 1. 2020. [Online]. Available: http://journal.um-surabaya.ac.id/index.php/JKM/article/view/2203

[102] F. Dabbaghi, A. Tanhadoust, M. L. Nehdi, S. Nasrollahpour, M. Dehestani, and H. Yousefpour, "Life cycle assessment multi-objective optimization and deep belief network model for sustainable lightweight

aggregate concrete," *J. Clean. Prod.*, vol. 318, no. August, p. 128554, 2021, doi: 10.1016/j.jclepro.2021.128554.

[103] F. Dabbaghi *et al.*, "Experimental and informational modeling study on flexural strength of eco-friendly concrete incorporating coal waste," *Sustain.*, vol. 13, no. 13, pp. 1–22, 2021, doi: 10.3390/su13137506.

[104] T. T. Lie and W. W. Stanzak, "FIRE RESISTANCE OF PROTECTED STEEL COLUMNS," *NRC Publ. Rec.*, vol. 10, no. 3, pp. 82–94, 1973.

[105] O. Bahr, P. Schaumann, B. Bollen, and J. Bracke, "Young's modulus and Poisson's ratio of concrete at high temperatures: Experimental investigations," *Mater. Des.*, vol. 45, pp. 421–429, 2013, doi: 10.1016/j.matdes.2012.07.070.

Appendices

A.1 Appendix

(According to ACI 318M-19,[18]) Analyzed of Lightweight Reinforced Concrete T-beam was done.

A.2 T-beam dimensions:

Total span = 1500 mm, center-to-center span length = 1300 mm, height = 250 mm, effective depth = 227.5 mm, beam width = 250 mm, beam depth = 100 mm, and cover thickness = 10 mm.

A.3 Min. reinforcement ratio

$a \leq hf$

$\sum Fx = 0$

$As * Fy = 0.85 * f`c * b * a$

$$a = \frac{4*\frac{Л}{4}*(12)^2*576*10^{-6}}{0.85*26.87*0.25} * 1000 = 45.63 \text{ mm}$$

$$\rho = \frac{As}{b*d} = \frac{4*\frac{Л}{4}*(12)^2}{250*200} = 0.00905$$

$\rho_{max} = 0.85 * \beta_1 * (f`c/Fy) * (\varepsilon_{cu}/(\varepsilon_{cu}+0.004))$

$$\rho_{max} = 0.85 * 0.85 * \frac{26.87}{576} * \frac{0.003}{0.003+0.004} = 0.01444$$

$$\rho_{min} = \max\left[\frac{1.4}{Fy} * \frac{bw}{b}\right] \text{ or } \left[\frac{\sqrt{f`c}}{4*Fy} * \frac{bw}{b}\right]$$

$$\rho_{min} = \max\left[\frac{1.4}{576} * \frac{100}{250}\right] \text{ or } \left[\frac{\sqrt{26.87}}{4*576} * \frac{100}{250}\right] = 0.00097 \text{ or } 0.00089$$

$\rho_{min} = 0.00097$

$\rho_{min} < \rho = 0.00905 < \rho_{max}$ ..... O.K

A.4 Flexure calculation

$Mu = \Phi * \rho * b * d^2 * (1 - 0.59 * \rho * Fy/f`c)$

$$Mu = 0.9 * 0.00905 * 0.25 * 0.2^2 * \left(1 - 0.59 * 0.00905 * \frac{576}{26.87}\right) * 10^{-3}$$

$Mu = 41.55$ kN.m

$Mn = Mu/1$ (Due to analysis purpose) $= 41.55/0.9$

$= 46.16$ kN.m

A.5 Shear calculation

$41.55 * 10^{-3} = 237.5\ Pu$

$Pu = 174.5\ kN$

$Vu\ .\ d = p/2 = 87.47\ kN$

$Vc = \frac{\sqrt{f`c}}{6} * bw * d * 10^{-3}$

$Vc = 43.19\ kN$

$4 * Vc = 172.787$

$2 * Vc = 86.3938$

$Vs = 73.43\ kN$

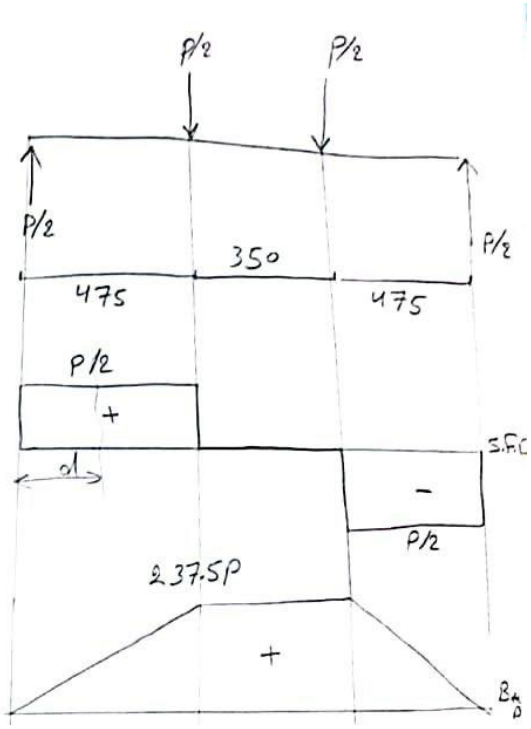

A.6 ABAQUS Appendix

The FEM result of strain behavior for sample are:

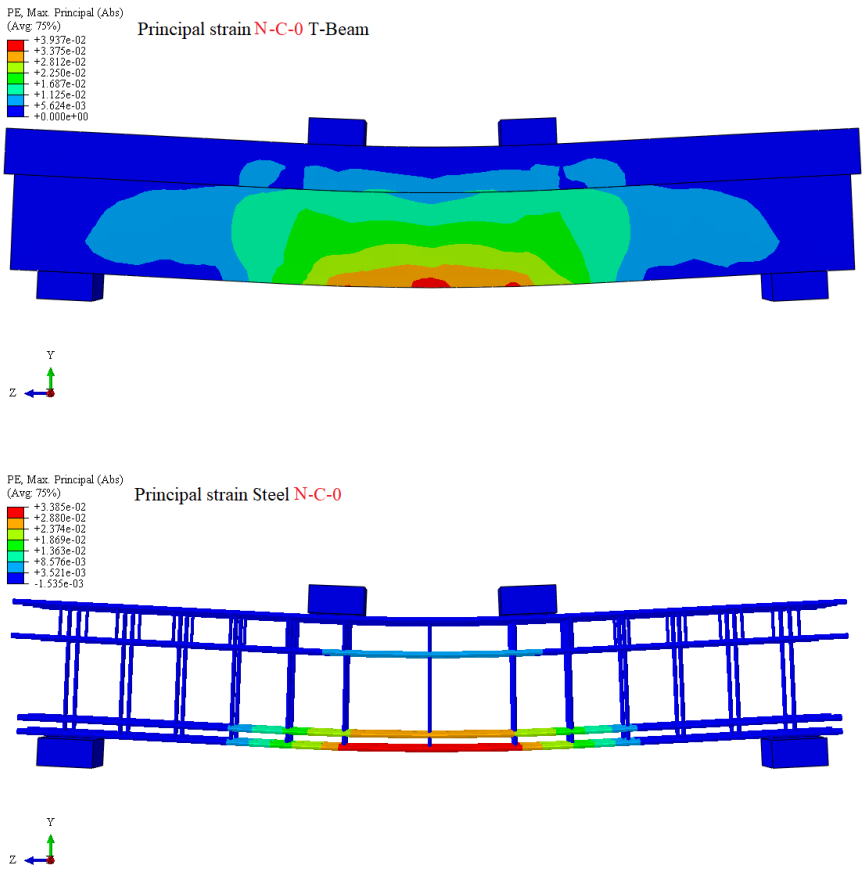

Figure A-1: Principal strain of the T-beam and steel reinforcement, N-C-0

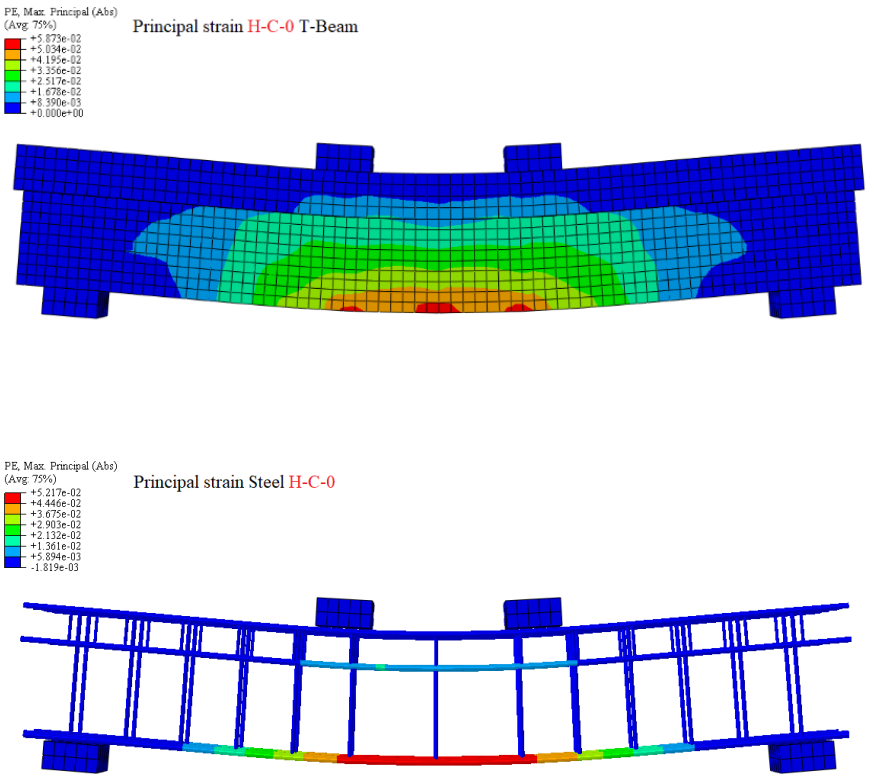

Figure A-2: Principal strain for H-C-0 T-beam and steel reinforcement

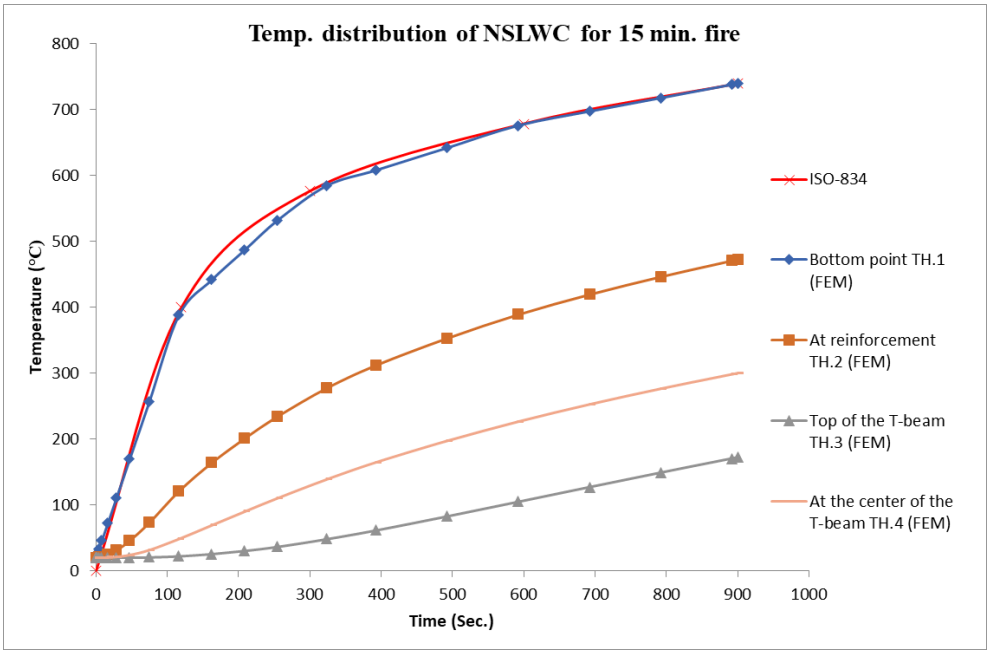

Figure A-3: Time- temperature distribution of NSLWC for 15 min. fire burning along the T-beam cross section

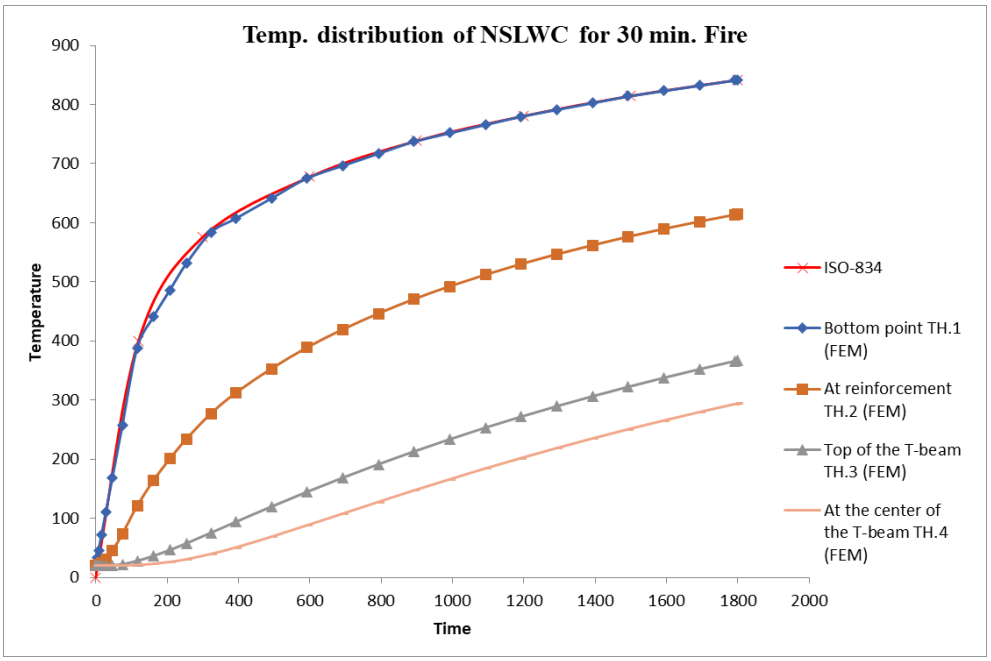

Figure A-4: Time- temperature distribution of NSLWC for 30 min. fire burning along the T-beam cross section

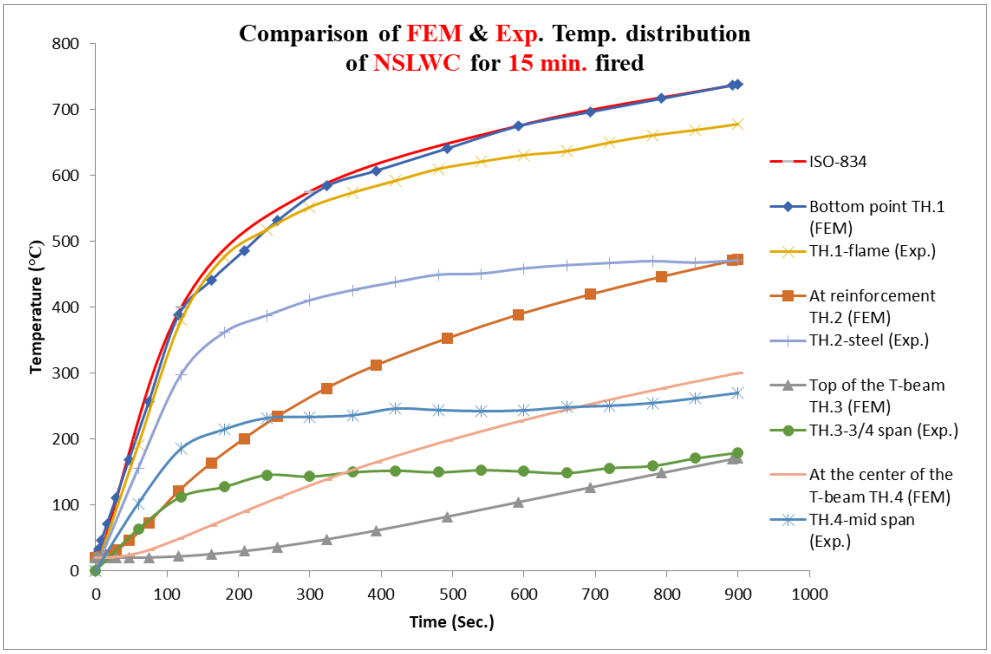

Figure A-5: Comparison of FEM & Exp. Temp. distribution of NSLWC for 15 min. fired

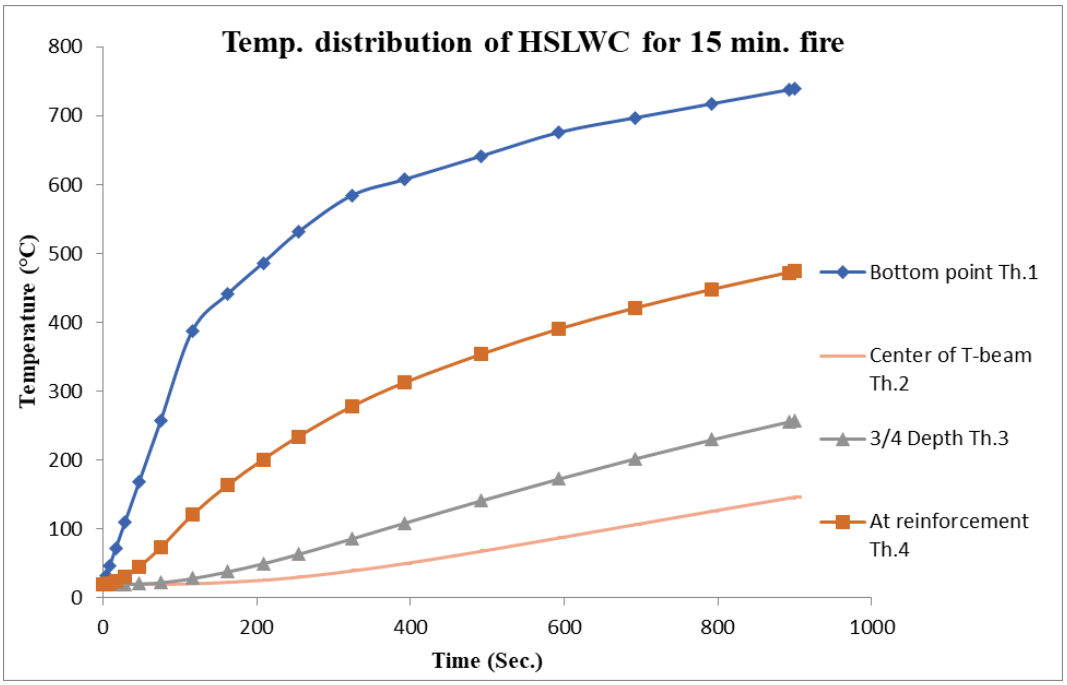

Figure A-6: Time- temperature distribution of HSLWC for 15 min. fire burning along the T-beam cross section

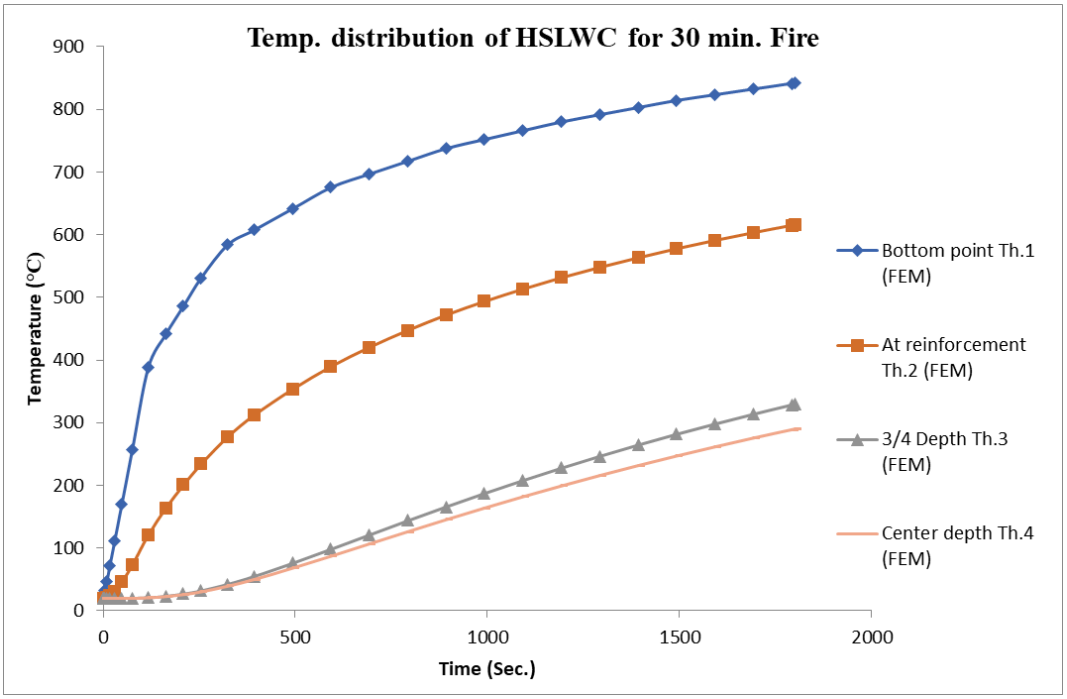

Figure A-7: Time- temperature distribution of HSLWC for 30 min. fire burning along the T-beam cross section

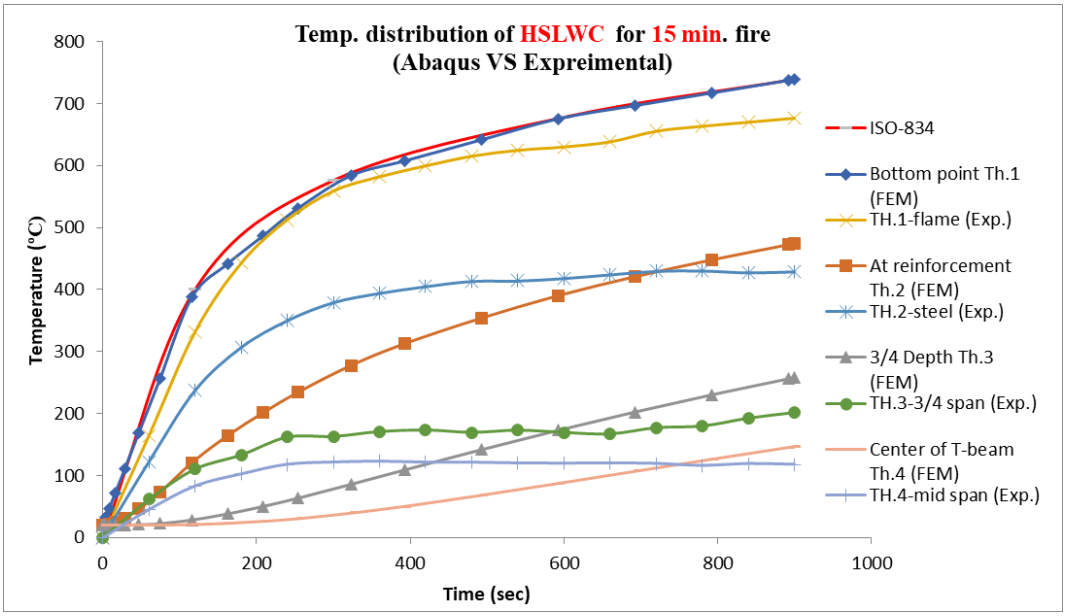

Figure A-8: Comparison of FEM & Exp. Temp. distribution of HSLWC for 15 min. fired

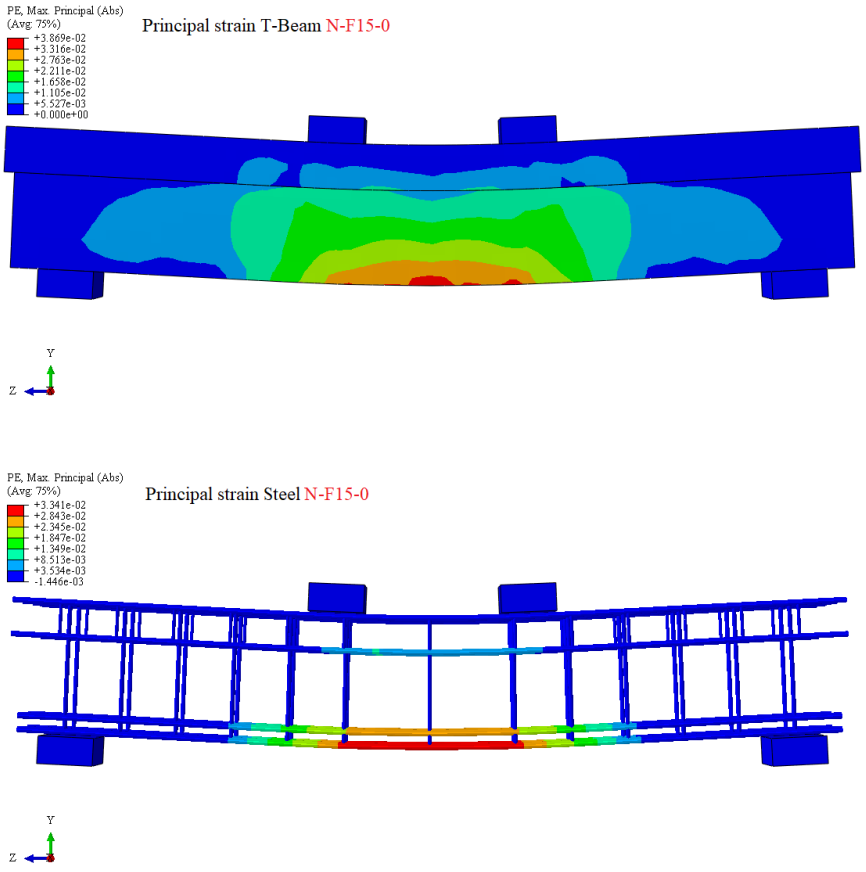

Figure A-9: Principal strain (concrete and steel) of N-F15-0

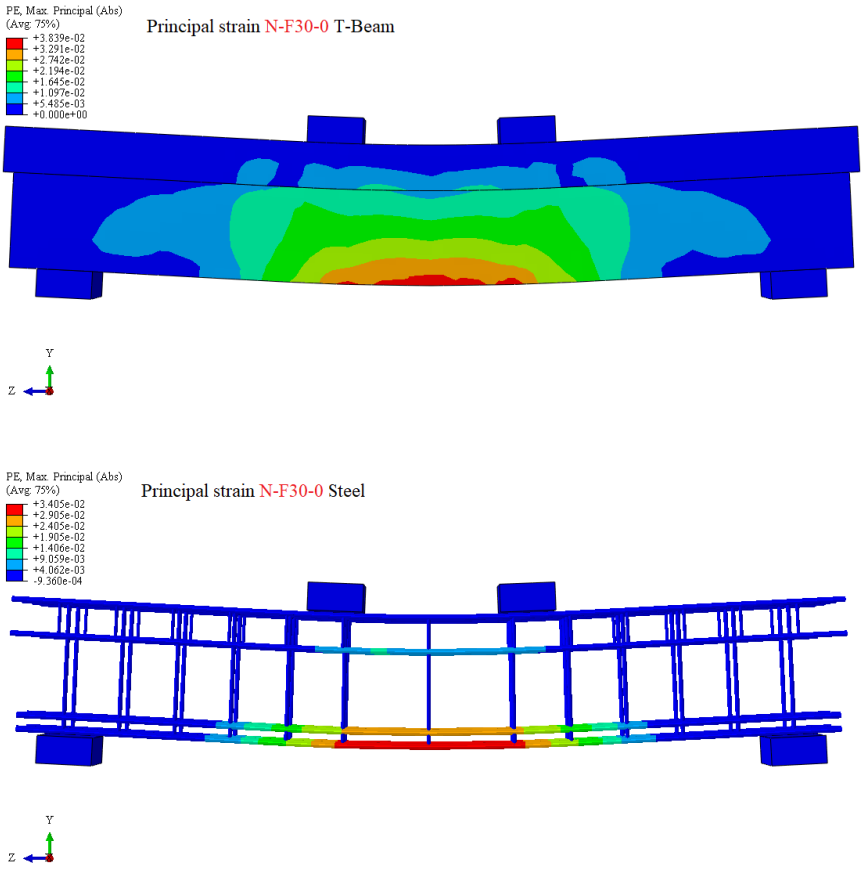

Figure A-10: Principal strain of N-F30-0

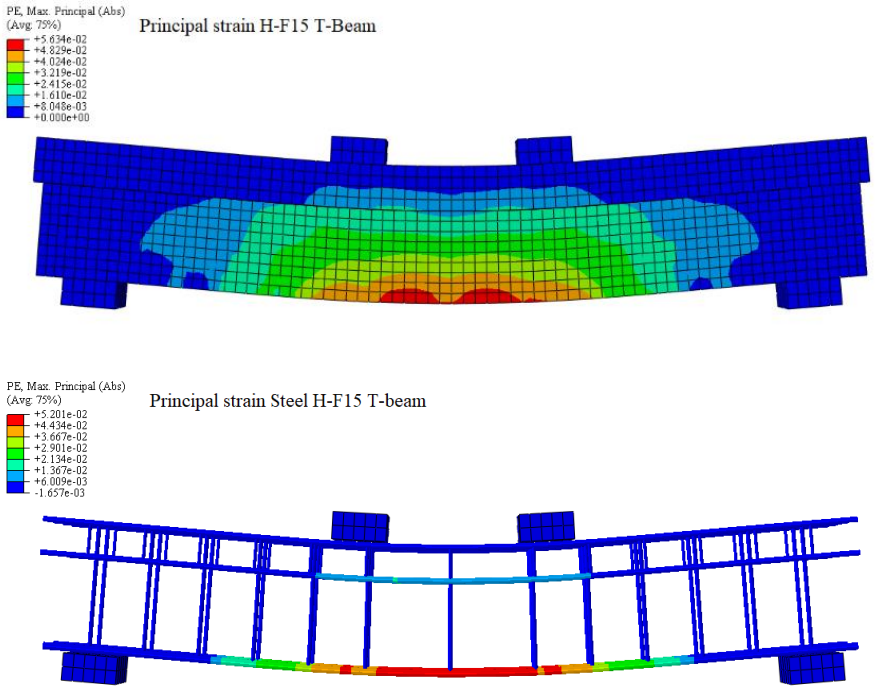

Figure A-11: Principal strain of H-F15-0

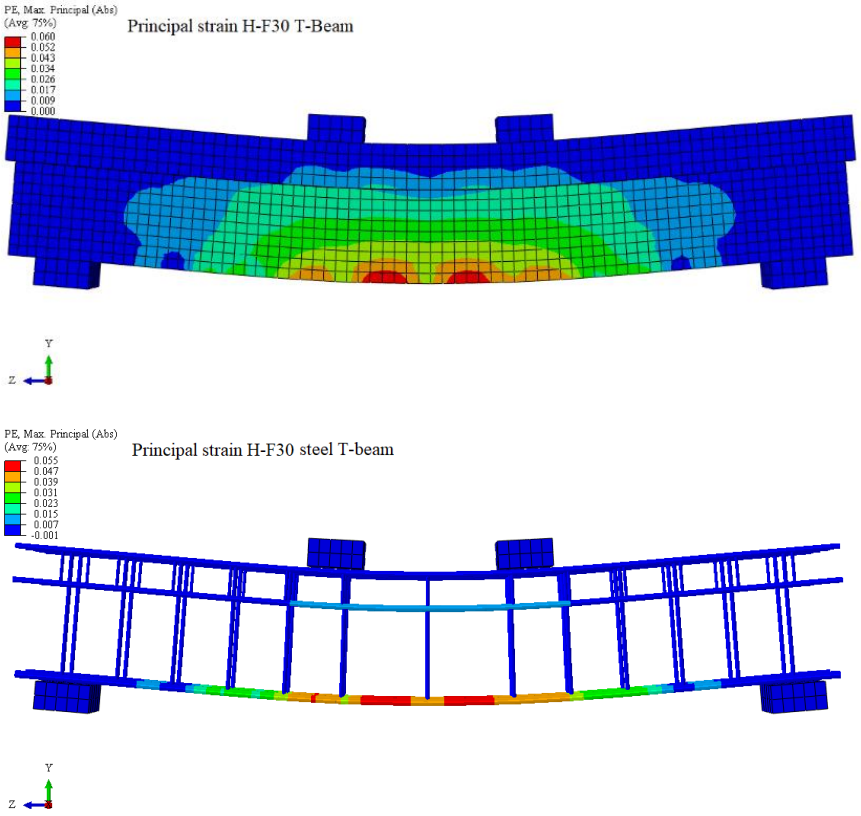

Figure A-12: Principal strain of H-F30-0

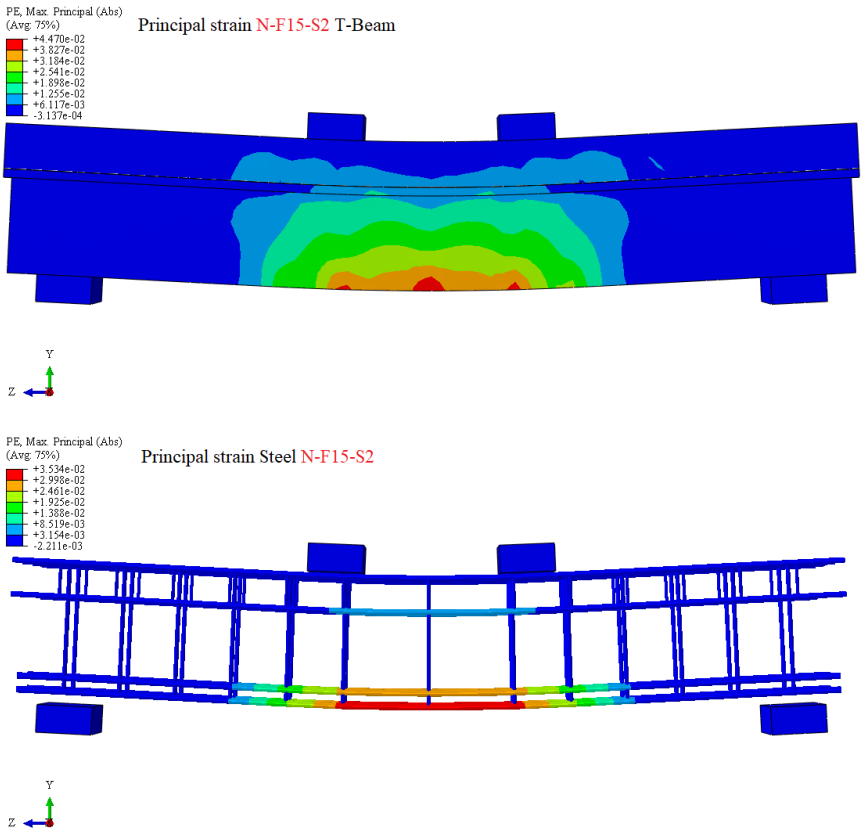

Figure A-13: Principal strain for T-beam N-F15-S2

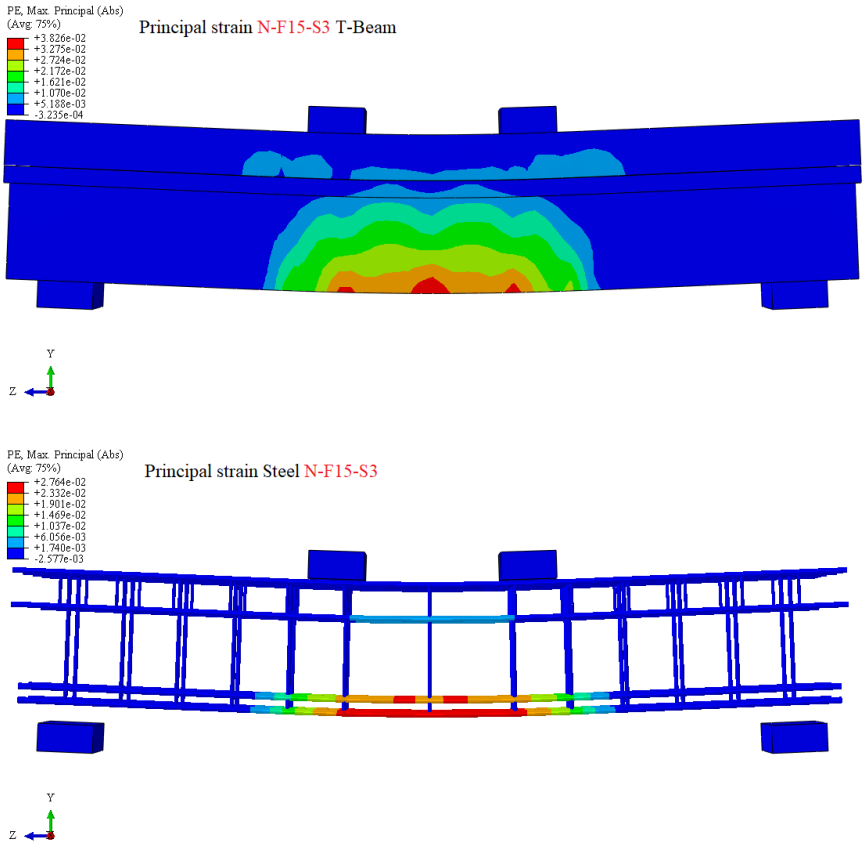

Figure A-14: Principal strain for the N-F15-S3 T-beam

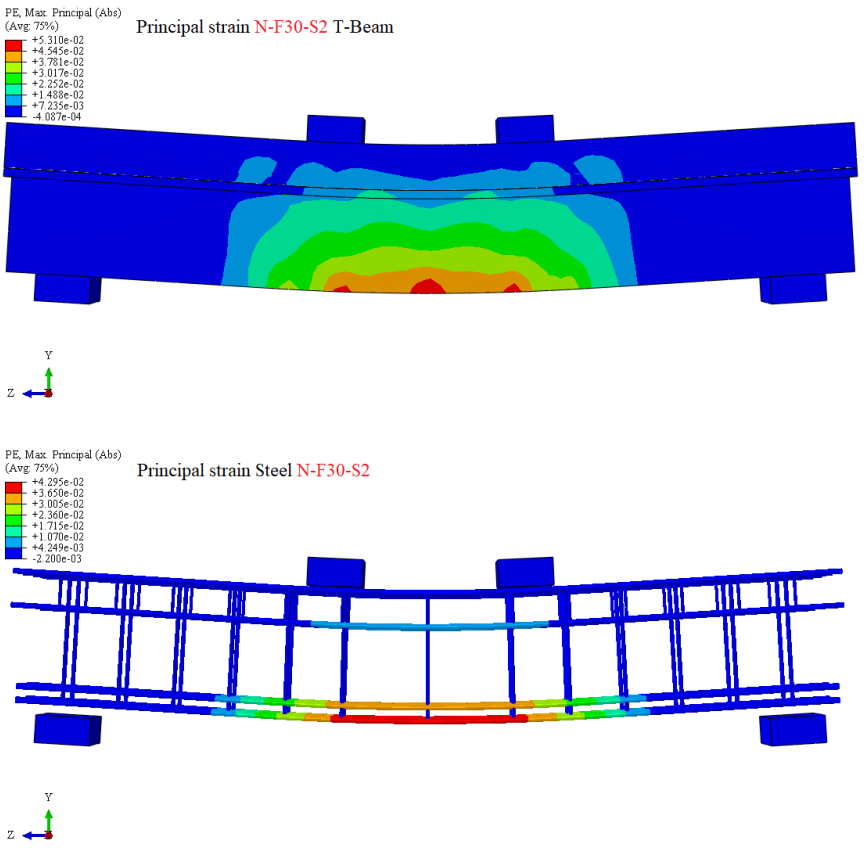

Figure A-15: Principal strain for the N-F30-S2 T-beam

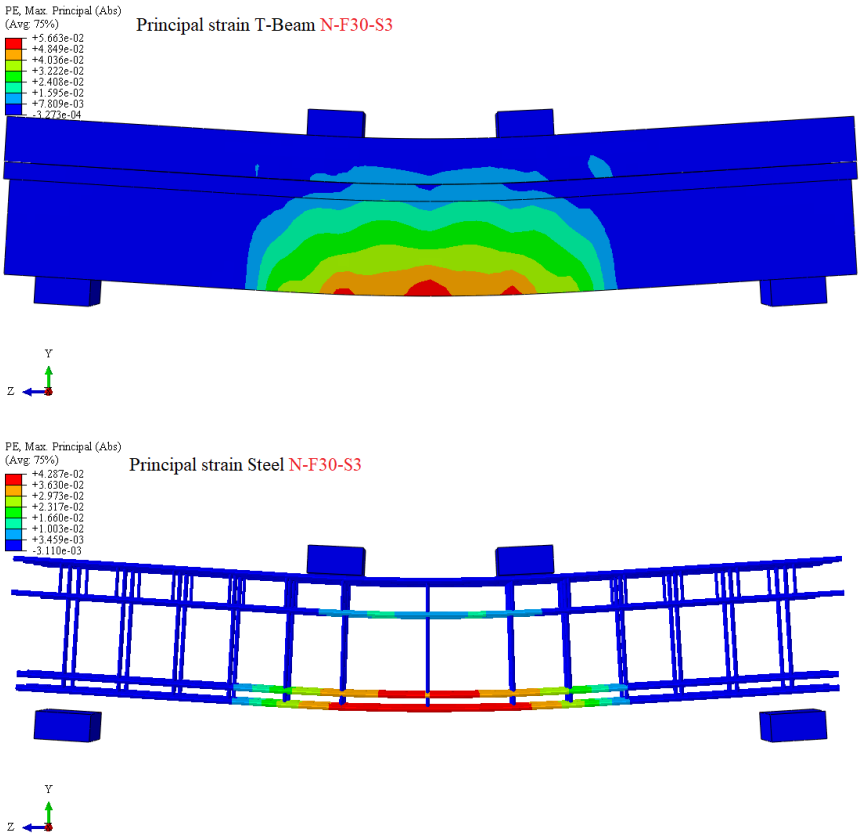

Figure A-16: Principal strain for N-F30-S2 T-beam and steel reinforcement

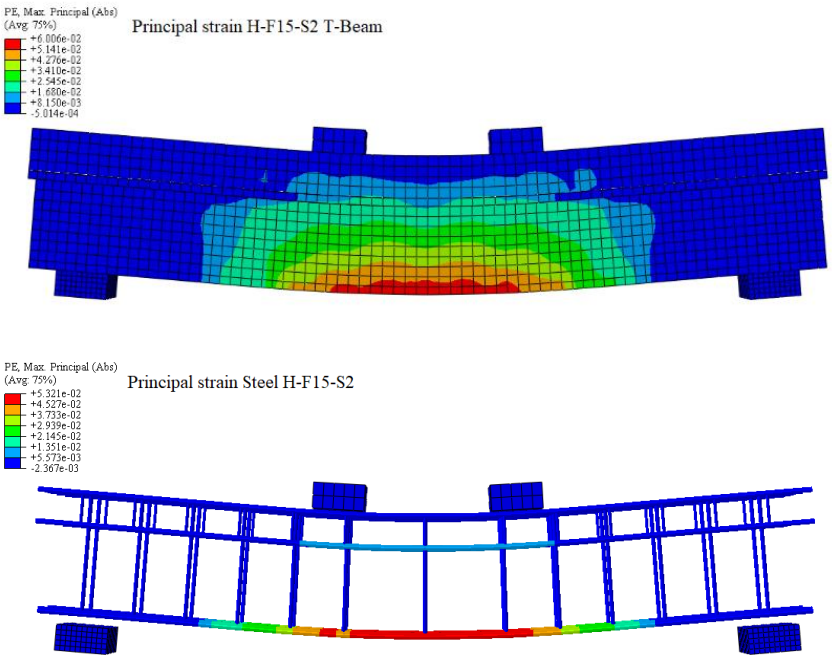

Figure A-17: Principal strain for H-F15-S2 T-beam and steel reinforcement

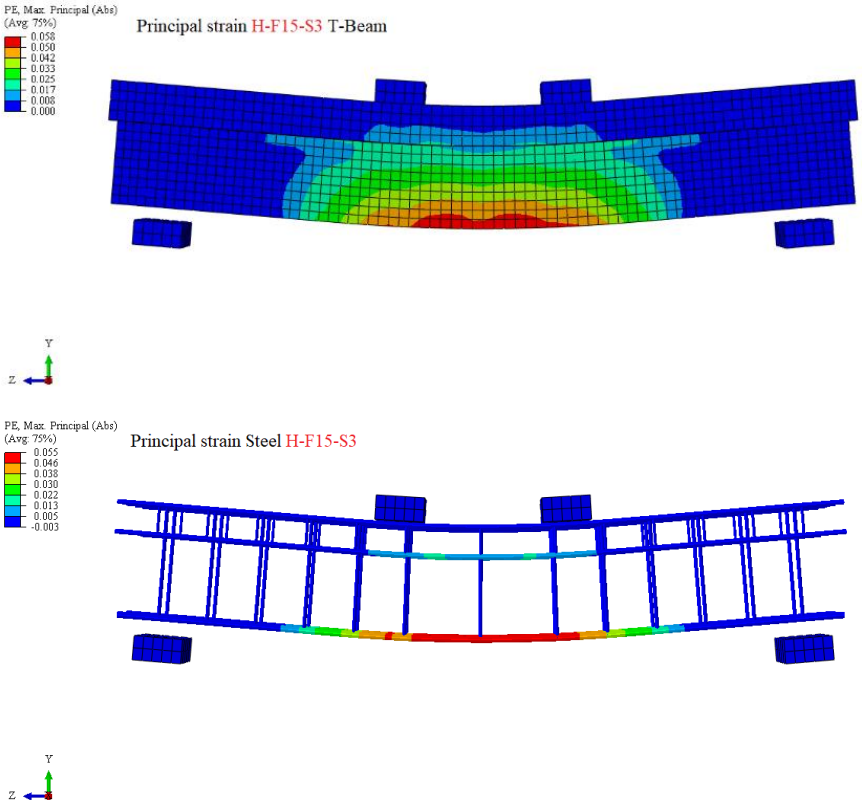

Figure A-18: Principal strain for H-F15-S3 T-beam

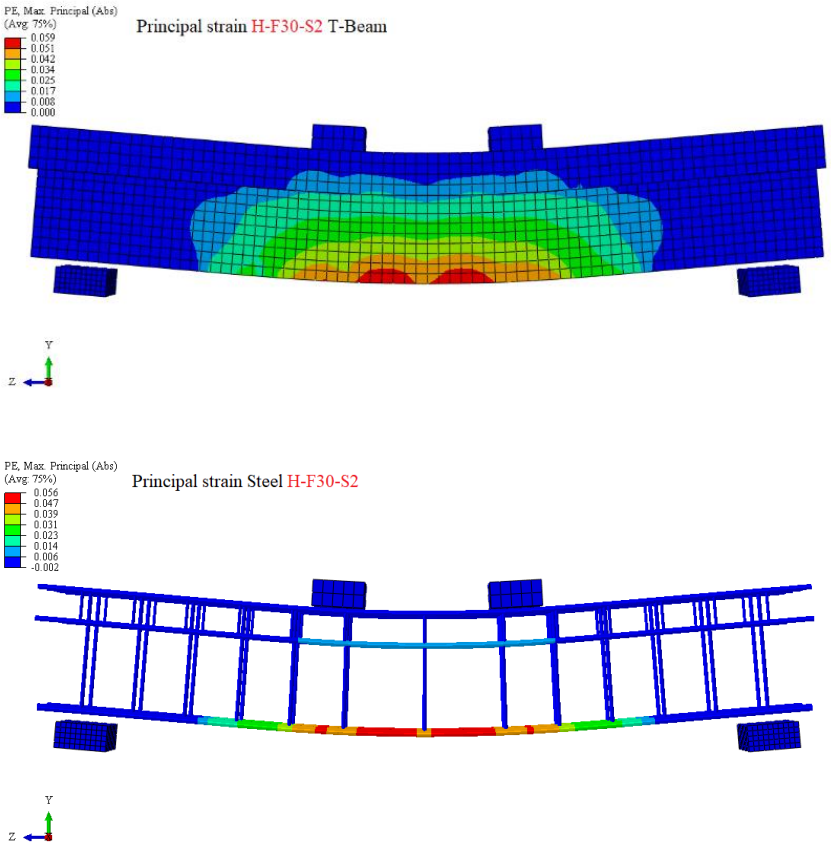

Figure A-19: Principal strain for the H-F30-S2 (T-beam and SIFCON) and Steel reinforcement

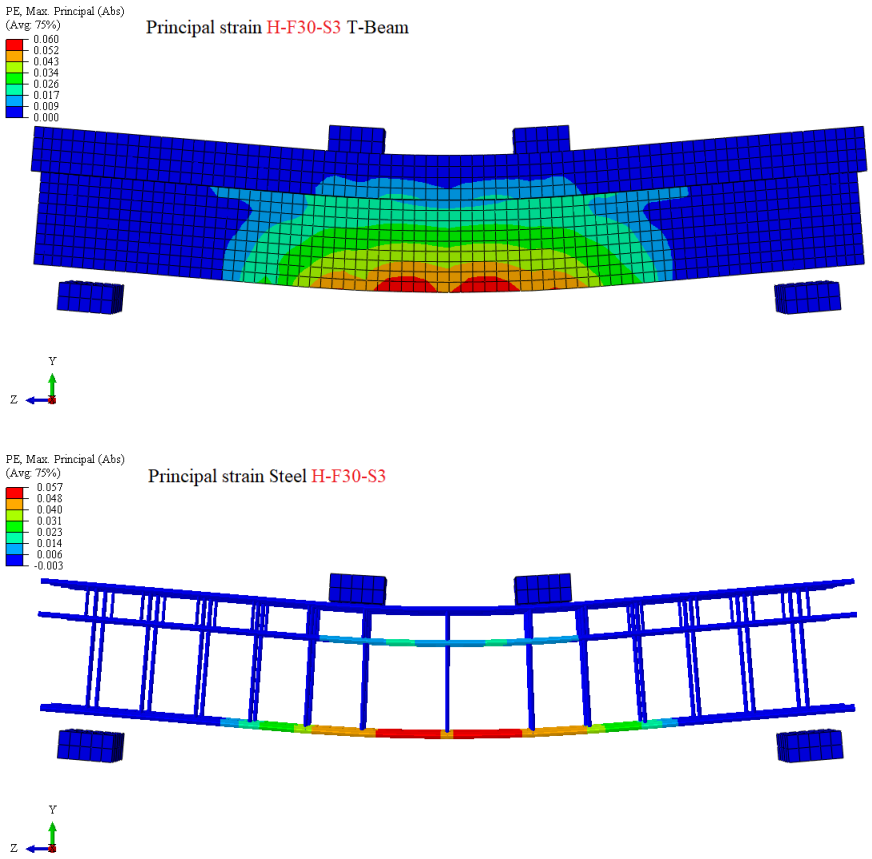

Figure A-20: Principal strain for H-F30-S3 (T-beam and SIFCON) and Steel reinforcement

الملخص

تم إجراء التحليل العملي لسلوك نماذج الاعتاب الخرسانية T-beam في هذه الدراسة، ومن أجل الحصول على خرسانة خفيفة الوزن، تم استخدام ركام الطين المحروق (LECA) كركام خشن.

تتضمن خطة العمل سلسلة من الفحوصات على أربعة عشر نموذج T-beam من الخرسانة المسلحة خفيفة الوزن ومسلط عليها لـ (Symmetric Two-Point Concentrated Loads) STPCL، حيث تكون أبعاد عينة T-beam ثابته لجميع العينات: (flange 25 x 7.5cm)، 10 web x 17.5 سم، وبطول 150 سم).

العوامل الأساسية التي تم أخذها في نظر الاعتبار لمعرفة كيفية تأثير الحريق على الخصائص الميكانيكية للخرسانة هي العينات غير المحروقة (العينات المرجعية) والمحروقة من الخرسانة المسلحة خفيفة الوزن التي تم صبها من نوعين مختلفين من الخرسانة خفيفة الوزنLWRC : الخرسانة ذات مقاومة الانضغاط العادية والخرسانة عالية المقاومة (NSLWC وHSLWC).

بعد ذلك يتم إصلاح وتقوية اعتاب LWRC المحروقة باستخدام طبقة (قميص خرساني على شكل حرف U ذات سمك قليل مصنوعة من خرسانة الملاط الاسمنتي المسلحة بالألياف الحديدية hook end steel fiber وتدعى اختصارا بـ(SIFCON) ،

يتم دراسة تأثير عدة عوامل على تصرف اعتاب T-beam، ductility, stiffness, and energy absorption ، كما تم دراسة الخصائص الميكانيكية للخرسانة وتحليلها من خلال فحص العينات الأسطوانية والمكعبة لكل مزيج حيث أظهرت النتائج أنه باستخدام LECA، يمكن تحقيق خرسانة خفيفة الوزن بكثافة جافة في حدود 1610-1965 كغم / م^3 وقوة انضغاط في حدود 34-67 ميكا باسكال بناءً على عينات فحص قياسية مكعبة بأبعاد 150*150 ملم.

تضمن الجزء العملي لهذه الدراسة ثلاثة أجزاء رئيسية: في الجزء الأول، قمنا بدراسة خصائص عينة T-beam المرجعية العادية والعالية مقاومة. وفي الجزء الثاني قمنا بدراسة التغيرات في الاعتاب NSLWC وHSLWC التي تم حرقها وفق منحنيات مواصفة IS0-834. وفي الجزء الثالث قمنا بدراسة خصائص العينات المحترقة بعد اجراء المعالجة والتقوية باستخدام طبقة من خرسانة الملاط الاسمنتي (SIFCON) ومقارنتها مع العينات المرجعية.

تم دراسة عوامل أخرى تؤثر على تصرف العتبات الخرسانية عند تعرضها الحريق. وتضمنت هذه العوامل مدة التعرض للحريق وسمك طبقة قميص SIFCON حيث تم تعريض النماذج للحريق لمدة 15 و30 دقيقة وبعد ذلك أجريت المعالجة (اصلاح العينات) بسمك 15 و30 ملم باستخدام قميص SIFCON.

تم وضع العديد من أجهزة الاستشعار الحرارية بشكل استراتيجي داخل T-beam لمراقبة توزيع درجة الحرارة عبر المقطع العرضي.

في المجمل، تم اختبار أربعة عشر عينة لدراسة الأجزاء الثلاثة وتضمنت (العينات المرجعية control، والعينات المتعرضة للحرق، والعينات التي تمت معالجتها بواسطة SIFCON) للأعتاب الخرسانية على شكل حرف T. تمت المقارنة بين عينات الفحص باستخدام عدة مقاييس، بما في ذلك

ultimate load capacity and deflection, ductility index, cracking load, initial stiffness, secant stiffness, and energy absorption

أظهرت نتائج الفحوصات العملية للنماذج تحسناً كبيراً في T-beam المدعمة بواسطة قميص SIFCON مقارنة بالعينات التي دمرتها النيران. كذلك استعادة نماذج T-beam لأدائها بشكل أفضل للخواص التصميمية والتشغيلية مقارنة مع العينات غير المتضررة (المرجعية) من خلال ملاحظة المقاييس أعلاه المحددة لهذه الدراسة.

كان أداء جميع الاعتاب الخرسانية T-beam المدعمة والمغلفة بـ SIFCON جيدًا في فحص الانثناء، أدى الحرق إلى خفض قيمة ultimate load capacity لأعتاب T-beam المحروقة حيث شهدت عينات الاعتاب NSLWC وHSLWC معدلات تدهور بلغت 24.4% و20.5% و41.5% و35.6% على التوالي لمدة 15 و30 دقيقة من التعرض للحريق على التوالي. واظهرت اعتاب T-beam المدعمة بواسطة SIFCON تحسن بشكل واضح في قيمة لـ load carrying capacity، بنسبة 159% و207% لـ NSLWC و180% و220% لـ HSLWC لسمك 15 و30 ملم من قميص SIFCON.

وأخيرا، تم استخدام طريقة العناصر المحددة (FEM) لنمذجة ومحاكاة العتبات الخرسانية T-beam التي تم التحقق منها عمليا في المختبر، وتم تمثيل النماذج بشكل نظري مع محاكاة لظروف الفحص المختبري لغرض المقارنة مع النتائج العملية.

تم استخدام طريقة العناصر المحددة للعينات باستخدام برنامج ABAQUS (بنسخة اصدار لعام 2021) لهذا الغرض، حيث أظهرت النتائج أن أدنى وأعلى قيم الأخطاء المطلقة ("التباين") في load carrying capacity للعينات كانت حوالي 1.97% و14.28%، على التوالي، لـ NSLWC وحوالي 0.39% و9.67%، على التوالي، لـ HSLWC.

كما لوحظ ان قيمة "التباين" او نسبة الخطأ المطلق الأدنى والأعلى لقيمة الهطول، 1.59% و13.43% لـ NSLWCعلى التوالي وكذلك3.93% و13.89% لـ HSLWC وكون نتيجة الخطأ المطلق بنسبة 15% أو أقل فإنها تعد مقبولة.

جمهوريـــــــــة العـــــــــراق
وزارة التعليم العالي والبحث العلمي
جامـــعة بابـــــــــــــل
كلية الهندسة
قسم الهندسة المدنية

إصلاح عوارض الخرسانة المسلحة خفيفة الوزن العادية وعالية المقاومة المتضررة من الحريق باستخدام ملاط الخرسانة المتخللة للألياف

رسالة

مقدمة الى كلية الهندسة / جامعِة بابل وهي جزءِ من متطلبات الحصول على درجة الماجستير في الهندسة / الهندسة المدنيِة / مواد إنشائية

من قبل

حسنين سمير حمدي العميدي

بأشراف

أ. د. محمد منصور كاظم **أ. د. نمير عبد الأمير علوش**

1445 A.H 2023 A.D.